NASA

60 GHz Intersatellite Communication

Link Definition Study

Baseline Document

Communications Sciences
Space System Operations
Western Development Laboratories
Ford Aerospace & Communications Corporation
Palo Alto, CA

NASA

60 GHz Intersatellite Communication

Link Definition Study

Baseline Document

Communications Sciences
Space System Operations
Western Development Laboratories
Ford Aerospace & Communications Corporation
Palo Alto, CA

TABLE OF CONTENTS

SECTION 1

SYSTEM DESIGN

TABLE OF CONTENTS, FIGURES & TABLES

SECTION 1

TABLE OF CONTENTS, FIGURES & TABLES (Cont)

1.0 OVERALL SYSTEM CONCEPT

With the launch of the NASA's first Tracking and Data Relay Satellite (TDRS), there is an overall trend in the satellite scientific and data collection communities toward the use of relay satellites for the return of mission data. This concept has a number of advantages over the previously used alternative of dedicated space-ground links (SGLs) to ground stations.

Most of these satellite platforms are in low-earth orbits (LEOs) that have limited and time-varying view of the earth. This means that either the satellite must provide some means of storing its collected data until it is in view of its ground station (and then transmit it very quickly during the short period of time the station is in view) or the system operator must provide ground stations that will be in the satellite's field of view for all times when the return of data is desired.

A relay satellite system with intersatellite communication links to the LEO satellite expands the available time of near real time contact by providing a relay (for the LEO satellite) that is in its field of view for longer periods of time. If there are two relay satellites in (nominally) geostationary earth orbits (GEOs), virtually continuous contact can be maintained with the LEO satellite. The SGLs are now from the relay satellites to ground stations. An additional crosslink between the two relay satellites to relay the mission data allows a single SGL to suffice. This eliminates the need for multiple overseas ground stations, which are expensive to maintain and are physically and politically vulnerable. An added benefit is that all mission data is received in a single ground station in real time and does not need to be relayed separately or spliced together. Additionally, the relay can also be configured to carry commands and telemetry to and from the mission satellite, allowing similar consolidation of T&C stations as in the mission data receiving stations.

NASA system studies have established that it is conceptually feasible to have a single satellite relay system to accommodate the needs of multiple mission satellites. (Within the context of this overall system, the mission satellites then become user satellites, or USATs, of the relay capability). This is the intent of the current Tracking and Data Relay Satellite System (TDRSS) and its anticipated successor, the Tracking and Data Acquisition System, or TDAS. The current TDRSS has intersatellite link capability at S-Band and Ku-Band. The data rate capacity of those systems, though, is not large enough to accommodate the expected rates for USATs in the post-1995 timeframe. It is necessary, then, to design an augmented capability for the post-1995 timeframe that will accommodate these new requirements.

The use of 60 GHz for intersatellite links has been judiciously chosen in the TDAS timeframe. Technology is currently being developed that will be able to support multigigabit data rates in the near future. Additionally, the attenuation of the earth's atmosphere at 60 GHz means that there is virtually no possibility of terrestrially generated interference (intentional or accidental) or terrestrially based intercept.

The ICLS (Intersatellite Communications Link System) includes the following functional areas:

1. The ICLS payload package on the GEO TDAS satellite that communicates simultaneously with up to five LEO USATs.

1-1

2. The ICLS payload package on the USAT that communicates with the TDAS satellite.

3. The crosslink payload package on the TDAS satellite that communicates with another TDAS satellite.

Figure 1-1 shows the overall ICLS concept of the TDAS and USATS.

Because of the similarities inherent in the above packages, the commonality of design should be maximized as much as possible (and reasonable). This includes not only the hardware but configuration and operational concepts as well. This approach minimizes the development necessary to implement the system and results in lower overall system costs with reduced risk.

Additionally, it is desirable to define clean, standardized interfaces between the ICL packages and the host satellites to which they are attached. It is especially critical in the case of the USAT. Whereas it is the purpose of a TDAS satellite to relay data, the prime mission of the USAT is to perform its scientific or collection mission. Therefore, it is the intent of this study to ensure that the impact and burden of the ICLS on the USAT is minimized. To this end, the simplest interfaces between the ICLS payload package and the host satellite have been defined as follows:

1. The ICLS packages will be modular in design. Mechanical interfaces will consist of a specified mounting area, mass and thermal transfer characteristics, and field-of-view requirements.

2. The communication interface will be (all or partially) baseband data at a user-specified rate, along with a suitable clock. This implies that the ICLS package will include modulators and demodulators.

3. There will be a data interface between the ICLS package and the host satellite for the purpose of transferring commands, telemetry, satellite attitude, and other data that would normally be resident in a satellite's command telemetry, and attitude control systems.

4. The host satellite will provide dc power to the ICLS package.

Two methods of data relay on-board the TDAS spacecraft were addressed in the study. One is a complete baseband system (demod and remod) with a bi-directional 2 Gbps data stream; the other is a channelized system conforming more to the current TDRSS channel structure, wherein some of the channels are baseband and others are merely frequency translated before re-transmission. This second concept, called "mixed baseband and IF signals" is documented in Appendix A to this report. Other than comparisons of the two systems, the information in the main body of this document refers to the "all baseband system".

Three standardized ICLS payload packages will be required, the TDAS GEO link, the TDAS LEO link, and the LEO USAT link. These payload packages for the "all baseband system" are illustrated in Figures 1-2 and 1-3. (Note that the packages involving the LEO USAT links will be the same regardless of the data relay system used on-board the TDAS). Table 1-1 highlights the resulting system commonality of the baseline design. Table 1-2 summarizes the major differences, both in equipment and performance, between the "all-baseband" and the "mixed IF and baseband" crosslink systems.

SYSTEM CONCEPT
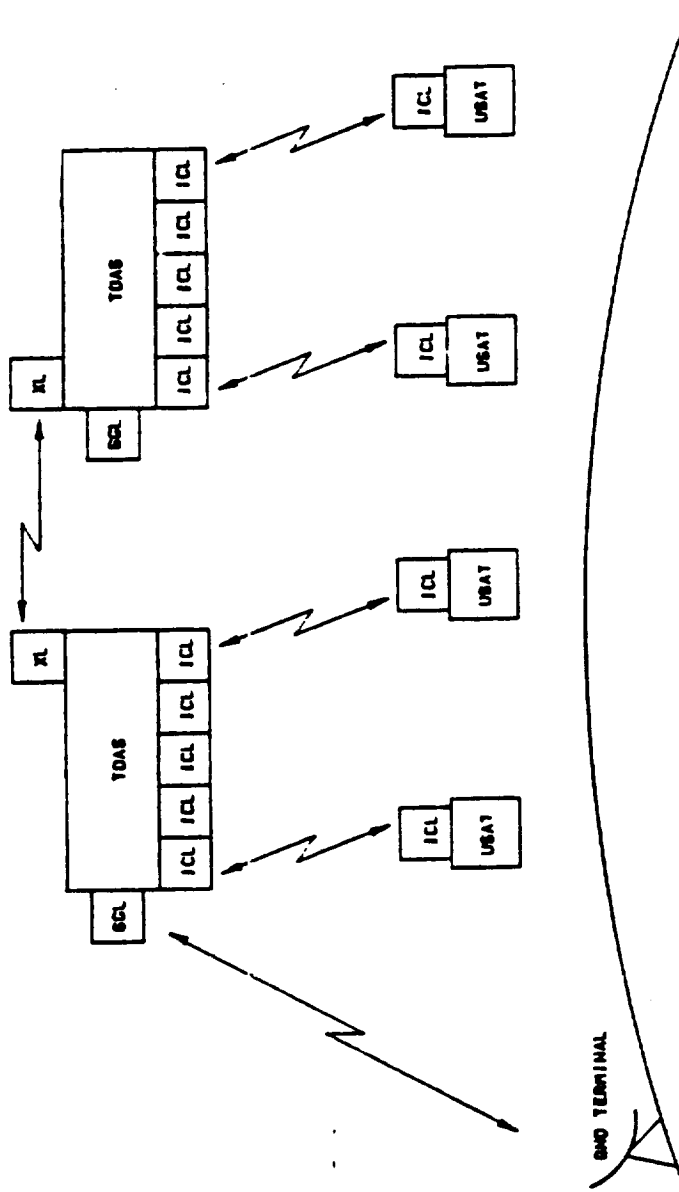
LEGEND:

TDAS - Tracking & Data Acquisition System (Satellite)
USAT - User Satellite
XL - Crosslink Package
ICL - Intersatellite Communication Link Package
SGL - Space/Ground Link Package

FIGURE 1-1

BASELINE ICLS/TDAS INTERFACE
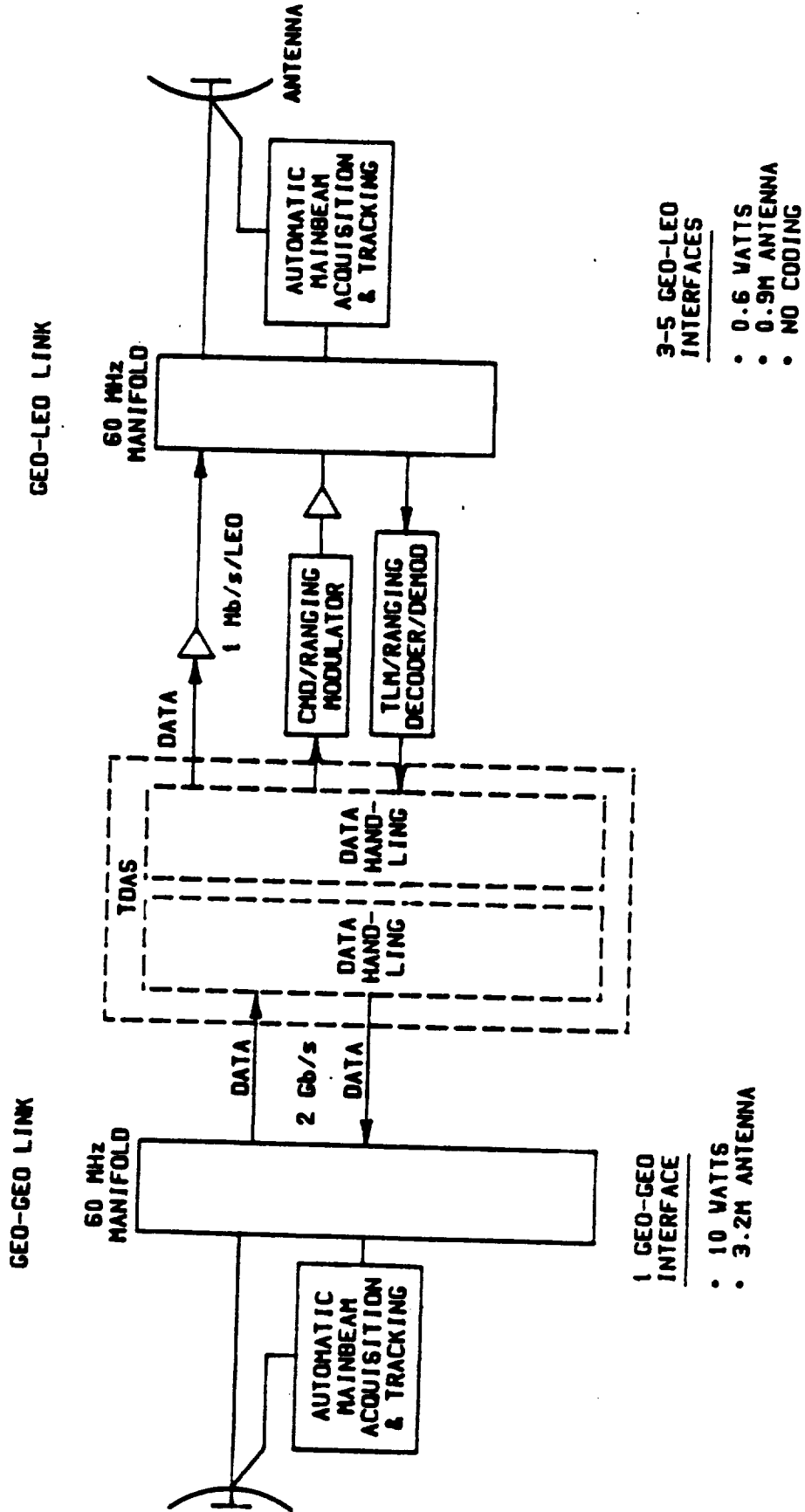
FIGURE 1-2

BASELINE ICLS/LEO USAT INTERFACE

LEO-GEO

INTERFACE

- 7.5V (300 Mb/s MAX)
- 4.6 FT ANTENNA
- 100 lb
- 200W DC POWER
- TLM DATA CDM 1 Mb/s
- DATA RATE USER SPECIFIED
- FEC ENCODING
- AUTOMATED MAINBEAM ACQISITION AND TRACKING

DATA HANDLING S/C

DATA

TLM/RANGING/ENCODER/MOD

CMD/RANGING/DEMOD

S-BAND XMTR/RCVR

60 GHz MANIFOLD

AUTOMATED ACQUISITION TRACKING PROCESSOR

ANTENNA

S-BAND ANTENNA
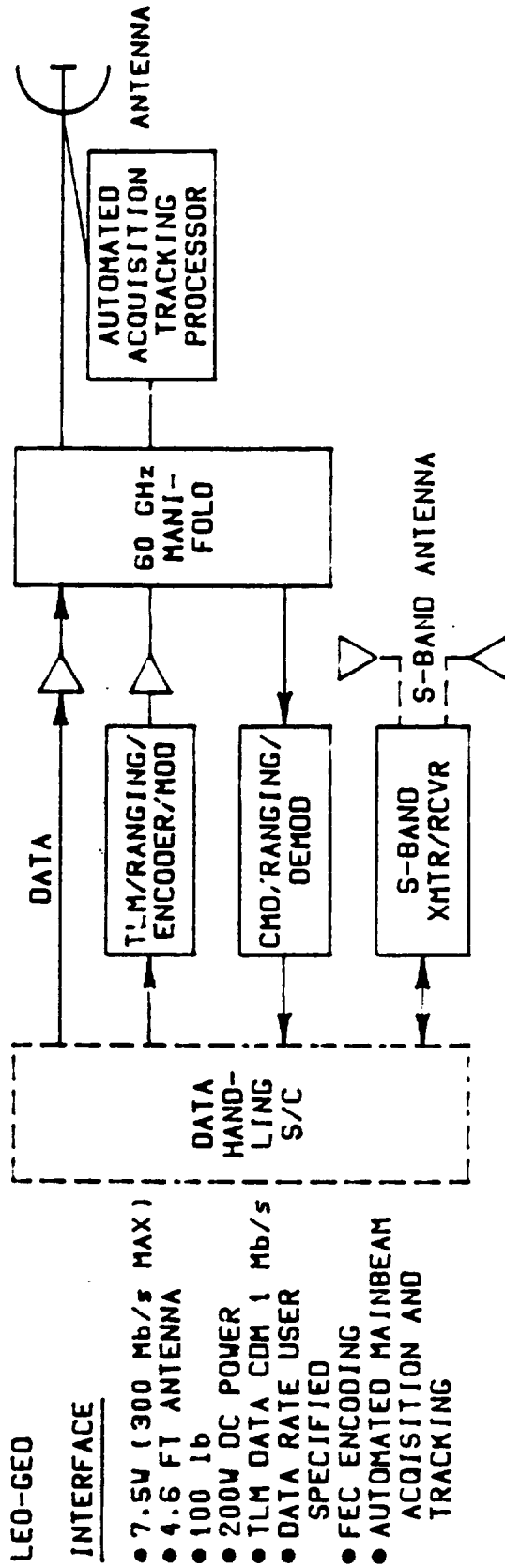
FIGURE 1-3

Table 1-1

System Commonality

	GEO TDAS (All Baseband)	LEO - USER

Common	o 360° K LNA
	   (GEO-GEO, LEO-GEO)
	
	o Acquisition Receiver
	
	o 10 W Xmitter Assembly
	   (GEO-GEO)
		o 360° K LNA
		   (GEO-LEO)
		
		o Acquisition Receiver
		
		o 7.5 W Xmitter Assembly
		   (LEO-GEO)

Unique	o 0.6 W Xmitter
	   (GEO-LEO)
	
	o 3.2 M antenna & gimbal
	   (GEO-GEO)
	
	o 0.9 M antenna & gimbal
	   (GEO-LEO)
	
	o 2 Gbps and 1 Kbps -
	   300 Mbps demodulators
	
	o 2 Gbps and 1 Mbps
	   modulator
	
	o FEC Decoder
		o 1.4 M antenna & gimbal
		
		o 1 Mbps demodulator
		   & user TT&C interface
		
		o 1 Kbps-300 Mbps modulator*
		
		o FEC Encoder

more complex   less complex

*Recommendation is that the following data rates be used:

100 Kbps
300 Kbps
500 Kbps
  1 Mbps
 10 Mbps
 30 Mbps
 50 Mbps
100 Mbps
300 Mbps

Table 1-2

Comparison: All Baseband vs Mixed IF and Baseband

	All Baseband	Mixed IF and Baseband
Number of GEO-GEO Channels		
Forward	1	13
Return	1	22
GEO-GEO Data Throughput (Mbps)		
Forward	2000	105.63
Return	2000	3124.60
GEO-GEO Antenna Size (Meters)	3.2	3.2
GEO-LEO Antenna Size (Meters)	0.9	0.9
Receiver Noise Figure (dB)	3.5	3.5
Highest Power Transmitter Req'd (Watts)	10	4
Weight (Pounds)		
GEO-GEO System	157.2	592.8
GEO-LEO (5 Systems)	414.5	414.5
LEO	99.6	99.6
DC Power (Watts)		
GEO-GEO Frontside	244	722
GEO-GEO Backside	244	914
GEO-LEO (5 Systems)	541	541
LEO	192	192
P_s (10 Year Life)		
GEO-GEO Forward or Return	0.7745	
e.g. WSA Return		0.8746 *
e.g. WSA Forward		0.8980 *
GEO-LEO	0.9425	0.9425

* For the complete reliability analysis of the Mixed IF and Baseband System, see Addendum A to this report.

1.1   Geosynchronous to Low-Earth Orbit System Design

The GEO-LEO link system design was based on NASA TDAS requirements. Specifically, the requirements were analyzed and allocated into functional areas within the architectural, operational and technical boundary of the projected 1989 time frame. The allocated functional areas offered a range of configuration possibilities suitable for parametric and qualitative trade off analyses and iterations.

In the course of this process, each major configuration component was addressed as a subset of interacting system parameters. Starting with the initial link interface definition and a set of judiciously selected candidate component items, the link system was designed iteratively. The impact and sensitivity of each component item upon the entire payload package as well as TDAS was assessed until a most viable design was developed. Also, the following ground rules were used as a measure of effectiveness to ensure an objective design optimization:

o   Use 1989 timeframe cutoff technology.

o   Maintain technology commonality among GEO-GEO crosslink and GEO-LEO intersatellite links.

o   Minimize burden to LEO user satellite.

o   Minimize overall weight and power needs imposed on TDAS.

During the course of the study it was found that certain key system requirements actually drove the baseline design. These included, but were not limited to:

o   The size of the antennas was limited by STS launch capability.

o   High GEO-GEO data rate forced a high EIRP.

o   WARC-79 frequency allocation forced QPSK modulation for the 2 Gbps GEO-GEO communication link and for the high data rate LEO-GEO link.

o   Potentially large LEO ephemeris errors (7-9 seconds) led to the choice of GEO-LEO antenna sizes. If the ephemeris uncertainty can be reduced, the GEO antenna size can be increased and the LEO decreased, thereby further reducing the user burden.

o   The simultaneous (3-5) LEO operations impact the system reliability, weight, and size. It was found that no more than 2 of the GEO-LEO antennas could slew simultaneously without creating unacceptable disturbances to the TDAS spacecraft.

o   Since the sun will be in the antenna field-of-view for a small percentage of the time, a low noise front end is required.

These system design drivers led to the identification of technology design drivers:

o   The high EIRP requirement, coupled with the limited antenna size, led to a 10 watt power amplifier.

o   The rate of IMPATT diode failures is critical in assessing the reliability of power amplifiers.

o   Gain, scanning and weight considerations led to a gimbal dish antenna configuration.

o   A low loss requirement from electronics package to antenna favored a beam waveguide approach.

o   The low loss requirement also forced performance improvements in EHF filters.

o   Gimbal velocity and acceleration (not EIRP and G/T) dominated the acquisition time.

o   Bandwidth considerations led to a rate 5/6 FEC code on the LEO-GEO link.

o   Complexity of the Viterbi decoder forced investigation of novel coding approaches such as AR (alphabet redundant) or LC (low complexity).

o   The low noise front end dictated a low noise amplifier instead of a mixer front end. In particular, the amplifier noise temperature requirement was less than 360° K.

Considering these hardware needs, most of the technology is currently available and all the enabling technologies are either in work or planned. Thus the prospects are excellent for all the required 60 GHz technology to be ready to support TDAS implementation. Reliability continues to be a major factor, however, and the achievable data rate is tied directly to the attainable reliability levels. In particular, improved parts characterization is essential, especially for transmitters. Techniques for hardware integration and cross-strapping must be improved. Other areas of suggested technology improvement are presented in Table 1-3.

1.1.1   Link Closure Parameters

The operational requirements of the LEO satellite coverage to orbital altitudes up to 5000 km was readily translated to the following system constraints as illustrated here in Figure 1.1.1-1, and frequency planning as shown in Figure 1.1.1-2.

TABLE 1-3

SUGGESTED TECHNOLOGY DEVELOPMENT

TRANSMITTERS

o Resolution of the stable amplifier vs injection-locked oscillator.
o Development of larger IMPATT devices to reduce parts count.
o Development of combiner techniques which allow graceful degradation
   or development of module cross-strapping techniques.
o Improvement of TWTA reliability.
o Improved parts characterization.

LOW NOISE FRONT ENDS

o Development of reliable 60 GHz low noise devices such as HEMTs.

DIGITAL EQUIPMENT

o Development of an 8-bit A/D converter with 150 to 200
   mega-conversions per second.
o Development of a multiplier capable of 300 to 500
   mega-multiplies per second.
o Development of 1-nanosecond RAM and ROM.
o Improved reliability consistent with mission life.

FILTERS AND MULTIPLEXERS

o Development of low-loss EHF band-pass filters.
o Development of narrow-band band-reject filters for power combining.
o Development of designs to maximize mechanical tolerances.
o Development of materials/heat-treating techniques to minimize
   thermal effects.

LINK ANALYSIS PARAMETERS AND CONVENTIONS

o LINE LOSSES:
   PER LOSS BUDGET ATTACHED

o CARRIER FREQUENCY:
   LINK 1: 62.75 GHz, 55.5 GHz
   LINK 2: 57.8 GHz
   LINK 3: 60 GHz

o MAX LINK DISTANCE:
   LINK 1: 83043 km
   LINK 2,3: 41660 km

o ACQUISITION TIME:
   (FOR GEO TDAS @ ±0.2°)
   (FOR LEO USAT @ ±2.0°)
   LINK 1: ≤27 sec (3.2 m ANT.)
   LINK 2: ≤44 sec (1.4 m ANT.)
   LINK 3: ≤ 3 sec (0.9 m ANT.)

o ANTENNA TEMPERATURE:
   LINK 1S = 5200°K   SUN
   LINK 2S = 5000°K   SUN
   LINK 3S = 4400°K
   LINK 2E, 3E = 250°K   EARTH
   LINK 1E, = 10°K
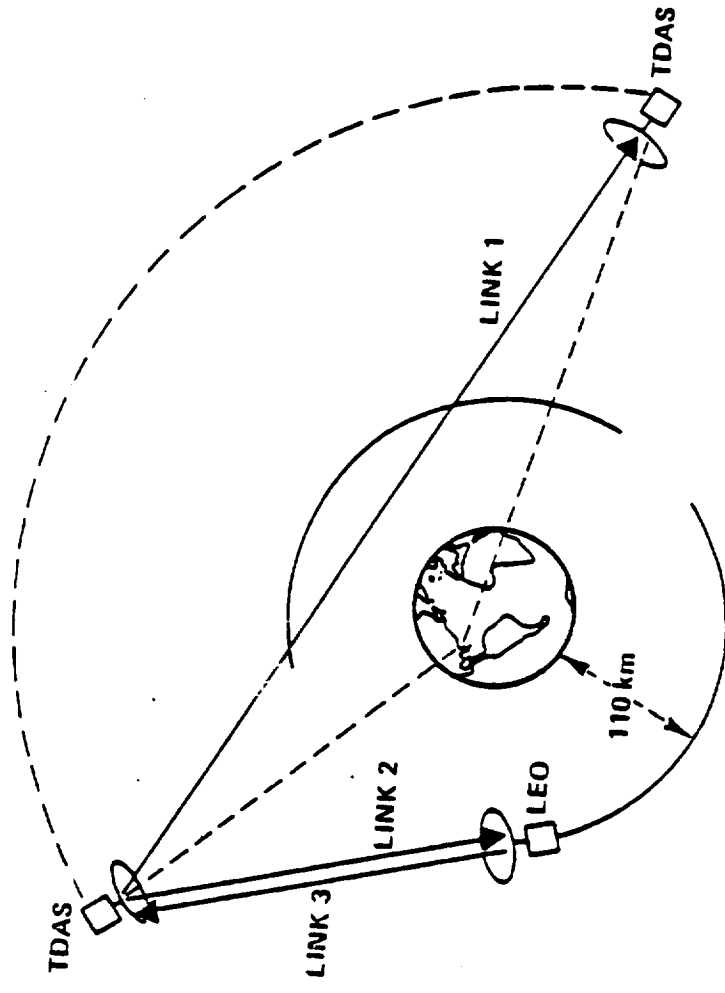
FIGURE 1.1.1-1

1 - 11
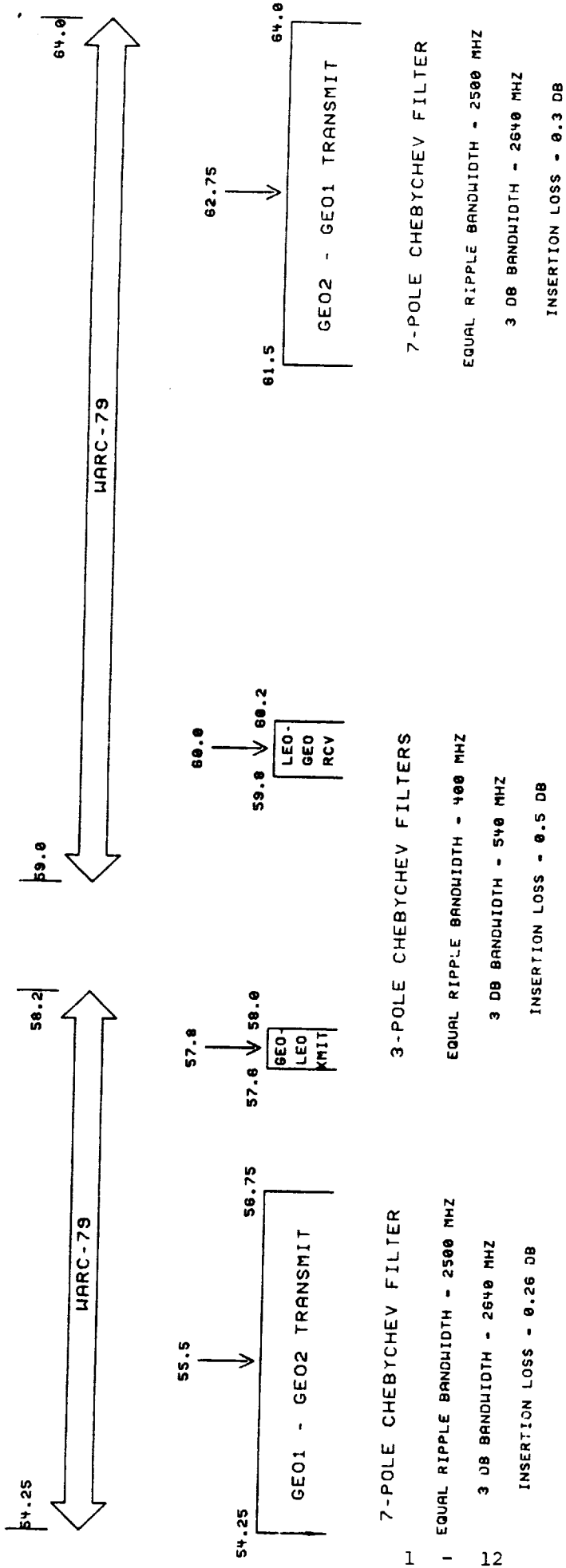
FREQUENCY PLAN & FILTER CHARACTERISTICS

FIGURE 1.1.1-2

The resulting all-baseband design is as follows: The crosslink between two geosynchronous TDAS with 160 degree separation (83,000 KM) is capable of simultaneous transmission and reception of 2 Gbps data through quadrature phase keying (QPSK) modulation using a 10 watt IMPATT diode stable amplifier and a gimbal mounted, 3.2 M parabolic dish Cassegrain antenna with low loss beam waveguide. This communication capability is maintained year round except for the brief periods (less than 0.01% per year total) when the sun is in conjunction with the antenna field of view. During these brief periods, the link is maintained at 300 Mbps. Automated acquisition/reacquisition and monopulse tracking are maintained at all times regardless of sun effect.

In addition to the TDAS-TDAS crosslink package above, there are five (5) link packages to provide simultaneous and independent intersatellite links between a geosynchronous TDAS and low earth orbiting (LEO) user satellites having a maximum altitude of 5,000 KM. Each forward link (from TDAS to LEO) is capable of a 1 Mbps data rate at all times using a 600 mW IMPATT transmitter and a 0.9 M gimbal mounted dish antenna, with binary phase shift keying (BPSK) modulation. Each return link (from LEO user to TDAS) is capable of reception of up to 300 Mbps, forward error correction (FEC) encoded QPSK information data. For LEO users equipped with a 1.4 M antenna and a 7.5 W transmitter, a 300 Mbps capability can be maintained at approximately 99.95% (for equatorial orbits) of time with 50 Mbps for the remaining 0.05% of time (for equatorial orbits) when the TDAS antenna is in conjunction with sun. A microprocessor controlled automated main beam acquisition algorithm receiver with monopulse tracking is capable of initiating and accomplishing fast TDAS-LEO link acquisition at any contactable time regardless of the effect of sun. With this design, high confidence (99.9%) acquisition can be accomplished in 50 seconds or better with very low (<0.01%) false acquisition rate for LEO users having an attitude plus ephemeris pointing error as large as ±2.0 degrees.

To accommodate a conglomerate of up to 5.5 Gbps traffic from all links per each TDAS, innovative frequency planning, along with key inter/intra system interference analyses have been conducted to ensure the adherence to the WARC 79 frequency allocation for the 60 GHz band.

The above mentioned design is based on 1989 technology projection and a number of system and design constraints as delineated in the NASA contract SOW (statement of work) none the least of which are to minimize the burden of LEO user satellites and provide proper thermal and mechanical interface to the TDAS. In a nut shell, the baseline design is modular and acquisition agile. The LEO user package can be "bolted" onto the user satellite as a secondary payload with simple interfaces and can be changed (before launch or through in-orbit service) to accommodate growth in data rate or service different mission needs.

Tables 1.1.1-1 through 1.1.1-6 show the link analyses of all intersatellite communication links under the effects of sun, earth or sky as appropriate. All analyses are based on the RF front end as illustrated in Figure 1.1.1-3 with its attendant loss budget shown in Figure 1.1.1-4. Figure 1.1.1-5 illustrates how system noise temperatures are calculated in each instance.

The data rate of the command link to the LEO satellite, calculated in Table 1.1.1-5, could be increased to 25 Mbps if a higher power transmitter (e.g. 5 watts) were to be utilized. The link performance would not be impacted and this would result in more commonality between TDAS and the current TDRSS.

Table 1.1.1-1. GEO-GEO Crosslink with Sun Effect

Modulation: QPSK
Coding: None

Carrier Frequency =   55.5 GHz

Parameter	Value	Units	Remarks
Transmitting S/C Power	10.00	dBW	10.0 watts
Transmit Line Loss	1.00	dB	
Feed Loss	0.60	dB	
Transmitting Antenna Gain	63.30	dBi	3.2-m dish
EIRP	71.70	dBW	
Free Space Loss	225.72	dB	83,043 km
Pointing Loss	0.10	dB	0.01 degree
Polarization Loss	0.20	dB	
Tracking Loss	0.10	dB	0.01 degree
Net Path Loss	226.12	dB	
Receiving S/C Antenna Gain	63.30	dBi	3.2-m dish; Temp. =5200 K
Feed Loss	0.60	dB	Temp.= 10 K
Receive Line Loss	1.20	dB	Temp.= 290 K
Receiver Temperature			360 K
System Noise Temperature	35.87	dB-K	3866.6 K at Receiver Input
Effective G/T	25.63	dB/K	
Received Carrier Level	-92.92	dBW	At Receiver Input
Boltzmann's Constant	-228.60	dBW/Hz-K	
Received C/No	99.80	dB-Hz	
Misc Hardware Losses	1.00	dB	
ISI Degradation	0.77	dB	
Modem Loss	2.00	dB	
Data Rate	84.77	dB-Hz	300 Mb/s
Available Eb/No	11.26	dB	
Required Eb/No	10.50	dB	BER = 10^{-6}, uncoded
Coding Gain	0.00	dB	
Eb/No Margin	0.76	dB	

Table 1.1.1-2. GEO-GEO Crosslink without Sun Effect

Modulation: QPSK
Coding: None

Carrier Frequency = 55.5 GHz

Parameter	Value	Units	Remarks
Transmitting S/C Power	10.00	dBW	10.0 watts
Transmit Line Loss	1.00	dB	
Feed Loss	0.60	dB	
Transmitting Antenna Gain	63.30	dBi	3.2-m dish
EIRP	71.70	dBW	
Free Space Loss	225.72	dB	83,043 km
Pointing Loss	0.10	dB	0.01 degree
Polarization Loss	0.20	dB	
Tracking Loss	0.10	dB	0.01 degree
Net Path Loss	226.12	dB	
Receiving S/C Antenna Gain	63.30	dBi	3.2-m dish; Temp. = 10 K
Feed Loss	0.60	dB	Temp.= 10 K
Receive Line Loss	1.20	dB	Temp.= 290 K
Receiver Temperature			360 K
System Noise Temperature	26.41	dB-K	437.6 K at Receiver Input
Effective G/T	35.09	dB/K	
Received Carrier Level	-92.92	dBW	At Receiver Input
Boltzmann's Constant	-228.60	dBW/Hz-K	
Received C/No	109.27	dB-Hz	
Misc Hardware Losses	1.00	dB	
ISI Degradation	0.92	dB	
Modem Loss	2.00	dB	
Data Rate	93.01	dB-Hz	2000 Mb/s
Available Eb/No	12.34	dB	
Required Eb/No	10.50	dB	BER = 10^{-6}, uncoded
Coding Gain	0.00	dB	
Eb/No Margin	1.84	dB	

Table 1.1.1-3. LEO-GEO Crosslink with Sun Effect

Modulation: QPSK
Coding: Rate 5/6 FEC

Carrier Frequency = 60.0 GHz

Parameter	Value	Units	Remarks
Transmitting S/C Power	8.75	dBW	7.5 watts
Transmit Line Loss	1.20	dB	
Feed Loss	0.60	dB	
Transmitting Antenna Gain	56.90	dBi	1.4-m dish
EIRP	63.85	dBW	
Free Space Loss	220.41	dB	41,660 km
Pointing Loss	0.07	dB	0.02 degree
Polarization Loss	0.20	dB	
Tracking Loss	0.03	dB	0.02 degree
Net Path Loss	220.71	dB	
Receiving S/C Antenna Gain	53.00	dBi	0.9-m dish; Temp. =4400 K
Feed Loss	0.60	dB	Temp.= 10 K
Receive Line Loss	1.40	dB	Temp.= 290 K
Receiver Temperature			360 K
System Noise Temperature	35.07	dB-K	3217.1 K at Receiver Input
Effective G/T	15.93	dB/K	
Received Carrier Level	-105.86	dBW	At Receiver Input
Boltzmann's Constant	-228.60	dBW/Hz-K	
Received C/No	87.67	dB-Hz	
Misc Hardware Losses	1.00	dB	
ISI Degradation	0.79	dB	
Modem Loss	2.00	dB	
Data Rate	76.99	dB-Hz	50 Mb/s
Available Eb/No	6.89	dB	
Required Eb/No	10.50	dB	BER = 10^{-6}, uncoded
Coding Gain	5.40	dB	
Eb/No Margin	1.79	dB	

Table 1.1.1-4. LEO-GEO Crosslink with Earth Effect

Modulation: QPSK
Coding: QPSK

Carrier Frequency =   60.0 GHz

Parameter	Value	Units	Remarks
Transmitting S/C Power	8.75	dBW	7.5 watts
Transmit Line Loss	1.20	dB	
Feed Loss	0.60	dB	
Transmitting Antenna Gain	56.90	dBi	1.4-m dish
EIRP	63.85	dBW	
Free Space Loss	220.41	dB	41,660 km
Pointing Loss	0.07	dB	0.02 degree
Polarization Loss	0.20	dB	
Tracking Loss	0.03	dB	0.02 degree
Net Path Loss	220.71	dB	
Receiving S/C Antenna Gain	53.00	dBi	0.9-m dish; Temp. = 250 K
Feed Loss	0.60	dB	Temp.= 10 K
Receive Line Loss	1.40	dB	Temp.= 290 K
Receiver Temperature			360 K
System Noise Temperature	27.77	dB-K	598.6 K at Receiver Input
Effective G/T	23.23	dB/K	
Received Carrier Level	-105.86	dBW	At Receiver Input
Boltzmann's Constant	-228.60	dBW/Hz-K	
Received C/No	94.97	dB-Hz	
Misc Harward Losses	1.00	dB	
ISI Degradation	1.03	dB	
Modem Loss	2.00	dB	
Data Rate	84.77	dB-Hz	300 Mb/s
Available Eb/No	6.17	dB	
Required Eb/No	10.50	dB	BER = 10^{-6}, uncoded
Coding Gain	5.40	dB	
Eb/No Margin	1.07	dB	

Table 1.1.1-5. GEO-LEO Crosslink with Earth Effect

Modulation: BPSK
Coding: None

Carrier Frequency =   57.8 GHz

Parameter	Value	Units	Remarks
Transmitting S/C Power	-2.22	dBW	0.6 watts
Transmit Line Loss	1.20	dB	
Feed Loss	0.60	dB	
Transmitting Antenna Gain	52.70	dBi	0.9-m dish
EIRP	48.68	dBW	
Free Space Loss	220.08	dB	41,660 km
Pointing Loss	0.03	dB	0.02 degree
Polarization Loss	0.20	dB	
Tracking Loss	0.07	dB	0.02 degree
Net Path Loss	220.38	dB	
Receiving S/C Antenna Gain	56.50	dBi	1.4-m dish; Temp. = 250 K
Feed Loss	0.60	dB	Temp.= 10 K
Receive Line Loss	1.40	dB	Temp.= 290 K
Receiver Temperature			360 K
System Noise Temperature	27.77	dB-K	598.6 K at Receiver Input
Effective G/T	26.73	dB/K	
Received Carrier Level	-117.20	dBW	At Receiver Input
Boltzmann's Constant	-228.60	dBW/Hz-K	
Received C/No	83.63	dB-Hz	
Misc Hardware Losses	1.00	dB	
ISI Degradation	0.00	dB	
Modem Loss	2.00	dB	
Data Rate	60.00	dB-Hz	1 Mb/s
Available Eb/No	20.63	dB	
Required Eb/No	10.50	dB	BER = 10^{-6}, uncoded
Coding Gain	0.00	dB	
Eb/No Margin	10.13	dB	

Table 1.1.1-6. GEO-LEO Crosslink with Sun Effect

Modulation: BPSK
Coding: None

Carrier Frequency =   57.8 GHz

Parameter	Value	Units	Remarks
Transmitting S/C Power	-2.22	dBW	0.6 watts
Transmit Line Loss	1.20	dB	
Feed Loss	0.60	dB	
Transmitting Antenna Gain	52.70	dBi	0.9-m dish
EIRP	48.68	dBW	
Free Space Loss	220.08	dB	41,660 km
Pointing Loss	0.03	dB	0.02 degree
Polarization Loss	0.20	dB	
Tracking Loss	0.07	dB	0.02 degree
Net Path Loss	220.38	dB	
Receiving S/C Antenna Gain	56.50	dBi	1.4-m dish; Temp. =5000 K
Feed Loss	0.60	dB	Temp.= 10 K
Receive Line Loss	1.40	dB	Temp.= 290 K
Receiver Temperature			360 K
System Noise Temperature	35.56	dB-K	3595.6 K at Receiver Input
Effective G/T	18.94	dB/K	
Received Carrier Level	-117.20	dBW	At Receiver Input
Boltzmann's Constant	-228.60	dBW/Hz-K	
Received C/No	75.84	dB-Hz	
Misc Hardware Losses	1.00	dB	
ISI Degradation	0.00	dB	
Modem Loss	2.00	dB	
Data Rate	60.00	dB-Hz	1 Mb/s
Available Eb/No	12.84	dB	
Required Eb/Nc	10.50	dB	BER = 10^{-6}, uncoded
Coding Gain	0.00	dB	
Eb/No Margin	2.34	dB	

ANTENNA SYSTEM SCHEMATIC
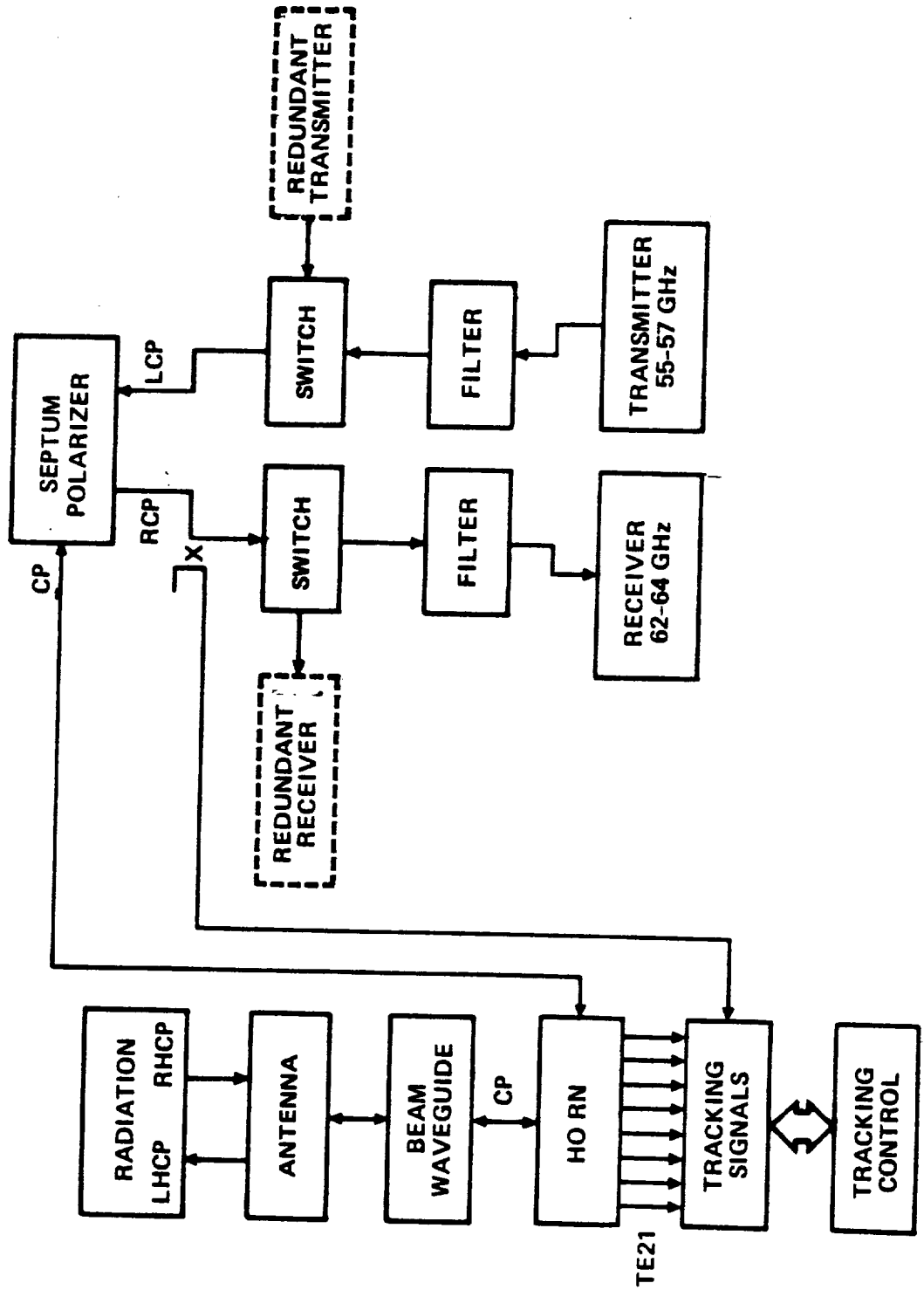
FIGURE 1.1.1-3

FEED AND NETWORK LOSS ASSESSMENT (1989)

(IN DB)

ITEM	GEO/GEO		GEO/LEO (GEO)		GEO/LEO (LEO)	
	XMIT	RCVR	XMIT	RCVR	XMIT	RCVR
SWITCH	0.1	0.1	0.1	0.1	0.1	0.1
OUTPUT FILTER	0.3		0.5		0.5	
INPUT FILTER		0.3		0.5		0.5
COUPLER		0.2		0.2		0.2
SEPTUM POLARIZER	0.2	0.2	0.2	0.2	0.2	0.2
HORN COUPLER	0.1	0.1	0.1	0.1	0.1	0.1
WAVEGUIDE (0.25 M)	0.3	0.3	0.3	0.3	0.3	0.3
NETWORK TOTAL	1.0	1.2	1.2	1.4	1.2	1.4
BEAM WAVEGUIDE	0.6	0.6	0.6	0.6	0.6	0.6

FIGURE 1.1.1-4

MAGNITUDE OF SOLAR INTERFERENCE

SUN AT 60 GHz

Taver = 7200K
= 0.53°

ANTENNA

Size = .9 to 3.2 M
Beamwidth = .3° to 0.11°
Efficiency = 0.62
Antenna Temperature (Sun)
Ta = 4400 to 5200K

NETWORK

Loss Total = 1.6-2.0 dB

RECEIVER

Tr = 360 K

SYSTEM TEMPERATURES

Point at Sun = Tsys 3200 to 3800K
Point at Earth = 600K
Point at Sky = 438K
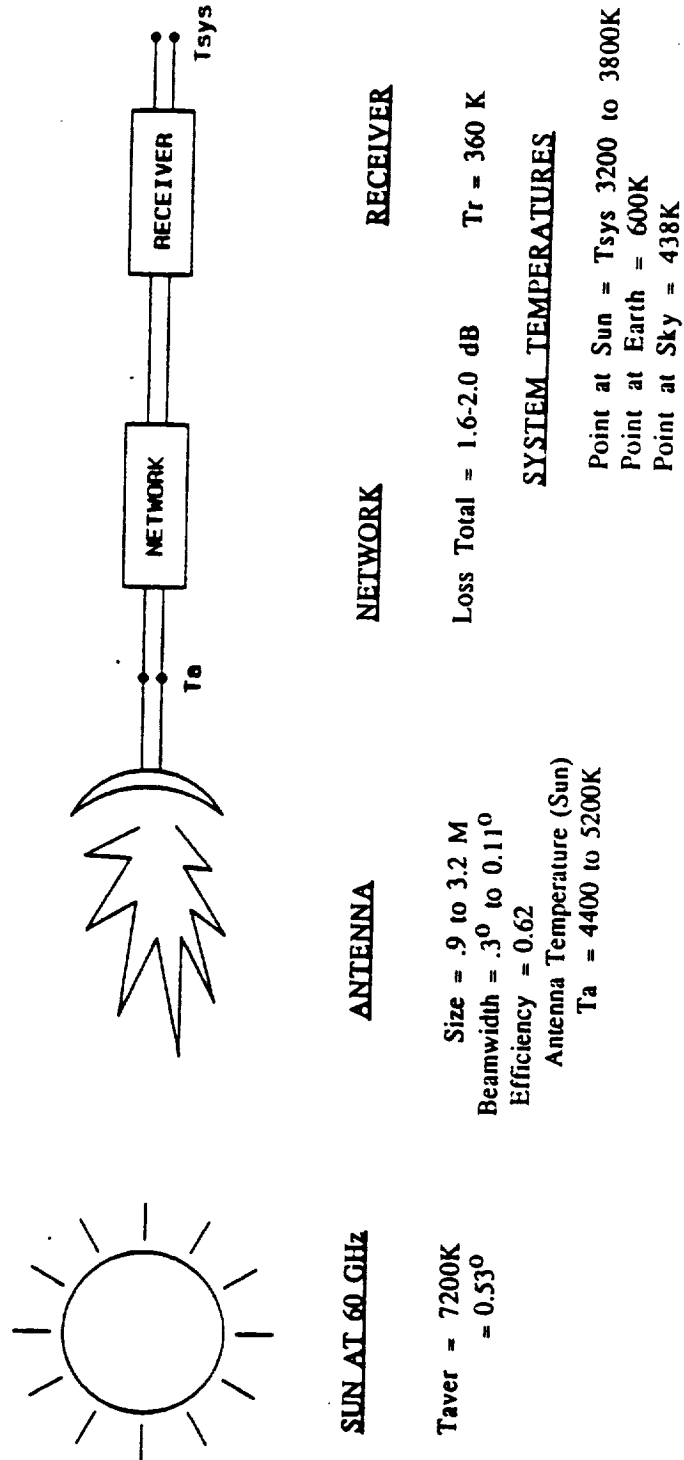
FIGURE 1.1.1-5

1.1.2 Acquisition and Tracking Analysis

1.1.2.1 Acquisition

In order to establish the GEO-LEO intersatellite link, both payload antennas must first be brought to within each other's field of view to allow spatial pull-in and signal acquisition. Post-acquisition tracking must then be initiated to ensure antenna spatial (line-of-sight) lock and signal lock for the case of coherent communication.

To the extent that signal condition is such that it achieves a given probability of detection (subject to a given false alarm rate), the antenna size must be small (or the beamwidth large) enough to allow the entire region of uncertainty in azimuth and elevation to be searched in a way such that the antenna spatial dwell time is equal to or greater than the signal energy detection time but is less than the time it will take for the target satellite to move from one field of view to another. The signal detection time usually includes the doppler sweep time, which is a function of detection bandwidth and doppler and carrier uncertainty. In most cases, however, minimum antenna size is bounded by the data communications requirements. A larger antenna requires a higher scanning (electronic or mechanical) rate, which dictates a narrower detection bandwidth, which increases the need for frequency sweeping. The situation is further complicated by the cases where signal to noise ratios are below the detection threshold and thus require post-detection integration, which effectively increases the signal detection time many fold. However, because of the relatively high C/kT values (more than 83 dB/Hz for the 50 Mb/s return link and almost 95 dB/Hz for the 300 Mb/s return link from LEO to GEO assuming coding is used) the recommended approach is to use an energy detector of wide enough bandwidth to eliminate doppler search.

To minimize burden to the LEO satellites, it is assumed that the GEO-LEO contact is on a scheduled basis (otherwise, at least one of the satellites needs to have an omni or hemispherical antenna). At the scheduled time the GEO TDAS positions its antenna through stored commands to illuminate the User satellite. The probability that the LEO satellite (not necessarily its antenna field of view) misses the GEO antenna footprint can be made very small using reasonable navigation accuracy requirements for the satellites. The LEO antenna will then scan the spatial uncertainty region of the GEO satellite, as illustrated in Figure 1.1.2-1. Since the worst case doppler is about ± 1.8 MHz, as illustrated in Figure 1.1.2-2, doppler sweeping is not necessary.

In either case, a 17 dB signal-to-noise ratio (SNR) in the detector is required to provide a 99.9% probability of detection with a 1% false alarm rate. This signal detection characteristic is shown in Figure 1.1.2-3. For the 50 Mb/s (case 1) data sending capability, a SNR of 7-8 dB would result for the 50 MHz detection. Thus post-detection integrations of approximately 20 times are required.

Upon signal detection, two more detections will be made to form a two-out-of-three majority decision (on detection). This unique verification process reduces the 1% false alarm rate to below 0.01% while reducing the probability of detection only very slightly. Upon detection, the LEO antenna will perform a side lobe check routine to ensure that it is dwelling on the antenna main beam. The LEO then starts to track the GEO using a simplified step track and radiates its own carrier to allow the GEO satellite to initiate

its tracking. The GEO at the same time enables its own carrier track and monopulse autotrack. Note that for high SNR situations the total acquisition time is not particularly dependent on the SNR as the detector response time is a relatively small percentage of the total. On the other hand, with low SNR (below 17 dB for specified performance) the detector must perform post-detection integration; e.g., approximately 20 integrations are required to provide a 10 dB improvement for a 7 dB SNR input, and the detection response time is now increased by 20 times, which may impact the overall acquisition time. However, its impact is still slight if the detector response time is negligible compared to other acquisition time components such as the spatial scan time required for the region of uncertainty. This is illustrated in Figure 1.1.2-4.

After having decided on the acquisition approach of GEO open loop radiating and LEO performing initial acquisition, as illustrated in Figure 1.1.2-5, a computer program has been developed to analyze the acquisition time and other related parameters for three different spatial search methods, as illustrated in Figure 1.1.2-6. The resulting computer analyses are presented in Table 1.1.2-1.

It may be more accurate and easier to simply provide ephemeris predic-tion and pointing vector calculation capability on board the satellites. There is a trade between the host satellite's computer and the ICL package's computer as to which one should perform the ephemeris calculations. This trade will likely be based on the processing load that would be placed on the computers by such a calculation, whether or not the host satellite would already be performing it for its own mission, the data transfer burdens between the host and the ICLS package, and how many users on the host required the information (e.g., on the TDAS satellite there would be six 60 GHz ICL and crosslink packages). This baseline is that the ICLS computer will do the pointing vector calculation, and the ephemeris calculation for the satellite will be supplied by the host.

If ephemerides are to be calculated on board, it should be remembered that two sets of calculations must be done on each satellite. Because the pointing vector is defined by the position of both the host and the target, ephemerides of both the host and target must be calculated at each satellite. The accuracy required of the ephemeris predictions defines what algorithms may be used, and thus the processing load that is placed on the computer for performing the function. Because of the desire to minimize the burden on the LEO host, it may be possible to use a simpler algorithm for any calculations that must be performed on the LEO, which may lead to simpler hardware. The potential for using this approach is improved if smaller antennas are used in the LEO, widening the beamwidth and minimizing the impact of pointing errors.

Whether the ephemeris and/or antenna pointing vectors are calculated on board the satellite or calculated on the ground and uplinked, it may be necessary to continually correct the (nominal) pointing vector with the actual spacecraft attitude. This is dependent on the magnitude of the attitude errors compared to the antenna beamwidths. The host spacecraft attitude will be resident in the host spacecraft's attitude control computer, so it is assumed that the information can be passed to the ICL computer for inclusion in the antenna pointing.

Once the link is set up, the ICLS packages will require very little information in order to maintain operation. Timing requirements will be less critical because the packages will be in communication with each other and will, by definition, be synchronized. Rather than having a command to stop

communication at some prescheduled time, a protocol can be established for dropping the link, virtually eliminating the timing requirement.

Because the baseline GEO-GEO and GEO part of the GEO-LEO antennas will be autotracking, knowledge of ephemeris and attitude is virtually unnecessary. The only real requirement is that the combination of host spacecraft attitude and host and target satellite positions not result in a change of antenna pointing vector that is faster than the antenna gimbals can track. This can be handled by specifying the gimbals to accommodate the expected change pointing vector. The baseline LEO part of GEO-LEO antenna will be steptracked. If a very small program-tracked antenna is used instead, the ICLS package will have a continuous requirement to know spacecraft attitude and ephemerides. This data transfer requirement may be more burdensome than simply steptracking or autotracking the antenna.

FIGURE 1.1.2-1

ACQUISITION BASELINE
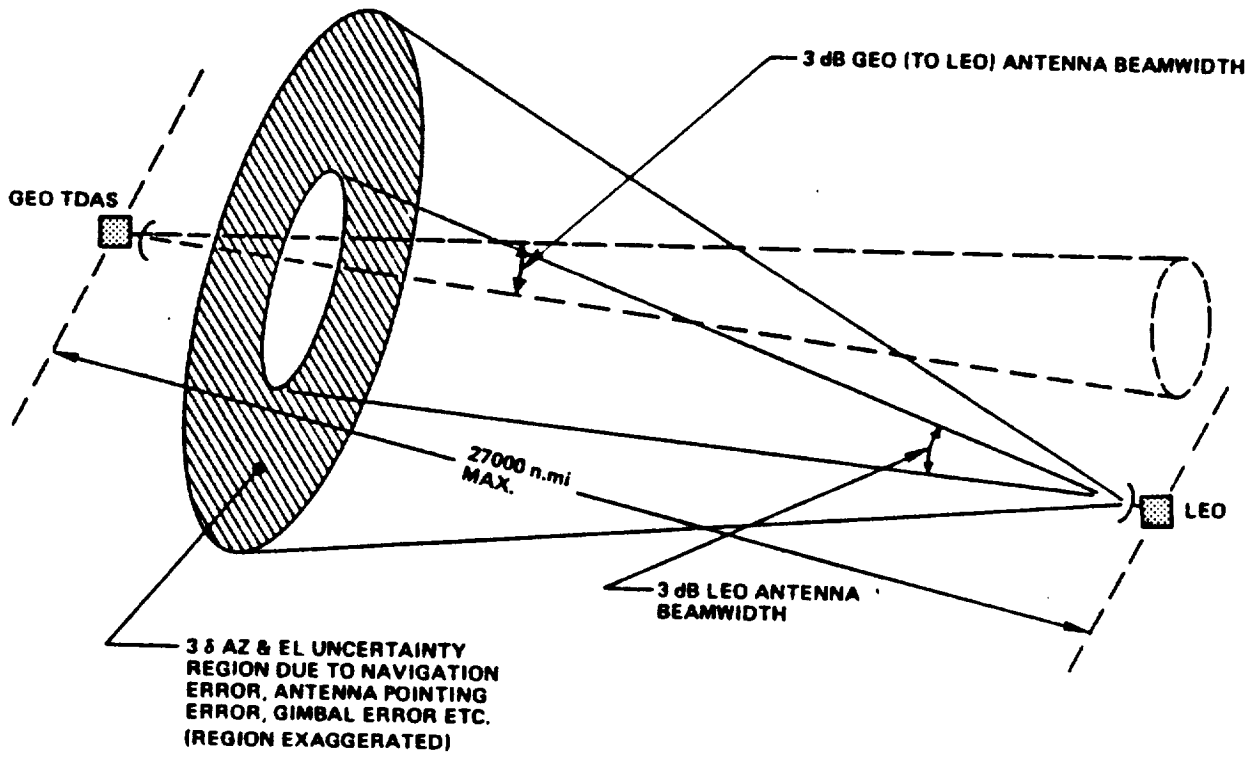
FIGURE 1.1.2-2
WORST CASE DOPPLER ESTIMATES
FOR LEO SATELLITES

WORST CASE DOPPLER ESTIMATES for LEO SATELLITES

Worst case estimate upper bound

Worst case estimate lower bound

DOPPLER FREQUENCY in MHz

LEO SATELLITE ALTITUDE in KM
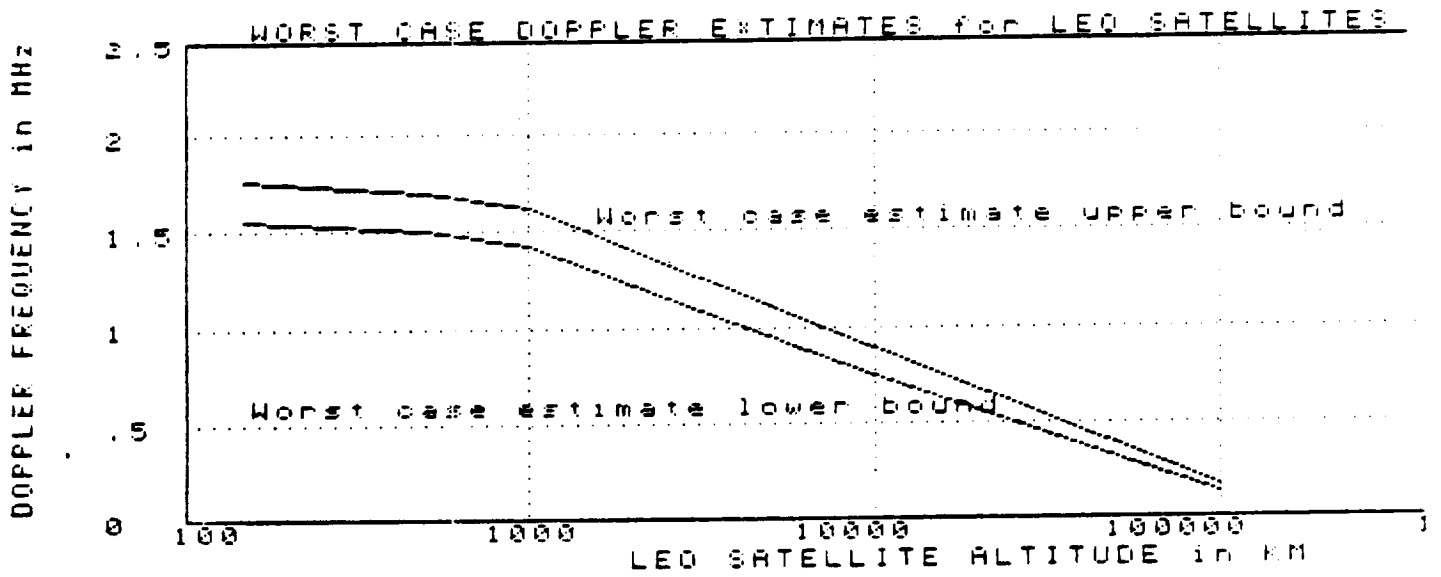
FIGURE 1.1.2-3

Signal Detection Characteristics
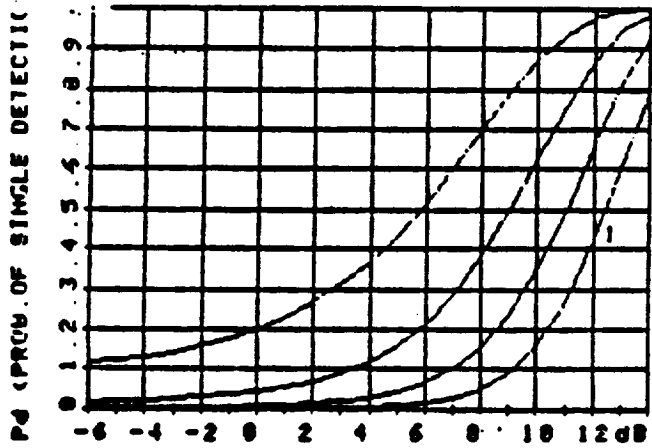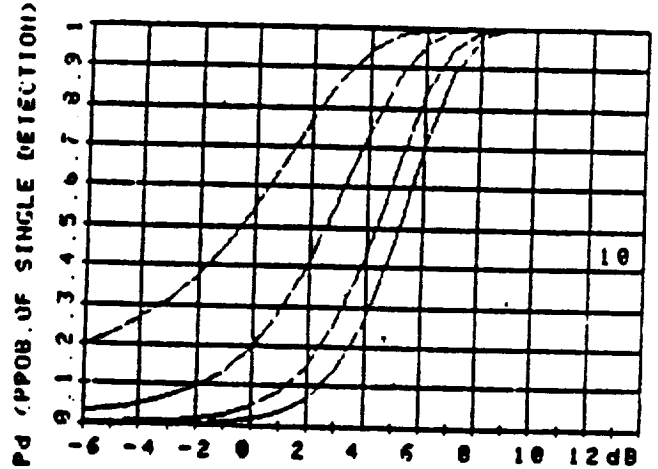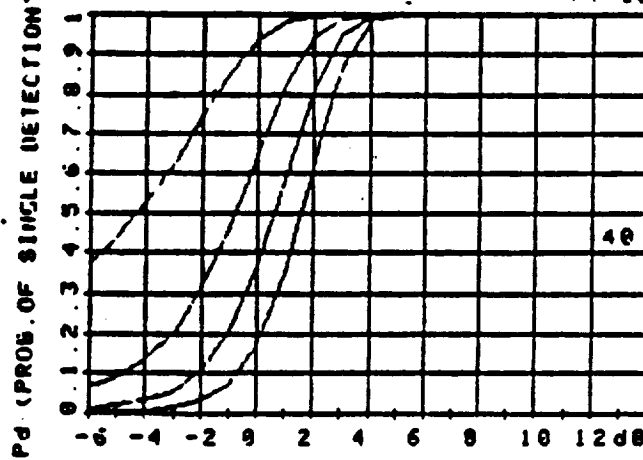
(NUMBER OF INTEGRATIONS)

FIGURE 1.1.2-4. ACQUISITION TIME
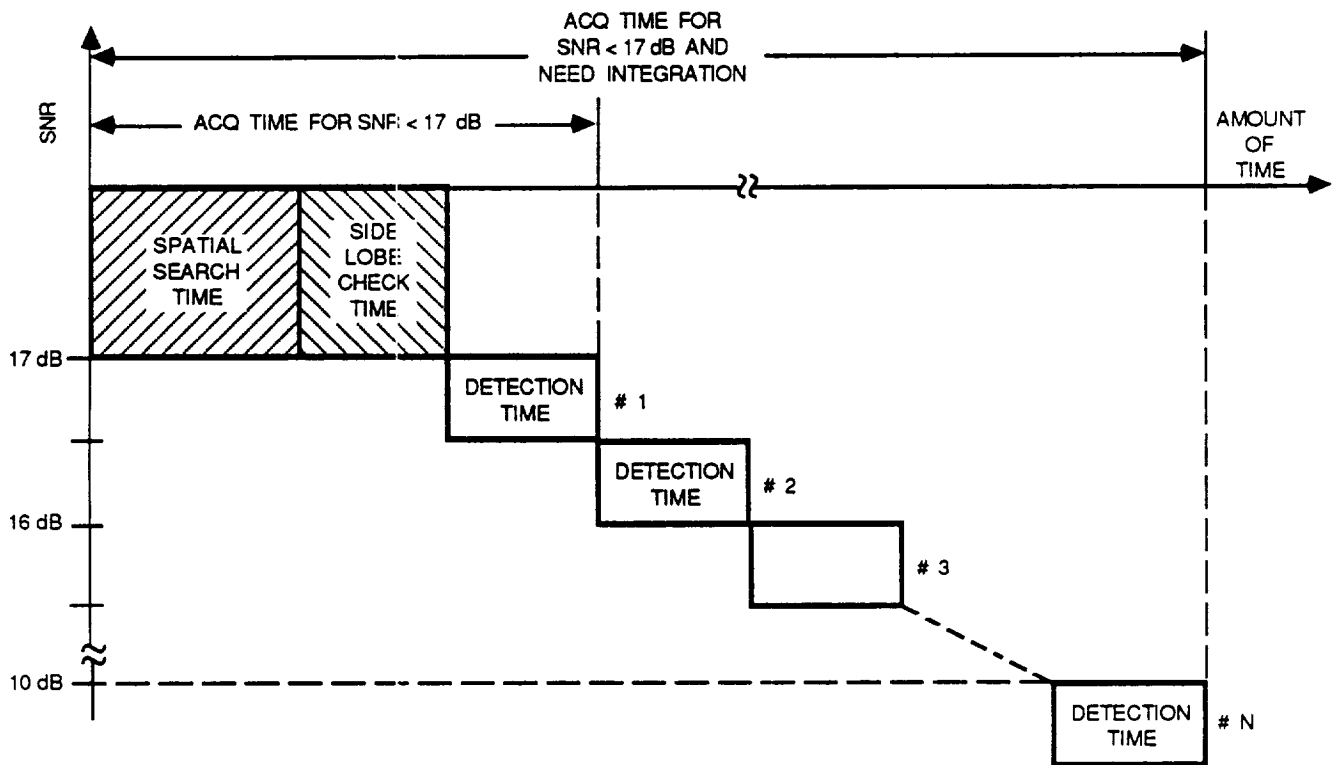
FIGURE 1.1.2-5

SELECTED APPROACH
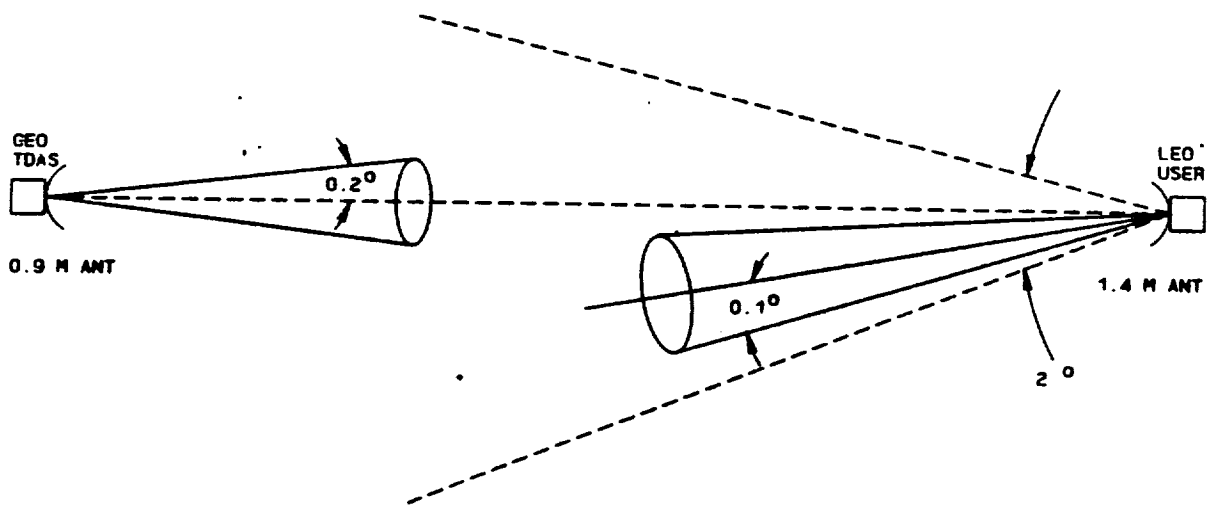
FIGURE 1.1.2-6

SPATIAL ACQUISITION

SPATIAL
SEARCH
APPROACH

(A) TACQ=50
TIME SEC.

(B) TACQ=82 SEC.

(C) TACQ=44 SEC.

SECTOR
SEARCH

VOLUME
SEARCH

OPTIMIZED
SEARCH

- SEARCH ONE DIMENSION(AZ)
  UNTIL TARGET CROSSES
  THE OTHER (EL)

- SEARCH 2-D SPACE DEFINED BY 3σ
  UNCERTAINTIES IN AZIMUTH
  AND ELEVATION

- SEARCH 2-D SPACE DEFINED
  IN (B) EXCEPT THE SEARCH
  START AT MOST LIKELY SPACE
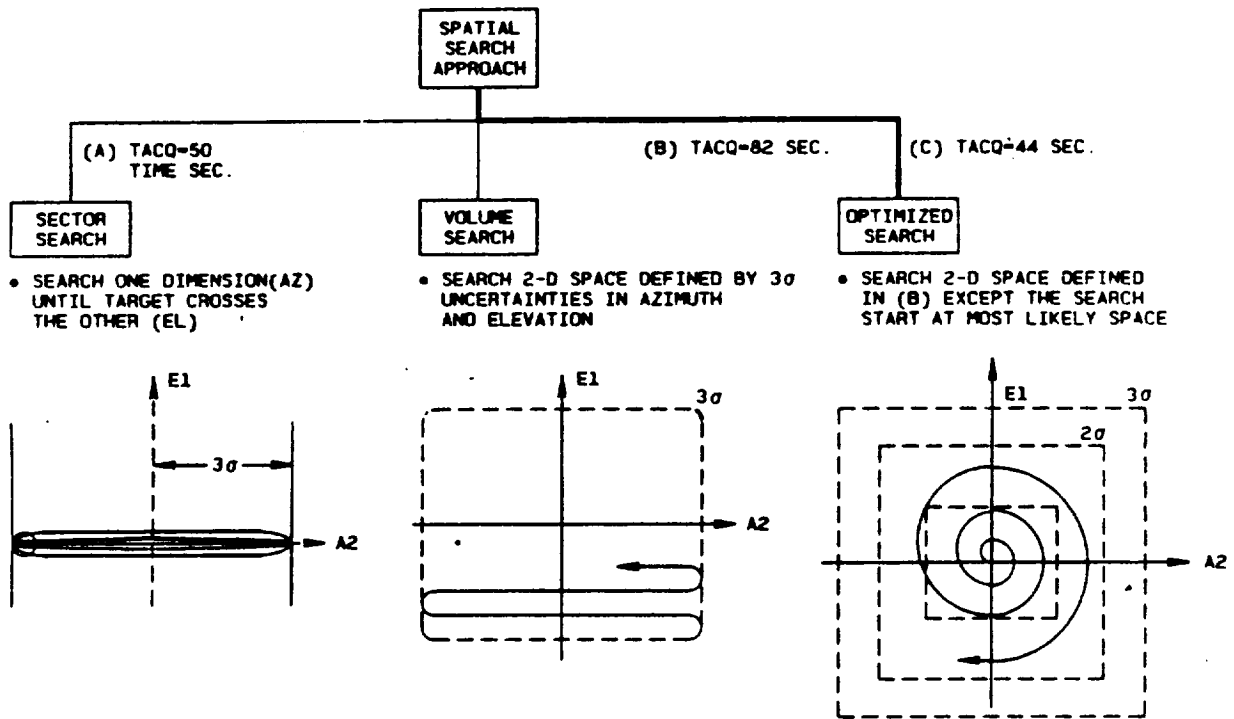
TABLE 1.1.2-1

60 GHz LEO-GEO ACQUISITION ANALYSIS

Target LEO Vehicle Parameters

o 3σ azimuth uncertainty $\pm2.0^{\circ}$

o 3σ elevation uncertainty $+2.0^{\circ}$

o   Nominal acquisition carrier frequency   57.8 GHz

o 3σ frequency uncertainty ±1.8 MHz

o   Nominal signal level referenced
       at receiver input   -117.2 dBW

o   Maximum LEO vehicle velocity $0.045^{\circ}/s$

Acquisition Conditions

o   Input signal level   -117.2   dBW
o   Acquisition antenna gain (1.4m)   56.6   dB
o. System noise temp (3417 K)   35.56   dB-K

o   Effective C/kT   75.84 dB/Hz
o   Effective 3 dB C/kT   72.84 dB/Hz

o   Effective 3 dB beamwidth 0.290°

o   Rated antenna velocity (azimuth and $1.0^{\circ}/s$
                        elevation)
o   Rated antenna acceleration (azimuth and $1.0^{\circ}/s^{-2}$
                        elevation)

SEARCH CASE 1: SECTOR SCAN ANALYSIS

o   Maximum azimuth antenna scan rate $1.0^{\circ}/s$
o   Acquisition bandwidth   4000.0 kHz
o   Prediction SNR   6.8 dB

o   Acquisition time   50.5 s
o   Probability of visibility   99.3266%
o   System availability (assumed)   100.0000%

o   Number of verifications   3
o   Number of integrations   16
o   Probability of detection   99.9702%
o   Probability of false alarm   0.0003%

o   Probability of acquisition   99.297 %

TABLE 1.1.2-1 (Continued)

SEARCH CASE 2: VOLUME SEARCH ANALYSIS

o	Maximum azimuth antenna scan rate	1.0°/s
o	Acquisitin bandwidth	4000.0 kHz
o	Predeteccion SNR	6.8 dB
o	Acquisition time	80.5 s
o	Probability of visibility	99.1923%
o	System availability (assumed)	100.0000%
o	Number of verifications	3
o	Number of integrations	16
o	Probability of detection	99.9702%
o	Probability of false alarm	0.0003%
o	Probability of acquisition	99.1627%

SEARCH CASE 3: OPTIMIZED SEARCH ANALYSIS

o	Maximum azimuth antenna scan rate	1.0%
o	Acquisition bandwidth	4000.0 kHz
o	Predetection SNR	6.8 dB
o	Acquisition time	42.9 s
o	Probability of visibility	99.1923%
o	System availability (assumed)	100.0000%
o	Number of verifications	3
o	Number of integrations	16
o	Probability of detection	99.9702%
o	Probability of false alarm	0.0003%
o	Probability of acquisition	99.1627%

1.1.2.2 Antenna Autotracking

1.1.2.2.1 System Description

The autotracking system for the GEO vehicle antennas is shown in the block diagram of Figure 1.1.2-7. Autotracking will be used on the GEO antennas because of the relatively narrow beamwidths of these antennas, and also because of the number of GEO/LEO antennas which are servicing a multiplicity of users. The continual moving from one user to another results in spacecraft platform perturbations which, at best, would be inconvenient to deal with by onboard ephemeris calculations and open loop program tracking.

The antennas on the GEO vehicle will use the single-channel monopulse technique (also called pseudo-monopulse or pseudo-conscan). In this particular application the reference (Σ) and difference (Δ) signals are derived from a single aperture feed horn. The difference output contains both (Az and El) components of the error signal, superimposed in quadrature. This composite error signal is processed through a 0°, 90°, 180°, 270° sequential phase shifter which is then coupled onto the reference channel to produce a multiplexed and amplitude modulated signal.

This signal is then AM detected and synchronously demodulated and demultiplexed in the tracking receiver (Figure 1.1.2-8) to generate dc error signals which are then compensated to generate axis drive rate commands. The narrowband filtering compresses the wideband PSK uplink signals (300Mb/s BPSK LEO/GEO and 2 Gb/s) to the point where they are operating at maximum signal spectral density which increases tracking system sensitivity by about 3 dB over full bandwidth tracking.

A special feature of this system is a technique for compensating for the space craft platform perturbations due to periodic high rate slewing of GEO/LEO antennas from one user to another. In this scheme the axis rates of slewing of the antennas are measured and converted into platform through mass-property transformations. These are then transformed into equivalent axis rates for the antennas which are currently autotracking. These are then applied as additive rate corrections to the tracking antenna drives.

An analysis of the tracking performance of this system follows, including optimization of servo parameters.

1.1.2.2.2 Tracking Error

Tracking Error is the angle between the antenna RF axis and the apparent line of sight to the target, when the antenna is operating in the automatic tracking mode. Thus for autotrack mode operation it is indicative of the tracking system effects on signal level losses. The significant sources of tracking error in single channel monopulse autotrack system are receiver noise and dynamic lag. These are evaluated in the following paragraphs. The generalized servo loop model used in this analysis is shown in Figure 1.1.2-9 which identifies the principal disturbances contributing to tracking error.
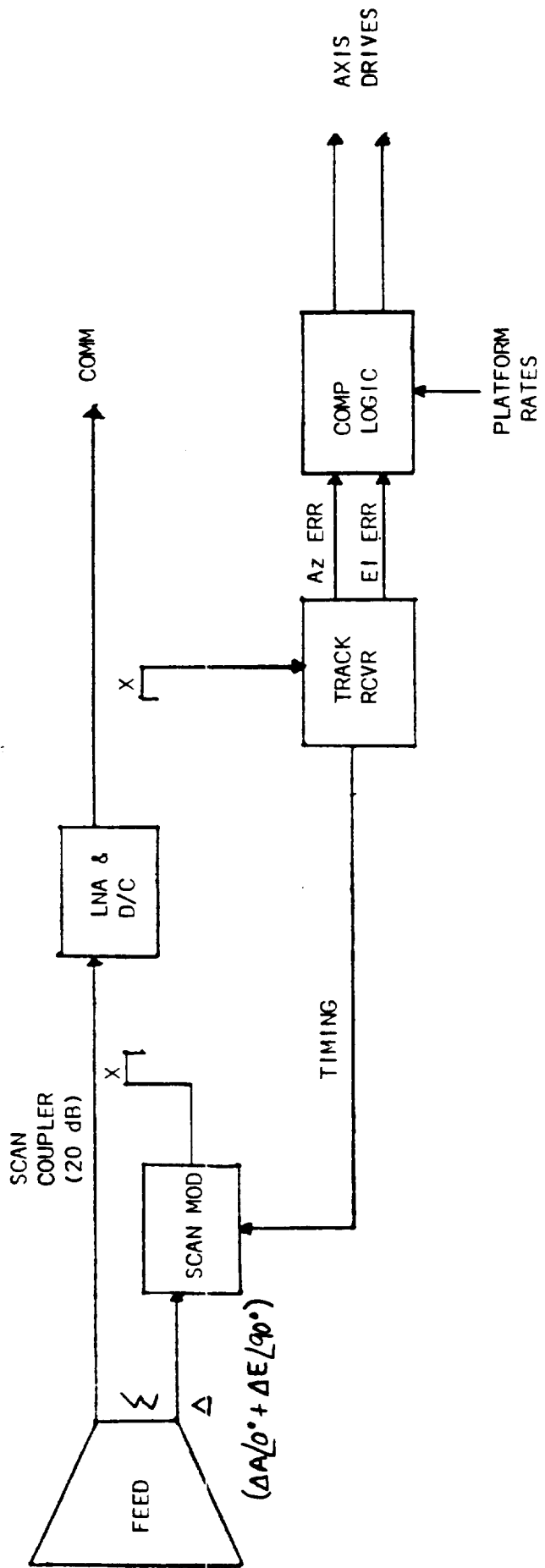
FIGURE 1.1.2-7   AUTOTRACKING SYSTEM

1-35
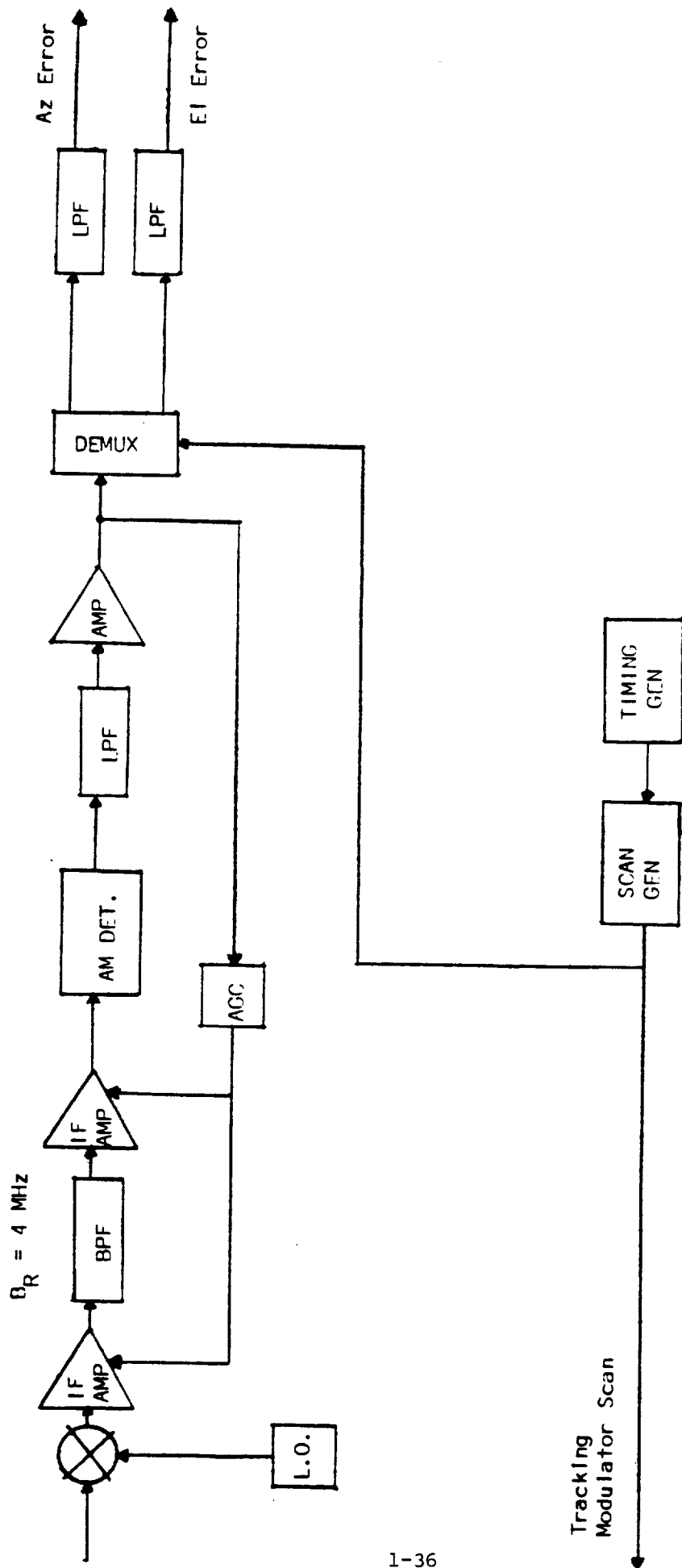
FIGURE 1.1.2-8   TRACKING RECEIVER/DEMODULATOR

FEED & TRACK RCVR
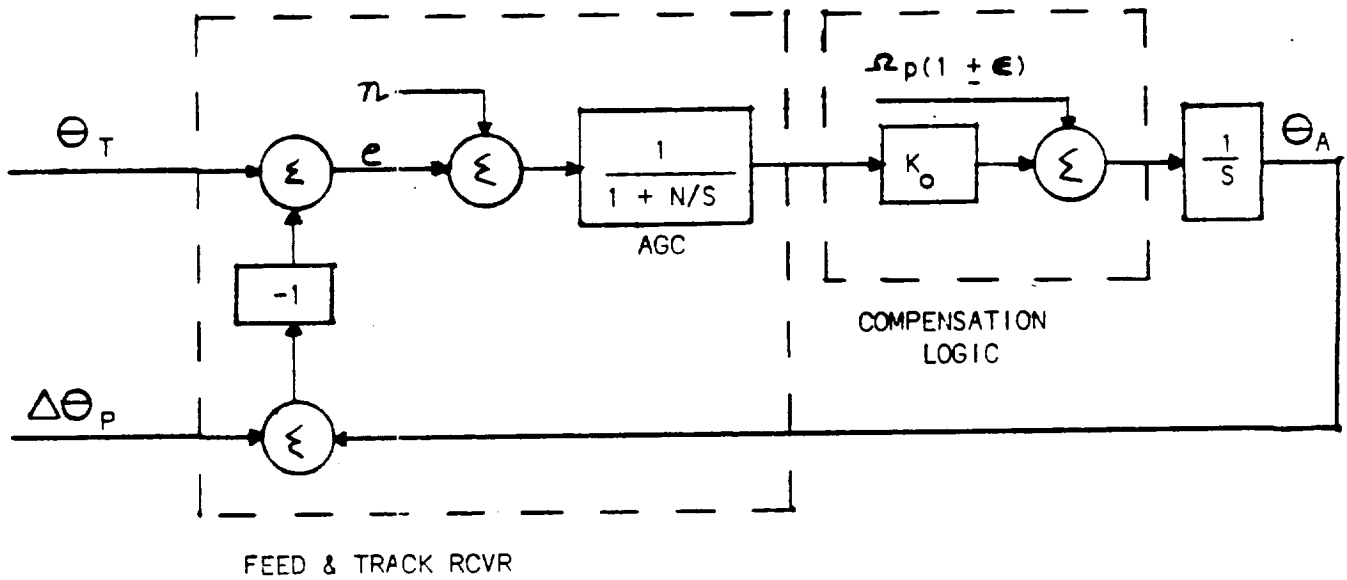
PARAMETERS

K_O = Noise-free open loop gain - (o/s)/s

N/S = Receiver noise/signal ratio

ϵ = Platform rate prediction accurace $\cong$ 10%

VARIABLES

θ_T = Target line-of-sight motion relative to stabilized platform

θ_A = Antenna motion relative to platform

$\Delta\theta_P$ = Platform motion due to other antennas slewing

Ω_P = d($\Delta\theta_P$)/dt

n = Receive system noise

e = Axis component of tracking error

FIGURE 1.1.2-9 SINGLE-AXIS TRACKING LOOP MODEL

1.1.2.2.2.2.1 Thermal Noise

Noise in the receiving system (primarily antenna and LNA) results in noise being superimposed on the dc Az and El error signals, which causes a low frequency random "jitter" about the target. The magnitude of this error is a function of system signal and noise parameters, the secondary pattern error gradient and single channel monopulse system modulation parameters, and the noise bandwidth of the antenna autotrack servo loop.

The crosslink signals which are being tracked by both the GEO/LEO and GEO/GEO antennas are PSK modulated at rates much greater than the tracking receive bandwidth. In such a case the magnitude of vector sum beam radial error can be characterized by the following:

σ_N = rms two-axis random error due to thermal noise

$\quad = (1/K_M) \ (B_S/B_R)^{1/2}$

B_S = 2-sided tracking servo loop noise bandwidth (Hz)

$\quad = (K_o/2)/(1 + N/S)$

B_R = Receiver predetection bandwidth

$\quad = 4 \ \text{MHz}$

K_M = normalized system modulation sensitivity

$\quad = K_\Delta \ / (F - 1)^{1/2}$

F = difference to sum coupling factor

$\quad = 100 \ (20 \ \text{dB})$

K_Δ = normalized antenna error gradient at tracking coupler

$\quad = 0.6/\Theta_{HP}$

Θ_{HP} = half-power beamwidth

K_o = noise-free open position loop gain

N/S = noise/signal ratio in tracking receiver predetection bandwidth

The selected coupling factor (20 dB) is typical for systems of this sort. The estimate of normalized error gradient is based on experience with other tracking systems using the same feed type.

These parameters are summarized in Table 1.1.2-2. Peak (3-sigma) thermal noise errors are plotted in Figure 1.1.2-10 as a function of servo loop gain for the GEO/LEO tracking antenna.

Table 1.1.2-2

Thermal Noise Error Parameters

		GEO/LEO	GEO/GEO
Θ_{HP}	= Antenna Beamwidth	0.4 deg	0.12 deg
K_{Δ}	= Antenna Error Gradient	1.5 deg-1	5.0 deg-1
B_R	= Receiver Bandwidth	4 MHz*	
C/kT	= System Signal/Noise Density	88.1 dBHz	107.9 dBHz (normal) 99.1 dBHz (eclipse)
N/S	= Receiver Noise/Signal Ratio = $B_R/(C/KT)$	0.006	0.0001 (normal) 0.0005 (eclipse)

* Selected to cover worst case doppler shift and long-term local oscillator drift.

1.1.2.2.2.2 Dynamic Lag

The autotracking position loop will be a Type I loop, which has dynamic lag errors proportional to the apparent target velocity as viewed from the vertical platform. The total apparent rate has two components:

o the line-of-sight (LOS) rate relative to a stable platform

o platform motion perturbations due to slewing of non-tracking GEO/LEO antennas for routine switches from one user to another.

Both of these factors are significant for GEO/LEO tracking; the second factor is dominant for GEO/GEO tracking.

861315
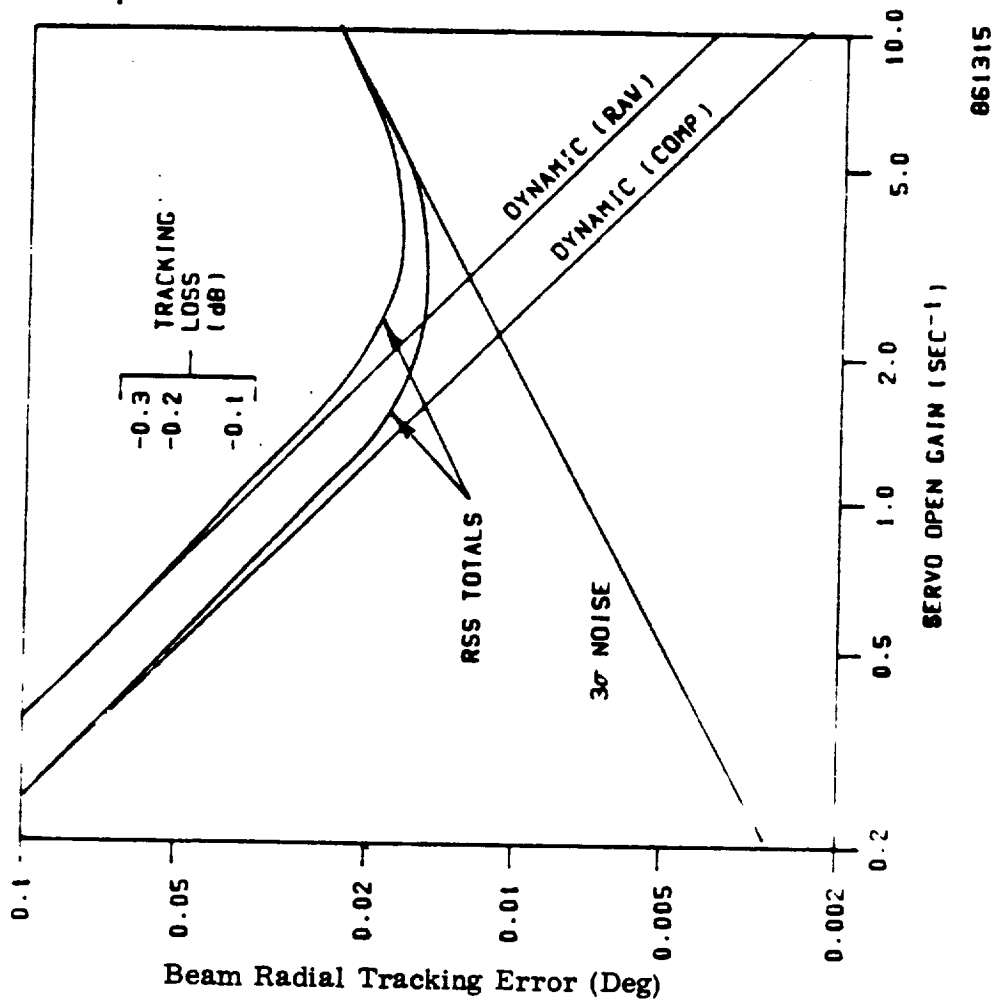
AUTOTRACKING ACCURACY - GEO/LEO

Figure 1. 1. 2-10

The effect of platform motion perturbations can theoretically be corrected in a Type 1 loop by adding known platform rates to the scaled drive error signals (this procedure is also known as rate feed-forward in systems where there is a prior knowledge of rates). The magnitudes of platform perturbation rates can be calculated by proportioning (in a two-dimensional manner) the other antenna slew rates by appropriate inertia ratios. These reaction momentum effects are expected to be estimated to within ±10%. The current estimates of the platform perturbation rates are given in Table 1.1.2-3 along with the basis LOS rates, which are based on the worst case of tracking 5000 km altitude satellite in a polar orbit.

The total two-axis dynamic lag error (beam radial error) for this loop configuration is given by:

$$e_D = \Omega/K_v$$

K_v = loop velocity error constant

$$= K_o/(1 - N/S)$$

Ω = total apparent target angular velocity

$$= \Omega_T + \Omega_P$$

Ω_T = LOS target angular rate relative to stabilized platform

Ω_P = platform perturbation rate (error in compensation corrections can be used if rate compensation is performed)

Estimates of these rates are summarized in Table 1.1.2-3 below. The estimates of disturbance rates are based on the assumption of two GEO/LEO antennas slewing at maximum of $5°/s$, and latest estimates of antenna inertias acting on a 2000 pound class spacecraft.

Table 1.1.2-3

Tracking Rates (Worst Case)

	GEO/LEO	GEO/GEO
o Unperturbed LOS	$0.015°/s$	0
o Perturbations Uncompensated	$0.01°/s$	$0.01°/s$
Compensated	$0.001°/s$	$0.001°/s$
o Total Uncompensated	$0.025°/s$	$0.01°/s$
Compensated	$0.016°/s$	$0.001°/s$

Dynamic tracking errors are plotted in Figure 1.1.2-10 as a function of position loop gain.

1-41

1.1.2.2.2.3 Combined Total Errors

Because dynamic lag and thermal noise errors are not spatially correlated, the peak total error is evaluated as the root-sum-square (RSS) of the maximum dynamic lag and the 3 sigma noise error:

$$e_{TOT} = (e_D^2 + (3\sigma_N)^2)^{1/2}$$

This error is also plotted in Figure 1.1.2-10 as a function of servo loop gain. Also shown are several levels of tracking loss given by

$$L_{dB} = 12(e/\Theta_{HP})^2$$

Since the dynamic lag errors decrease with loop gain and the noise errors increase with loop gain there is an optimum gain which will yield minimum total error for any given set of conditions. The practical "optimization" for the GEO/LEO tracking system is discussed below. For a discussion of the GEO/GEO tracking system see Section 1.2.2.2.

1.1.2.2.2.4 GEO/LEO Tracking

From Figure 1.1.2-10 it can be seen that the optimum value of loop gain is about 2-3/s depending on whether platform rate compensation is used. In this case there is not a great deal of difference between the theoretical minimum total errors. In both cases it is important to note that the predicted error levels at the optimum loop gain are relatively low with respect to beamwidths (less than 0.1 dB predicted tracking loss). However, there are other factors to be considered.

There are two general reasons why it is desirable to select a loop gain lower that the theoretical optimum:

1) The optimum is posited on worst case relative target rates which occur infrequently. On the other hand the thermal noise errors, which are always present, decrease with servo loop gain/bandwidth.

2) The attainable loop gain is limited by antenna structural natural frequencies, in particular the fixed-based locked-rotor frequency for low inertia-ratio antennas. A very conservative theoretically and experimentally derived rule-of-thumb is that Ko, the open loop gain (which is also the nominal loop 3 dB bandwidth (in rad/s) can't be made much greater than the structural locked rotor frequency (in Hz) and still have a stable loop. Reducing the loop gain requirements reduces requirements on structural stiffness design.

The GEO/LEO antennas can achieve tenth beamwidth tracking (0.1 dB tracking loss) with a loop gain of the order of 1/sec or less, which implies a required locked-rotor frequency of 1 Hz which is probably not difficult to attain with a 0.9 m diameter antenna. The requirement could be reduced by about 40% by 10% accuracy body rate compensation.

1.1.3 Baseline Ranging System

The baseline two-way ranging system consists of a PN code generated in the GEO and transmitted to the USAT; then recovered and re-transmitted to the GEO by the LEO satellite. The block diagrams of the baseline system are presented; the equipment aboard the LEO is shown in Figure 1.1.3-1, that aboard the GEO is shown in Figure 1.1.4-6.

The ranging is complicated by the various data rates expected. The GEO-LEO data rate is set at 1 Mbps. With a PN code rate of 3 Mbps the code can be easily modulo 2 added to the forward data stream and transmitted to the LEO on the data channel. The USAT data rates, however, have been specified to be between 1 Kbps and 300 Mbps. The recommendation is to design for some judiciously-chosen subset of rates (see Table 1-1) between 100 Kbps and 300 Mbps.

This wide disparity in data rates implies that the method of returning the PN code to the GEO will not be the same for all of the possible users. It appears that for the range code to be returned to the GEO via the LEO-GEO data stream, at last two techniques will have to be implemented: 1) For data rates much higher than the PN code, the code can be muxed into the data stream. This will require a preamble for accurate re-construction of the range code. 2) For data rates lower than the chipping rate, the code can be modulo 2 added to the data.

At this time we recommend not using return data rates at or near the chipping rate of 3 Mbps although alternate techniques, if substituted, could include these rates as well.

1.1.3.1 Ranging Accuracy

Potential navigation performance has been evaluated by identifying and budgeting timing uncertainty sources. There are essentially three types of sources that affect the ranging accuracy:

a. Hardware induced uncertainty

b. Processing induced uncertainty

c. Link induced uncertainty

Hardware Induced Error

Circuit components contributing to group delay are bandpass filters, transmission line, amplifiers, mixers, etc. Group delay in a filter is proportional to bandwidth. However, the wide bandpass filters in this system have very little group delay. In fact the 400 MHz bandpass filters will exhibit group delay of less than 1 nanosecond at band edge. The bandwidth of a flight quality filter of this type will change 0.01% over a 50°C temperature range. The group delay variance of the filter is thus negligible. Transmission lines generally have low temperature coefficient expansion, especially waveguides. However, if the transmission line is very long, the group delay uncertainty will be significant. A typical semirigid copper-jacketed cable has a phase-vs.-temperature coefficient of approximately -50 ppm/$^{\circ}$C, or 2.7 ns for 50°C change. Wideband mixers and amplifiers do not contribute a significant amount of group delay uncertainty.
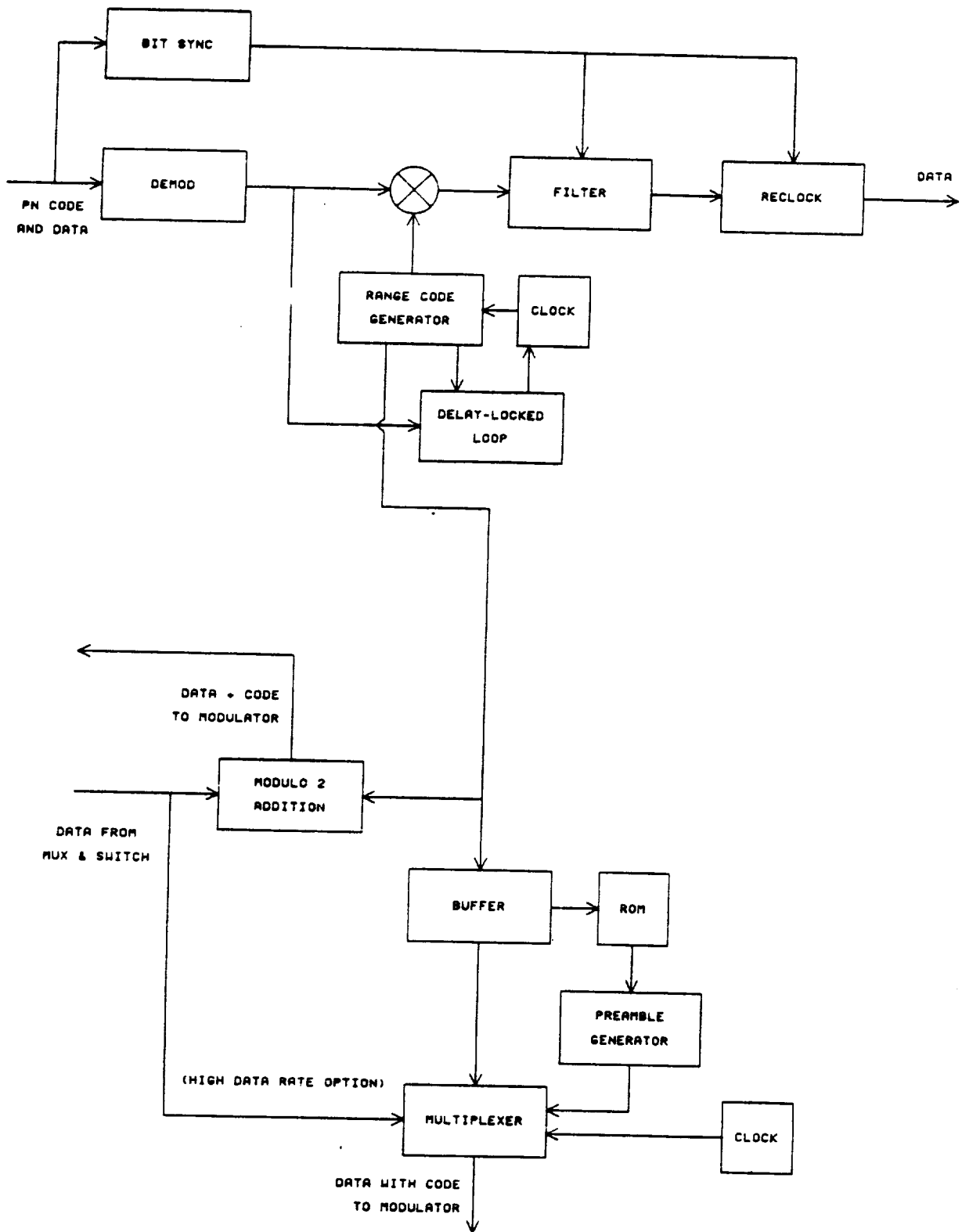
LEO RANGING SUBSYSTEM

Figure 1.1.3-1

Processing Induced Error

Timing error due to less than "real-time" data processing is a matter meriting consideration. Initial analysis indicates that by using buffer memory readout, data processing can be treated as essentially real-time.

Timing error introduced by code tracking has been assessed in the study. Our experience in space-delivered DLL technology implies that a 5% tracking error performance is easily obtainable. Assuming that a 3 Mb/s ranging code is used, this code error would be about 16.67 ns.

Link Induced Error

Link induced timing error includes the error due to uncertainties which are functions of such items as receiver noise, oscillator stability, quantization, and time measurement.

Since a ground based link is not involved, no timing error is introduced by atmospheric propagation and tropospheric error. Link induced error can be made very small by providing a strong SNR.

Accuracy specifications should be broken down into bias and noise components. Hardware induced errors are really bias errors and should not be lumped with the code tracking loop error to yield the total rms ranging error. Since the ranging scheme assumes that the return link code is identical in length to the forward link range code and is synchronized to both the forward link clock and epoch, then it is reasonable to assume that half of the ranging error budget be allocated to the LEO and the other half to the GEO. In other words, the range error budget of 5 meters may be treated as two separate one-way errors of 5 meters each. Therefore the allowable rms noise errors in the code tracking loop can be, as stated above, of the order of 5% of a range chip period. As such the range determination can be designed to be within the requirements of the SOW.

There are several schemes to improve ranging performance, if a more definitized analysis shows such a need. The simplest is to increase the range clock rate and/or provide for smoothing of the range code tracking noise. With the inclusion of a data processing capability, ranging accuracy can be further improved through smoothing algorithms and inclusion of Doppler derived range-rate data.

1.1.3.2 Range Rate

The best method of extracting and measuring Doppler must be developed in concert with the ranging concept and the total system design. Consideration must be given to other sources of error and contributing factors in the point design trades. Our analysis has shown no need for Doppler compensation due to the orbital dynamics. The range rate 1.0uracy requirement of ±0.2 cm/sec is very demanding on careful system design and will require a frequency stability of $1x10^{-10}$. Nevertheless this performance has been demonstrated in ATS-6 experiments under conditions of average Doppler measurement. Our analysis has assumed an averaging time of 2.5 seconds.

1.1.4   Block Diagrams

The block diagrams of the GEO-LEO equipment aboard the GEO satellite are presented in Figures 1.1.4-1 through 1.1.4-9.

1.1.5   Navigation Attitude and Timing Requirements

The accuracy of satellite navigation and attitude control are important parameters in designing the link acquisition and tracking approach. As target LEO satellite spatial uncertainty is a major factor in acquisition design, it impacts the selection of antenna, its steering, and even the acquisition signal detection bandwidth. It also has profound impact on acquisition time. The acquisition base line design has been determined for LEO attitude errors as much as $\pm 2.0^{\circ}$. The range rate requirement of ± 0.2 cm/sec translates to a timing and clock stability requirement of 1×10^{-10}.

1.1.6   Telemetry and Command Requirements

The telemetry and command system approach will be modular to allow system capacity to be optimized for either the LEO or GEO mission without major redesign. The system will use a central microprocessor to control telemetry and command functions. This approach has been selected to allow operation with a variety of host spacecraft configurations. Figure 1.1.6-1 shows the telemetry and command system interfaces.

For a spacecraft of the assumed size represented here, 500 commands of the discrete type should be adequate. These would be divided into about 300 discrete pulses, (28 v, 100 ms) and 200 relay closure commands. Serial data load commands can also be accommodated. A total of 50 data load commands should be adequate. Within the central processor, time tagged stored commands for later execution can be loaded as a serial data stream into the central memory in the order of desired execution and the stored time tag compared with onboard generated time. When the two coincide, the stored command is shifted from memory, decoded, and executed.

When the spacecraft is configured with redundant units, selection is made by discrete commands which choose the desired member of the redundancy pair. Where operation of both redundant units simultaneously is undesirable (resulting in damage or mutual interference), the command outputs are interlocked so that the situation is prevented.

Critical commands require a multiple command sequence (enable, arm, fire) before they may be executed. A critical command disable is also provided to reset the sequence if necessary.

INTERSATELLITE LINK
ANTENNA (0.9 M)

EIRP = 48.68 DBW
G/T = 23.23 DB/K (WITH EARTH EFFECT)
G/T = 15.93 DB/K (WITH SUN EFFECT)

BEAM WAVEGUIDE

FEED

0.6 WATT TRANSMITTER SUBSYSTEM

BPSK MODULATOR SUBSYSTEM

BASEBAND SWITCH & MUX

GEO RANGING SUBSYSTEM

LEO-GEO RECEIVER SUBSYSTEM

VARIABLE DATA RATE DEMODULATOR

DEMUX & BASEBAND SWITCH

GIMBAL SUBSYSTEM

GIMBAL DRIVE ELECTRONICS

TRACKING & ACQUISITION RECEIVER

ANTENNA CONTROLLER

ANTENNA CONTROL MICROPROCESSOR

SPACECRAFT BUS

GEO-LEO

INTERSATELLITE LINK COMMUNICATION SYSTEM

GEO EQUIPMENT

Figure 1.1.4-1

60 GHZ BPSK MODULATOR

Figure 1.1.4-2

FROM
60 GHZ BPSK
MODULATOR

0 DBM

FET
PREAMP

20 DBM

CIRCULATOR

1-IMPATT
STAGE

CIRCULATOR

28 DBM

BANDPASS
FILTER
2-POLE

27 DBM

TO
INTERSATELLITE
LINK ANTENNA

GEO-LEO

0.6 WATT TRANSMITTER SUBSYSTEM

Figure 1.1.4-3

RF EQUIPMENT

ISL LEO-GEO RECEIVER SUBSYSTEM

Figure 1.1.4-4
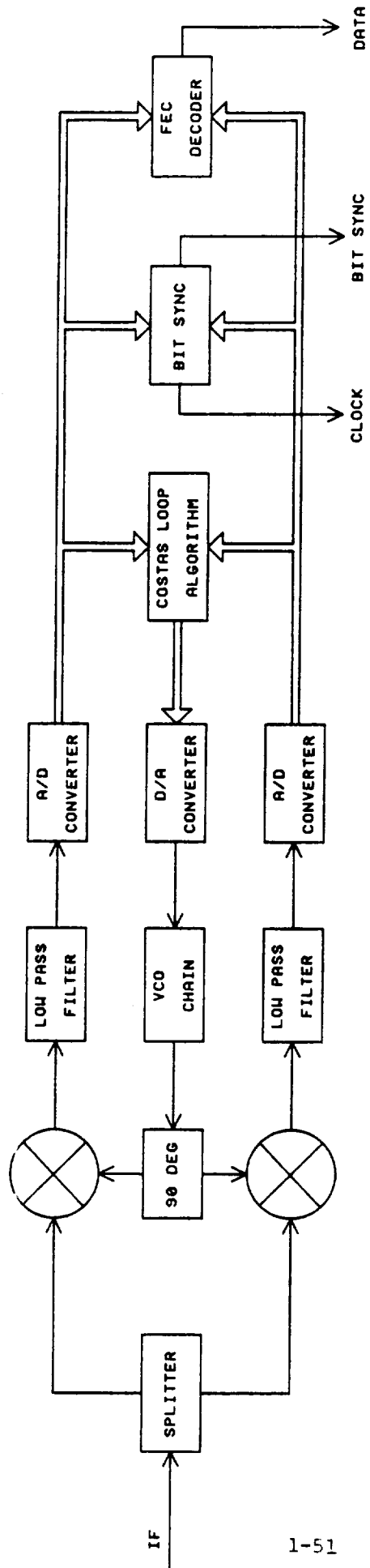
VARIABLE DATA RATE DEMODULATOR

Figure 1.1.4-5
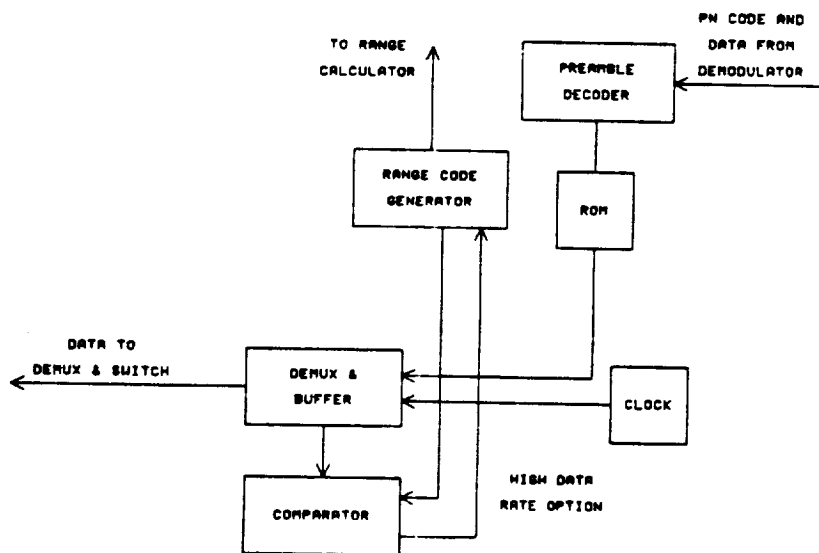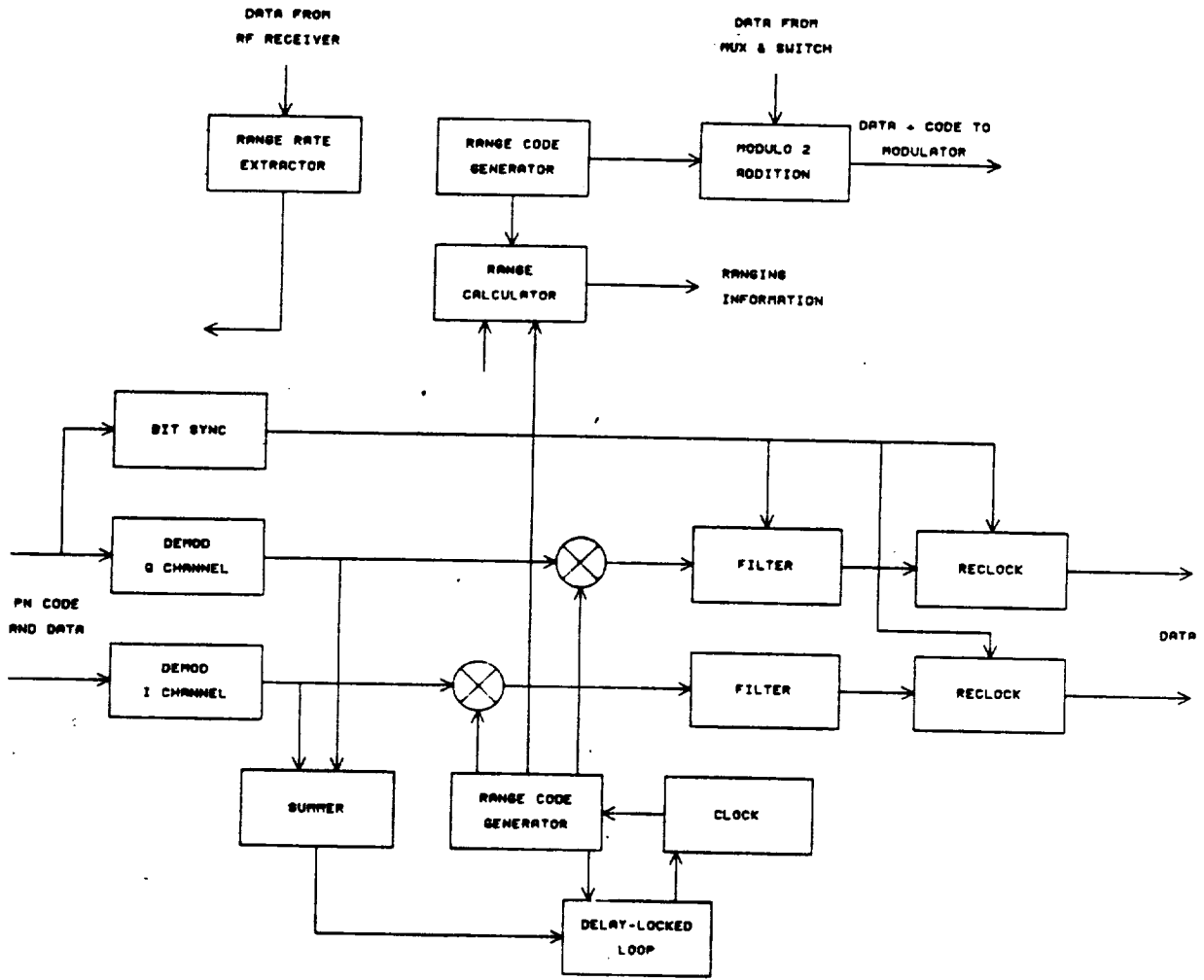
GEO RANGING SUBSYSTEM

Figure 1.1.4-6

FIGURE 1.1.4-7. ACQUISITION AND TRACKING RECEIVER
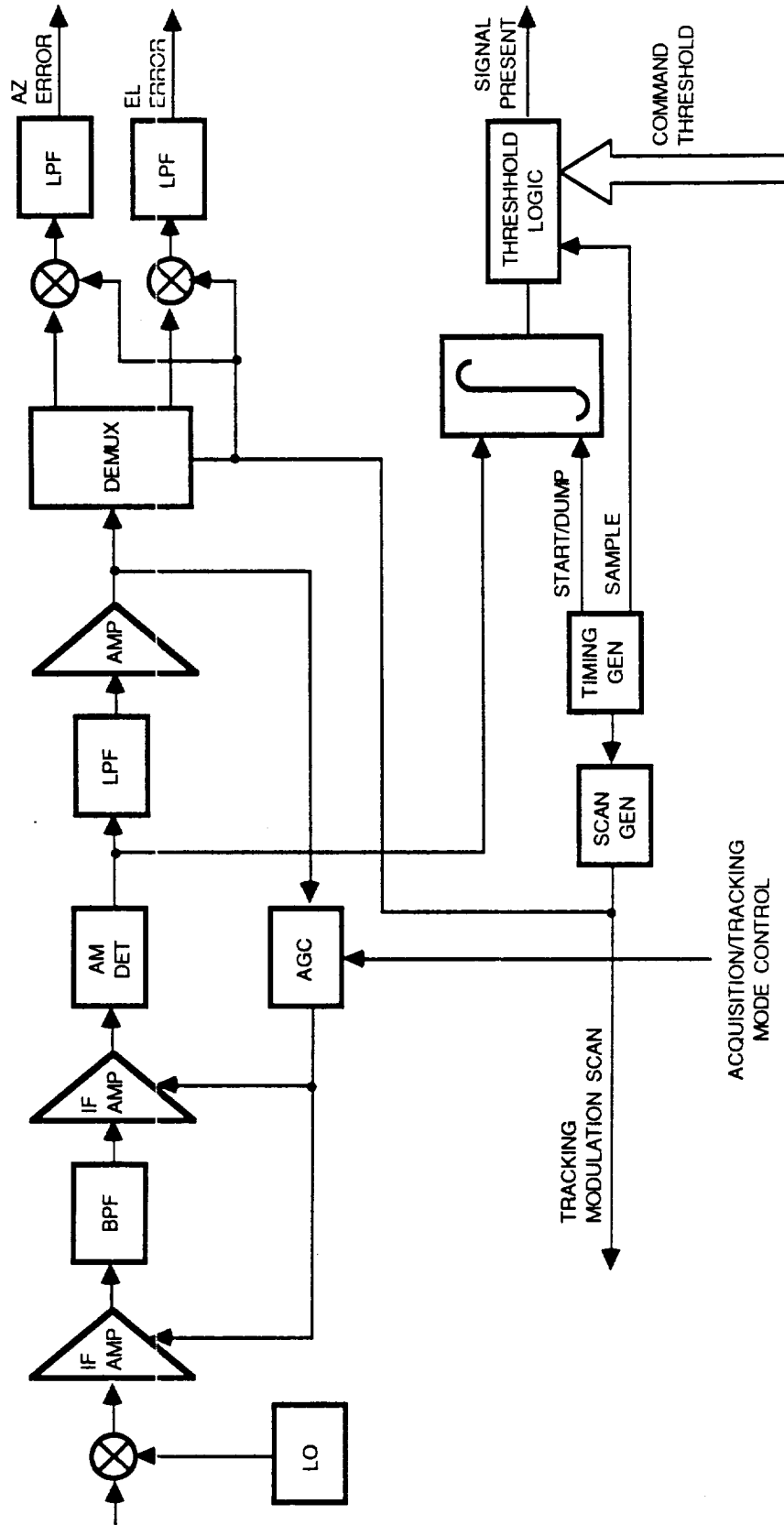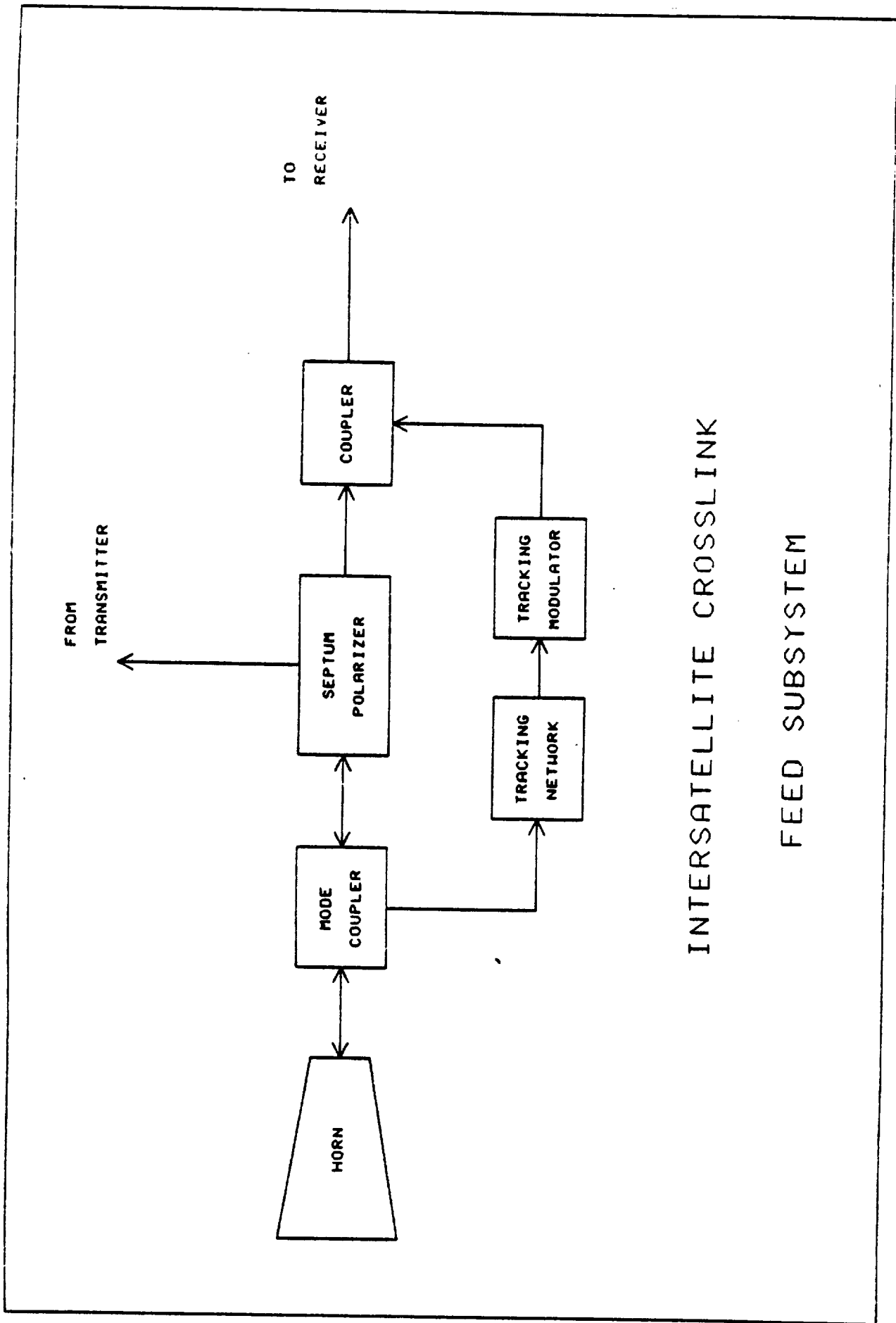
INTERSATELLITE CROSSLINK

FEED SUBSYSTEM

Figure 1.1.4-8

DRIVE
MOTORS

ENCODERS

GIMBAL DRIVE
ELECTRONICS
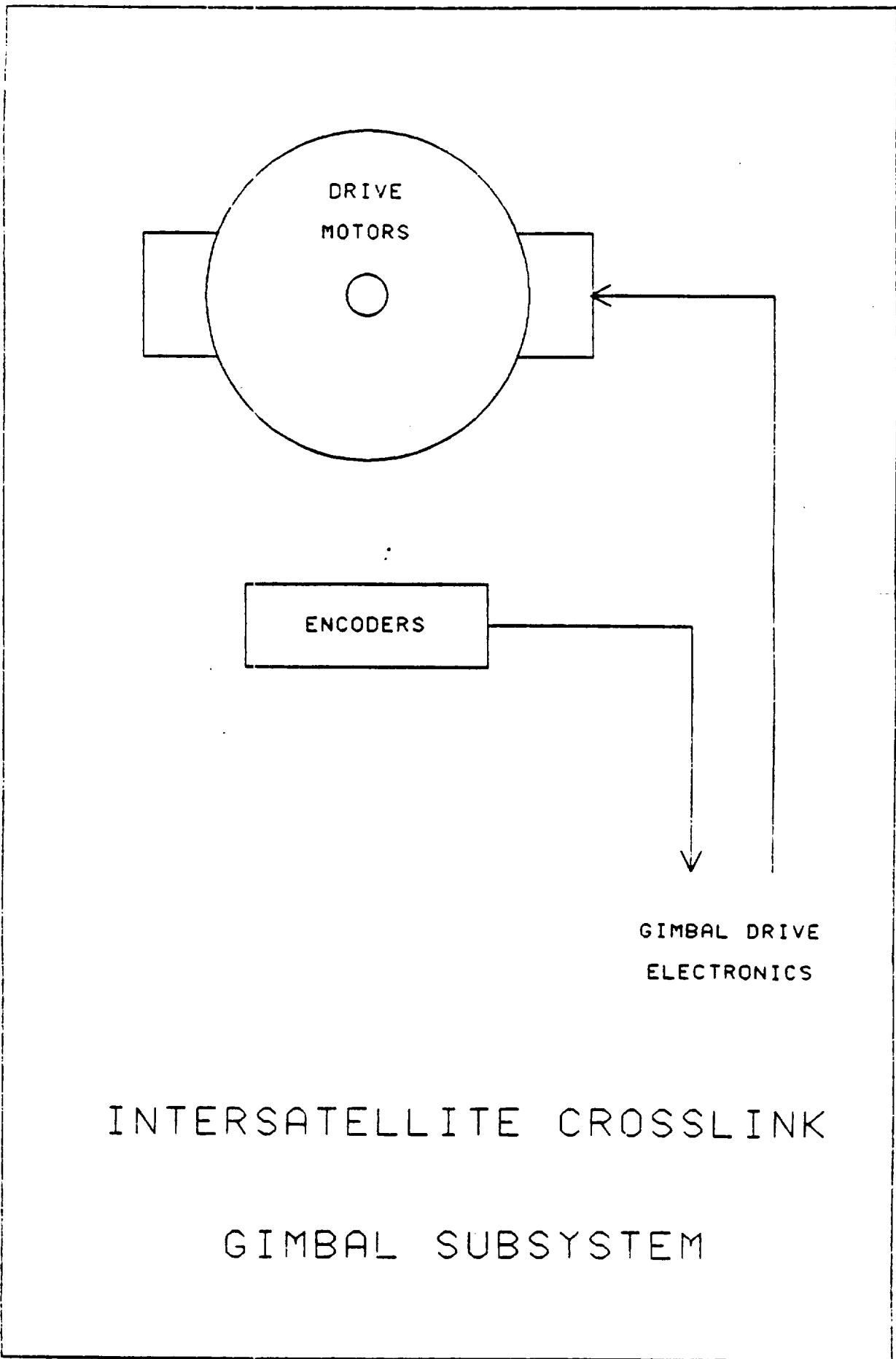
INTERSATELLITE CROSSLINK

GIMBAL SUBSYSTEM

Figure 1.1.4-9

Some form of error detection/correction coding is desirable in the command link. A polynomial

$$X^7 + X^6 + X^2 + 1$$

(from ADS 7.1, "Inner Convolutional and Block Error Control Coding Standard") gives satisfactory protection for discrete commands. The decoded command can be telemetered to the ground for verification prior to execution if necessary.

Three types of command output interfaces will be used. Discrete commands will either be a 28 volt pulse or a relay closure. Data load commands will be serial digital data streams with appropriate clock and enable signals. Levels for these signals will be TTL. Redundancy control and mode changes will be exercised by the ground control station via the command link. The command processor will generate (and telemeter) the spacecraft clock. This will allow time tagged commands to be loaded and autonomously executed.

Various formats and bit rates have been considered. The most desirable appears to be one conforming to ADS Standard 4.5. The formats and bit rates are adequate to support either the LEO or GEO mission. The standard provides for either a discrete/proportional command frame of 48 bits including 7 bit address and a standard Hamming error control code or a memory load message structure. Use of this format has no impact on spacecraft hardware complexity and it allows use of existing ground station equipment without modification.

For ground checkout, it is assumed that the command link would be utilized for test purposes. Access to the system can be obtained by either a low power RF link (radiated or hardlined to the spacecraft) or by means of a baseband interface through the spacecraft umbilical connector. The same umbilical interface can be utilized by the shuttle for access to the spacecraft. It would require a small (approximately 10 inches of 19-1/2 inch rack space) command generator which would generate manually selected commands or interface with one of the on-board computers.

The telemetry system will accept analog signals, bi-level status signals, serial digital data, and will provide conditioning for ISL package temperature measurements. The mainframe will be either 64 or 128 words long. Status and temperature data will be subframe with a maximum length of 32 words. Final frame length decision will be made when more complete system definition exists. A word length of 8 bits provides adequate resolution for housekeeping data.

The system will include the ability to dwell, on command, up to six words. This dwell mode will be provided on a dedicated output port simultaneously with the normal PCM frame. Outputs from the telemetry will be:

o Normal PCM data stream
o Dwell PCM data stream
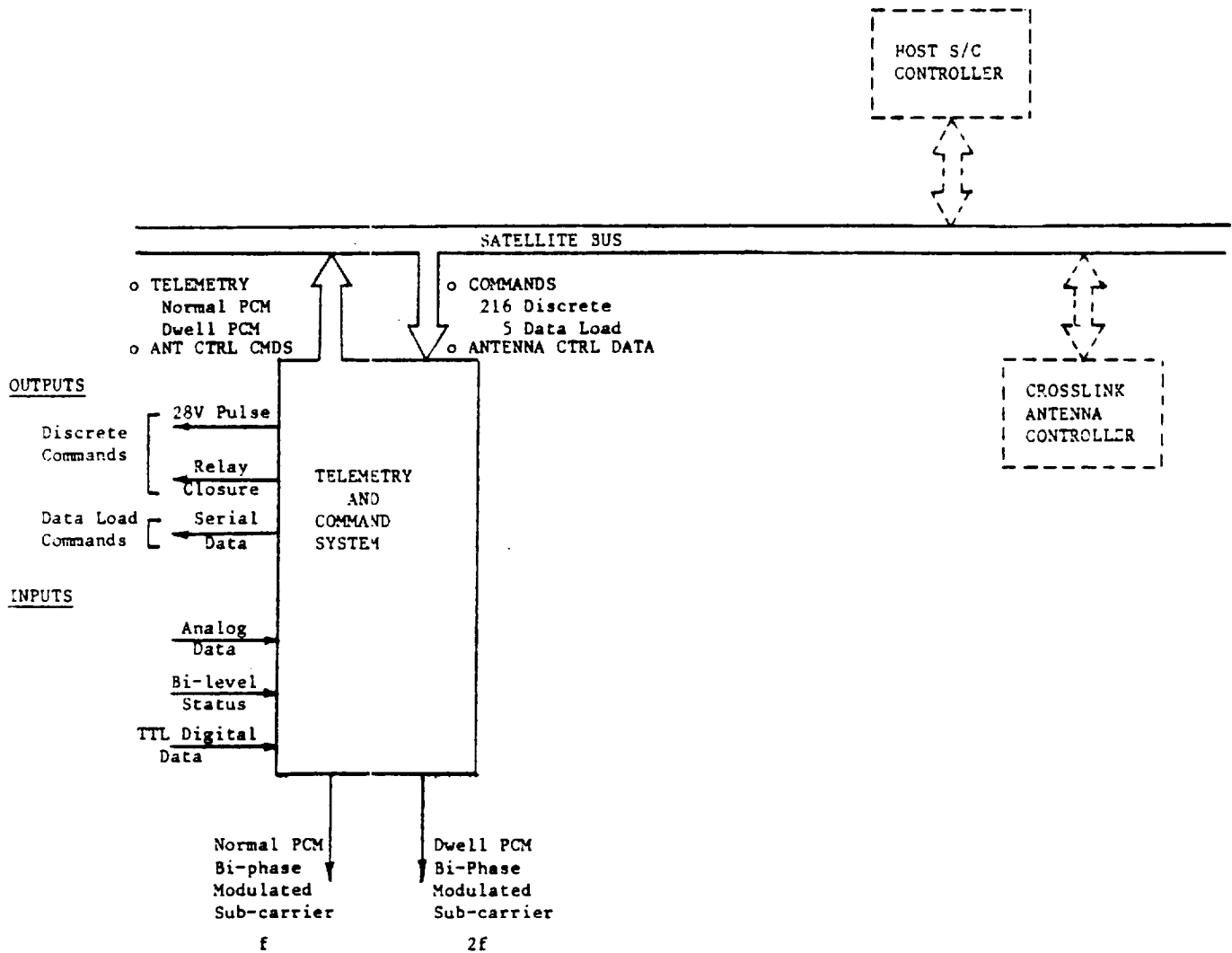
FIGURE 1.1.6-1
TELEMETRY AND COMMAND SYSTEM INTERFACES

The recommended PCM format is NRZ-L to conserve bandwidth on the downlink. A separate baseband output in an NRZ-M format for use by the shuttle can also be provided.

A telemetry unit will accept analog data from the various sources conditioned to a 0 to 5 volt range. Bilevel data will be used for status (on, off, configuration selection) and digital data (TTL level) will be clocked out of source units as a serial data stream to the telemetry.

Because the backside satellite requires multiplexing of TT&C data into the crosslink data, a digital output will be provided. To maintain uniformity of hardware the telemetry data should also be multiplexed into the downlink. For initial sizing purposes the following housekeeping assumptions have been made:

MINOR FRAME DATA	NUMBER OF WORDS
Analog (Minor Frame)	64
Status (Sub Frame)	4x16
Serial Digital	22
Temperature (Sub Frame)	3x32
Analog (Sub Frame)	4x16
Status (Minor Frame)	2
Spare (Minor Frame Analog)	14
Spare (Minor Frame Digital)	9
Overhead	7

This leads to a 128 word minor frame, word length 8 bits, and a major frame consisting of 32 minor frames. A bit rate of 4 Kbps results in a time of 256 ms per minor frame and produces a major frame every 8.192 seconds.

As shown in Figure 1.1.6-2, the output of the telemetry unit is stored in a memory for later readout and transmission on either the crosslink or on the down link in the case of a LEO. The memory will be configured so that one minor frame word is being loaded into memory while the preceding word is being read out for transmission.

Pre-launch checkout (in the Orbiter bay) can cover any of the functions monitored by telemetry. A separate telemetry bit stream will be returned to the orbiter for pre-launch checkout through a hardwired umbilical connection.

Modular design of the telemetry and command system will allow easy reconfiguration of the system for the various mission host spacecraft. Typical telemetry and command lists are shown in Table 1.1.6-1.
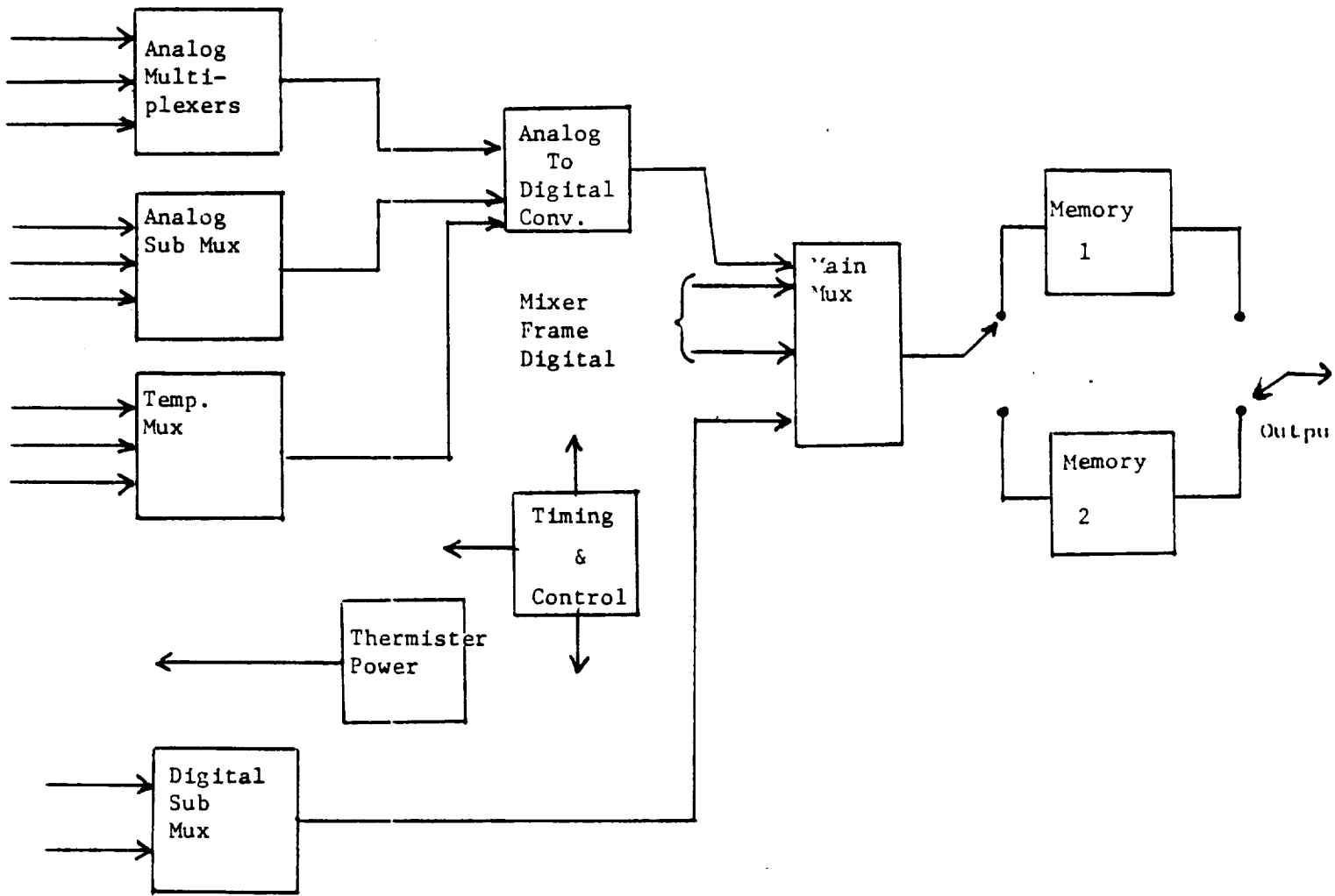
TELEMETRY FUNCTION

Figure 1.1.6-2

Table 1.1.6-1

Typical Telemetry and Command List

Unit: Command

Commands	Telemetry
Command address (selects unit to process data) Critical command enable/disable Data load to controller Stored program time lag	Command verification Execute flag Stored and sequence readout

Unit: Telemetry

Commands	Telemetry
Unit on/off Dwell mode select Dwell word(s) select	Frame sync Subframe counter Dwell word i.d. Spacecraft i.d. Telemetry unit on/off status

Unit: Transmitter

Commands	Telemetry
Unit on/off Mod index select Mod source select	On/off status Mod index selected Mod source selected

Unit: Receiver

Commands	Telemetry
	Phase lock loop lock status Phase lock loop stress Receiver AGC voltage

Unit: System Controller and Gimbal Drive

Commands	Telemetry
Unit on/off Track auto/manual Slew, manual pitch Slew, manual yaw Pitch, slew limit Yaw slew limit Auto scan select Data load	On/off status Mode, auto scan/manual slew Controller data dump Pitch Drive to motor Yaw drive to motor

1.1.7 Operational Concepts

1.1.7.1 Launch Sequence

The TDAS launch sequence is described in Section 1.2.6.1.

1.1.7.2 Acquisition

The original contact with a target satellite for each of the five ISL payloads is necessarily a part of the in-orbit testing of the comm payloads. First all ISL components are enabled and checked for turn-on. When all the operating systems are powered-up and prepared for operation, acquisition and testing can begin.

The ephemeris, data rate, Doppler profile and time of contact of a target satellite (LEO) is sent to the TDAS from the ground (via the GEO-GEO comm system in the case of the GEO #2), as is the ephemeris of the TDAS. The ISL computer calculates the pointing vector given this information and the antenna of the ISL payload under test is slewed to the target's location. A 60 GHz signal (locked to a master .frequency source) is beamed towards the USAT. The transmitted signal is sampled by calibrated couplers and sent to the ground via telemetry so that test personnel can verify proper power levels.

A time-line command containing pointing vector information has also been sent to the LEO so that its ISL comm system attempts acquisition with the TDAS simultaneously. The baseline acquisition strategy (see Section 1.1.2.1) ensures that the GEO antenna (assuming reasonable navigational accuracy) will illuminate the USAT. The USAT then moves its antenna through a series of pre-programmed steps until the GEO signal is locked onto and the tracking is controlled by the tracking receiver. At this time a 60 GHz signal is returned to the GEO; carrier lock is achieved and acquisition is complete.

If acquisition should fail and the USAT is still in the TDAS field-of-view, one of the other TDAS ISL comm systems should attempt acquisition (of course with an updated pointing vector) with that particular target. This may give some indication of the cause of acquisition failure e.g., antenna pointing error due to launch damage, receiver malfunction, etc. Attempted acquisition of more than one USAT (if available) by each of the five ISL payloads is also important in this phase to aid test personnel in determining which of the payloads (TDAS or USAT) is the cause of the failure.

1.1.7.3 On-Orbit Test

All of the five ISL payloads must be checked out for target acquisition. It is considered unlikely that there will be more than one LEO target satellite available for initial test. To reduce the time spent on initial test as much as possible, we recommend test of an ISL payload to begin immediately after acquisition and to continue through the time the USAT is in the field of view for that orbit, if necessary. When one ISL payload is checked out for acquisition and performance, tests on the next payload (acquisition and performance) can begin.

This next phase of the on-orbit test is to ensure that the performance of the link is adequate. These tests are the same as those described in

Section 1.2.6.3. Additionally, the ranging system and the range rate extractor must be tested. All the redundant paths shall be checked out.

Since there will probably be long time gaps between the initial checkout and launch of LEOs transmitting at the other data rates, it may be a very long time before all of the equipment (demodulators, etc) is checked out. This should not preclude utilization of the operational crosslink equipment for traffic during this time.

In the interest of more rapid checkout of the five GEO-LEO payloads aboard the TDAS, it may be economically feasible to utilize the STS as a special test USAT. A customized USAT package containing the diversity of LEO options could be placed aboard the STS. Not only could all options be checked out, but the STS could act as a simulated ground station with trained personnel to interpret test results and direct any trouble-shooting.

1.1.7.4 Normal Operation

Scheduling the crosslink resources will be a ground function. Priorities and anomalies (such as solar or user conjunction) will be resolved prior to commanding the intersatellite link. To reduce the computational load on the ISL controller, ephemeris information in the form of a time- position look-up table will be supplied for the ISL antenna for use during the acquisition phase. Two modes should be provided--a closed-loop self track where the antenna autotracks the user and a time-position mode. This mode is used for special applications where the antenna (as in the acquisition mode) is driven from a look-up table up-loaded from the ground. Gimbal position and error telemetry will be available at all times.

Various receiver states (bandwidth, data rate, etc.) as well as the crosslink interconnections will be under ground control. As in the case of the antenna this information is up-loaded ahead of time and executed on a time-line. This mode of operation circumvents the long delays associated with real-time ground control, allowing maximum utilization of the intersatellite links. A back-up real-time control mode will be provided for back-up and trouble-shooting.

1.1.7.5 Re-Acquisition

Re-acquisition of target USATs will be according to the time-line up-loaded from the ground. The re-acquisition technique is the same as that for original acquisition. Since ephemeris computations are not being done on a real-time basis, some method of terminal pre-positioning should be available to further minimize time spent in slewing to the target location.

1.1.8   The Effects of Earth, Sun and Polarization

1.1.8.1 Earth

The effect of earth basically adds an added noise temperature of 290°K. The GEO-LEO link accomodates this effect without the loss of any required data transmission and receiving capability.

1.1.8.2 Sun

1.1.8.2.1   General Discussion

Solar radiation falling in the main beam or sidelobes of a 60 GHz intersatellite link antenna adds to the system noise temperature. Since the apparent temperature of the sun is 7200 K at 60 GHz, the impact on a system with a 360 K noise temperature receiver is large.

1.1.8.2.2   The Sun At 60 GHz

The 60 GHz solar radiation originates from near the visible surface of the sun. As viewed from the earth, the mean angular size of the optical sun is 32 arcmin (0.533 degrees) and varies ± 0.5 arcmin over the year. Although some limb brightening is observed, to first order the sun at sunspot minimum appears to have uniform brightness. The total 60 GHz solar flux changes by less than 10% from sunspot minimum to maximum, but at solar maximum "hot" spots from a few tens of arcseconds to an arcminute in size may appear above sunspots. These "hot" spots are circularly polarized and may be more than 100 times hotter than the average solar temperature. They will cause increasing interference as antenna beamwidths approach their angular size. However, since the antenna sizes considered for the crosslink system have beamwidths many arcminutes in size, the sun can be considered a one half degree disk of uniform temperature.

Since the intersatellite link antenna beamwidths are smaller than the angular size of the sun, the sun cannot be considered as a point source of noise. Instead of using solar flux density, an apparent temperature is assigned to the disk of the sun. The apparent temperature of the sun is defined as the black body temperature of the visible disk which would result in the observed solar flux density, and is 7200 K at 60 GHz ("Astrophysical Quantities", Allen, p. 192). A 60 GHz antenna in the surface of the sun will have an antenna temperature of 7200 K.

1.1.8.2.3 Estimate of Maximum Antenna Temperature due to Solar Interference

The sun is assumed to be a uniform 7200 K disk of 0.53 degrees diameter. Antenna full power beamwidths range from 0.84 to 0.23 degrees, depending on antenna size and illumination function. The maximum antenna temperature occurs when the antenna is pointed at the center of the sun. An area integration of the antenna power pattern over the disk of the sun gives the percentage of antenna power falling on the sun. The antenna temperature is this percentage multiplied by 7200 K, since the remaining 60 GHz sky is filled with 3 K background radiation.

The calculation was carried out for a uniform aperture antenna with 4% blockage of the area of the antenna. An additional factor of 1.2 dB loss (76% efficiency) was required to account for the additional energy scattered into sidelobes. The resultant antenna temperature for different antenna sizes are tabulated in Table 1.1.8.2-1. As contrast, two other cases are considered; the antenna pointing at cold sky (3 K), and pointing at an 18 degree diameter earth (290 K).

TABLE 1.1.8.2-1

ANTENNA TEMPERATURES BEFORE NETWORK

	0.9	1.0	1.4	1.5	2.0	3.0
Antenna diameter (m)	0.9	1.0	1.4	1.5	2.0	3.0
Full power beamwidth (degrees)	0.84	0.76	0.54	0.50	0.38	0.25
Diameter between 2nd nulls (deg)	1.73	1.73	1.11	1.04	0.78	0.52
Antenna temperature (K)						
Pointed at sun @ 7200 K	4400	4500	5000	5000	5100	5200
Pointed at earth @ 290 K	250	250	250	250	250	250
Pointed at sky @ 3 K	10	10	10	10	10	10

1.1.8.2.4 Size of Solar Interference Region

If 1% (-20 dB) of the antenna energy is received from an area corresponding to the disk of the sun, up to 72 K increase in antenna noise temperature could occur. For a 60 GHz receiver noise temperature of 500 K, for example, this would cause up to 0.6 dB link margin degradation.

Solar interference will stay below this level (with careful antenna design) if the sun stays beyond the first sidelobe ring around the main beam. This criteria gives a circular "solar interference" area around the antenna boresight direction. If the sun comes within this area significant interference can occur. The solar interference area is defined in terms of the position of the center of the sun, and thus its minimum diameter is that of the sun, 0.53 degrees. Table 1.1.8.2-2 gives the solar interference area for different antenna sizes. A tapered aperture illumination (see Monthly Progress Report #6 for March, 1985) is assumed for calculation of the solar interference region.

TABLE 1.1.8.2-2

SIZE OF SOLAR INTERFERENCE REGION

Antenna diameter (m)	0.9	1.0	1.4	1.5	2.0	3.0
Full power beamwidth (degrees)	0.84	0.76	0.54	0.50	0.38	0.25
Diameter between 2nd nulls (deg)	1.73	1.56	1.11	1.04	0.78	0.52
Solar Interference Region						
Diameter (degrees)	2.3	2.1	1.6	1.6	1.3	1.1
Area (% of sky)	.0097	.0083	.0051	.0047	.0033	.0021

1.1.8.2.5 Duration of Solar Effects

Table 1.1.8.2-2 has given data on the size and area of the region in the sky which causes solar interference. If the solar plus satellite motions were random, the "% of sky" indicates a probability of solar interference between 1:10,000 to 1:48,000 for different antenna sizes. This translates to from 11 to 51 minutes link degradation per year. However, the motions of the sun and satellites are precisely known so a better estimate of maximum total "solar interference" time can be given. Two different links are considered in this section: from low earth orbit (LEO) to GEO, and from GEO to LEO. The link from geostationary orbit (GEO) to GEO is considered in Section 1.2.7.

LEO-GEO Links (Using 1.5 m LEO and 1 m GEO antennas)

Figure 1.1.8.2-1 shows the view of the earth and LEO satellite orbits (altitudes from 100 to 3100 mi) as viewed from the GEO satellite. The earth has an apparent radius of 8.75 degrees and the LEO satellites' orbits range in radius up to 9.0 degrees for 100 mi orbit and up to 15.7 degrees for 3100 mi orbits. The path of the sun varies from -23.4 to +23.4 degrees depending on time of year. For solar declinations above and below 16.3 degrees for 3100 mi LEO orbits, and declinations above and below 9.65 degrees for 100 mi LEO orbits, the LEO-GEO link cannot experience solar interference since the sun will never pass close enough to the LEO satellite. As shown in Table 1.1.8.2-3, solar interference cannot occur for 73% of the year for 100 mi LEO orbits, and for 51% of the year for 3100 mi LEO orbits.

As viewed from GEO orbit, the sun will appear to pass from west to east across the region potentially occupied by satellites. Since the solar motion is 4 degrees/hour, there can be potential solar interference for as much as 39 min (100 mi LEO) to 65 min (3100 mi LEO) every day. However, the disk of the earth will block the sun for part of this time. For 100 mi LEO satellites there will only be 6 minutes a day as the LEO satellite comes around the limb of the earth that solar interference is possible. At higher LEO satellite altitudes, depending on orbital inclination, more solar interference time is possible within the 39 to 65 min window each day.

TABLE 1.1.8.2-3

SUMMARY OF SOLAR EFFECT FOR LEO-GEO LINK

| | | LEO ALTITUDE | |
		100 mi	3100 mi
LEO satellite period	(minutes)	90	200
Time LEO satellite eclipsed by earth	(minutes)	49	47
% of time	(%)	55	24
Maximum orbital radius as viewed from GEO	(degrees)	9.0	15.7
Including antenna solar interference	(degrees)	9.6	16.3
Time for solar transit of region	(minutes)	39	65
Maximum increase in receiver noise temperature	(K)	3250	3250
Dates of possible solar interference		Feb24-Apr15	Feb4-May5
number of days	(days)	50	90
other dates of solar interference		Aug28-Oct17	Aug8-Nov6
number of days	(days)	50	90
% of year	(%)	27	49
Maximum continuous duration of noise >70 K	(minutes)	6	varies
(for single LEO satellite)			with orbit

DURATION OF SOLAR INTERFERENCE
GEO Satellite Looking at LEO Satellite
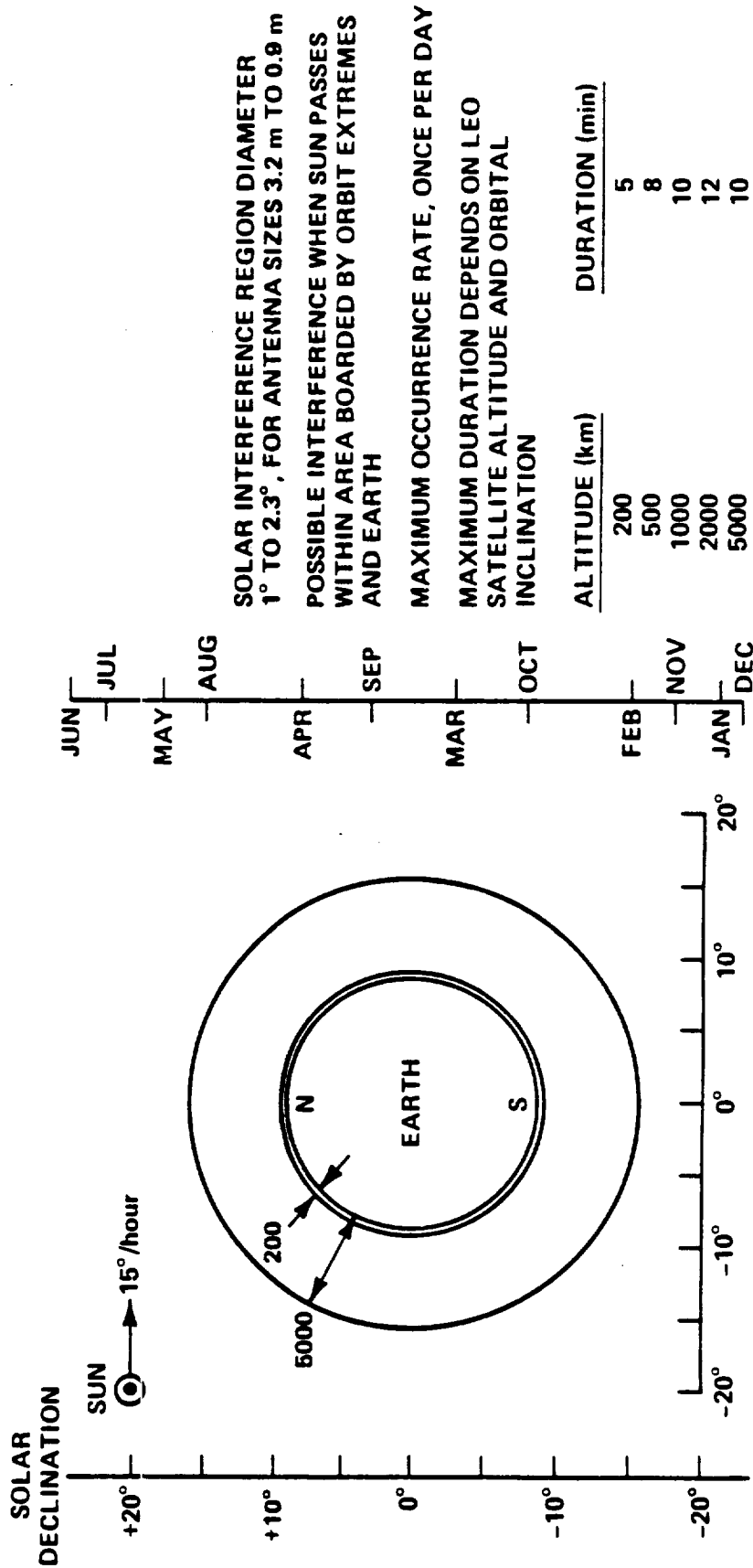
SOLAR INTERFERENCE REGION DIAMETER 1° TO 2.3°, FOR ANTENNA SIZES 3.2 m TO 0.9 m

POSSIBLE INTERFERENCE WHEN SUN PASSES WITHIN AREA BOARDED BY ORBIT EXTREMES AND EARTH

MAXIMUM OCCURRENCE RATE, ONCE PER DAY

MAXIMUM DURATION DEPENDS ON LEO SATELLITE ALTITUDE AND ORBITAL INCLINATION

ALTITUDE (km)	DURATION (min)
200	5
500	8
1000	10
2000	12
5000	10

GEO SATELLITE VIEW OF EARTH

• LEO ORBITS FROM 200 TO 5000 km

• SOLAR MOTION W TO E, UNIFORM 0.25 DEGREES PER MINUTE N S MOTION MAXIMUM OF 0.4 DEGREES PER DAY AT EQUINOX

SOLAR DECLINATION

SUN

15°/hour

FIGURE 1.1.8.2-1

As seen from Table 1.1.8.2-3, solar interference is limited in duration and in occurrence. The recommendation is to size the LEO-GEO link for two modes:

i. No solar interference. Lower power and/or higher data rates can be used. (Antenna temperature will be 240 K due to disk of earth being in the field of view).

ii. With 3250 K sun increasing antenna noise temperature. Higher power and/or lower data rates could be used.

The change between modes could be based on ephemeris calculations or sun sensors. The alternate to dual mode operation is to shut down the link during solar "outages", which are predictable far in advance. It is not recommended to size the link to include solar margin at all times as this would be a great waste in capacity.

GEO-LEO Links (using 1 m GEO and 1.5 m LEO antennas)

The geometry of the GEO-to-LEO link is the same as for the LEO-to-GEO link except for being in the opposite direction. A major difference is that as viewed from the LEO satellite, the earth cannot come between the target GEO satellite and the sun. Thus more solar interference time can occur. However, there is no 240 K increase in antenna temperature due to the earth being in the field of view. Table 1.1.8.2-4 summarizes the solar interference effects for the GEO-LEO link.

Since data transfer is primarily from LEO to GEO satellite, the required data rate is much lower for the GEO-LEO link than for the LEO-GEO link, 1 Mbps vs as much as 300 Mbps. Thus the GEO-LEO link, with its antenna sizes based on the LEO-GEO requirements, will have more than adequate margin to operate with full 3600 K solar interference.

TABLE 1.1.8.2-4

SUMMARY OF SOLAR EFFECT FOR GEO-LEO LINK

| | | LEO ALTITUDE | |
		100 mi	3100 mi
Maximum increase in receiver noise temperature (K)		3600	3600
Dates of possible solar interference		Feb24-Apr15	Feb4-May5
number of days	(days)	50	90
other dates of solar interference		Aug28-Oct17	Aug8-Nov6
number of days	(days)	50	90
% of year	(%)	27	49
Maximum continuous duration of noise >70 K (for single LEO satellite)	(minutes)	6	varies with orbit

1.1.8.3 Polarization

1.1.8.3.1 General Discussion

A receiving antenna extracts the maximum amount of energy from an incident electromagnetic wave when it is polarization matched to the wave. This means that the polarization ellipse of the incident wave is identical to and oriented in space identically with the wave that would result from transmitting with the receiving antenna. The polarization of an electromagnetic field is described in terms of the direction in space of the electric field which will always be normal to the direction of propagation. If the electric field vector is always directed along a line the field is said to be linearly polarized. In general, however, the terminus of the electric field vector does not trace a straight line but rather it describes an ellipse. These polarization ellipses can vary between two extremes: a straight line (linear polarization) and a circle (circular polarization). Elliptical polarization results from the electric field vector rotating clockwise or counter clockwise at the excitation frequency about an axis parallel to the direction of propagation. It can be shown that linear polarization is composed of two counter rotation (orthogonal) circular polarizations of equal amplitude. Elliptical polarization can be broken into two counter rotating circular polarizations of unequal amplitude, and perfect circular polarization contains only one sense of circular polarization and none of the opposite (orthogonal) sense of polarization. Efficiencies of unity can be achieved from any of the polarizations as long as the condition is met that the receiving antenna is polarization matched to the incident wave. Linearly and elliptically polarized antennas must be aligned to the polarization ellipse of the incident wave to achieve maximum efficiency while circular polarization requires no angular alignment because of its symmetry. If the incident wave originates from a source that is moving with respect to the receiving antenna, there will usually be a variation in the polarization orientation of the linearly polarized wave as the source moves and for maximum efficiency the receiving antenna must acquire and track this variation. Likewise there will be a variation in the orientation of the polarization ellipse for elliptically polarized waves as the source moves and again the receiving antenna must acquire and track the polarization ellipse in order to achieve maximum efficiency. If both the incident wave and the receiving antenna are circularly polarized, no polarization orientation acquisition and tracking is required. Thus circular polarization is normally the best choice for systems where the transmitting source and the receiving antenna are moving with respect to one another.

It has been assumed that there is no effect on the polarization of the wave due to the propagating medium, therefore, the polarization of the wave incident on the receiving antenna is the same as the polarization of the antenna that launched the wave.

The most common method of describing the ellipticity of the polarization is in terms of axial ratio. The axial ratio is the major to minor axis ratio of the ellipse that the terminus of the electric field vector traces. Linear polarization has an infinite axial ratio while circular polarization has an axial ratio of unity. Expressed in dB the axial ratio varies from infinite for linear polarization to 0 dB for circular polarization. Figures 1.1.8.3-1 and 1.1.8.3-2 can be used to determine the range of polarization loss between any two antennas. Figure 1.1.8.3-1 is "best" case when both transmitting and receiving polarization ellipses are aligned and Figure 1.1.8.3-2 is a "worst" case when the polarization ellipses are orthogonal. The energy lost to polarization mismatch in one polarization shows up in the

orthogonal polarization resulting in degradation of polarization isolation. Figure 1.1.8.3-3 gives the level of cross-polarized energy as a function of axial ratio for the circular polarization case.

In an antenna system, it is theoretically possible to have infinite isolation between two orthogonal polarizations. However, in practice something less than infinite isolation is achievable due to difficulties in maintaining polarization purity within the antenna feed. An example of an orthogonal polarization pair is horizontal and vertical linear polarization. For circular polarization the orthogonal pair is right hand circular and left hand circular. Systems take advantage of this polarization isolation to increase the isolation between communication channels. Three ways have been considered for configuring the communication systems for polarization utilization:

1. Co-Polarized

    The transmit and receive channels have the same polarization. Isolation between them is achieved by frequency multiplexing.

2. Orthogonally Polarized

    The tranmsit and receive channels are placed on polarizations orthogonal to each other. Isolation between them is achieved by the inherent isolation between orthogonal polarizations and by frequency multiplexing.

3. Frequency Re-Use

    Two transmit channels utilizing the same frequency bands are placed on two orthogonal polarizations. Likewise, two receive channels utilizing the same frequency band are placed on two orthogonal polarizations.

Figure 1.1.8.3-4 gives a graphical illustration of these three ways that polarization is used to isolate channels. The co-polarized systems depend solely on filters to multiplex the transmit and receive channels into the antenna. The orthogonally polarized system also multiplexes the transmit and receive channels into the antenna with filters. However, it takes advantage of the orthogonal polarizations to achieve further isolation between transmit and receive channels. It can be seen from Figure 1.1.8.3-4 that frequency re-use almost doubles the traffic bearing capacity of the link. The transmit to receive isolation depends solely on filtering while isolation between transmit channels and between receive channels relies solely on the isolation between orthogonal polarizations. Consequently, re-use systems place more stringent polarization purity requirements on antenna systems.

POLARIZATION LOSS
SAME SENSE

$(\beta = 0°)$
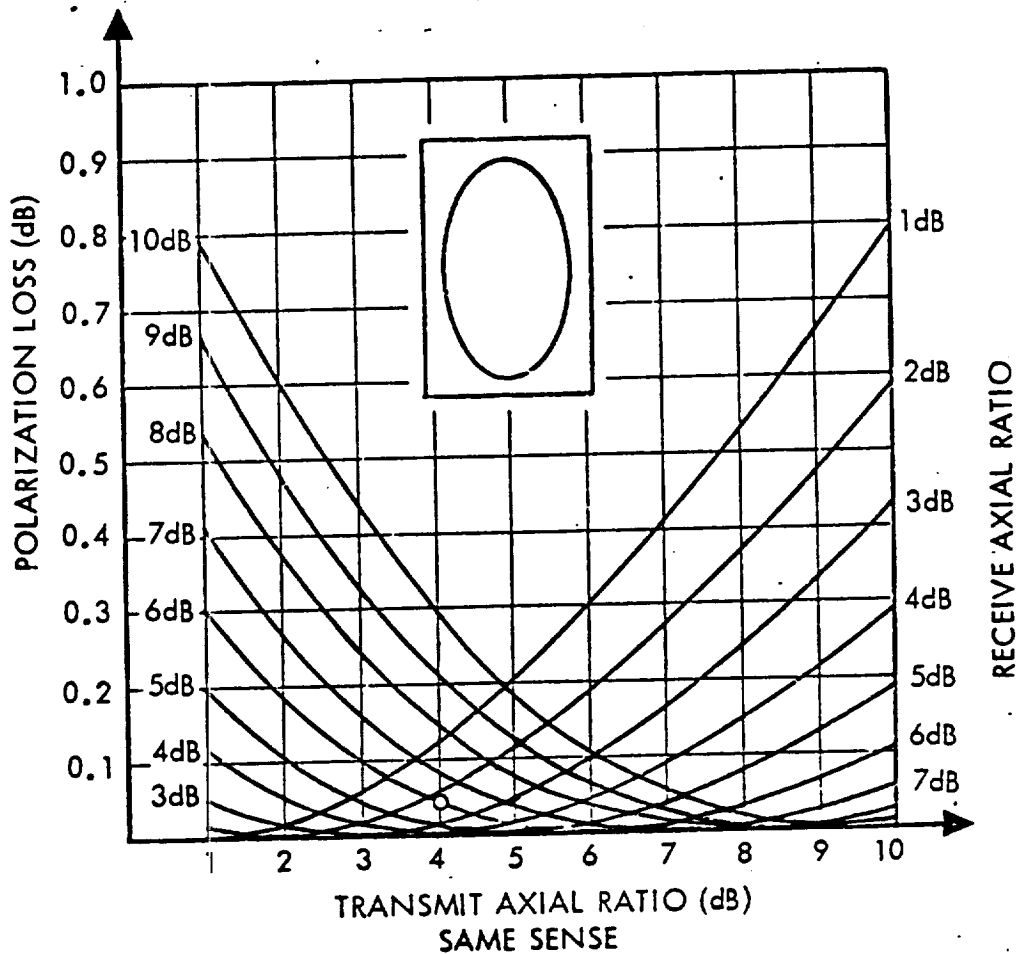
POLARIZATION LOSS BETWEEN ELLIPTICALLY POLARIZED ANTENNAS
WHEN THE ELLIPSES ARE ALIGNED (MINIMUM LOSS)

FIGURE 1.1.8.3-1

POLARIZATION LOSS
(SAME SENSE)
$(\beta = 90°)$
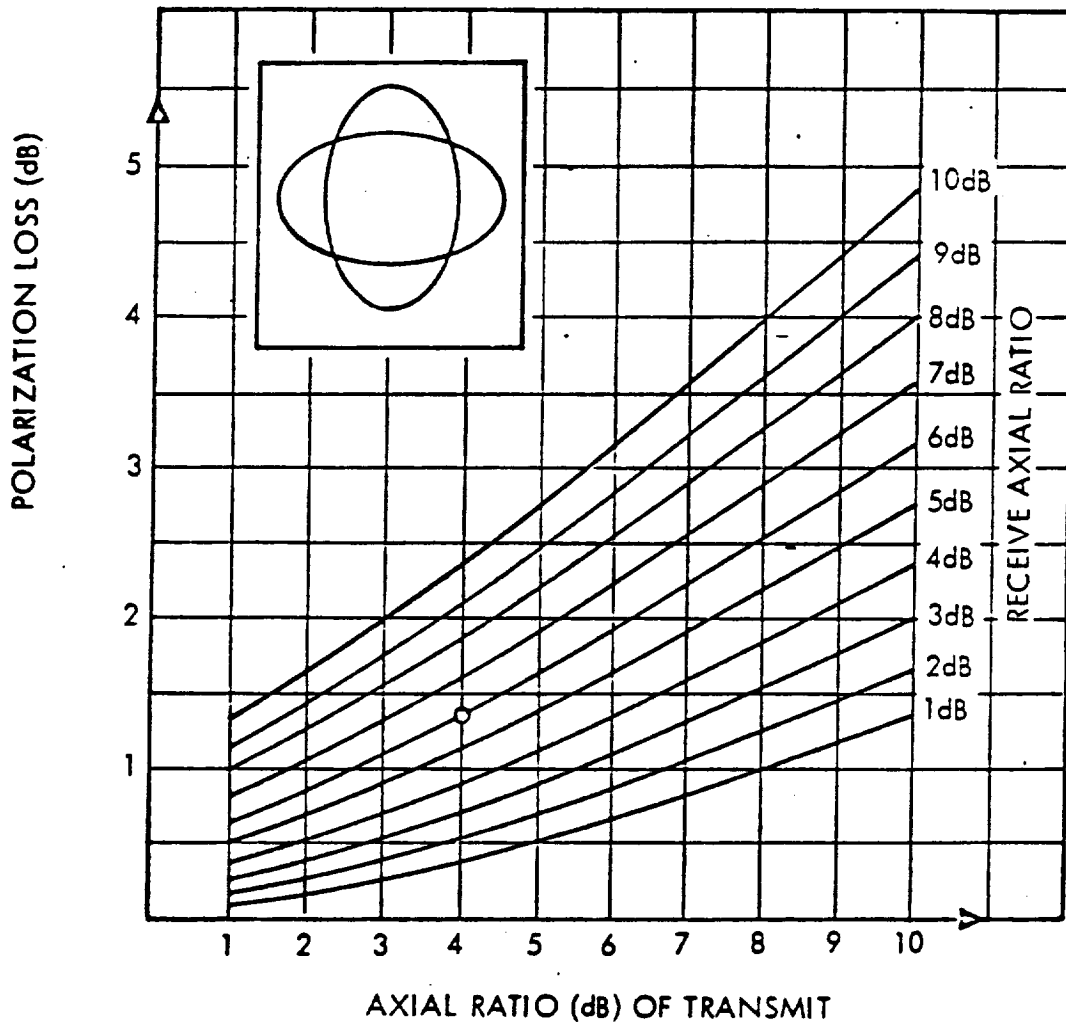
POLARIZATION LOSS BETWEEN ELLIPTICALLY POLARIZED ANTENNAS
WHEN THE ELLIPSES ARE ORTHOGONAL (MAXIMUM LOSS)

FIGURE 1.1.8.3-2
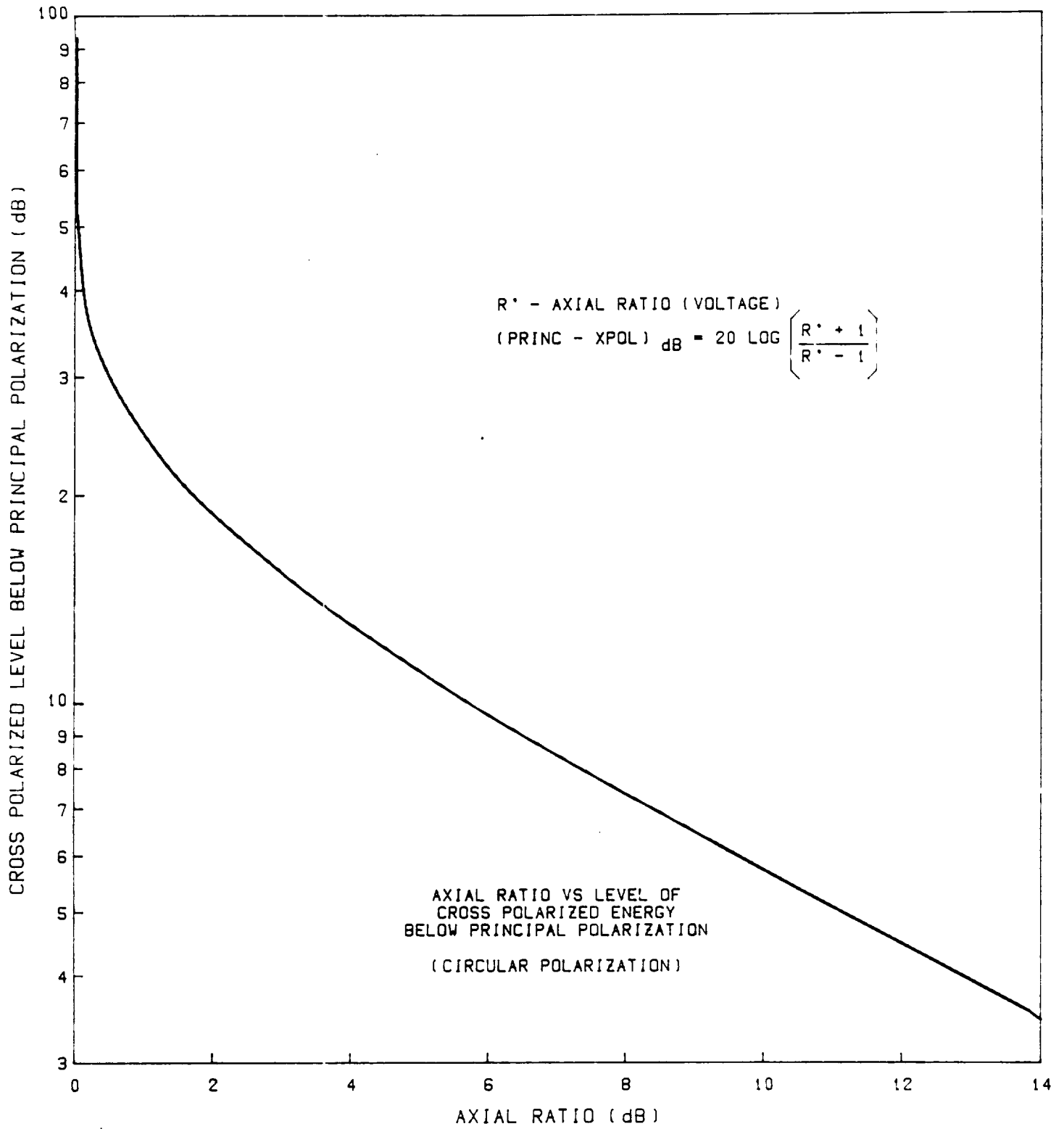
Figure 1.1.8.3-3

FIGURE 1.1.8.3-4. POLARIZATION UTILIZATION

CO-POLARIZED

TRANSMIT (BAND 1) RECEIVE (BAND 2) A

(NOT USED) B

FREQUENCY ⟶

ORTHOGONAL POLARIZATION PAIR

ORTHOGONALLY POLARIZED

TRANSMIT (BAND 1) A

RECEIVE (BAND 2) B

FREQUENCY ⟶

FREQUENCY RE-USE

TRANSMIT (BAND 1) RECEIVE (BAND 2) A

TRANSMIT (BAND 1) RECEIVE (BAND 2) B

FREQUENCY ⟶
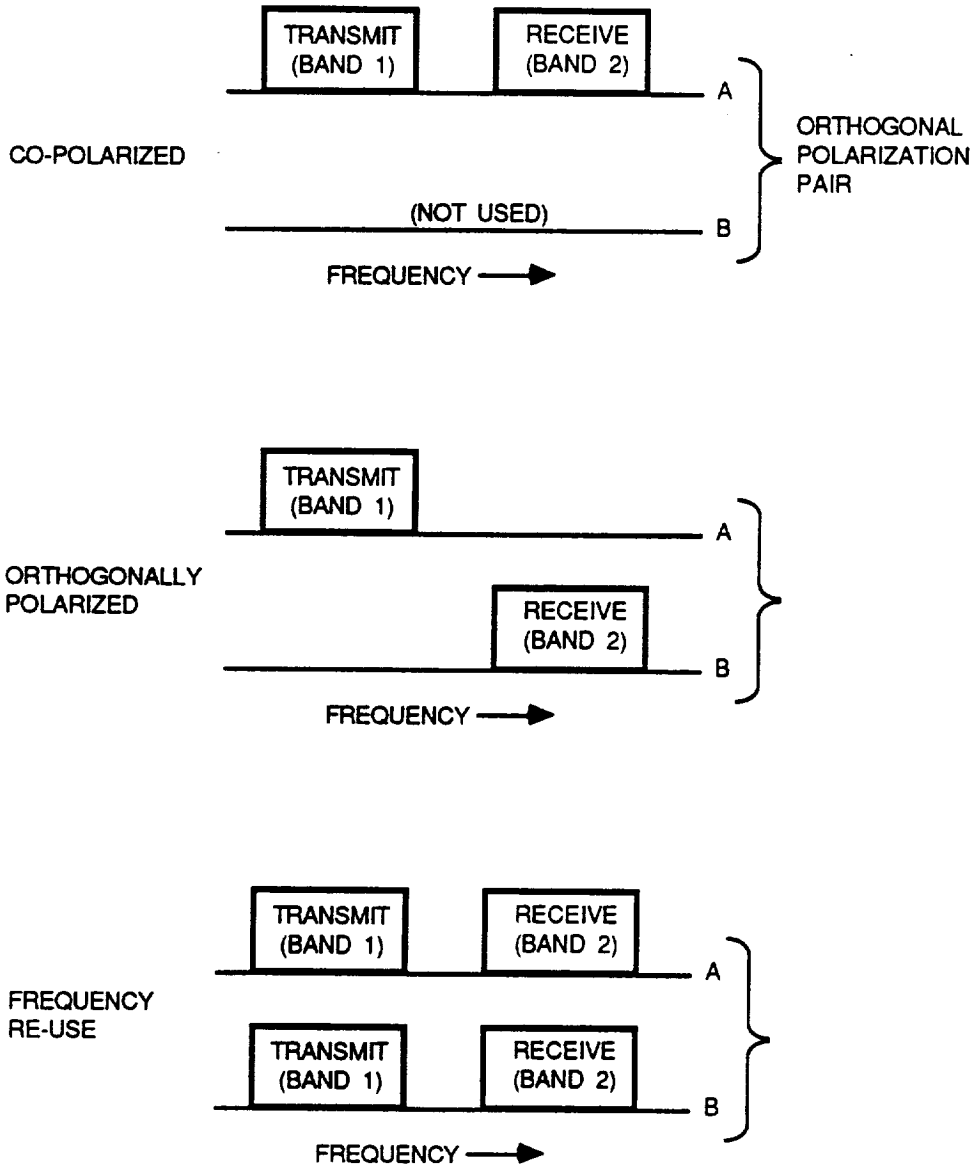
When reflector type antennas are used, the polarization of the electromagnetic wave is usually accomplished in the feed. The degree to which polarization purity car be achieved depends upon the symmetry and reflections within the feed. Based on experience at C-Band, isolation between orthogonal circular polarizations of up to 27 dB are readily achieved with typical machining and fabrication techniques and reasonable VSWRs. Isolations between 27 dB and 35 dB are typical of frequency re-use feeds and require much more attention to fabrication and matching techniques.

1.1.8.3.2 In-Orbit Spare Considerations

The impact of each of the three polarization utilization schemes on the in-orbit spare has been investigated. These three schemes are: 1) co-polarized 2) orthogonally polarized, and 3) frequency re-use. Briefly, a single in-orbit spare has been assumed which can be configured to replace either of the two GEO satellites. The objective is to determine if the choice of polarization utilization schemes has any impact on the complexity of the in-orbit spare.

In summary, as far as the impact on the in-orbit spare, all polarization utilization schemes are equal. Figures 1.1.8.3-5, -6 and -7 are simplified block diagrams showing the two GEO satellites and the required in-orbit spares for implementing co-polarized, orthogonally polarized, and frequency re-use systems, respectively. On the diagrams, polarization A and polarization B represent any two orthogonal polarization. From these block diagrams it can be seen that the switching required to configure the in-orbit spare is the same for all three polarization utilization schemes. None of the schemes require the in-orbit spare to perform polarization switching in the antenna.

FIGURE 1.1.8.3-5. BLOCK DIAGRAM FOR GEO - GEO LINK USING CO - POLARIZED TRANSMIT AND RECEIVE
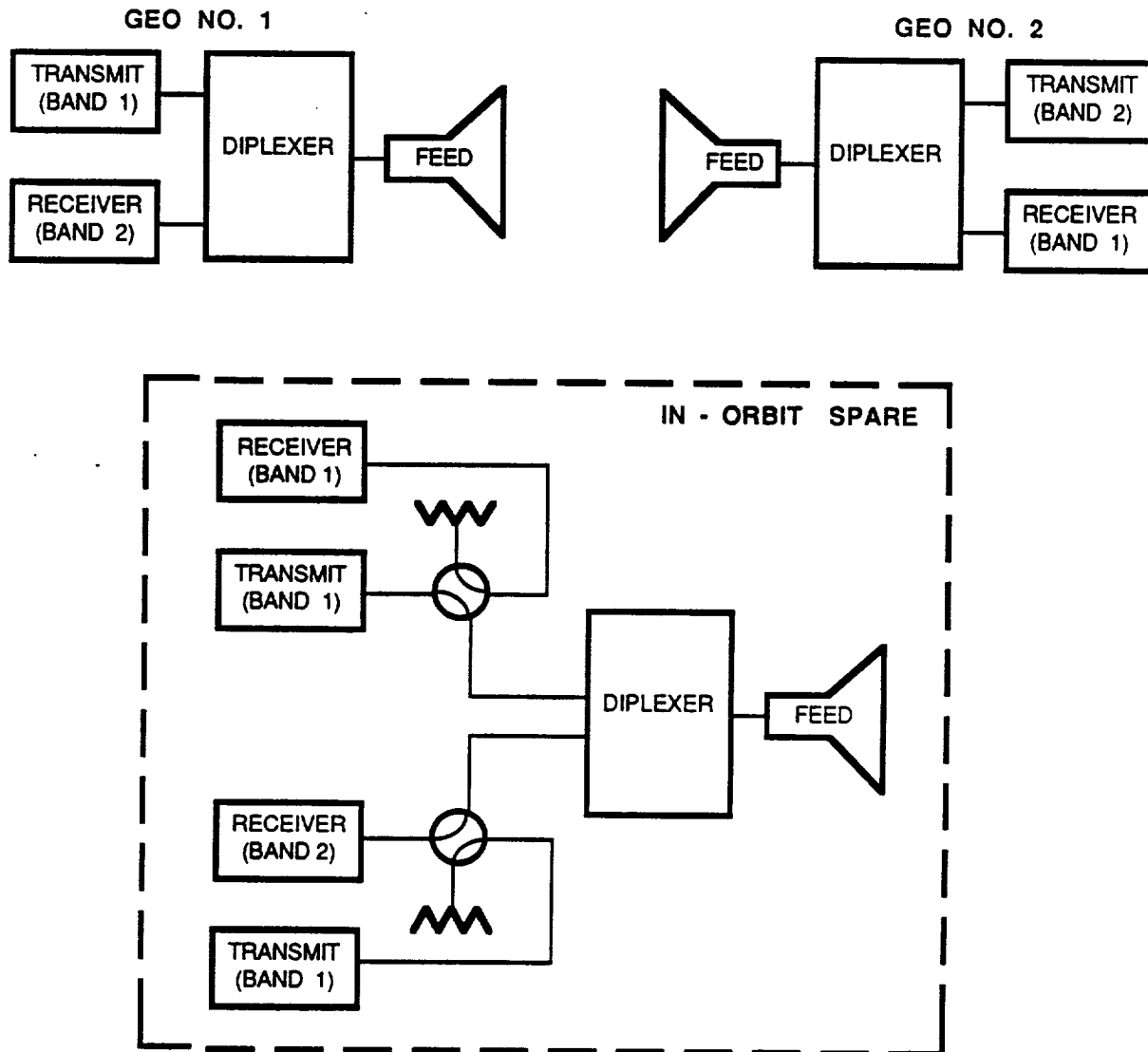
FIGURE 1.1.8.3-6. BLOCK DIAGRAM FOR GEO - GEO LINK USING ORTHOGONALLY POLARIZED TRANSMIT AND RECEIVE

GEO #1

XMTR
(BAND 1)

RCVR
(BAND 2)

DIPLEXER

POL A

FEED

XMTR
(BAND 1)

RCVR
(BAND 2)

DIPLEXER

POL B

GEO #2

XMTR
(BAND 2)

DIPLEXER

POL A

FEED

RCVR
(BAND 1)

POL B

XMTR
(BAND 2)

DIPLEXER

RCVR
(BAND 1)

IN-ORBIT SPARE

XMTR
(BAND 2)

RCVR
(BAND 1)

DIPLEXER

XMTR
(BAND 1)

RCVR
(BAND 2)

DIPLEXER

POL A

FEED

XMTR
(BAND 1)

RCVR
(BAND 2)

DIPLEXER

POL B

XMTR
(BAND 2)

RCVR
(BAND 1)

DIPLEXER
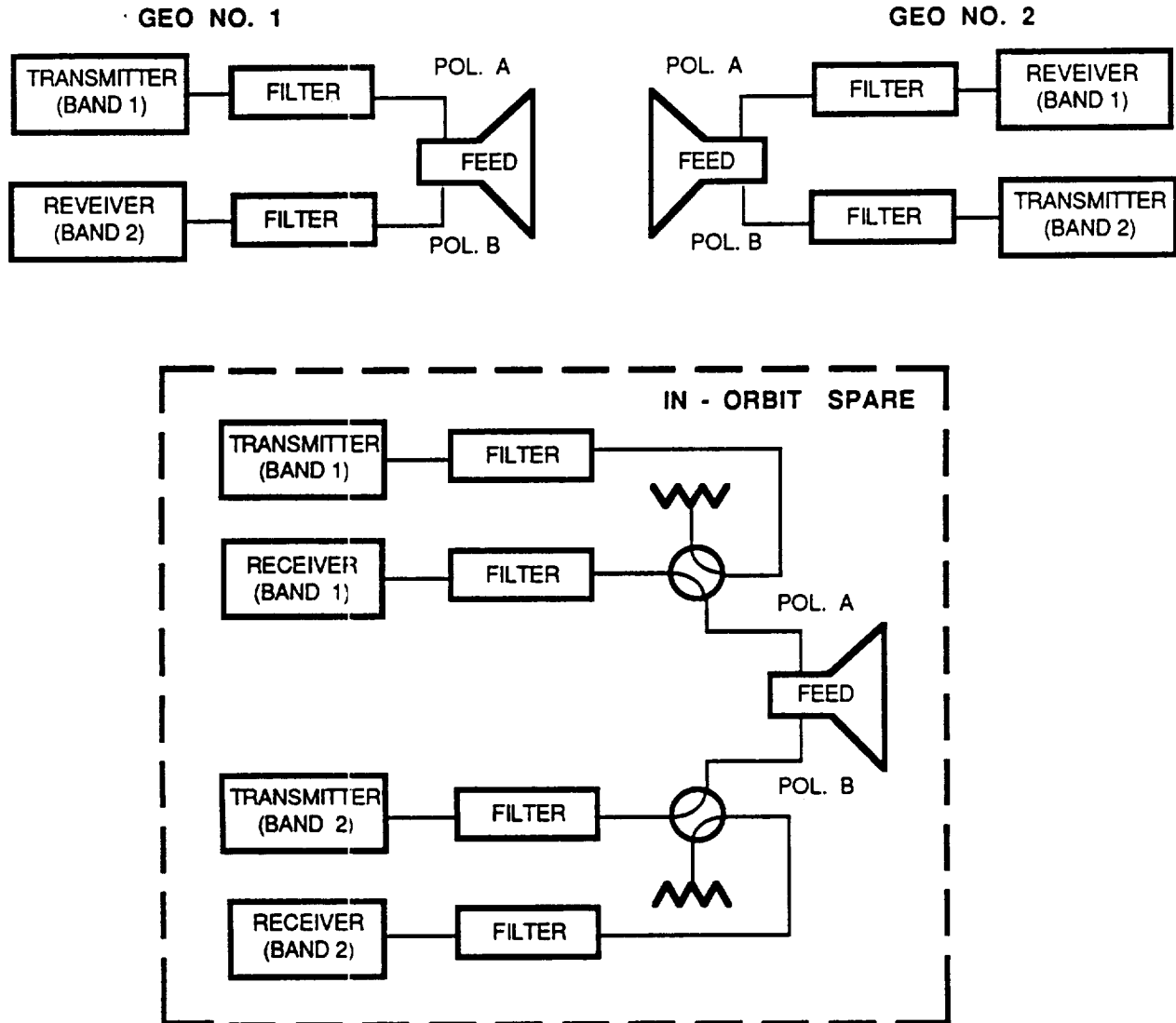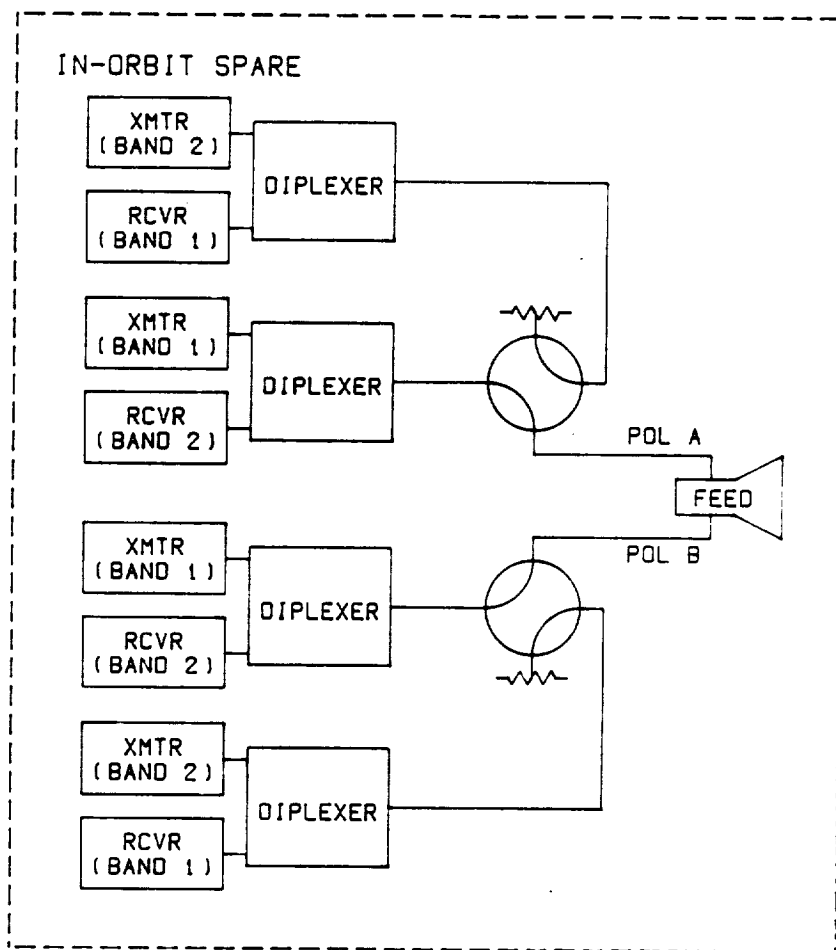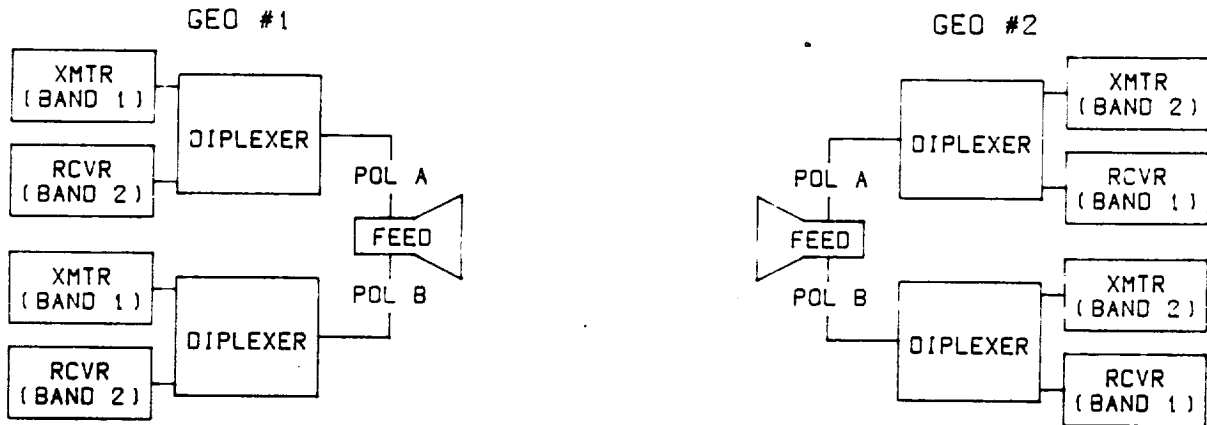
FIGURE 1.1.8.3-7
BLOCK DIAGRAM FOR GEO-GEO LINK USING FREQUENCY RE-USE

1-78

1.1.8.3.3 Baseline Polarization Utilization

Because circular polarization does not require polarization tracking, it will be used for all intersatellite links. In order to take advantage of the achievable polarization isolation, transmit and receive channels have been placed on orthogonal polarizations within each antenna system. The following polarizations will be used for the baseline system:

```
GEO#1  to   GEO#2   Transmit--------------RHCP
GEO#1 from  GEO#2   Receive---------------LHCP

GEO#2  to   GEO#1   Transmit--------------LHCP
GEO#2 from  GEO#1   Receive---------------RHCP

GEO    to   LEO     Transmit--------------RHCP
GEO   from  LEO     Receive---------------LHCP

LEO    to   GEO     Transmit--------------LHCP
LEO   from  GEO     Receive---------------RHCP
```

The configuration of each GEO depends on its role, not its location. The location of the two GEOs can be interchanged and communication will still occur: GEO #1 will still transmit on Frequency Band 1, which is the GEO #2 receive band. Note that GEO #1 is only equipped to transmit on Frequency Band 1; transmission on Frequency Band 2 would require the use of another transmitter tuned to that frequency. Similarly, reception by GEO #2 on Frequency Band 2 would imply another RF receiver. The spare satellite, however, must be equipped with transmitters and receivers tuned to both frequency bands, as shown in Figure 1.1.8.3-6, along with two polarizers and necessary switches.

1.1.9 System Test and Verification Approach

To verify the system performance of the 60 GHz crosslink, the system test and verification plan addresses the three primary functional areas of:

a. Data communication links
b. Acquisition and tracking
c. Command and telemetry digital interface

System verification involves the combination of analysis, simulation, and performance tests at subsystem and system level. Analysis is used to predict the system performance parameters early in the development cycles so the system performance can be tracked as measurements are made. Simulation is used for those dynamic elements such as acquisition that can not be easily determined by analysis. The performance tests at subsystem and system level under various environmental conditions are the final verification of the system performance.

FIGURE 1.1.9-1
SIMPLIFIED PERFORMANCE VERIFICATION
FLOW DIAGRAM
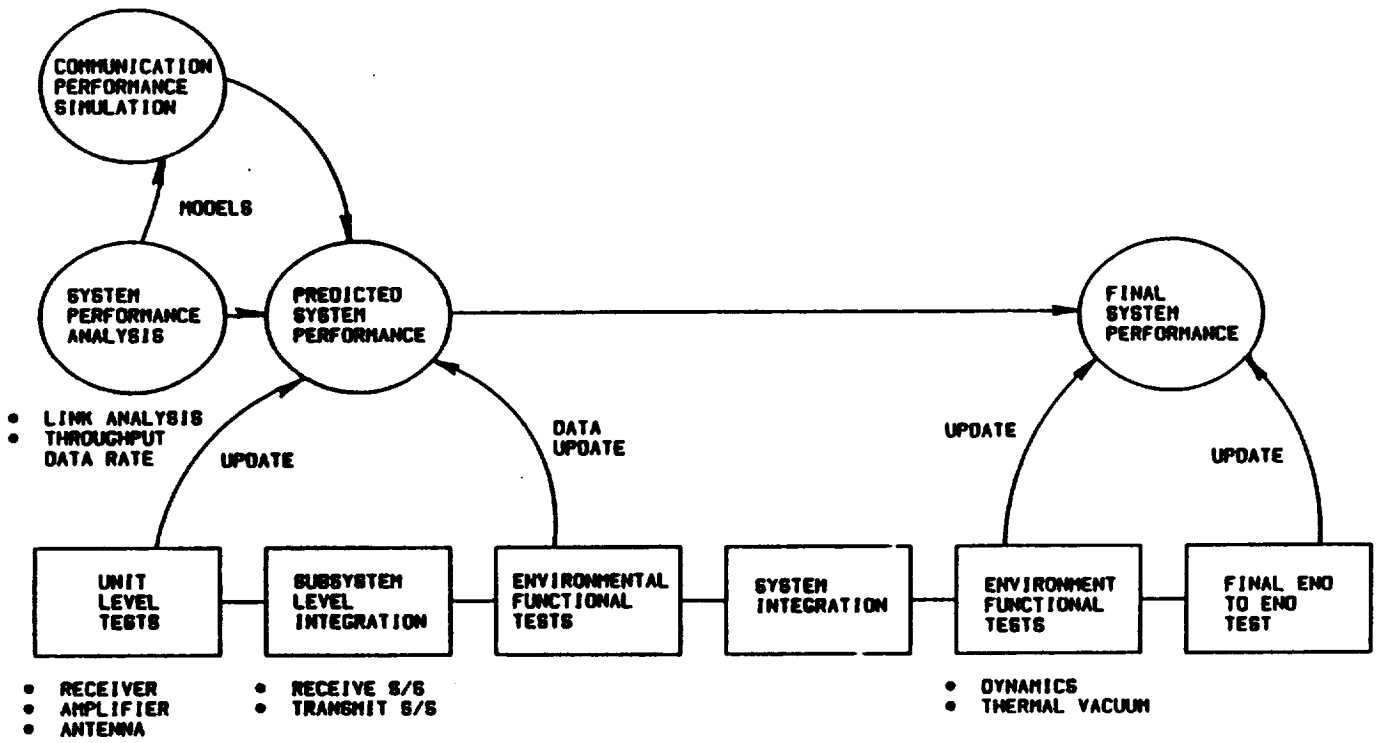
1.1.9.1 Performance Verification Approach

A baseline communication performance verification plan has been developed to functionally test the crosslink during subsystem development and system qualification and acceptance. A flow diagram of the baseline communication performance sequence is shown in Figure 1.1.9-1. Note that this performance sequence uses a link performance analysis to predict the throughput data rate capability of the intrasatellite system as measurements are made early in the development process.

Functional testing is to be performed throughout the qualification and acceptance test sequence at the subsystem and system level. The environmental conditions include thermal, thermal vacuum, mechanical vibration and shock, and acoustic load. The RF functional testing includes measurements of:

o Saturated power output
o Transmitter gain
o Phase error (AM/PM nonlinearity, phase noise)
o Frequency stability (local oscillator, frequency conversion)
o Frequency response (channel BW, gainslope, group delay, spurious output)
o Noise figure, C/N
o Transmit/receive isolation

Investigations performed during the study show that the equipment will be available in the predicted time frame to implement standard test set-ups at 60 GHz. Testing on the antenna for gain, polarization loss, pattern measurements, and isolation will primarily be done at the subsystem level. Test methods will allow the system testing for BER performance and transmit/receive isolation with the antenna.

One of the most important system performance measurements is the evaluation of the end-to-end BER. The baseline approach is to build a satellite simulator using ground test equipment to form one end of a 60 GHz crosslink. In this way we can verify BER for both the receive and transmit subsystems of the flight system under test.

One area of concern for system verification is the development of a calibration procedure for the RF tests at the subsystem and system level. Because the 60 GHz frequency band suffers large attenuation due to oxygen and accepted standards at this frequency are not readily available, the accuracy of the performance measurements will depend on an adequate calibration procedure. To maximize control of the measurement environment, waveguide, purged with an inert gas, should be utilized whenever possible. As much as possible, the system verification should use the same ground test equipment at the subsystem and the system level testing to minimize the variables that affect calibration.

In ground based satellite tracking systems the ranging performance is usually tested by a loop back scheme to verify equipment selected noise performance and to measure and calibrate biases. The same approach can be used for TDAS range testing except that the loop-back will be through an actual or simulated LEO "transponder".

1.1.9.2 Built-in Test Concept

The purpose of the built-in-test feature of the intrasatellite crosslink system is to verify the performance of the link from the transmitter input to the receiver output while the system is on-orbit. Since the system will have a demodulation/modulation function, a test concept that evaluates BER is adopted as the baseline method to verify end-to-end system performance. The forward data rate (GEO-LEO) is only 1 Mb/s while the return rate (LEO-GEO) may be as high as 300 Mb/s. Thus buffering will be required in the TDAS for a complete round-trip check.

Some of the built-in test concepts include:

a. Self contained built-in BER test pattern measurement.

   This concept uses a test pattern that is transmitted, received and tested for errors all within the 60 GHz package. It requires the addition of processors and memories in the 60 GHz package for buffering and data comparison.

b. Cooperative BER test with host satellite processor on test pattern transmission.

   This concept is identical to a. except it utilizes the host computer processor. The impact on the host processor must be considered before selecting this concept.

c. Continuous data test pattern check on each transmitted/received data frame.

   This concept is similar to attaching a known check sum tail on every data frame that would be continuously checked by the intrasatellite system processor to verify that the link quality is adequate. This concept has the advantage of providing a continuous monitor on the system but it does use some of the data link capability for the test overhead.

d. Telemetered transmit power and receive C/N measurements.

   This concept measures transmitted power and received power. This concept provides the most direct measurement of the performance of the 60 GHz crosslink equipment for diagnostics and making corrective decisions. This concept can supply benchmark information on transmitted and received power on a continuous basis, however, a C/N measurement will require an interruption of crosslink traffic.

e. Monitoring of the activity of the FEC decoder.

   On the links containing coding, the number of errors detected by the FEC decoder can be monitored as a direct measurement of BER using mission data without any additional off-line processing, overhead, or traffic interruption.

For the GEO-GEO crosslinks the baseline BER test concept is to use telemetered transmit power and C/N measurements as described in d-above. This link is uncoded, therefore there is no FEC decoder to

monitor for errors. Benchmarks can be established at the factory and during the in-orbit test phase for real-time monitoring. Interruption of traffic need only occur when the degradation in the BER warrants further diagnostics that can only be made with a C/N measurement.

For the GEO-LEO return link, the baseline BER test concept is to monitor the activity of the FEC decoder. This concept as described in e. above provides a direct BER measurement with minimal impact on the 60 GHz system hardware and no impact on the overhead or traffic.

1.1.10 Communication System Ground Test Equipment and Bench Test Equipment

To the maximum extent possible, the same GTE should be used to perform tests at the subsystem and system level to minimize calibration problems and cost. The GTE will be computer automated. To simulate the host satellite baseband interface with the 60 GHz crosslink package it must be able to transmit and receive modulated 60 GHz signals. For this reason the GTE will be functionally similar to a 60 GHz crosslink package. A simplified block diagram of the GTE is shown in Figure 1.1.10-1. Most of the testing with the GTE will be through RF waveguide. Additional IF and digital ports are provided for test ports and the baseband data interface. The GTE will have a built in BER tester and the capability of generating data patterns up to 300 Mb/s. The BTE used for unit level testing of receivers, converters and TWTAs should be a subset of the GTE. These unit level tests may not need the baseband modulation, but will require RF signals and measurement equipment such as power meters and spectrum analyzers which are also a part of the GTE.

Considerable progress has been made in the past year towards extending the frequency range of commercially available test equipment. At this time spectrum analyzers operating at frequencies up to 110 GHz are available. Typical values at frequencies needed for the crosslink test equipment (up to 70 GHz) are a noise level of -95 dBm with a 1 kHz bandwidth and an accuracy of ±2.5 dB.

Vector and scalar network analyzers, signal sources, and waveguide accessories (e.g. isolators, attenuators, terminations, etc.) operating at U-band frequencies (40 to 60 GHz) are currently available. A typical vector network analyzer offers 80 dB dynamic range and resolutions of 0.05 dB and 0.1 degree phase. Signals up to 60 GHz with a frequency resolution of 9 Hz can be generated at this time.

Network analyzers, signal sources, and waveguide accessories for use at V-band (50 to 75 GHz) are currently in development, as are counters and power meters for both U-band and V-band. Indications are that with the current rate of development there will be adequate test equipment to test the crosslink system in the 1989 time frame.

FIGURE 1.1.10-1

GTE SIMPLIFIED BLOCK DIAGRAM
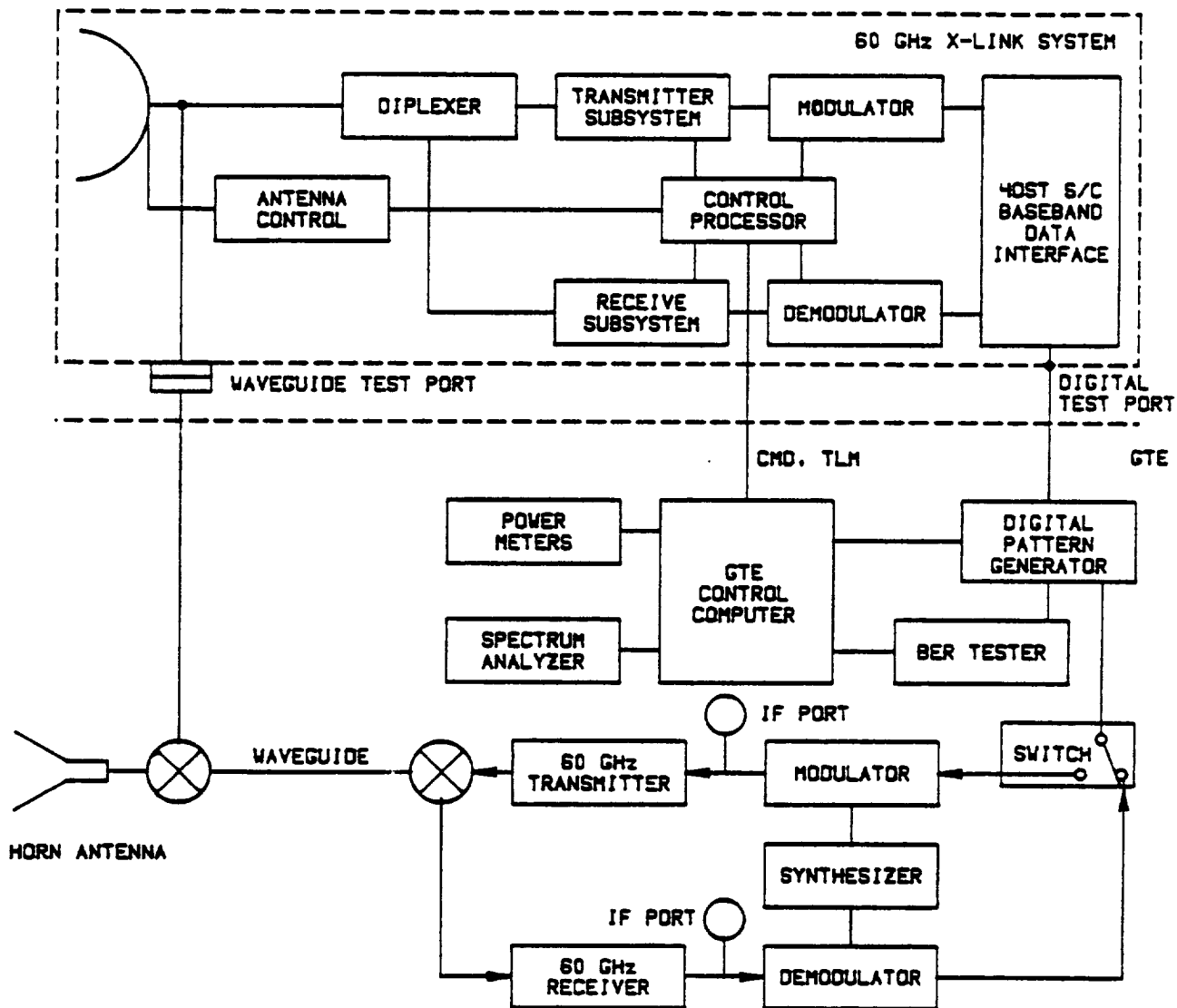
LH3047
HCL39056/KEN2/4-23-84

1.1.11 Interference Analysis and Transmit/Receive Isolation Requirements

Assuming a baseline frequency plan as shown in Figure 1.1.1-2, the intra-system interference among the intersatellite links is assessed and the input/output isolation requirements among the GEO-GEO and GEO-LEO links are addressed. Filters are recommended which will give the required isolation.

1.1.11.1 Interference to GEO-GEO Crosslink Receiver

In the GEO-GEC headend as illustrated in Figure 1.1.1-3, a major source of interference to the receiver is the septum polarizer feed-thru of the transmitter's out-cf-band emissions. Other sources include the command (forward link) transmitter's out-of-band emission through lower order antenna sidelobe intercepts or coupling.

Assuming the GEO transmitter has an effective EIRP of 71 dBW realized by the use of a 3.2 M antenna and a 10 W transmitter, and that the septum polarizer provides a minimum of 27 dB polarization isolation, the interference of the GEO transmitter feedthru presented to the receiver input is

$$I1 = 10 - 27 - Jt(f) - Jr(f) - J(f) \text{ dBW}$$

Similarly, the interference due to the Forward (command) link transmitter is:

$$I2 = -2 \ (0.6W) - 40 \ (\text{Ant. isolation}) - JF(f) - Jr(f) - Jc(f) \text{ dBW}$$

where $Jt(f)$, $Jr(f)$ and $JF(f)$ are filter responses of GEO transmit, GEO receive and Forward transmit in dB, respectively, and $J(f)$ and $Jc(f)$ are modulation spectral factors. Isolation between GEO-GEO and GEO-LEO antennas is assumed to be 40 dB as expressed above.

If the intended signal at the same input is taken to be:

$$C = 70 - 226 \ (\text{path loss}) + 63 \ (\text{ant. gain}) = -93 \text{ dBW}$$

the resulting C/N (thermal) is about 15 dB (at 2 Gbps without sun effect). The C/I due to transmitters are therefore:

$$C/I1 = -76 + [\ Jt(f) + Jr(f) + J(f) \ ] \text{ dB}$$

$$C/I2 = -51 + [\ Jf(f) + Jr(f) + Jc(f) \ ] \text{ dB}$$

where the notation [ ] denotes averaging in frequency. If the total allowable loss due to C/I is 0.1 dB, the minimum C/I (for C/N (thermal) = 15 dB) due to either transmitter is then 33 dB (assuming equal contribution).

As such the conbined filtering must provide a minimum rejection of:

$$[\ Jt(f) + Jr(f) + J(f) \ ] > 109 \text{ dB}$$

$$[\ Jf(f) + Jr(f) + J(f) \ ] > 84 \text{ dB}$$

The above requirements can be met with the following considerations: For the GEO-GEO interface, the assessment is as illustrated below:

FREQ (GHz)	Jr(f) (dB) 7-pole Chebyshev fo=55.50 GHz	Jt(f) (dB) 7-pole Chebyshev fo=62.75 GHz	Jr(f) (dB) 2 Gbps QPSK	Total (dB) Rejection
54.25 (band edge)	0	> >	36	> >
54.50	0	> >	35	> >
Rx 55.50 (band center)	0	136	32	168
56.50	0	125	28	153
56.75 (band edge)	0	123	28	151
57	11	120	26	157
58	53	106	25	184
59	74	90	22	186
60	89	68	20	177
61	101	34	15	150
61.50 (band edge)	105	0	12	117
61.75	108	0	10	118
Tx 62.75 (band center)	115	0	0	115
63.75	> >	0	- -	> >
64.00 (band edge)	> >	0	- -	> >

The above isolation characteristics can be implemented with 7-pole Chebyshev receive and transmitter filters, assuming a 0.1 dB ripple for the filters.

The interference due to forward link transmitters can be similarly assessed as illustrated below:

FREQ (GHz)	Jr(f) (dB) 7-pole Chebyshev fo=55.50 GHz	Jc(f) (dB) 1 Mbps BPSK	Jf(f) (dB) 3-Pole Chebyshev fo=57.800 GHz	Total (dB) Rejection
54.25 (band edge)	0	> >	> >	> >
54.50	0	>46	70	>116
Rx 55.50 (band center)	0	>46	60	>106
56.50	0	>46	45	>91
56.75 (band edge)	0	>46	39	>85
57.00	11	>46	31	>88
57.250	26	>46	21	>93
57.30	28	>46	19	>93
57.395	33	>46	13	>92
57.600 (band edge)	40	>46	0	>86
57.725	45	46	0	91
57.736	45	40	0	85
57.796	47	20	0	67
57.798	47	15	0	62
57.799	47	10	0	57
Tx 57.800 (band center)	47	0	0	47
58.000 (band edge)	53	- -	0	- -

The above performance, which results in an average rejection of 58 dB, can be implemented with a 3-pole, 400 MHz equal ripple bandwidth Chebychev filter in conjunction with the 7-pole GEO receiver filter. An additional 30 dB IF quieting will exceed the required 84 dB, so no interference problem due to the forward transmitter is expected. The 30 dB additional rejection at IF can be obtained by another 7-pole filter.

1.1.11.2 Interference to LEO-GEO Link Receiver

Interference to the return link receiver can be similarly analyzed. We will calculate the interference due to the closest GEO-GEO transmitter and refer to it as I3. The interference due to the Forward link transmitter is called I4.

Following the analysis of the previous section, I3 and I4 are expressed as:

I3 = 10 (EIRP) - 40 (Ant. isolation) - Jt(f) - J(f) - Ju(f) dBW

I4 = -2 (0.6 W) - 27 (SP isolation) - Jf(f) - Jc(f) - Ju(f) dBW

where Ju (f) is the return link input filter response.

Let the intended signal at the same input be:

C = 64 - 221 (path loss) + 54 (Ant. gain) = -103 dBW

which results in a C/N (thermal) of about 10 dB (at 300 Mbps with earth effect and FEC encoding). The minimum C/I3 or C/I4 should then be 25 dB or more. As such the minimum rejections required are:

[Jt(f) + J(f) + Ju(f)] > 98 dB

[Jf(f) + Jc(f) + Ju(f)] > 99 dB

for I3 and I4 respectively.

The interference to the return link due to GEO-GEO transmission (I3) is analyzed first:

FREQ (GHz)		Ju(f) (dB) 3-pole Chebyshev fo=60.00 GHz	Jt(f) (dB) 7-pole Chebyshev fo=62.75 GHz	Jf(f) (dB) 2 Gbps QPSK	Total (dB) Rejection
59.80	(band edge)	0	73	>19	>92
59.85		0	72	>19	>91
Rx 60.00	(band center)	0	68	>19	>87
60.15		0	64	>19	>83
60.20	(band edge)	0	63	19	82
60.56		21	52	17	90
60.74		29	45	16	90
60.92		34	37	15	86
61.10		39	28	14	81
61.28		43	17	13	73
61.46		46	4	12	62
61.50	(band edge)	47	0	12	59
61.75		51	0	10	61
Tx 62.75	(band center)	62	0	0	62

The average isolation is about 60 dB. The required minimum of 98 dB can be implemented with a 3-pole Chebychev receive filter, the 7-pole Chebyshev transmitter filter and 40 dB of IF quieting. The interference due to the forward link transmitter can be similarly assessed.

FREQ (GHz)	Ju(f) (dB) 3-pole Chebyshev fo=60.00 GHz	Jc(f) (dB) 1 Mbps BPSK	Jf(f) (dB) 3-pole Chebyshev fo-57.800 GHz	Total (dB) Rejection
57.800 (band center)	59	0	0	59
57.801	59	10	0	69
Tx 57.802	59	15	0	74
57.804	59	20	0	79
...				
57.864	58	40	0	98
57.875	58	46	0	104
58.000 (band edge)	56	>46	0	>102
58.200	53	>46	12	>111
59.000	37	>46	41	>124
...				
59.500	19	>46	50	>115
...				
59.800 (band edge)	0	>46	54	>100
Rx 60.000 (band center)	0	>46	57	>103
60.200 (band edge)	0	>46	59	>105

The average interference rejection is about 70 dB, which, with 40 dB IF quieting, provides a total rejection of 110 dB. This is greater than the required minimum of 99 dB. The 40 dB of IF quieting can be obtained with another 3-pole Chebyshev filter in the receiver.

1.1.11.3 Image Rejection Considerations

Because of the wide data bandwidths involved, demodulation must occur at relatively high IF frequencies. An IF frequency centered at 26 GHz has been selected for all receivers on the GEO spacecrafts. Image and 3rd order product frequencies that result from mixing of the receiver local oscillators and the various 60 GHz transmit frequencies have been evaluated. We have ensured that none fall in the receiver band of any of the 60 GHz crosslink receivers or in the band of any of the other TDRSS receivers on board the GEO.

1.1.11.4 Interference with other TDAS Systems

Although other communications systems on-board the TDAS are not defined in the SOW, it is expected that both S-Band and Ku-Band capabilities will be retained per current generation TDRSS. THe TDRSS receive frequencies are:

Receiver	Frequency Band			
MA Users	2.2845	to	2.2905	GHz
Shuttle KSA User	14.887	to	15.119	GHz
SSA User	2.0204	to	2.1233	GHz
TDRSS Uplink	14.59	to	15.25	GHz
	2.0359625			GHz
	2.200	to	2.300	GHz
	14.887	to	15.119	GHz

No image or 3rd order products fall within the receive bands of the receivers listed above. Tables 1.1.11.4-1,1.1.11.4-2, and 1.1.11.4-3 contain the calculated image and 3rd order products for each of the crosslink receivers on board the GEO spacecraft.

Because of the extreme atmospheric absorption attenuation at the 60 GHz band, no noticeable interference is anticipated to or from any terrestrial source, as long as out-of-band emissions and rejections are properly handled.

GEO #1 Receiver:
(GEO-GEO crosslink)
Freq 61.500 to 64.000 GHz
L.O.: 36.750 GHz

Source	Image	3rd Order Products
GEO to LEO Transmit (Forward) Freq: 57.600 to 58.000 GHz	20.850 to 21.250 GHz 94.350 to 94.750 GHz	15.500 to 15.900 GHz 78.450 to 79.250 GHz 131.100 to 131.500 GHz 151.950 to 152.750 GHz
LEO to GEO Transmit (Return) Freq: 59.800 to 60.200	23.050 to 23.450 GHz 96.550 to 96.950 GHz	13.300 to 13.700 GHz 82.850 to 83.650 GHz 133.300 to 133.700 GHz 156.350 to 157.150 GHz
GEO#1 to GEO#2 Transmit Freq: 54.250 to 56.750 GHz	17.500 to 20.000 GHz 91.000 to 93.500 GHz	16.750 to 19.250 GHz 72.750 to 76.750 GHz 127.750 to 130.250 GHz 145.250 to 150.250 GHz

TABLE 1.1.11.4-1

GEO #2 Receiver
(GEO-GEO crosslink)
Freq: 54.250 to 56.750 GHz
L.O.: 29.500 GHz

Source	Image	3rd Order Products
GEO to LEO Transmit (Forward) Freq: 57.600 to 58.000 GHz	28.100 to 28.500 GHz 87.100 to 87.500 GHz	1.000 to 1.400 GHz 85.700 to 86.500 GHz 116.600 to 117.000 GHz 144.700 to 145.500 GHz
LEO to GEO Transmit (Return) Freq: 59.800 to 60.200 GHz	30.300 to 30.700 GHz 89.300 to 89.700 GHz	.800 to 1.200 GHz 90.100 to 90.900 GHz 118.800 to 119.200 GHz 149.100 to 149.900 GHz
GEO#2 to GEO#1 Transmit Freq: 61.500 to 64.000 GHz	32.000 to 34.500 GHz 91.000 to 93.500 GHz	2.500 to 5.000 GHz 93.500 to 98.500 GHz 120.500 to 123.000 GHz 152.500 to 157.500 GHz

TABLE 1.1.11.4-2

Return Link Receiver
(LEO-GEO crosslink)
Freq: 59.800 to 60.200 GHz
L.O.: 34.000 GHz

Source	Image	3rd Order Products
GEO to LEO Transmit (Forward) Freq: 57.600 to 58.000 GHz	23.600 to 24.000 GHz 91.600 to 92.000 GHz	10.000 to 10.400 GHz 81.200 to 82.000 GHz 125.600 to 126.000 GHz 149.200 to 150.000 GHz
GEO#1 to GEO#2 Transmit Freq: 54.250 to 56.750 GHz	20.250 to 22.750 GHz 88.250 to 90.750 GHz	11.250 to 13.750 GHz 74.500 to 79.500 GHz 122.250 to 124.750 GHz 142.500 to 147.500 GHz
GEO#2 to GEO#1 Transmit Freq: 61.500 to 64.000 GHz	27.500 to 30.000 GHz 95.500 to 98.000 GHz	4.000 to 6.500 GHz 89.000 to 94.000 GHz 129.000 to 132.000 GHz 157.000 to 162.000 GHz

TABLE 1.1.11.4-3

1.1.11.5 EHF Filter and Multiplexer Technology

To reduce the intrasystem interference among the intersatellite links, proper filtering at receive and transmit frequencies is required. The filter requirements are defined in Paragraph 1.1.11.1. In this section, the feasibility of actual filter implementation is briefly discussed.

Operation at high microwave frequencies (e.g., 60 GHz) imposes new and difficult demands on passive components of the system. This is especially true in the filter and multiplexer areas. Two critical factors which have to be taken into consideration are:

o Additional losses due to decreased conductivity of metal surfaces and increased dielectric losses in dielectrics.

o Extremely small dimensions of typical components and very stringent mechanical accuracy requirements.

In wide band applications (5% and above), lower Q elements can be used in filter design and insertion loss is still acceptable. Typical implementations include:
o Suspended substrate stripline
o Fin line
o Metal strip or septum

Suspended substrate striplines are susceptible to moding at these frequencies; therefore fin line or metal septum (Figure 1.1.11-1) designs present a better choice. Achievable Q's are on the order of 500 and typical losses are on the order of 1.5 dB for a 2% filter.

Higher Q implementations necessary for narrow band filters require the use of waveguide type resonators. Dielectric resonators can also be used; however, substantial development is required in this area.

One of the possible, high Q candidate resonators is the TE011 mode resonator. Field distribution in such a resonator is presented in Figure 1.1.11-2. Typical design parameters (center frequency, physical dimensions, and Q) of the TE011 resonator are shown in Figure 1.1.11-3 (spurious mode frequencies are also shown). The theoretical Q of such a resonator is on the order of 12,000. However, the expected practical value of this parameter is about 40-50% (5000 - 6000) in very narrow bandwidth filters. In addition, the Q of TE011 mode cavity is reduced when it is heavily loaded, a condition that occurs for surprisingly small relative bandwidths on the order of .2% or greater. Taking all these facts into consideration (proposed filters have approximately 3% bandwidth) a realistic Q expectation is on the order of 4000.

The proposed 3-pole and 7-pole Chebyshev filters using assumed Q=4000 are presented in Figures 1.1.11-4 and 5. Theoretically, these filters will give the required performance. However, filter and multiplexer art at EHF frequencies is far away from maturity, and further development of these important components is necessary.
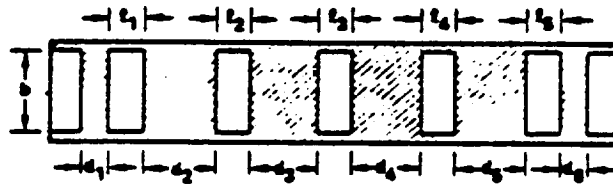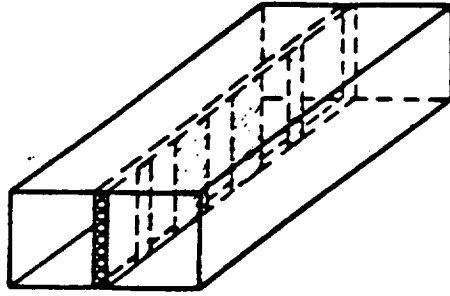
FIGURE 1.1.11-1

METAL SEPTUM (FIN-LINE) FILTER CONFIGURATION.
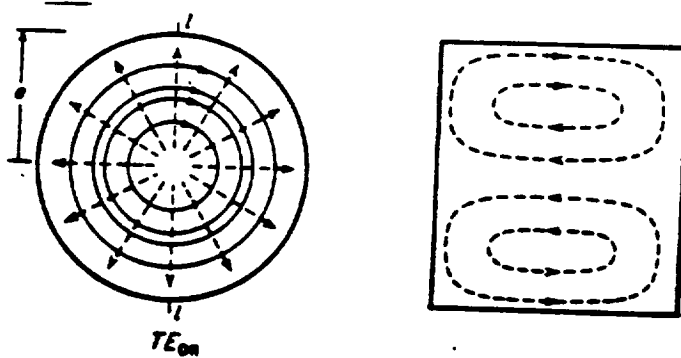
FIGURE 1.1.11-2

TE011 MODE FIELD CONFIGURATION.

TE011

F=   63000.00
D=   .   0.25000

L=   0.23058   V=   0.01132
Q=   11913.40

TE11
     37682.78   58174.45
TM01
     44274.47   62645.86
TE21
     52540.47   68737.00
TE01
     63000.00   77027.75
TM11
     63000.00   77027.75
TE31
     68110.11   81260.45
TM21
     81292.34   92588.98
TE41
     83891.23   94878.94
TE12
     84090.00   95054.73
TM02
     86794.03   97455.00
TM31

FIGURE 1.1.11-3

TE011 MODE RESONATOR DESIGN.

REJECTION/RETURN LOSS DB

3-POLE, 400 MHZ, Q=4000, EHF FILTER

FREQUENCY MHZ

REJECTION/RETURN LOSS DB

FIGURE 1.1.11-4

REJECTION/RETURN LOSS DB
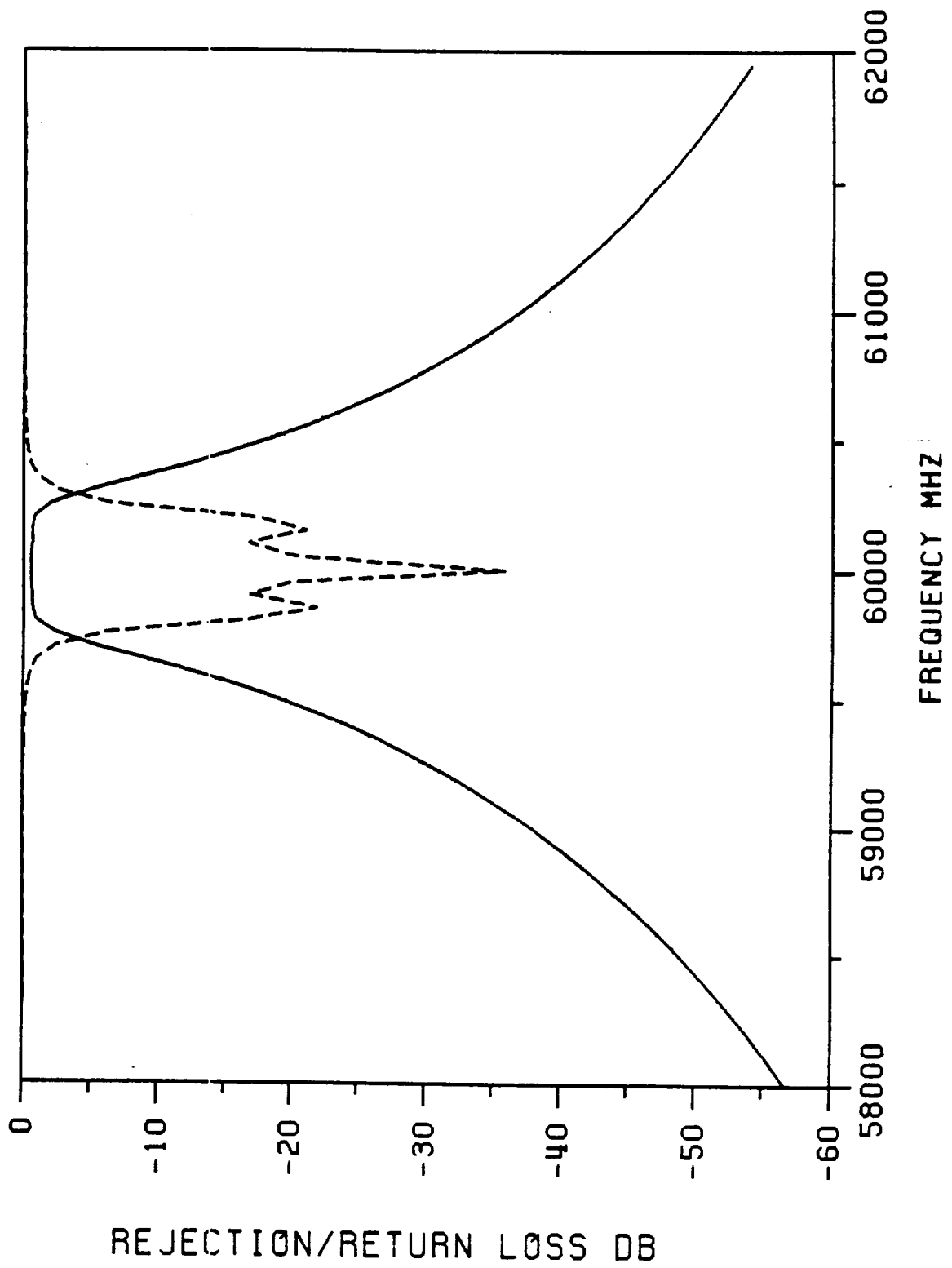
7-POLE, 2500 MHZ, Q=4000, EHF FILTER

FREQUENCY MHZ

FIGURE 1.1.11-5

REJECTION/RETURN LOSS DB
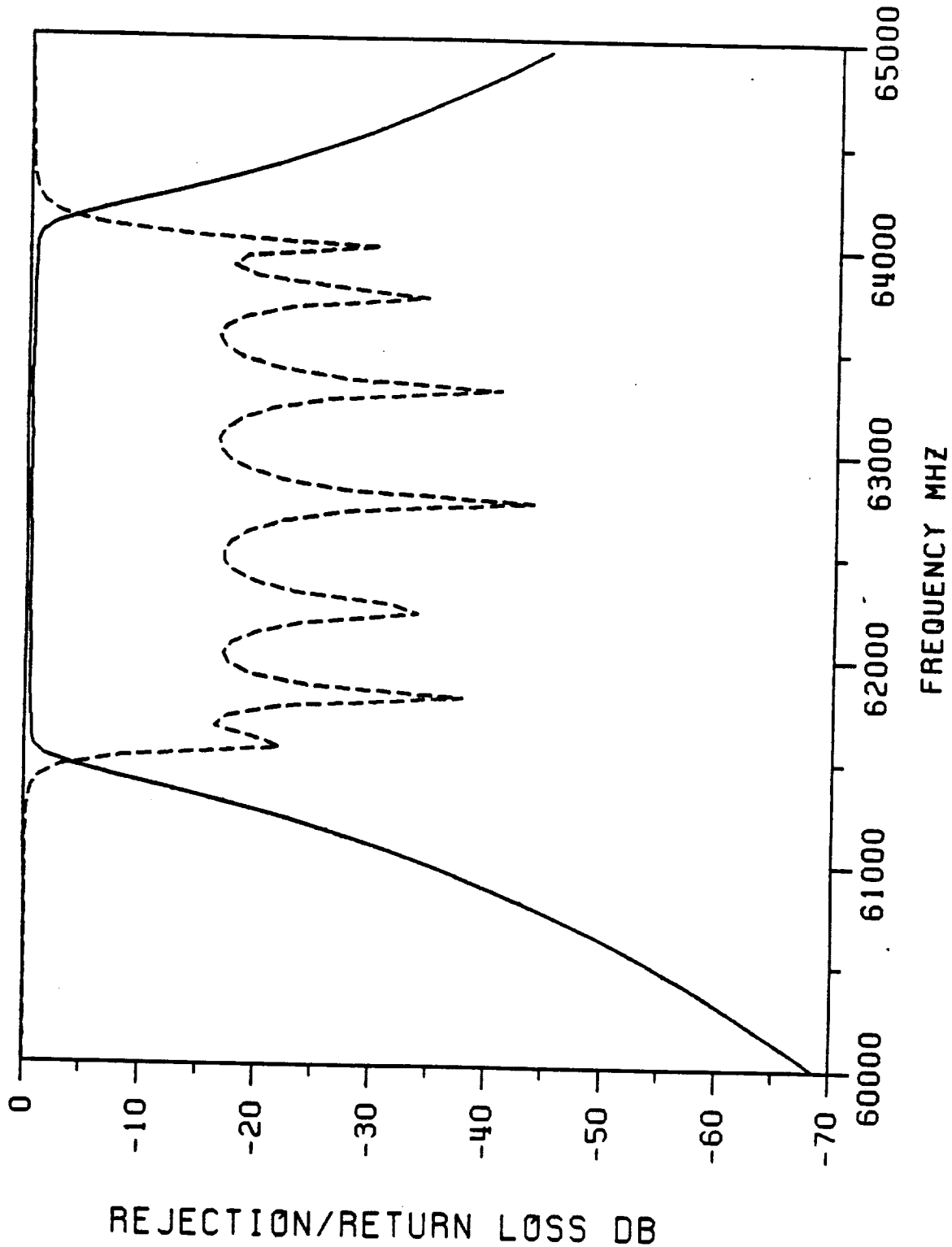
1.1.11.6 Filtering-Caused Link Degradation

Filtering of QPSK data can lead to link degradation due to group delay distortions and intersymbol interference. The group delay of the 7-pole filters will be 1.2 nsec, that of the 3-pole filters is 0.5 nsec. Therefore, in the case of these wide filters, group delay caused degradation is considered to be negligible.

Extensive research has been done on filter distortion and intersymbol interference (1,2,3) and sophisticated computer programs have been developed to simulate these effects. The simulation was applied to the cascaded filters in the crosslink system and the results are shown in the following tables. The results are in the form of the additional power required in the link in order to maintain a given BER.

A parameter used to optimize the system performance is "Clock Phase Offsets" or sampling time error. In the case of an ideal channel with a perfectly matched data detection filter, the optimum sampling time is the data transition time. However, with a mismatched data filter, the optimum sampling time is dependent on the phase transfer function of the filter. For example, usually when a 2-pole Butterworth data detection filter is used, the sampling time should be delayed about 2% for QPSK signals.

Table 1.1.11-1 shows that an additional 0.83 dB of power will be needed to maintain a BER of 10^{-6} in the LEO-GEO link using one 3-pole transmit and one 3-pole receive filter. Adding another 3-pole receive filter at IF increases the link degradation to 1.03 dB when the data rate is 300 Mbps, as shown in Table 1.1.11-2. The data detection filter is an "Integrate & Dump" type; optimum performance is obtained at 2.5% clock phase offsets. Replacement of the I&D filter by a 2-pole Butterworth in this configuration increases the ISI to only 1.06 dB (at clock phase errors of 0%). Table 1.1.11-3 presents the filtering-caused degradation when operating in the sun, i.e. at a data rate of 50 Mbps. In this case the second receive filter (at IF) has been reduced in bandwidth to correspond to the data rate. Results for both an I&D and a Butterworth data detection filter are given. The minor performance improvement resulting from utilization of a matched I&D filter in this application is not deemed significant enough to warrant the technology development that would be required.

Table 1.1.11-4 shows that the normal operating mode of the crosslink (2 Gbps with no sun present) will experience degradation of 0.92 dB utilizing the 7-pole transmit filter and 2 (one at IF) 7-pole receiver filters. The clock phase offsets are -2.5%. The data detection filter is a 2-pole Butterworth with a bandwidth equal to the symbol rate, i.e. 1000 MHz. The Butterworth is a better match for the extreme distortion caused by the 7 poles.

The degradation expected in the GEO-GEO link when in solar conjunction is presented in Table 1.1.11-5. The data rate is reduced to 300 Mbps; thus the IF receiver filter is narrowed to 320 MHz and the Butterworth to 150 MHz. The link degradation is 0.77 dB at a BER of 10^{-6}.

If determined that this degradation will severely impair the quality of the link, a possible compensating technique is to develop transversal filters and/or equalizers to overcome the loss due to bandlimiting.

REFERENCES

1. J. Y. Huang, "Filter Distortion and Intersymbol Effects on BPSK/QPSK/SQPSK/MSK Signals", Final Report, Technical Memo 289, September 1979, Systems Analysis and Synthesis Department, WDL Division, Ford Aerospace and Communications Corporation, Palo Alto, California.

2. J. Jay Jones and W. K. S. Leong, "Analysis of Performance Degradation for a PSK Communication Satellite Channel", Final Report, Technical Memo 242, December, 1974, Communication Sciences Department, WDL Division, Ford Aerospace and Communications Corporation, Palo Alto, California.

3. J. Jay Jones, "Filter Distortion and Intersymbol Interference Effects on PSK Signals", IEEE Trans. on Communication Technology, Vol. COM-19, No. 2, April, 1971, pp. 120-132.

Table 1.11-1

LEO-GEO: No Sun Effect: 2 Cascaded Filters

Number of Chebychev Transmitter Filters   1

Number of Chebychev Receiver Filters   1

Number of Poles, 3-dB Bandwidth (MHz), and Ripple (dB) for Transmit Filters

3, 540, 0.1

Number of Poles, 3-dB Bandwidth (MHz), and Ripple (dB) for Receiver Filters

3, 540, 0.1

Data Rate (Ms/sec)   180

Data Detection Filter   Integrate & Dump

Results

CLOCK PHASE OFFSET = 2.5 PERCENT

AVERAGE BIT ERROR PROBABILITY	QPSK LOSS (DB)
1 e-01	0.45
1 e-02	0.52
1 e-03	0.61
1 e-04	0.69
1 e-05	0.76
1 e-06	0.83
1 e-07	0.88
1 e-08	0.93
1 e-09	0.96

Table 1.1.11-2

LEO-GEO: No Sun Effect: 3 Cascaded Filters

Number of Chebychev Transmitter Filters   1

Number of Chebychev Receiver Filters   2

Number of Poles, 3-dB Bandwidth (MHz), and Ripple (dB) for Transmit Filters

                                            3, 540, 0.1

Number of Poles, 3-dB Bandwidth (MHz), and Ripple (dB) for Receiver Filters

                                            3, 540, 0.1

Data Rate (Ms/sec)   180

Data Detection Filter   Integrate & Dump

Results

CLOCK PHASE OFFSET = 2.5 PERCENT

AVERAGE BIT ERROR PROBABILITY	QPSK LOSS (DB)
1 e-01	0.51
1 e-02	0.62
1 e-03	0.74
1 e-04	0.85
1 e-05	0.95
1 e-06	1.03
1 e-07	1.10
1 e-08	1.15
1 e-09	1.19

Table 1.1.11-3

LEO-GEO: With Sun Effect: 3 Cascaded Filters

Number of Chebychev Transmitter Filters   1

Number of Chebychev Receiver Filters   2

Number of Poles, 3-dB Bandwidth (MHz), and Ripple (dB) for Transmit Filters

                                            3, 540, 0.1

Number of Poles, 3-dB Bandwidth (MHz), and Ripple (dB) for Receiver Filters

                                            3, 540, 0.1
                                            3, 60, 0.1

Data Rate (Ms/sec)   25

Results

CLOCK PHASE OFFSET = 1.0 PERCENT

AVERAGE BIT ERROR PROBABILITY	QPSK LOSS(DB) I&D FILTER	QPSK LOSS(DB) BUTTERWORTH FILTER
1 e-01	0.34	0.65
1 e-02	0.40	0.68
1 e-03	0.48	0.71
1 e-04	0.55	0.74
1 e-05	0.62	0.76
1 e-06	0.68	0.79
1 e-07	0.73	0.81
1 e-08	0.77	0.84
1 e-09	0.81	0.86

Table 1.1.11-4

GEO-GEO: No Sun Effect: 3 Cascaded Filters

Number of Chebychev Transmitter Filters   1

Number of Chebychev Receiver Filters   2

Number of Poles, 3-dB Bandwidth (MHz), and Ripple (dB) for Transmit Filters

7, 2640, 0.1

Number of Poles, 3-dB Bandwidth (MHz), and Ripple (dB) for Receiver Filters

7, 2640, 0.1

Data Rate (Ms/sec)   1000

Data Detection Filter   2-Pole Butterworth, 1000 MHz BW

Results

CLOCK PHASE OFFSET = -2.5 PERCENT

AVERAGE BIT ERROR PROBABILITY	QPSK LOSS (DB)
1 e-01	0.68
1 e-02	0.73
1 e-03	0.79
1 e-04	0.84
1 e-05	0.88
1 e-06	0.92
1 e-07	0.95
1 e-08	0.98
1 e-09	1.00

TABLE 1.1.11-5

GEO-GEO: With Sun Effect: 3 Cascaded Filters

Number of Chebychev Transmitter Filters   1

Number of Chebychev Receiver Filters   2

Number of Poles, 3-dB Bandwidth (MHz), and Ripple (dB) for Transmit Filters

7, 2640, 0.1

Number of Poles, 3-dB Bandwidth (MHz), and Ripple (dB) for Receiver Filters

7, 2640, 0.1
7, 320, 0.1

Data Rate (Ms/sec)   150

Data Detection Filter   2-Pole Butterworth, 150 MHz BW

Results

CLOCK PHASE OFFSET = -1.5 PERCENT

AVERAGE BIT ERROR PROBABILITY	QPSK LOSS (DB)
1 e-01	0.59
1 e-02	0.63
1 e-03	0.67
1 e-04	0.70
1 e-05	0.74
1 e-06	0.77
1 e-07	0.80
1 e-08	0.82
1 e-09	0.84

1.1.12   Codulation Method

The LEO-GEO modulation system concept provides a QPSK modulated signal encoded with a rate 5/6 algebraic code over a 400 MHz bandwidth. The code chosen will be either the low complexity (LC) code of Tanner or the alphabet redundant (AR) Ungerboeck code.

1.1.12.1   Modulation and Coding Issues

The choice of the AR coding technique of Ungerboeck is motivated by the need to obtain high bandwidth efficiency while maintaining a bit error rate of 10^{-6}. The underlying philosophy of AR coding is to integrate coding and modulation to achieve coding gain without increasing bandwidth in a way that is not possible when the modulation and the coding are created independently. To clarify the issues of the combined design, we will discuss in this section the design principles of Ungerboeck and their application in AR coding. The same principles can be applied to the low-complexity (LC) codes of Tanner (1981), an alternative which is attractive because of its potential circuit complexity advantages in a 300 Mb/s system. Our discussion will start from a general setting that ignores the problems of the complexity of implementation; we then discuss why complexity considerations lead to approaches such as AR coding or LC coding.

1.1.12.2   Coding and its Limitations

As is well known in information theory, to achieve the lowest probability of error for transmitting data at a fixed rate across a given channel, the optimum code will map as many data bits as possible into channel codewords or signals that are chosen from the allowed channel sequences. The signals are chosen to be as far apart as possible in the signal space, where the separation is measured in terms of the noise characteristics. For the band-limited AWGN (additive white Gaussian noise) channel the signal space is a Euclidean space of dimension proportional to the duration of the transmission and the signal separation is measured in terms of Euclidean distance. If the mapping is constrained to operate on only small subsets of the data bits into some subspace of the signal space, the achievable probability of error is unavoidably larger than if it is unconstrained. For example, uncoded BPSK is a bit-by-bit mapping of one data bit into a two-dimensional signal space that cannot achieve the BER possible with coded QPSK.

On an AWGN channel, the probability of bit error is affected by three major factors: first, the Euclidean distances between pairs of signals and the shapes of the optimal decision regions; second, the shapes of the decision regions that are realized by the actual decoding algorithm being used; and finally, the distance-preserving properties of mapping of data bit sequences to signals.

To simplify analysis of the first factor, one initially focuses on the minimum Euclidean distance between any pair of signals. At high SNR the probability of error is dominated by the errors due to confusion of the two signals that are closest. If the signal set formed by the combined digital code and modulation scheme is weak, in that there are many pairs of signals that are much closer than they need to be in the Euclidean space, there is no possibility of approaching optimal performance no matter how complex a demodulator-decoder is used. Consider a system where a digital error correcting code with minimum Hamming distance D_{free} is used in combination with a

modulation scheme wherein, in the two-dimensional symbol space, two symbols are separated by a minimum Euclidean distance D_{min}. If the mapping of sets of binary bits to symbols is arbitrary, the square of the minimum Euclidean distance between the ultimate signals can be as low as $D_{free} \cdot D_{min}^2$ because the minimum can be obtained by unconstrained minimization of both parts of the decomposition independently.

The importance of the second issue, the ability of the demodulating-decoding algorithm to achieve optimal decision regions, is widely recognized. Hard decision demodulation followed by algebraic decoding of the binary sequence creates sub-optimal decision regions in the Euclidean signal space. (In some instances, particularly at high SNR, it can be justified on the basis that the effective D_{free} of algebraic error-correcting codes is much greater than that of competing convolutional codes). Convolutional codes are commonly used on satellite channels because the Viterbi algorithm can perform optimal decoding. It should be noted, however, that the exponential dependence of the complexity of Viterbi decoding on the number of encoder states generally means that the convolutional code used is weak. In practice the Viterbi algorithm often is used to decode optimally an error-correcting code that is itself far from optimal.

To reduce the BER that will result from the use of any fixed coding-modulation scheme and algorithm, the mapping of data bit sequences to signals must try to achieve a monotonic relation between the Hamming distance separating data bit sequences and the Euclidean distance separating the corresponding signals. As much as possible, the signals that are closest in the signal space should correspond to data sequences that differ in only one bit. Sequences that differ in two bits should be further apart in the signal space than those differing in one bit, and so forth. In standard convolutional code systems, this motivates the use of noncatastrophic codes and Gray code mapping of encoded bits to symbols. The distance property is usually guaranteed a coarse level by the mapping of small subsets of bits to channel symbols, e.g., 3 bits to one 8-PSK symbol, which permits bounding of the BER in terms of symbol-error probabilities. However, the optimal combined system with this distance-preserving property does not necessarily use a Gray code for each modulation symbol.

1.1.12.3 Shannon Bound on Coding Gain

Like any other communications resource, coding gain is not without its limit. Coding gain can be upper bounded by the Shannon capacity theorem. For a PSK satellite communication channel, the Shannon bound for coding gain (with respect to an $E_b/N_o = 9.6$ dB at BER $= 10^{-5}$) is

Code Rate R	Shannon Bound On Coding Gain (dB)
1/3	10
1/2	9.4
3/4	8.4
7/8	7.1

Since the current state of the art for coding gain is about 5 dB depending on the code rate R, a head room of 2 to 5 dB is theoretically available for future improvement.

1.1.12.4 Elias Bound on Coding Gain

For algebraic block codes, the existence of any particular code is further bounded by an Elias bound (Elias, 1955) as illustrated by Figure 1. The Elias bound is expressed in terms of the normalized Hamming distance versus the code rate R (i.e., the normalized information bit size).

Since the Hamming distance D_{min} is related to coding gain, the Elias bound presumably bounds the coding gain as well. A survey of block codes documented in the literature indicates that the more efficient codes listed are very near the Elias bound itself, suggesting no significant improvement in coding gain is foreseen over those already listed without an inordinate reduction in code rate R. Figure 2 illustrates a few BCH block codes and Reed-Soloman block codes as a function of code rate. The left-hand side ordinate denotes the normalized Hamming distance and the right-hand side ordinate denotes the coding gain.

All coding gains are referenced to the AWGN threshold $Eb/No = 9.6$ dB at a BER = 10^{-5}. For other BER, these gains will be adjusted accordingly.

Figure 3 suggests the following:

a. BCH codes and R-S codes can be used to provide 3-4 dB coding gain. The code rate R should not be less than R = 1/2.

b. Viterbi decoding of convolutional code provides up to 5 plus dB coding gain.

1.1.12.5 Advanced Decoding

By concatenating a suitable block code with a convolutional code, additional coding gain beyond that of Viterbi decoding may be achieved. JPL has reported such a scheme showing a coding gain improvement of 2 dB over the Viterbi at BER = 10^{-5} and even greater gain at lower BER. This scheme requires a great deal of processing and is not considered to be suitable for space borne applications at this time. With the advent of VHSIC and parallel computation algorithm developments of recent years, however, the block/convolutional hybrid approach may be the next technology advance in coding.

1.1.12.6 AR Coding

With this background, the philosophy of AR coding can be addressed. Ungerboeck's technique is to use the finite state memory of a convolutional code to govern and thereby constrain the mapping of subsets of data bits to channel symbols. As in convolutional codes, the data bits select a path through a trellis diagram, and the emitted sequence of channel symbols can be read off of the path edges. The minimum Euclidean distance between signals in the signal space can be determined by finding the minimum sum of squared distances separating signals corresponding to distinct paths in the trellis diagram. The key to the significant coding gain of AR coding is that the minimization of distance is constrained by the carefully selected assignments of bits to channel symbols in the trellis. Simple heuristics for making the assignments are used to guarantee that paths that differ only over relatively few edges are nonetheless separated by a large Euclidean distance because the channel symbols in which they differ are themselves chosen to be far apart.

In contrast with the result of the arbitrary mapping found in a completely independent construction, when the underlying convolutional code achieves its D_{free}, the D_{min} of the modulation is deliberately not achieved. Thus the constrained minimization of the Euclidean distance yields a much larger minimum than for the independent system. To take advantage of this improvement in the ultimate signal set, Ungerboeck uses the optimal Viterbi decoder.

Using computer search techniques common in the construction of standard convolution codes, Ungerboeck (1982) demonstrated that AWGN coding gains of up to 6 dB in the error-event probability are possible. Biglieri (1984) confirmed this potential on the nonlinear satellite channel.

1.1.12.7 LC Coding

Another technique is the low-complexity coding technique of Tanner (1981). Tanner has shown that it is possible to combine the power of algebraic code construction with probabilistic decoders that are very well adapted to high-speed parallel implementations in VLSI. In contrast to convolutional codes with Viterbi decoding, Tanner's algebraic techniques permit the construction of codes with minimum Hamming distances comparable to those of the best algebraic codes. Indeed, in Tanner (1983) an algebraic theory is developed that leads to the construction of codes more efficient than any previously known code of any type. The decoding algorithm B of Tanner (1981, pp. 541-542) can be used to decode many such codes using Euclidean distance information. Although algorithm B is not optimal, it has been shown to approximate an optimal decoding algorithm in a number of cases. LC coding may be able to outperform a Viterbi algorithm used on a weaker AR code by using this suboptimal algorithm on a stronger code. To compete with AR coding, it is necessary to show that the assignment of channel symbols to subsets of bits for these LC codes can be done in accordance with the philosophy of AR coding, and thus yield a combined code-modulation scheme with superior Euclidean distance properties. At the current time, by use of the flexible algebraic theory of Tanner this appears plausible, and Ford Aerospace has thus chosen LC coding as the baseline approach to the problem.

The advantage of LC decoding is its potential for reducing hardware complexity. As stated by Ungerboeck, "Improvements on the order of 6 dB require codes with about 2^{10} states." A Viterbi decoder requires real number computations for each state as each channel symbol arrives. In contrast, Tanner's algorithm B uses bounded precision integer arithmetic and is amenable to complete parallelism and pipelining at many levels. In an unpublished study, preliminary VLSI floorplans for a decoder for a (4968, 4096) block code to operate on a 10 Mb/s disk channel were developed. The decoder could fit on a single VLSI chip of complexity roughly equivalent to that of an NMOS 64K RAM. Comparable miniaturization of the satellite decoder would have substantial power and weight advantages.
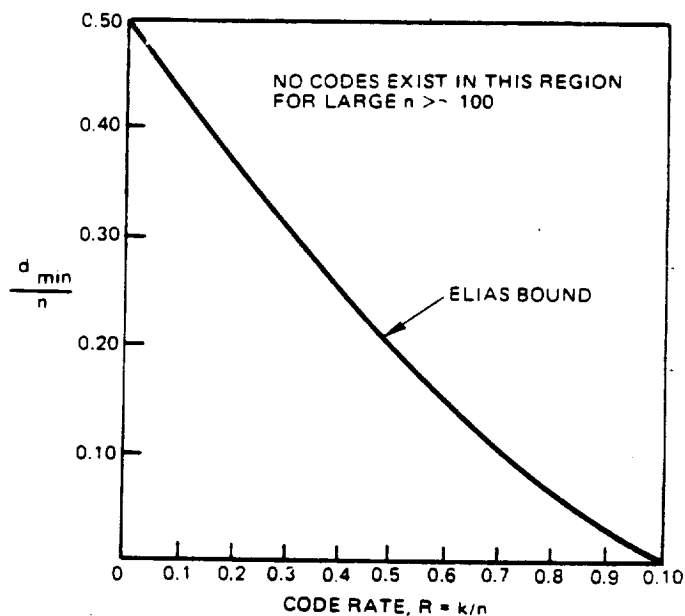
FIGURE 1.1.12-1

Elias Bound on Coding Gain
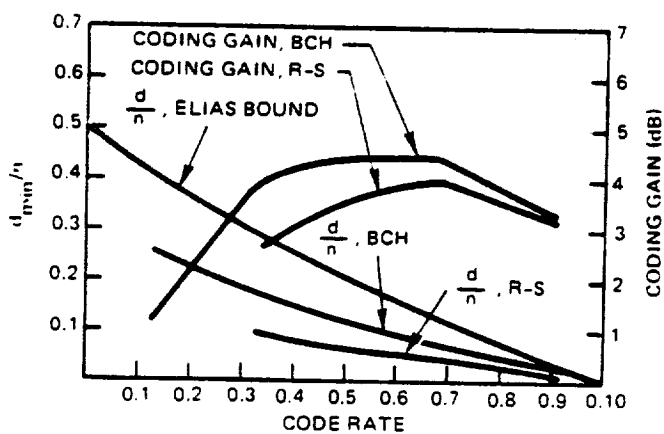
FIGURE 1.1.12-2

R-S and BCH Code Performance Envelope
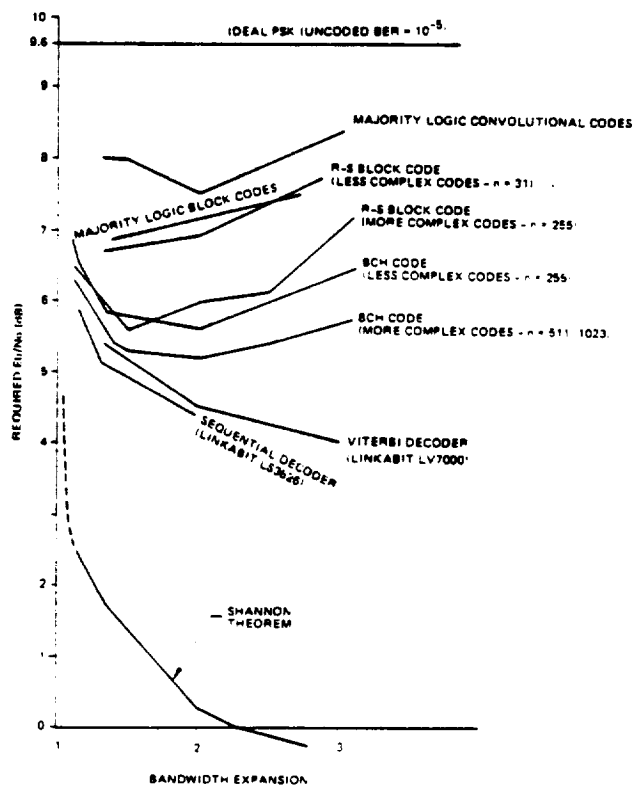
FIGURE 1.1.12-3

State-of-the-Art Decoder Envelope

REFERENCES

1. Elias, P., "Coding for Noise Channels," IRE Convention Record, Part 4, 1955

2. Tanner, R.M., "A Recursive Approach to Low Complexity Codes", IEEE Trans. Inform. Theory, Vol. IT-27, No. 5, pp. 533-547, September, 1981

3. Tanner, R.M., "A Transform Theory for a Class of Quasi-Cyclic Codes", IEEE International Symposium on Information Theory, Quebec, Canada September, 1983

1.1.13 Weight, Power and Size

The weight, size and power table for the intersatellite link equipment aboard the TDAS follows. The increased weight in the TOTAL PER USAT row reflects the weight of the redundant equipment. The power consumption does not increase with the addition of the redundant units because only one of any redundant pair will be operational at any one time. The TOTAL PER SPACECRAFT weight and power reflects the 5 USAT systems aboard the TDAS; the DC/DC converters are dependent on the power requirements of the other equipment. The microprocessor and antenna controllers are not considered in this table. Weights and powers of this equipment for all the systems (including the crosslink) are given in Table 1.2.8. The redundancy levels assumed herein are the same as those assumed in Section 1.1.14, Reliability Prediction Assessment.

GEO EQUIPMENT (GEO-LEO LINK)	Qty	PER UNIT DATA Weight lbs.	Power W	Size in x in x in	Redundancy
LEO-GEO Receiver (RF Portion)	1	4.3	28	5 x 4 x 2 / 1 x 3 x 3/4	1
QPSK Demodulator & FEC Decoder	1	4	16	3 x 6 x 2	1
GEO Ranging Subsystem	1	0.5	0.6	4.5 x 4.5 x 3/4	-
BPSK Modulator (1Mb/s) & L.O.	1	4.1	18.2	3 x 4 x 1 / 5 x 4 x 2	1
Transmitter (0.6 W)	1	0.3	6.3	3.3 x 2 x 1	1
Feed Assembly	1	3.3	-	4 x 4 x 18	-
Antenna (0.9 m)	1	7.3	-	0.9 m x .9 x .3	-
Gimbal Subsystem	1	28	9*(32**)	14 x 13.5 x 11	-
Gimbal Drive Electronics	1	5	4.5	8.5 x 2.6 x 5.7	1
Acquisition & Tracking Receiver	1	1.2	4	3 x 6 x 2	1
TOTAL PER OPERATIONAL SYSTEM PER USAT		58.0	86.6		
TOTAL PER USAT		76.9			
TOTAL PER SPACECRAFT		384.5	483.0		
DC/DC Converter	1	10.0	108.0	3 x 6 x 2	2
TOTAL PER SPACECRAFT		414.5	541.0		
* Average ** Peak					

1-111

1.1.14 Reliability Prediction Assessment

The reliability prediction assessment has been updated to incorporate current design information for the ISL with both GEO to GEO and GEO to LEO configurations considered. The reliability aspects of the design are discussed in more detail in the following sections. The reliability assessment compares ISL design configurations with and without hardware redundancy. The reliability results for 10 years are summarized as follows:

ISL 10 year Reliability

	GEO to GEO*	GEO to LEO*
ISL without redundancy	0.2588	0.4911
ISL with redundancy	0.7745	0.9425

*Results do not include the antenna microprocessor or controllers

1.1.14.1 Reliability Model without Redundancy

The ISL reliability model (baseline) for the ISL without redundancy is shown in Figure 1.1.14-1. the basic reliability assumptions for the baseline reliability model include:

o High reliability parts and components in accordance with typical long life spacecraft

o Part derating policies in accordance with MIL-STD-1547 and PPL-17 for 10 year mission life

o 12 year design life for electronics and active mechanical assemblies

o Operating temperatures for assemblies typical of 3-axis spacecraft operating in geosynchronous orbit

o Failure rates for piece parts in accordance with MIL-HDBK-217D, Notice 1

FUNCTIONAL MODEL

	1	2	3	4	5	6	7	8
	ANTENNA AND FEED	FILTER	RECEIVER	DEMOD	TRACKING & ACQUISITION RECEIVER	MODULATOR	TRANSMITTER	FILTER

GEO - GEO*

	1	2	3	4	5	6	7	8
F.R. (10^{-9})	—	5	1508	1095	1721	1545	8430	5
Ps (10 YRS)	0.9066	0.9996	0.8763	0.9085	0.8601	0.8734	0.4778	0.9996
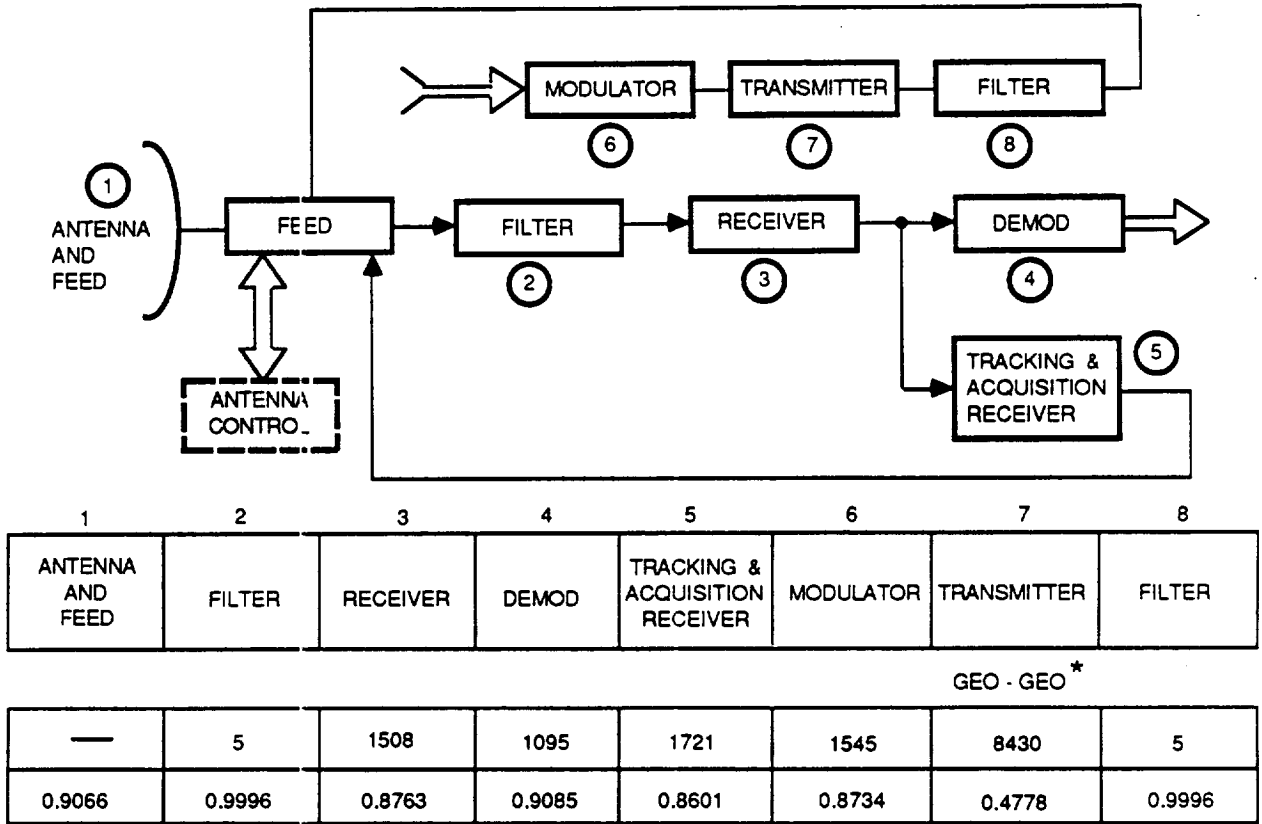
RELIABILITY BLOCK DIAGRAM

MATH MODEL

$$Ps(t) = P_1 \ P_2 \ P_3 \ P_4 \ P_5 \ P_6 \ P_7 \ P_8$$

* NOTE: GEO TO LEO TRANSMITTER F.R. = 1120, Ps (10 YRS) = 0.9065

Ps (10 YRS)	
GEO TO GEO	0.2588
GEO TO LEO	0.4911

ISL RELIABILITY MODEL
(NO REDUNDANCY)

FIGURE 1.1.14-1

1.1.14.2 ISL with Redundancy

Figure 1.1.14-2 provides a design for the ISL incorporating two for one redundancy for all active electronics including the input receiver, tracking and acquisition receiver, demodulator, modulator, and transmitter. Two for one redundancy is also incorporated in the antenna and feed design for the gimbal driver circuitry, motor windings, optical encoders, and the modulator drivers. This level of redundancy is considered the minimum required for a spacecraft design. It is also sufficient at this time to meet the 10 year mission requirements. Higher levels of redundancy could be required if transmitter reliability is lower than assumed in this analysis. The reliability considerations in addition to those assumed for the baseline ISL design include:

o A minimum two for one redundancy is required for all powered electronic assemblies including motor windings for 10 year mission life and avoidance of single point failures

o Redundancy is not practical for passive items such as filters, switches, and passive mechanical items in the antenna and feed assembly

o A standby failure rate of 10% of the active rate for nonoperating electronic assemblies

1.1.14.3 Antenna and Feed Reliability

The antenna and feed reliability model is shown in Figure 1.1.14-3. The appropriate results from this model are included in the higher level reliability models of Figures 1.1.14-1 and 1.1.14-2. The antenna and feed configuration has a 10 year probability of success of 0.9066 without redundancy in the design. The reliability improves to 0.9846 when two for one redundancy is incorporated in the gimbal drive electronics, motor windings, optical encoders, and modulator drivers. This level of redundancy is considered both practical and necessary for a 10 year mission. Redundancy for other components in the antenna and feed is not practical to implement and the risk of failure for the passive components is sufficiently low (primarily restricted to low probability structural or mechanical failures).

1.1.14.4 Hardware Reliability

The following sections provide the details for the reliability estimate of the hardware items in the ISL. The failure rates for the component items are derived from similar component designs on current programs, MIL-HBDK-217D estimates for piece parts, and engineering estimates.

FUNCTIONAL MODEL
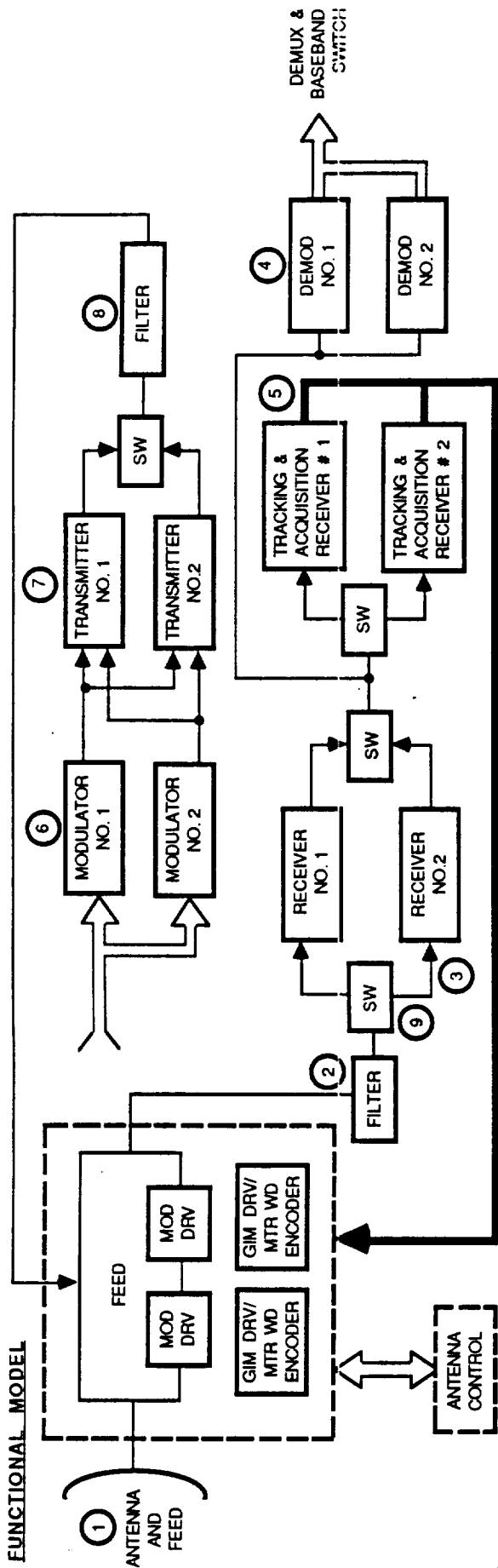
	1	2	3	4	5	6	7	8	9
	ANTENNA AND FEED	FILTER	RECEIVER	DEMOD	TRACKING & ACQUISITION RECEIVER	MODULATOR	TRANSMITTER	FILTER	SWITCH PORT
F.R. (10⁻⁹)	—	5	1508	1095	1721	1545	4210	5	10
Ps (10 YRS)	0.9346	0.9996	0.8763	0.9085	0.8601	0.8734	06916	0.9996	0.9991

* GEO TO GEO

RELIABILITY BLOCK DIAGRAM

Ps (10 YRS)	
GEO TO GEO	0.2588
GEO TO LEO	0.4911

ISL RELIABILITY MODEL
(WITH REDUNDANCY)
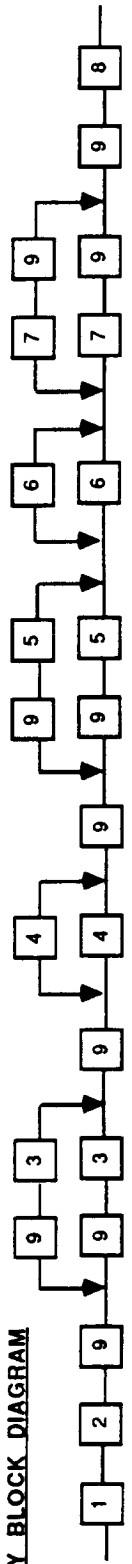
MATH MODEL

$$Ps(t) = P_1 P_2 P_9 (P_9 P_3) \{11 \cdot 10 (P_9 P_3)^{0.1}\} P_9 P_4 \{11 \cdot 10 P_4^{0.1}\} P_9 (P_9 P_5) \{11 \cdot 10 (P_9 P_5)^{0.1}\} P_6 \{11 \cdot 10 P_6^{0.1}\} (P_7 P_9) \{11 \cdot 10 (P_7 P_9)^{0.1}\} P_9 P_8$$

* NOTE: GEO TO LEO TRANSMITTER Ps (10 YRS) = 0.9065 (λ = 1120)

FIGURE 1.1.14-2

FUNCTIONAL MODEL:

TO RECEIVER

HORN — MODE COUPLER — SEPTUM POLARIZER — COUPLER

TRACKING NETWORK — TRACKING MODULATOR — DRIVER

FEED LAYOUT

ANTENNA CONFIGURATION

PLANAR MIRROR

INTERFACE TUBE
PARABOLIC MIRROR
OPTICAL MIRROR
GIMBAL DRIVE ELECTR
DC TORQUE MOTOR

GIMBAL/BEAM WG LAYOUT

FEED

	1 SUBREFLECTOR AND SUPPORT	2 MAIN REFLECTOR	3 GIMBAL/BEAM WG/MOTOR	4 SHAFT/GEARS	5 GIMBAL DRIVE ELECTR	6 MOTOR WINDINGS	7 OPTICAL ENCODER	8 FEED HORN	9 MODE COUPLER	10 SEPTUM POLARIZER	11 COUPLER	12 TRACKING NETWORK	13 TRACKING MODULATOR	14 DRIVER
F.R.(10^{-9})	5	3	105	12	674	100	50	0.3	2.7	5.6	0.3	1.6	10	150
P_s(10 YRS)	0.999562	0.999737	0.990844	0.998949	0.942667	0.991278	0.995630	0.999974	0.999764	0.999510	0.999974	0.999860	0.999124	0.926946

RELIABILITY BLOCK DIAGRAM

(NO REDUNDANCY)

1 — 2 — 3 — 4 — 5 — 6 — 7 — 8 — 9 — 10 — 11 — 12 — 13 — 14

(WITH REDUNDANCY)

1 — 2 — 3 — 4 — [5 6 7 / 5 6 7] — 8 — 9 — 10 — 11 — 12 — 13 — [14 / 14]
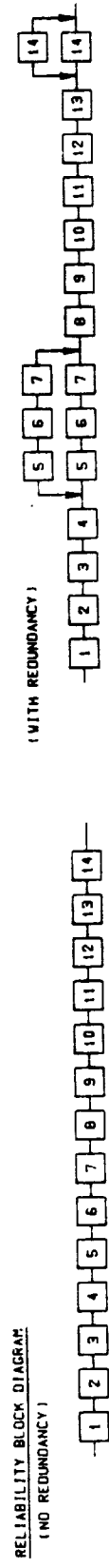
MATH MODELS

(NO REDUNDANCY) $P_s(t) = \pi_{i=1}^{14}\, P_i = 0.9066$

(WITH REDUNDANCY) $P_s(t) = \pi_{i=1}^{14}\, P_i \left[1-(1-(P_5 P_6 P_7)^{0.1}\right]\left[1-(1-P_{14})^{0.1}\right] = 0.9846$

ANTENNA AND FEED RELIABILITY MODEL

Figure 1.1.14-3

1.1.14.4.1 Input Receiver

The failure rate of the input receiver is calculated as follows:

Input Receiver Failure Rate (10^{-9})

Item	Component failure rate	n	Total failure rate
RF preamp (HEMT)	50	1	50
Mixer	100	1	100
IF Amplifier (GaAs FET)	103	1	103
V-Band L.O.		1	
Isolator	5	4	20
Power Divider	10	2	20
Mixer	100	3	300
V-Band GUNN Osc.	600	1	600
Loop filter	10	1	10
Band pass filter	5	2	10
Amplifier	20	1	20
Low pass filter	5	1	5
Correction amplifier	20	1	20
Multiplier	30	1	30
Divider	30	1	30
SAW VCO (UHF)	30	1	30
XTAL oscillator	50	1	50
Loop amplifier	20	1	20
DC/DC converter	90	1	90
	Total failure rate		1508

1.1.14.4.2 Demodulator

The failure of the demodulator is calculated as follows:

Demodulator Failure Rate (10^{-9})

Item	Component failure rate	n	Total failure rate
Mixer	100	5	500
Low pass filter	5	4	20
Loop filter	20	1	20
Limiter	20	2	40
VCO	25	1	25
Summer	75	1	75
Sample/latch	50	2	100
Bandpass filter	5	1	5
T/2	30	2	60
PPL	60	1	60
Clock	100	1	100
DC/DC converter	90	1	90
	Total failure rate		1095

1.1.14.4.3 Acquisition and Tracking Receiver

The failure rate of the acquisition and tracking receiver is calculated as follows:

Acquisition and Tracking Receiver Failure Rate (10^{-9})

Item	Component failure rate	n	Total failure rate
Mixer	100	3	300
IF Amplifier (GaAs FET)	103	2	206
Bandpass filter	5	1	5
AM detector	20	1	20
Lowpass filter	5	3	15
DC amp	20	1	20
L.O.	400	1	400
Scan generator	200	1	200
Timing generator	250	1	250
Summer	75	1	75
Threshold logic	90	1	90
Demux	50	1	50
DC/DC converter	90	1	90
	Total failure rate		1721

1.1.14.4.4 Modulator

The failure rate of the modulator is estimated as follows:

Modulator Failure Rate (10^{-9})

Item	Component failure rate	n	Total failure rate
V-Band oscillator (see input receiver)	1165	1	1165
3 db power divider	10	1	10
Biphase switch	130	2	260
3 db power combiner	10	1	10
Microstrip/WG transition	10	1	10
DC/DC converter	90	1	90
	Total failure rate		1545

1.1.14.4.5 GEO to GEO Transmitter

The failure rate of the GEO to GEO transmitter is almost entirely dependent upon the assumptions concerning the IMPATT diode failure rate and the number of allowable diode failures. In this analysis, it is assumed that the diode failure rate is 500 FITs (see 1.1.14.5) and that all diodes are required for successful transmitter operation. The estimate is as follows:

GEO to GEO Transmitter Failure Rate (10^{-9})

Item	Component failure rate	n	Total failure rate
Mixer	100	1	100
Crystal controlled osc (temp controlled over)	250	1	250
Isolator	10	3	30
Amplifier (1 IMPATT)	520	1	520
Amplifier (2 IMPATTs)	1050	1	1050
Amplifier (4 IMPATTs)	2120	1	2120
8-way combiner & ampl. (8 IMPATTs)	4240	1	4240
DC/DC Converter	120	1	120
		Total failure rate	8430

1.1.14.4.6 GEO to LEO Transmitter

The failure rate of the GEO to LEO transmitter is estimated as follows:

GEO to LEO Transmitter Failure Rate (10^{-9})

Item	Component failure rate	n	Total failure rate
Mixer	100	1	100
Crystal controlled osc. (temp controlled oven)	250	1	250
FET preamp	150	1	150
Isolator	10	1	10
Amplifier (1 IMPATT)	520	1	520
DC/DC converter	90	1	90
		Total failure rate	1120

1.1.14.5 IMPATT Diode Reliability

The reliability estimates provided in this assessment are heavily dependent on the assumptions for transmitter reliability which in turn are dependent on IMPATT diode reliability. The best source for IMPATT diode reliability is MIL-HDBK-217D, Notice 1. The point estimate is 500 FITs (10^{-9}) per diode. The 217D data, however, is based on a small amount of available IMPATT diode data as well as some engineering data. The IMPATT diode data provided in 217D does not differentiate failure rates for power ratings, application frequencies, or the nature and history of the technology.

Previous discussions with researchers and users of IMPATT diodes uncovered no substantial reliability data. These discussions clearly indicated that 1) there is apparently no serious work in progress to characterize failure rates for IMPATT diodes by the Air Force, Aerospace Corporation or RADC (the authors of 217D); 2) more definitive failure rate data on IMPATT diodes is unlikely in the near future. It can only be hoped that manufacturers of these devices will provide some useful data. As a result of the reliability risk associated with using IMPATT diodes, which is attributed to lack of data, a conservative design approach is required both in terms of redundancy and derating.

1.1.14.6 Antenna Control Electronics

The baseline antenna control electronics in the ISL concept design consists of a centralized antenna control microprocessor (ACM) which feeds 6 antenna controllers (AC). A separate AC provides the positioning signals to the antenna gimbal mechanism for each ISL transponder. The failure rates for the ACM and AC electronics are estimated as follows:

ACM Failure Rate (10^{-9})

Item	Component failure rate	n	Total failure rate
Processor circuits	500	1	500
4K x 8 ROM	250	1	250
8K x 8 RAM	600	1	600
Interface circuits	150	6	900
DC/DC converter	90	1	90
		Total failure rate	2340

ACM Failure Rate (10^{-9})

Item	Component failure rate	n	Total failure rate
Processor circuits	500	1	500
4K x 8 ROM	250	1	250
8K x 8 RAM	600	1	600
Interface circuits	150	2	300
DC/DC converter	90	1	90
		Total failure rate	1740

Figure 1.1.14-4 provides three concepts for implementation of the ACM and AC processors. The simplest concept is the use of one ACM and six ACs without redundancy. The ten year probability of success for this scheme is 0.3264. This approach is not considered viable for a spacecraft application and some concept with full redundancy of the ACM and AC processors is required.

One redundancy approach is to use 2 for 1 redundancy for the ACM and full cross-strapping to 6 sets of 2 for 1 redundant ACs. It is further assumed that some sort of communication bus scheme between the ACMs and ACs is used to minimize the number of signal paths. It is estimated that the 10 year probability of success for such a scheme would be greater than 0.91.

A second redundancy approach could be to integrate an ACM with 6 ACs. This approach would reduce the number of DC/DC converters from 14 to only two for the processor electronics and also would reduce the number of interface circuits between the ACM and AC functions since internal busing could be used. A second integrated backup unit would be used for 2 for 1 redundancy. The 10 year probability of success for this type of scheme with the assumed failure rate for each unit being 3540 FITs is greater than 0.95.

Further work is required to optimize the reliability of the entire antenna positioning electronics scheme. However, some sort of integrated (combined) electronics approach is suggested. At this time it is assumed that cross-strapping would take place at the output of the 6 ACs within each unit for the integrated approach for cross-strapping to the gimbal drive circuits. The integration could also include the gimbal drive circuits with cross-strapping to the motor windings (or dedicated motor windings to each integrated unit).
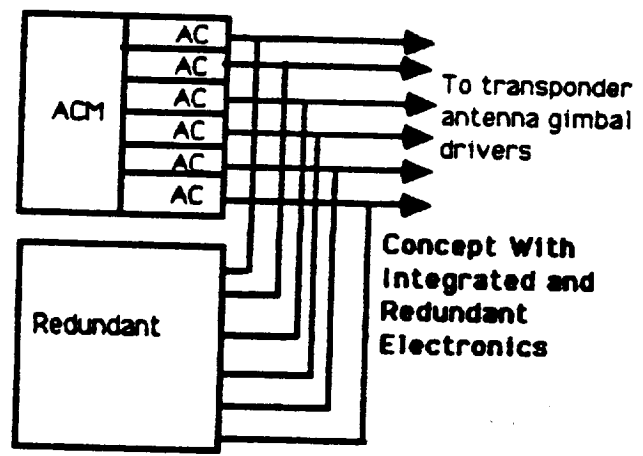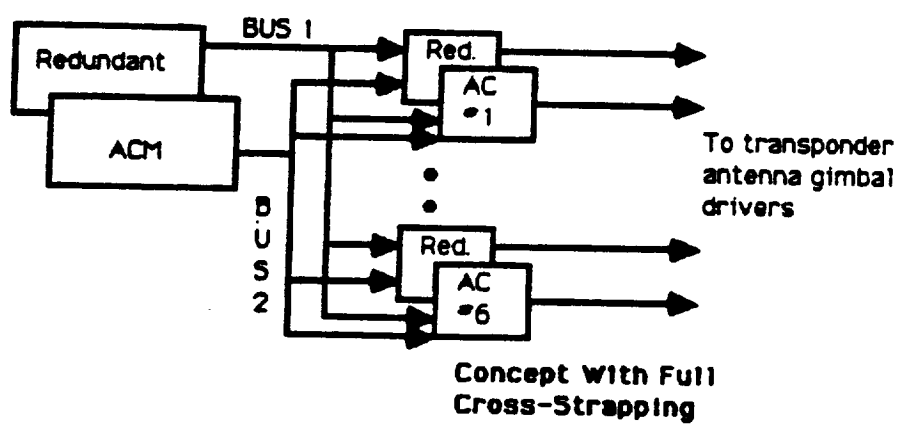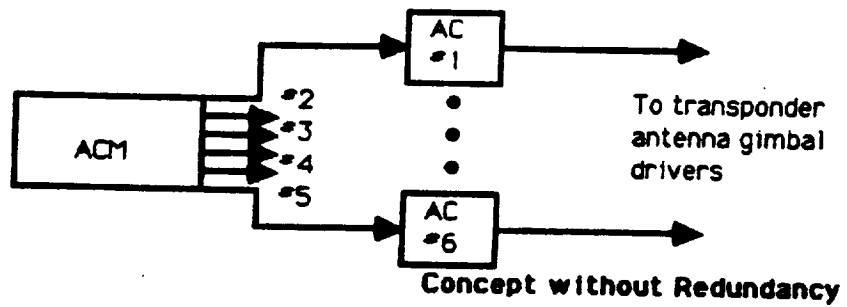
Figure 1.1.14-4 - ANTENNA CONTROL

1.2　Geosynchronous-Geosynchronous System Design

The GEO-GEO link system design is based on NASA requirements. The requirements have been analyzed and allocated into functional areas within the architectural, operational and technical boundary of the projected 1989 time frame. The allocated functional areas in turn offered a range of configuration possibilities suitable for parametric and qualitative trade off analyses and iterations.

In the course of this process, each major configuration component was addressed as a subset of interacting system parameters. Starting with the initial link interface definition and a set of judiciously selected candidate component items, the link system was designed iteratively. The impact and sensitivity of each component item upon the entire payload package as well as TDAS was assessed along the way until a most viable design was developed. Also, the following ground rules were used as a measure of effectiveness in order to ensure an objective design optimization:

o　Use 1989 timeframe cutoff technology.

o　Minimize overall weight and power needs imposed on TDAS.

1.2.1　Link Closure Parameters

Link closure parameters are presented in Tables 1.1.1-1 and 1.1.1-2.

1.2.2　Acquisition and Tracking

1.2.2.1 Acquisition

It is intended that the two geosynchronous satellites maintain contact at all times, including solar conjunctions, therefore the acquisition sequence should be performed only once. At worse, we assume that re-acquisition will occur rarely. The GEO-GEO acquisition sequence is as illustrated in Figure 1.2.2-1.

The GEO 1 satellite points its antenna to position 1 of its scanning pattern (see Figure 1.2.2-1). The GEO 2 satellite then searches through the seven positions of its scan pattern. If the GEO 2 finds the signal from the GEO 1, it signals the GEO 1 of acquisition and starts monopulse tracking. The GEO 1 satellite, upon receiving the success signal from the GEO 2, also initiates monopulse tracking. If the GEO 1 does not receive a success signal from the GEO 2 within a fixed time period, it moves its antenna to position 2 of its scanning pattern and the GEO 2 again searches through its seven scan locations. This process continues until acquisition is achieved.

1.2.2.2 GEO/GEO Tracking

From Figure 1.2.2-2, it can be seen that the situation for the GEO/GEO antenna is somewhat different from that of the GEO/LEO discussed in Section 1.1.2.2.

o Platform rate compensation can be quite important, because platform motion is its only dynamic tracking requirement.

o The loop gain/bandwidth required to meet 0.1 beamwidth/0.1 dB tracking loss is 0.1/sec, implying that all that is needed from 3.2 m antenna structure is a little better than a 0.1 Hz locked-rotor-frequency.

The later factor dramatically illustrates the utility of the platform motion compensation scheme. By making use of a relatively straightforward onboard computation process, the mechanical design constraints on the gimbal system for this antenna are relayed, with a presumed subsequent weight reduction advantage.

1.2.3 Block Diagrams

The block diagrams unique to the GEO-GEO system are shown in Figures 1.2.3-1 through 1.2.3-5.

FIGURE 1.2.2-1

GEO-GEO ACQUISITION

Either one of the 2 GEO can acquire the other as follows:

1. GEO 1 - rotates its axis to form 7 sequential main
    lobes, as shown

2. GEO 2 - Perform optimized spatial
    search requiring 4 sec. for
    each of GEO #1 main lobe.

    - Worst case total search
      time is 27 sec.

3. GEO 2 - Signal GEO #1 of acquisition

4. Both GEO #1 and GEO #2 initiate monopulse tracking

BEAMWIDTH
0.117°

0.3°
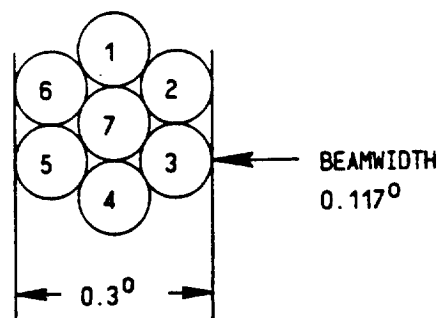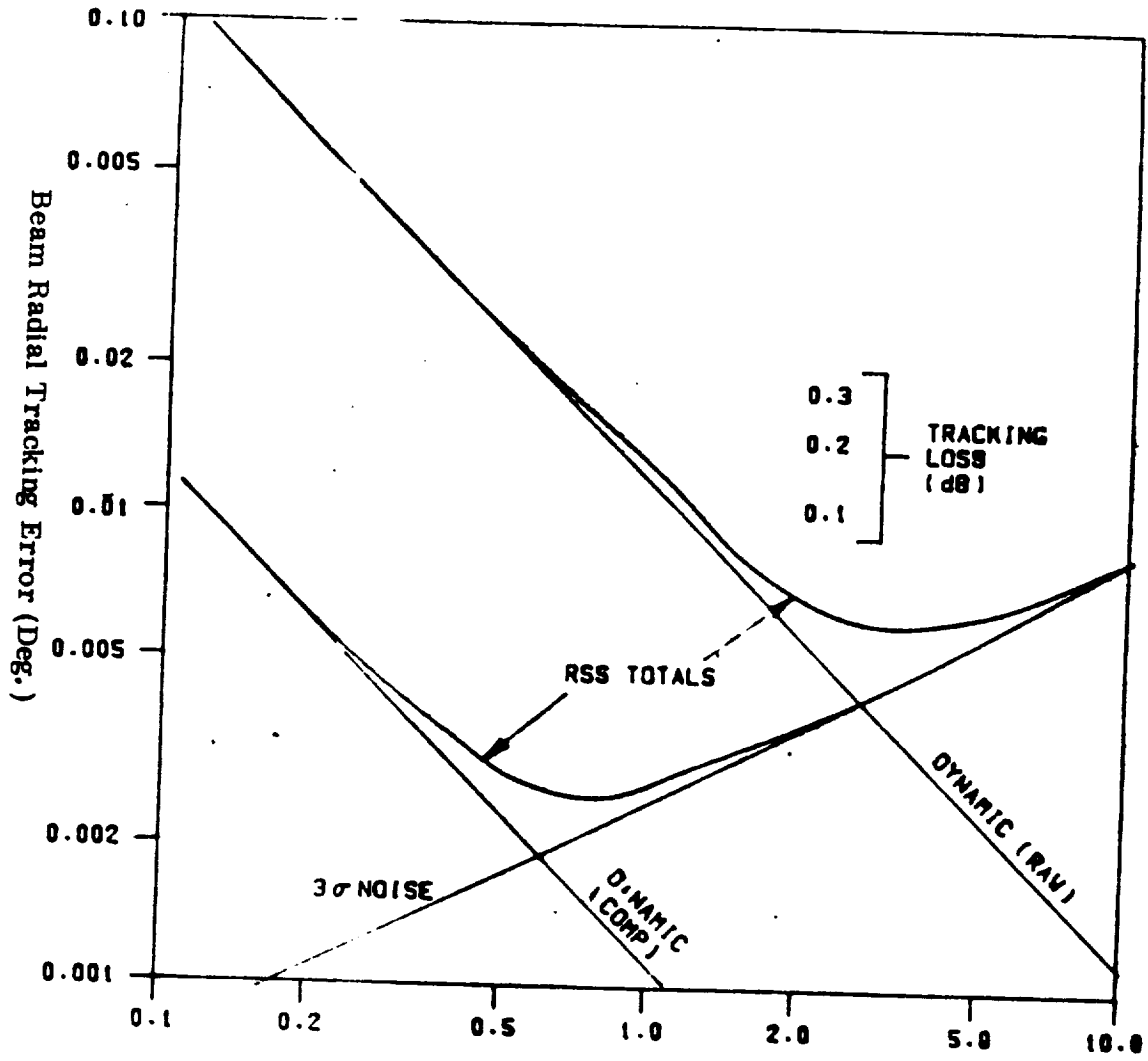
AUTOTRACKING ACCURACY - GEO/GEO

Figure 1. 2. 2. -2

EIRP = 71.7 DBW
G/T = 25.63 DB/K (WITH SUN EFFECT)
G/T = 35.09 DB/K (NO SUN EFFECT)
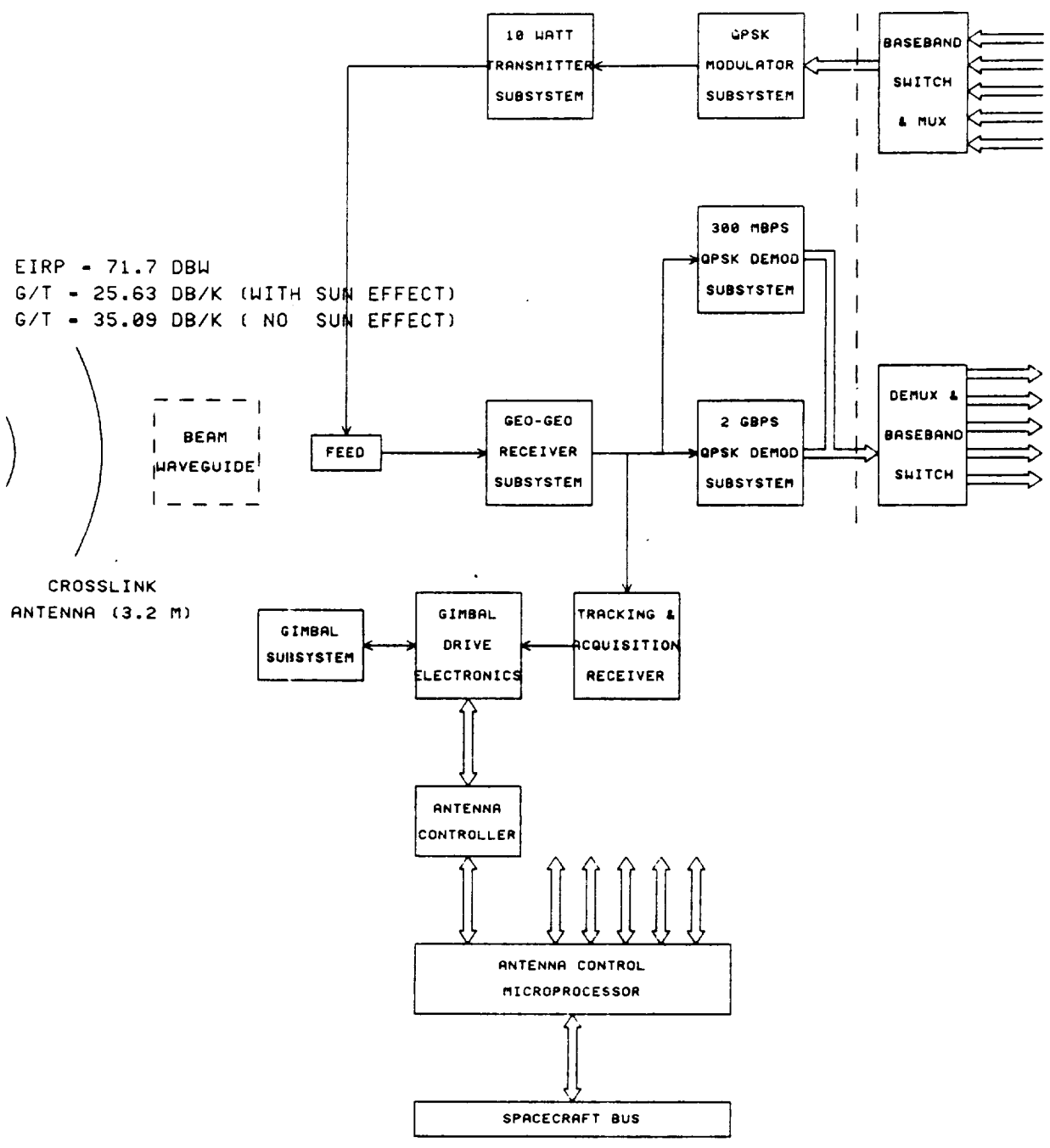
GEO-GEO

CROSSLINK COMMUNICATION SYSTEM

Figure 1. 2. 3-1

10/7.5 WATT IMPATT AMPLIFIER
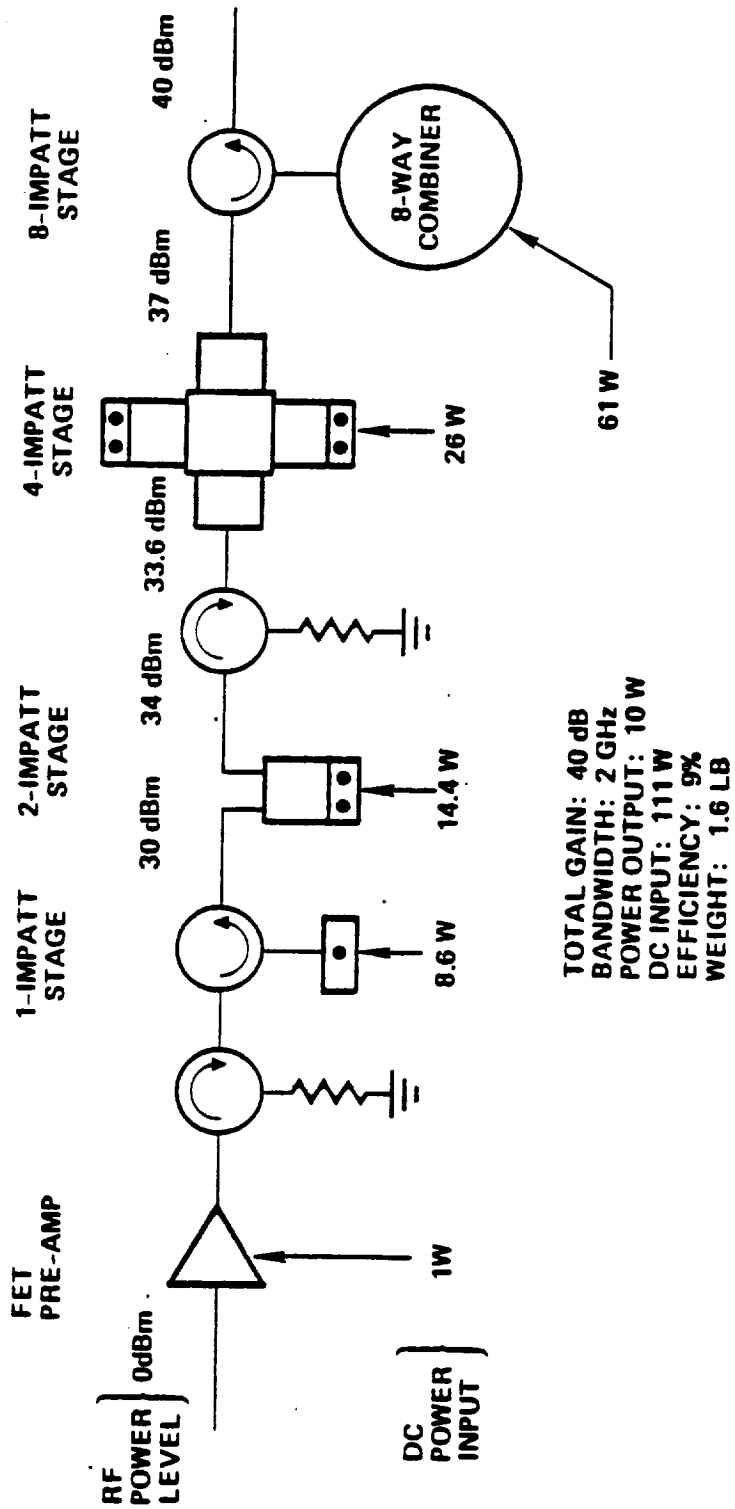
FIGURE 1.2.3-2
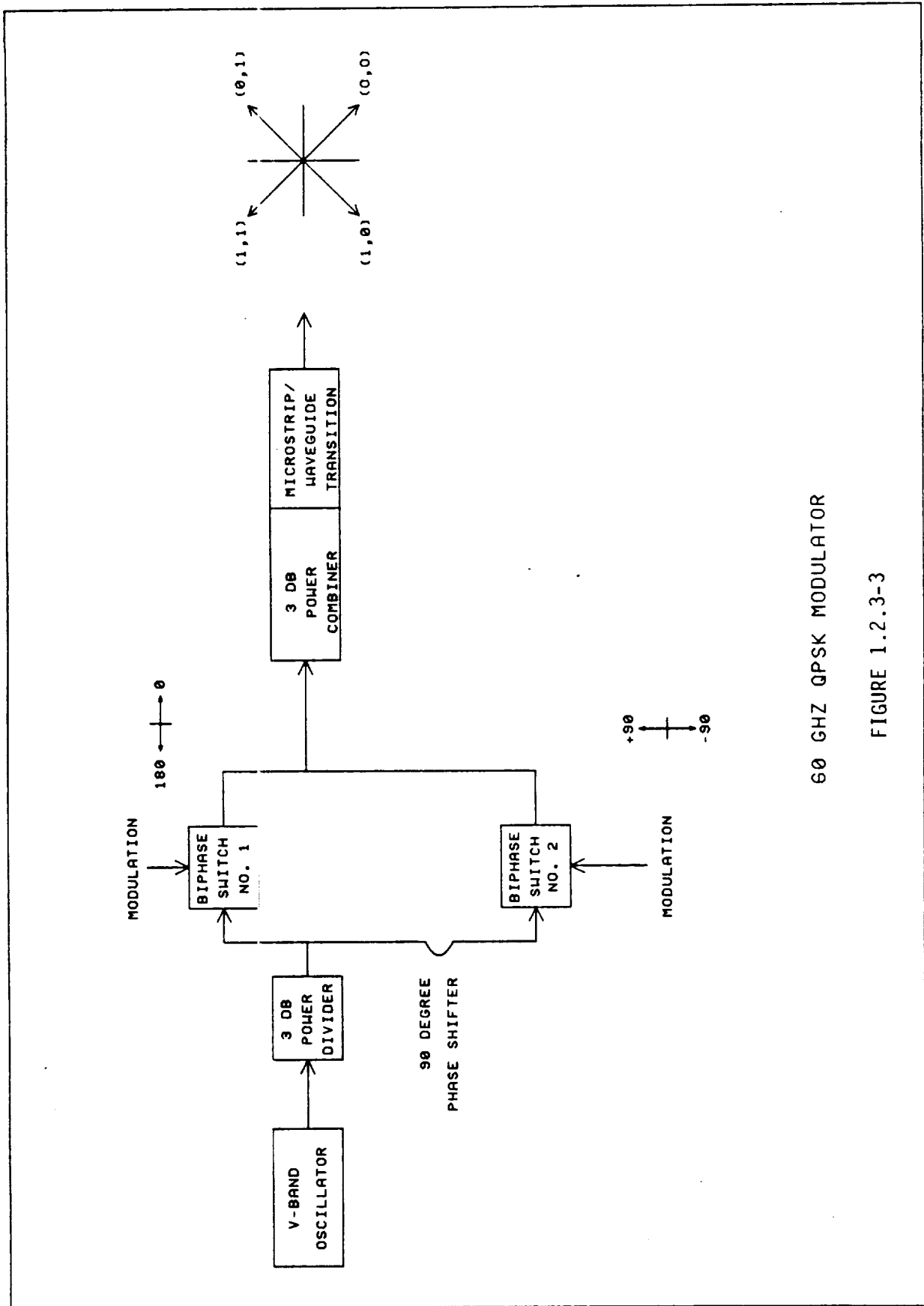
60 GHZ QPSK MODULATOR

FIGURE 1.2.3-3

RF EQUIPMENT

ISL GEO-GEO RECEIVER SUBSYSTEM

FIGURE 1.2.3-4

FROM ANTENNA

-93.08 DBM
1) 55.50 GHZ
2) 62.75 GHZ

BPF
7-POLE

L = 0.3 DB

-93.38 DBM

RF PREAMP
(HEMT)

G = 30 DB

-63.38 DBM

LO
34 GHZ

-71.38 DBM

SWITCHABLE
BP FILTER
7-POLE

L = 0.2 DB

-71.58 DBM

IF AMPL
(GaAs FET)

G = 25 DB

-46.58 DBM
1) 21.50 GHZ
2) 28.75 GHZ

TO
DEMODULATOR

QPSK DEMODULATOR SUBSYSTEM

(1) ELIMINATES HIGH FREQUENCY SPURIOUS MIXING PRODUCTS

(2) SETS NOISE BANDWIDTH
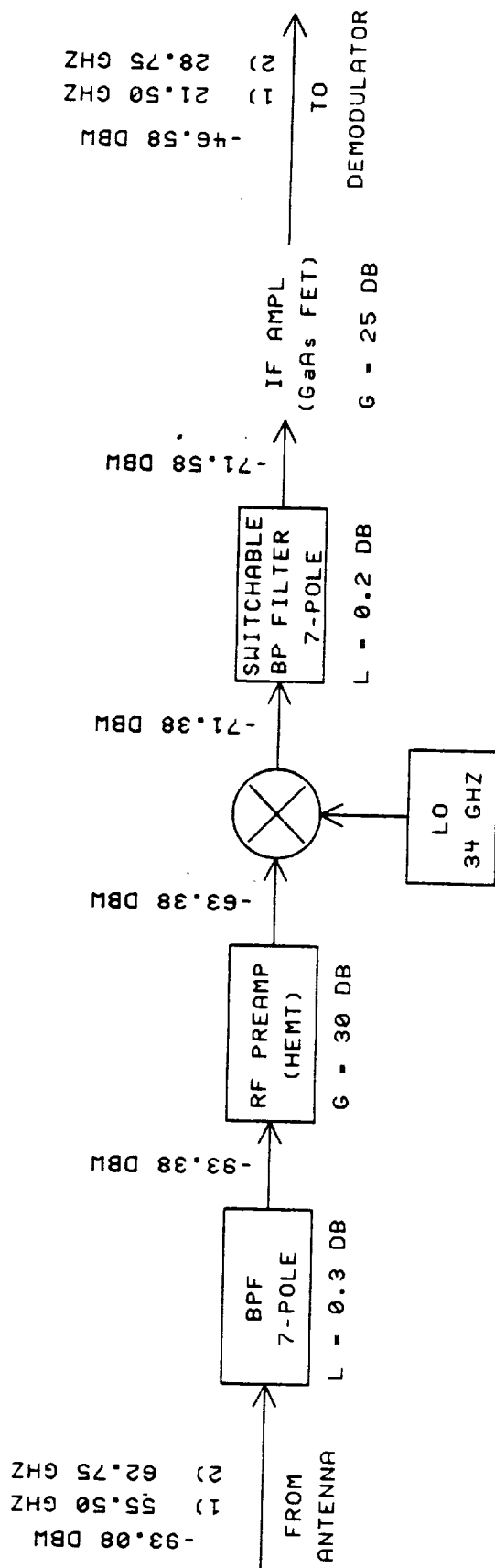
1.2.3.1 Modes of Operations

The following Tables 1.2.3.1-1 and 1.2.3.1-2 define the modes of operation for the units in Figure 1.2.3-1. Note that "normal operation" implies a data rate of 2 Gbps. During solar conjunction the 300 Mbps modulator and demodulator will be operational.

1.2.4 Navigation, Timing/Clock Requirement

See Section 1.1.5.

1.2.5 Telemetry and Command Structure

See Section 1.1.6.

Modes: Normal, Acquisition, Re-Acquisition, System Evaluation

Satellite	Unit	Configuration	Power	Status
TDAS #1	10 Watt Transmitter	ON	ENABLED	ACTIVE
	2 GBPS Modulator	ON	ENABLED	OPERATING
	300 MBPS Modulator	OFF	ENABLED	NON-OPERATING
	GEO-GEO Receiver	ON	ENABLED	OPERATING
	2 GBPS Demodulator	ON	ENABLED	OPERATING
	300 MBPS Demodulator	OFF	ENABLED	NON-OPERATING
	Tracking & Acquisition Receiver	ON	ENABLED	OPERATING
	Antenna Control Microprocessor	ON	ENABLED	OPERATING
TDAS #2	10 Watt Transmitter	ON	ENABLED	ACTIVE
	2 GBPS Modulator	ON	ENABLED	OPERATING
	300 MBPS Modulator	OFF	ENABLED	NON-OPERATING
	GEO-GEO Receiver	ON	ENABLED	OPERATING
	2 GBPS Demodulator	ON	ENABLED	OPERATING
	300 MBPS Demodulator	OFF	ENABLED	NON-OPERATING
	Tracking & Acquisition Receiver	ON	ENABLED	OPERATING
	Antenna Control Microprocessor	ON	ENABLED	OPERATING

TABLE 1.2.3.1-1

Stand-by Mode

Satellite	Unit	Configuration	Power	Status
TDAS #1	10 Watt Transmitter	OFF	ENABLED	PASSIVE
	2 GBPS Modulator	OFF	ENABLED	NON-OPERATING
	300 MBPS Modulator	OFF	ENABLED	NON-OPERATING
	GEO-GEO Receiver	OFF	ENABLED	NON-OPERATING
	2 GBPS Demodulator	OFF	ENABLED	NON-OPERATING
	300 MBPS Demodulator	OFF	ENABLED	NON-OPERATING
	Tracking & Acquisition Receiver	OFF	ENABLED	NON-OPERATING
	Antenna Control Microprocessor	OFF	ENABLED	NON-OPERATING
TDAS #2	10 Watt Transmitter	OFF	ENABLED	PASSIVE
	2 GBPS Modulator	OFF	ENABLED	NON-OPERATING
	300 MBPS Modulator	OFF	ENABLED	NON-OPERATING
	GEO-GEO Receiver	OFF	ENABLED	NON-OPERATING
	2 GBPS Demodulator	OFF	ENABLED	NON-OPERATING
	300 MBPS Demodulator	OFF	ENABLED	NON-OPERATING
	Tracking & Acquisition Receiver	OFF	ENABLED	NON-OPERATING
	Antenna Control Microprocessor	OFF	ENABLED	NON-OPERATING

TABLE 1.2.3.1-2

1.2.6   Operational Concepts

1.2.6.1   Launch Sequence

The spacecraft will be launched by the space shuttle (STS) from Kennedy Space Center. The STS will place the spacecraft into a nominal 160-nm circular parking orbit at 28.5-degree inclination, from which an upper stage will inject the satellite into an elliptical geosynchronous transfer orbit (GTO). The restartable main satellite thruster will then be fired multiple times to raise perigee radius and reduce the orbit inclination such that a circular equatorial geosynchronous orbit is established.

Following launch, the spacecraft is first powered up about two hours prior to deployment from the shuttle orbiter. Spacecraft systems are checked out and the spacecraft attitude reference is established and calibrated. The orbiter will maneuver to the desired deployment attitude shortly before deployment and the spacecraft will be switched to internal battery power. The particular parking orbit rev chosen for deployment is based on STS constraints and the desire to obtain early ground communication following the injection burn. To this end, the TT&C antenna boom is extended, if necessary, soon after deployment from the orbiter. A non-spinning deployment is effected by means of separation springs; after the spacecraft has achieved a safe distance from the orbiter, its thrusters are enabled to recapture and maintain the injection attitude. Depending on the type of upper stage selected, the spacecraft may be spun up for stability just prior to the injection burn. The upper stage is fired to inject the spacecraft into GTO about 45 minutes after deployment. Injection occurs near local noon or midnight, and may be on an ascending or descending node. From deployment through injection, all spacecraft activities are controlled by the automatic sequencer on the spacecraft.

Shortly after injection, the spacecraft will come into view of a ground station. Support will be provided by the dedicated mission ground station as well as the three DSN stations and TDRSS. Ground controllers will evaluate health status and command separation of the upper stage, followed by spindown if required. The satellite will be maneuvered into a sun orientation, and the solar array will be partially deployed to provide power during the transfer orbit phase. After sufficient time has elapsed for orbit determination, the first of three apogee maneuver firings will be executed. Attitude sensors are calibrated and the satellite is reoriented to the required AMF attitude. The main satellite thruster is fired by ground command to impart a fraction of the total impulse required to raise perigee to synchronous altitude and reduce inclination to zero. The exact split among the three AMFs is determined by phasing requirements for arrival at the desired station longitude with minimal maneuvering. Between AMFs, the satellite is returned to sun-pointing mode to maintain power.

Following the three AMFs and a maneuver at perigee to adjust the apogee altitude, the satellite is in near-geosynchronous equatorial orbit. At this point the smaller satellite thrusters will be used for maneuvering, so the solar array may be fully deployed and the satellite transitioned to the on-orbit earth-oriented control mode. Once this mode is established the large antenna reflectors will be deployed and minor maneuvers will be performed to fine-tune the station position and establish stationkeeping cycles. Payload testing can then begin, prior to the start of normal on-orbit operations.

The sequence of major mission events is presented in Table 1.2.6-1. Figure 1.2.6-1 shows the satellite orbit geometry.
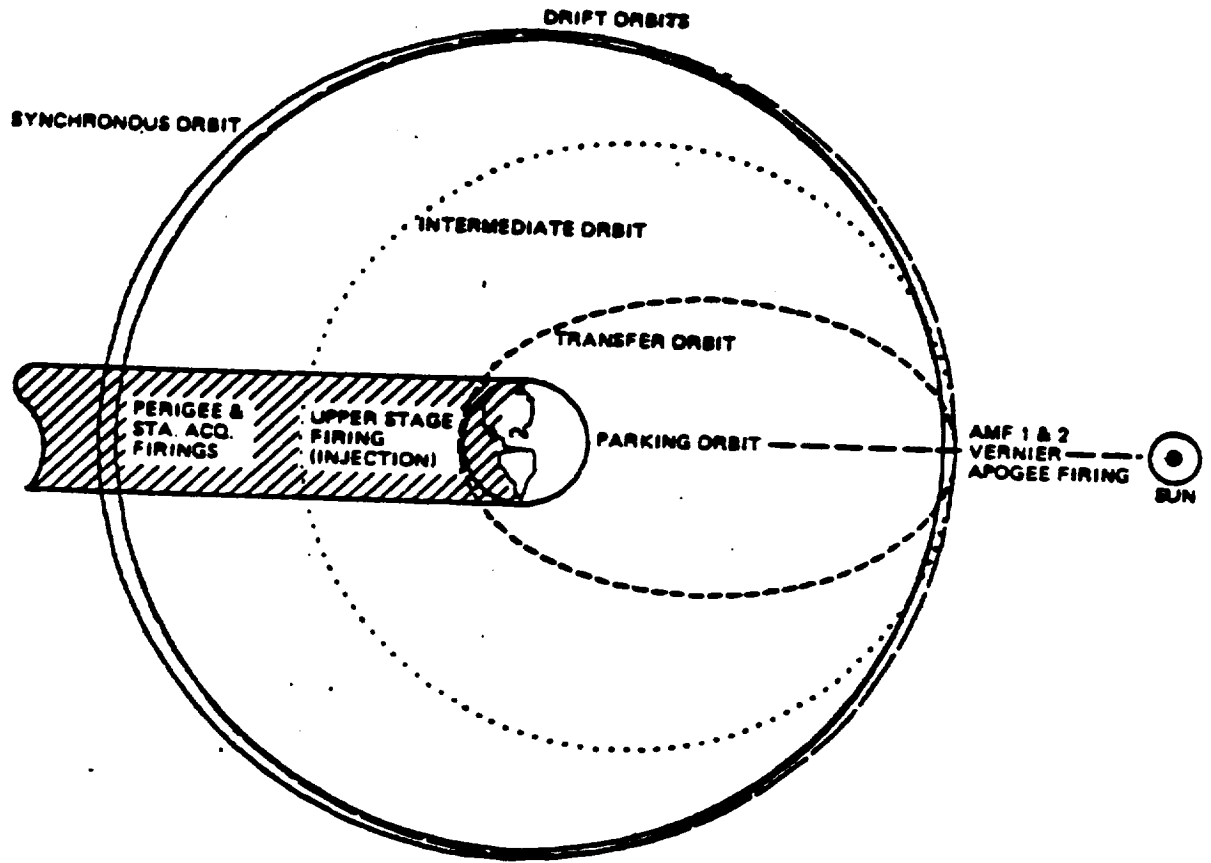
Satellite Orbit Geometry

FIGURE 1.2.6-1

SEQUENCE OF MAJOR MISSION EVENTS

EVENT	EVENT TIME (HR:MIN)
STS liftoff	T0 = TBD
Spacecraft power on	T1 - 2:00
Begin S/C checkout	T1 - 2:00
Calibrate S/C attitude reference	T1 - 0:30
Orbiter maneuver to deployment attitude	T1 - 0:15
Switch to S/C internal power	T1 - 0:05
Spacecraft deployment from orbiter	T1 = TBD
Deploy TT&C antenna, if required	T1 + 0:03
Arm S/C thrusters; initiate injection attitude maintenance	T1 + 0:04
Spin up S/C, if required	T1 + 0:30
Transfer orbit injection (upper stage burn)	T2 = T1 + 0:45
Initial acquisition of signal (AOS) by ground station	T2 + 0:20
Upper stage separation (ground command)	T2 + 0:25
Initiate spin-down (if required); sun acquisition	T2 + 0:30
Partial deployment of solar array	T2 + 0:45
Transfer orbit determined	T2 + 22:35
Prepare for 1st AMF (calibrate; reor)	T3 - 0:50
1st apogee maneuver firing (3rd apogee)	T3 = T2 + 26:22
Return to sun acquisition mode	T3 + 0:25
Prepare for 2nd AMF	T4 - 0:50
2nd apogee maneuver firing (6th apogee)	T4 = T3 + 50:00
Return to sun acq mode	T4 + 0:15
Prepare for apogee adjust maneuver	T5 - 0:20
Apogee adjust maneuver (7th perigee)	T5 = T4 + 35:20
Return to sun acq mode	T5 + 0:10
Prepare for 3rd AMF	T6 - 0:30
3rd apogee maneuver firing (9th apogee)	T6 = T5 + 35:00
Return to sun acq mode	T6 + 0:10
Switch to earth aquisition mode	T6 + 4:30
Deploy solar array and slew to sun	T6 + 4:40
Spin-up momentun wheel	T6 + 5:50
Switch to on-orbit (3-axis) control mode	T6 + 6:10
Deploy KSA/SSA reflectors	T6 + 23:00
Uncage and reorient crosslink reflector	T6 + 24:00
Begin station acquisition maneuvers	T7 = T6 + 48:00
Start on-orbit testing	T7 + 24:00
Start normal on-orbit operations	T7 + 72:00

TABLE 1.2.6-1

1.2.6.2 Ground/Satellite Communication Concepts

The GEO-GEO crosslink provides, among other things, for communication between a ground station and a Geostationary satellite which is not in view of that station. While data between the ground and the visible GEO satellite (TDAS #1) is transmitted on the TT&C channel, the satellite-to-satellite relay will be accomplished by baseband multiplexing the commands, test data, etc., on the 60 GHz data stream.

Examples of commands to the non-visible satellite (TDAS #2) from the ground will include

        A)   Equipment Turn-on Commands
        B)   On-Orbit Test Commands
        C)   Redundancy Switching Commands

Examples of data which will be sent to TDAS #2 via the TDAS #1 are updated contacts with User satellites. Included for each USAT will be

        A)   Time of Contact
        B)   Ephemeris Information
        C)   Data Rate for LEO-GEO communication
        D)   Doppler Profile

Other data which will be communicated comprises timed switching (data rate) for solar conjunction and operating instructions for expected times of two or more USATs in conjunction.

Component operating status and test measurements will be sent from the GEO #2 to the ground station via the 60 GHz crosslink and the GEO #1 TT&C channel. The USAT's mission data will be transmitted to its ground station via TDAS #2 and TDAS #1 for mission analysis.

1.2.6.3 Acquisition and Initial On-Orbit Test

Because of the absorption by oxygen of EHF energy at 60 GHz, normal operational tests (signals transmitted to and from the ground) of the orbiting TDAS spacecraft are not possible. The on-orbit testing will be directed from the ground with commands up-linked to the TDAS via the TT&C channel. The other orbiting TDAS will act as a simulated ground station with the test results (e.g. received C/N measurements) relayed to the ground for evaluation by test personnel.

Therefore initial acquisition and on-orbit testing are necessarily linked. The following sequence of events will be used to validate performance of the two TDAS spacecraft.

        A.   Initial system/payload turn-on for each host vehicle.
             (The assumption is that the TDAS #1 will be in view
             of the dedicated White Sands facility and that the TDAS #2
             will be controlled initially from one of the DSN
             stations).

B. Transmission of 60 GHz signal, assuming the use of a master frequency source in the spacecraft (transmitter power shall be measured and relayed to ground control station).

C. Slewing of 3.2 meter antenna to estimated position of other TDAS. (Initial ephemeris data may be provided via TT&C or may be in processor ROM).

D. Timed co-operative search for other TDAS antenna (see Section 1.2.2). When antenna is locked onto signal, comm testing can begin.

E. Comm testing (bi-directional). The testing will be done using the other TDAS as a simulated ground station with the test results telemetered to the ground for validation of system operation. Some of the tests are:

1. Transmit power
2. Receiver C/N
   Carrier lock
   Demodulator lock
3. Power levels after amplification in receivers
4. Frequency response
5. End-to-end system verification using known bit pattern
6. Data routing and switching test.

F. Antenna pattern testing. Once operation of electronics is verified, the antennas will be moved a small amount off boresight. The resultant drop in received C/N is measured to verify the antenna alignment.

1.2.6.4 Normal Operation

Normal operation of the GEO-GEO link can commence when the two spacecraft are completely checked out. The communications link is assumed to be continuous at 2 Gbps except during the small portion of time when the satellites are in solar conjunction. Commands to reduce the data rate (perform the necessary switching) are under ground control.

During spacecraft operation the performance is monitored continuously and status telemetered to the ground for performance verification.

Failure Monitoring

The crosslink communication package will have the ability to provide performance and status of each unit defined in Figure 1.2.3-1. On/off status and temperature measurements for each component will be provided. Gimbal/antenna read-out positions will be continuously monitored and relayed. Accurately calibrated couplers can provide RF power levels.

A system that evaluates BER is planned as the method to verify end-to-end system performance (see Section 1.1.9.2). If the quality of the link degrades, the traffic will be interrupted for a C/N measurement which will be automatic in the satellite whenever the BER threshold is exceeded. Further trouble-shooting will be directed by ground personnel using the telemetered measured data.

Examples of other hardware failures/operating discrepancies which will cause immediate reaction and diagnostic testing are loss of carrier lock and loss of receiver lock.

Redundancy Control

Except in rare instances, redundancy control will be retained by TDAS ground control. Failure analysis will be initiated once an operational discrepancy and/or hardware failure has been detected. Once the trouble area has been identified, redundancy switching will be accomplished through the ground generated telemetry data (via the Frontside TDAS if the failure occurred in the Backside Satellite).

Automated Sequences

The possibility of simplifying operations of the TDAS XL exists by using automated command sequences that allow for fast redundancy switching and routine command sequences. These are extremely useful in the event of a detected component power outage. However, the number of automated command sequences should be kept to a minimum so that functional verification between commands can be ensured. Due to the high reliability of flight qualified hardware, frequent redundancy switching/failure analysis is not expected. On the contrary, every effort will be made during the design of the crosslink system to ensure maximum reliability.

1.2.6.5 Re-Acquisition

It is assumed that tracking will be continuous and that re-acquisition will not be necessary. In the unlikely event that the communication stream is broken, re-acquisition can be obtained in the same manner as the original acquisition.

1.2.7 Effects of Earth, Sun and Polarization

1.2.7.1 Earth

The earth will have no appreciable effect to the GEO-GEO links.

1.2.7.2 Sun

A detailed study has been conducted to determine the percentage of the time the sun intrudes into the antenna beam when two linked geostationary (GEO) satellites are positioned 160 degrees (β) apart as shown in Figure 1.2.7-1.

The total beam width view angle (Θ) was assigned values from 0.05 degrees to 0.20 degrees, and the probability of the sun intruding into the beam of one satellite on any day was calculated as shown in Figure 1.2.7-2. The figure shows that for the narrow beam widths used, sun intrusion only occurs twice a year for two to three days during the equinox periods. It is also important to note that as long as the two GEO antennas are within line-of-sight of each other (not eclipsed by the earth), their separation angle does not affect the probability of intrusion values. The information in Figure 1.2.7-2 is presented as the percent of a day that the sun is intruding into the antenna beam of one satellite. It also intrudes into the beam of the other satellite the same percentage of a day but at a different time of day.

1.2.7.3 Polarization

The polarization effects are discussed in Section 1.1.8.

FIGURE 1.2.7-1

Intersatellite Link Geometry
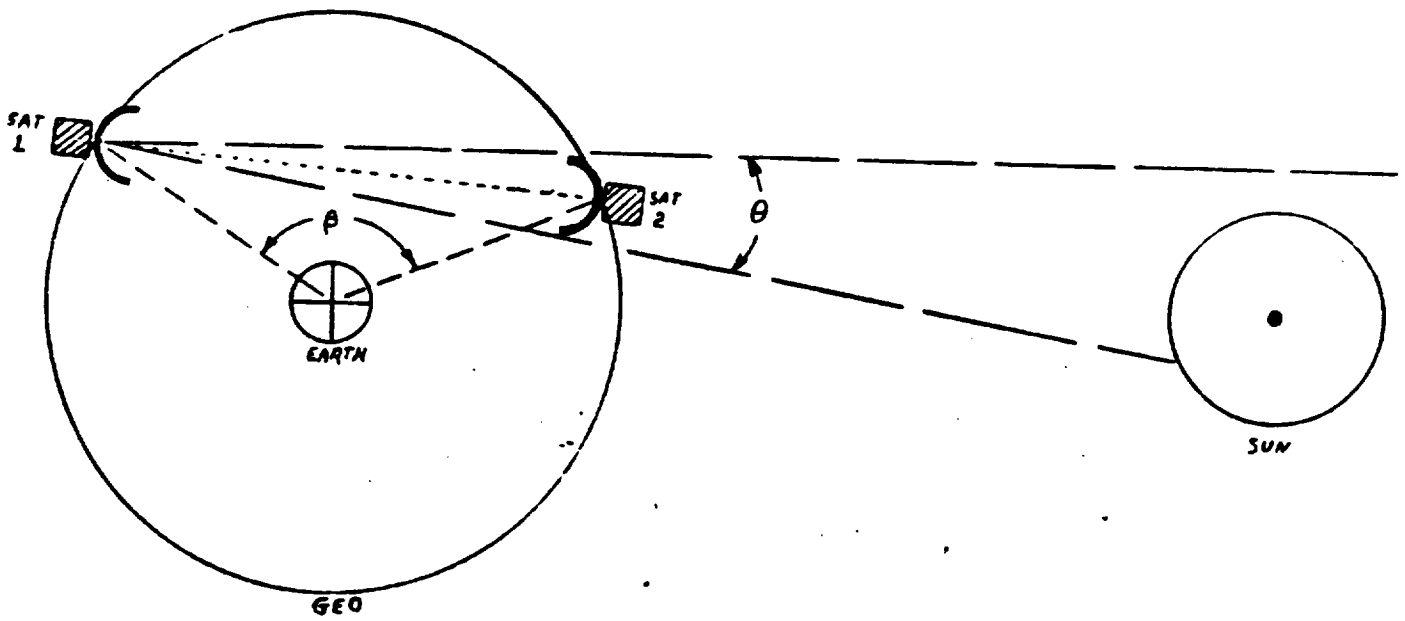
FIGURE 1.2.7-2
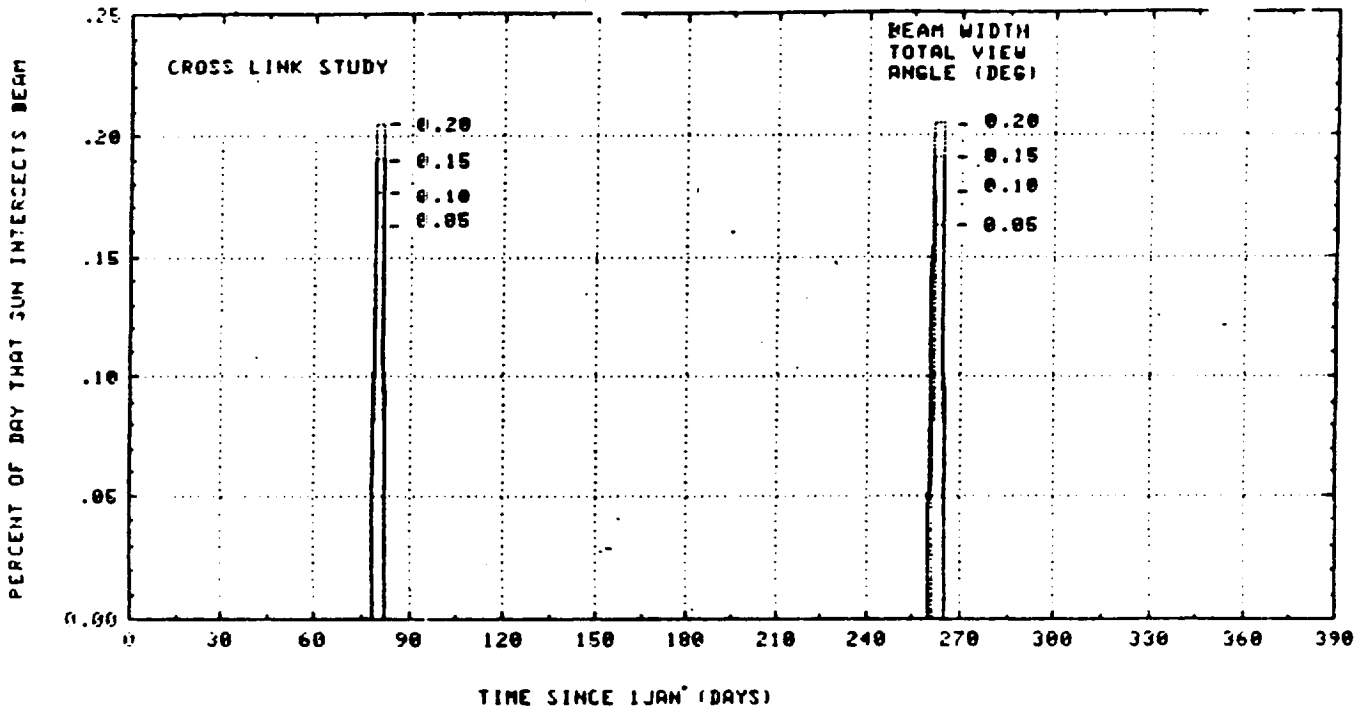
1.2.8   Weight, Power and Size

GEO-GEO EQUIPMENT	Qty	Weight lbs.	Power W	Size in x in x in	Redundancy
Receiver (RF Portion)	1	4.3	28	5 x 4 x 2 / 1 x 3 x 3/4	1
2 GBPS Demodulator (QPSK)	1	3	6	3 x 4 x 2	1
QPSK Modulator & L.O.	1	5	24	3 x 4 x 1 / 5 x 4 x 2	1
Transmitter (10W)	1	1.6	111	14 x 5 x 1.5	1
Feed Assembly	1	3.5	-	4 x 4 x 18	-
Antenna (3.2 m)	1	60.5	-	3.2m x 3.2 x .9	-
300 MBPS QPSK Demodulator	1	3	6	3 x 4 x 2	1
Gimbal Subsystem	1	28	9*.(32**)	14 x 13.5 x 11	-
Gimbal Drive Electronics	1	5	6	8.5 x 2.6 x 5.7	1
Acquisition & Tracking Receiver	1	1.2	4	3 x 6 x 2	1
TOTAL PER OPERATIONAL SYSTEM		115.1	194		
TOTAL PER SPACECRAFT		138.2			
DC/DC Converter	1	4	49	3 x 6 x 2	2
Antenna System Control Electronics	1	3.5	1.0	112 in.^{3}	1
Antenna Controller	6	0.5	0.1	4 x 8 x 1/2	6
Antenna Control Microprocessor	1	0.5	0.4	4 x 8 x 1/2	1
TOTAL PER OPERATIONAL SYSTEM		3.5	1.0		
TOTAL PER SPACECRAFT (CONTROLLER)		7.0			
TOTAL PER SPACECRAFT		157.2	244		
* Average					
**Peak					

1.2.9   Reliability

The reliability is discussed in Section 1.1.14.

SECTION 2

ANTENNAS

TABLE OF CONTENTS, FIGURES & TABLES

2.0 ANTENNA DESCRIPTION

The TDAS satellite (Figure 2-1) will have a 60 GHz communications "crosslink" with another TDAS satellite in geosynchronous orbit (GEO) and five "command/data links" with satellites in low earth orbit (LEO). Three antenna systems are required.

    (1) TDAS antenna for GEO - GEO crosslinks
    (2) TDAS antennas for GEO - LEO command links
    (3) LEO satellite antenna for LEO - GEO data link

The baseline designs for these antenna systems will be described.
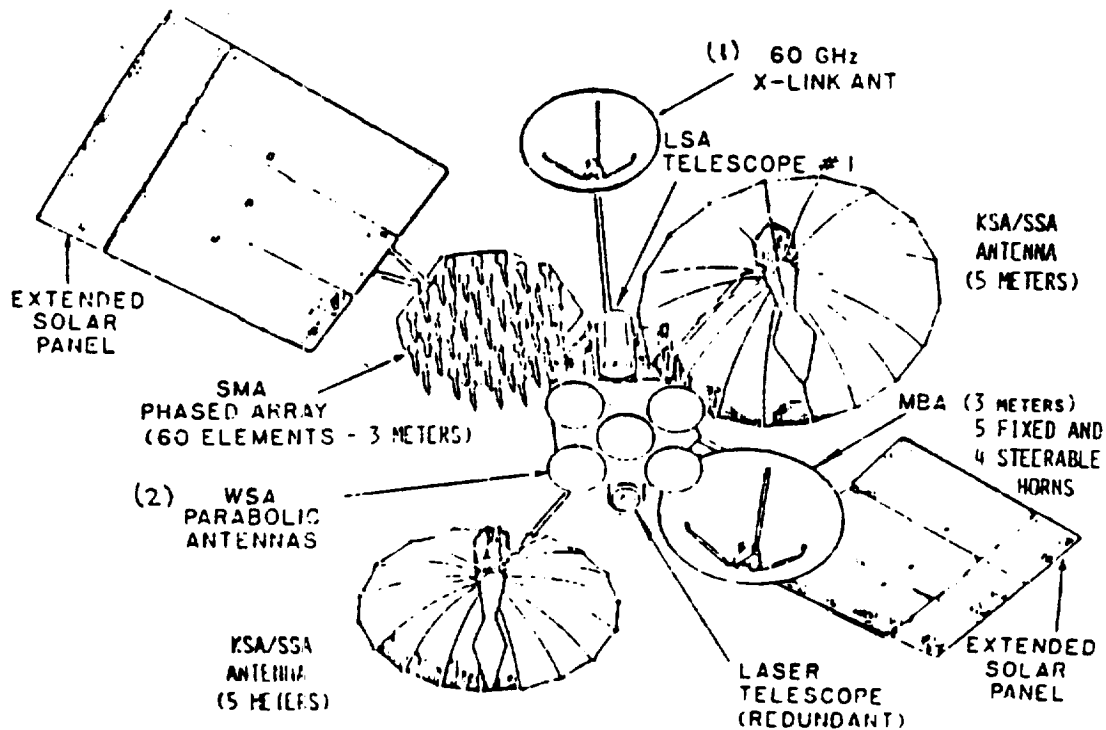
FIGURE 2-1. ANTENNA SYSTEMS ON TDAS SATELLITE

2.1 TDAS ANTENNA DESIGN FOR GEO-GEO LINK

2.1.1 System Considerations

The factors determining antenna design for the high data rate crosslink are as follows.

- o Up to 2 Gbps data rate, full duplex operation
- o Frequency and polarization plan: 54.25-56.75 GHz and 61.5-64.0 GHz, opposite senses of circular polarization.
- o Satellites spaced from 25 to 160 degrees apart in the GEO plane, [18,000 to 83,000 km range, 213 to 226 dB path loss, 77.5 to 10 degree azimuths]
- o Duplex communications link with other TDAS satellite
- o Link operation at full capacity with sun in field of view not required
- o 10 W RF power amplifiers available (early 1990's)
- o 360 K low noise receiver available (early 1990's)

The GEO-GEO link budget calculation (Table 1.1.1-2) based on these factors requires antenna gain around 63 dB, or 3.2-m diameter antennas on both ends of the link. Larger antennas and/or increased transmit power would be required to operate at full data rate with the sun in the field of view. Since solar noise degradation of GEO-GEO links occurs for only a few minutes a year, the link is not sized to accommodate it.

The baseline antenna system description and performance estimate is given in Table 2-1. The antenna is shown in Figure 2-1 as the "60 GHz X-LINK ANT". The different system components are shown in schematic form in Figure 2-2 and will be discussed in the remaining subsections of Section 2.1.

2-2

TABLE 2-1. BASELINE GEO-GEO LINK ANTENNA

DESCRIPTION

o Axially fed Cassegrain antenna with shaped reflectors for best efficiency.
o Mechanically steered around two axes via gimbals to cover required field of view with necessary acquisition and slew speeds.
o Each TDAS spacecraft contains a single GEO-GEO antenna to support the communication operation regardless of TDAS orbital position (frontside, backside, or spare).
o Each antenna has two channels for the transmit and receive links. Separation between channels will be on the basis of frequency and polarization, with channels capable of being switched between links.

PERFORMANCE ESTIMATE

Loss Budget

Factor	Efficiency (dB)
Aperture	-0.40
Blockage	-0.50
Spillover	-0.70
Phase	-0.10
Polarization	-0.10
Surface RMS (.12 mm)	-0.40
NET EFFICIENCY	-2.10

Antenna Gain

The ideal gain of a 3.2-m reflector at 55.5 GHz (wavelength = 5.4 mm) is 65.4 dB. The net gain, using the above efficiency, is 63.3 dB. Table 1.1.1-2, the link budget, includes losses for components before the antenna per the loss budget in Figure 1.1.1-4.

FEED DESIGN

o The feed is an aperture-matched horn with -20 dB subreflector edge taper.
o Circular polarization is implemented via a septum polarizer.
o System magnification is three. Focal length is chosen such that the feed to receiver/transmitter unit connection is short.
o Beam waveguide (a system of guiding mirrors) is used to transmit the RF signal through the center of gimbals. This allows the receiver/transmitter unit to be located on the body of the satellite and reduces inertial loads.
o Tracking is achieved by a monopulse system (single horn) using TE21 modes for the error pattern and TE11 for the main beam.
o Acquisition is accomplished by mechanically steering the antenna to each search position.

MECHANICAL DESIGN

o Composite materials will be used for maximum strength, minimum weight, and thermal stability in the space environment.
o Mass of the antenna system is estimated as follows.

3.2-m dia. reflector	24.0 kg
0.48-m subreflector	1.1 kg
Subreflector support	2.3 kg
Feed horn assembly	1.6 kg
TOTAL	29.0 kg

o The 3.2-m reflector will fit in the shuttle for launch, but may pose packaging and deployment problems.

```
RADIATION
LHCP  RHCP
      ↕
   ANTENNA
      ↕
  BEAM
  WAVEGUIDE
      ↑ CP
  MEANDERLINE
  POLARIZER
      ↑ LP
   HO RN ←——— LP ———→ ORTHOMODE
                       JUNCTION
      ↓↓↓↓ V         V ↓     H ↑
  TRACKING
  SIGNALS    ←————————X
  (RECEIVE ONLY)
      ⇕              DIPLEXER    DIPLEXER
  TRACKING           ↓ ↑         ↓ ↑
  CONTROL
                        SWITCH
                        ↓     ↑
                   RECEIVER   TRANSMITTER
```
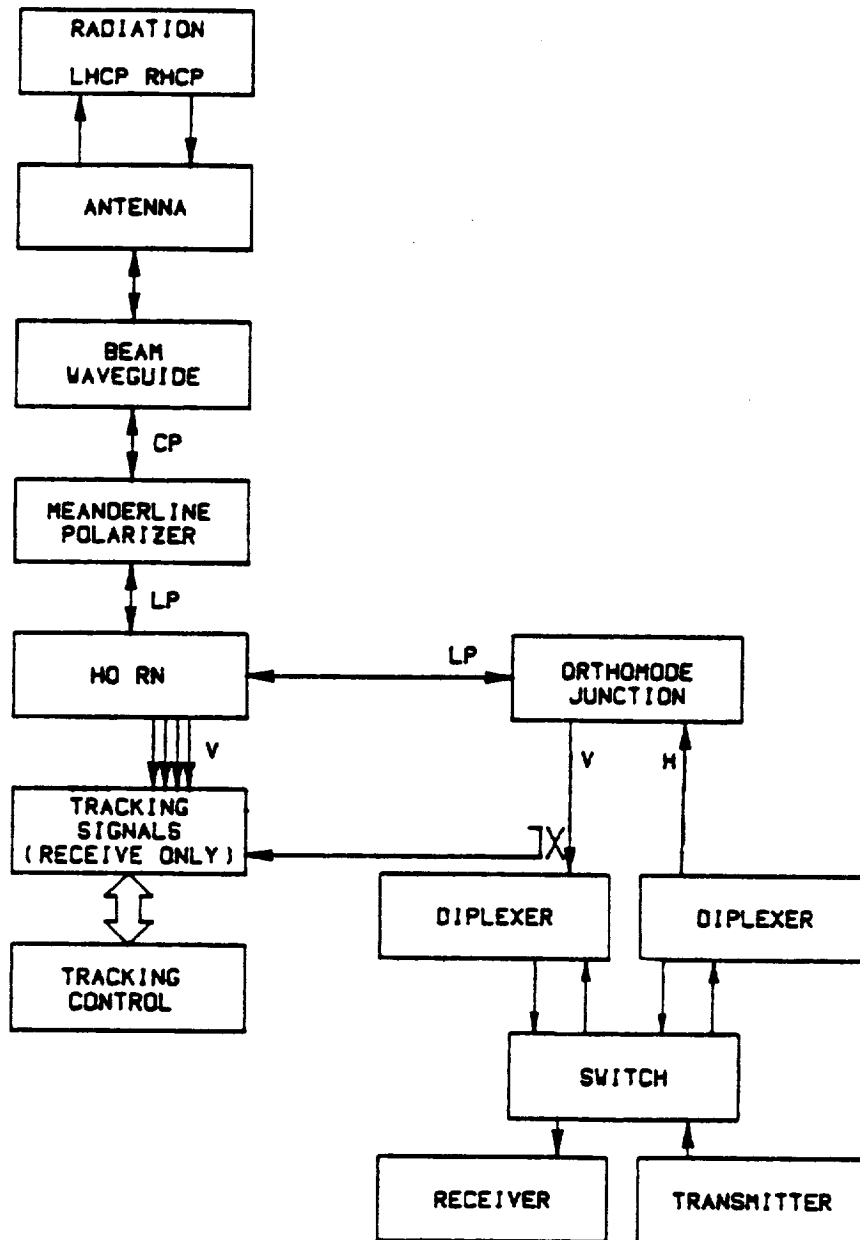
500351
KE650035/JIM
1-28-85/M1

FIGURE 2-2. ANTENNA SYSTEM SCHEMATIC

2 - 4

2.1.2 Antenna Geometry

Antenna geometry is shown in Figure 2-3. The major design consideration is high efficiency in order to keep antenna size to a minimum. An axially fed Cassegrain antenna design is used with reflectors shaped for enhanced efficiency. The combination of feed horn taper and shaped subreflector gives low aperture and spillover losses (0.3 dB). Magnification and focal length are chosen to minimize blockage and to place the feed position close to the vertex of the antenna.

2.1.3 Beam Waveguide

Beam waveguide is used for low loss transmission of RF energy through the gimbals to the body of the spacecraft. The baseline assumption was that the loss due to beam waveguide (0.5 to 1.0 dB) would be offset by the electrical and mechanical advantages of having the electronics package (receivers and transmitters) on the body of the spacecraft rather than rotating with the antenna. Alternates to beam waveguide, such as waveguide and rotary joints, or flexguide are much more lossy.

FIGURE 2-3. DIMENSIONS OF BASELINE GEO-GEO LINK ANTENNA

2-5

2.1.4 Feed Horn

An aperture-matched horn (Burnside) with -20 dB subreflector edge taper is chosen. For the required 20 degree coverage angle, the smooth, flared horn will be 3 to 5 wavelengths long.

2.1.5 Monopulse Tracking System

The monopulse tracking system couples TE21 mode energy from the feed horn to produce the error pattern signals. For each H and V polarization, signal coupling from 4 symmetric positions around the waveguide are required. Tracking will be carried out only on the receive signal. However, due to possible link reconfiguration, either polarization could be the receive signal, and 8 coupled signals must be brought out. Some of the direct TE11 mode (H and V) as shown in Figure 2-2 is also coupled off to produce the sum and difference tracking signals.

2.1.6 Septum Polarizer

The septum polarizer separates the circularly polarized incoming signal into RHCP and LHCP components. Due to possible link reconfiguration, the signals may be either frequency (55.5 or 62.75 GHz) and either polarization (RHCP or LHCP) The outputs of the septum polarizer go to filters for separation into the two frequency bands. A switch is used to connect the receiver and transmitter to the correct combination of frequency and polarization. The unused outputs of the switch are connected to matched loads.

2.1.7 Mechanical Design

Composite materials

The proposed design uses a machined sacrificial layer on the front surface of a rib stiffened to meet the required RMS error. The structure is a combination of a thin honeycomb sandwich shell and stiffening ribs attached to the backside. It provides the reflector that meets all the structural and thermal requirements with the lowest possible weight.

The reflector shell is a lightweight sandwich composed of a 6 mm Kevlar core with faceskins of unidirectional graphite epoxy prepreg. A quasi-isotropic laminate (0/±45/90 degrees) of pitch 75 fibers radially oriented in a gore lay-up provides excellent structural and thermal stability. The sandwich shell will be fabricated in one curing cycle under vacuum pressure on a precision graphite mold. A sacrificial layer of low modulus graphite fibers is added to the reflector shell front surface. Its thickness will be kept to a minimum amount in order to minimize the weight increase.

The inner and outer rings are connected by radial ribs and constitute the main back-up rib structure. The ribs are of the same type of construction as the basic reflector shell, with each facesheet consisting of three plies of high modulus pitch 100 material in a 0/±60 degree lay-up configuration which provides high bending and shear stiffness. Load continuity across rib joints is assured by splice caps and shear angles are held in place by doublers and angle clips, all attached with room-temperature-curing adhesive.

After completion of the shell/rib structure assembly, the contour of the reflector will be measured, best-fitted and then machined in order to achieve the required surface RMS. Only a portion of the sacrificial layer thickness will be removed. The remaining broken fibers (which do not contribute to the structural integrity) will be coated with a layer of vapor deposited aluminum passivated with a thin layer of silicon dioxide in order to enhance RF reflectivity. The subreflector will be a monocoque graphite design with tubular graphite epoxy struts.

Misalignments and Surface Distortion

The 3.2 meter GEO-GEO reflector has a maximum allowable surface distortion of 0.12 mm (0.0047 inch) and about one-fourth of this has been allocated for distortion due to thermal effects. A distortion analysis for a 3.0 meter reflector using two different coefficients of thermal expansion (one theoretical and one experimental) was done. Six cases of solar position with respect to the GEO-GEO antenna were considered. In all cases the RMS distortion of the reflector caused by thermal expansion was within the 0.001 inch allocation. The analysis results are contained in Table 2-2. The 60 GHz gain loss vs rms reflector surface tolerance is shown in Table 2-3.

TABLE 2-2. PREDICTED REFLECTOR RMS DISTORTIONS

THERMAL CASE	Reflector RMS Distortion, Inches	
	$CTE=-0.754\times10^{-6}$	$CTE=+0.540\times10^{-6}$
1) Full sun normal to front (concave) side of primary antenna (E.O.L.).	0.00012	0.000089
2) Full normal sun on 1/2 of primary antenna frontside (E.O.L.).	0.00021	0.00015
3) Full sun normal to back (convex) side of primary antenna.	0.00035	0.00025
4) Full normal sun on 1/2 of primary antenna backside.	0.00042	0.00031
5) Full side sun. (Solar vector normal to antenna focal axis).	0.00047	0.00033
6) Worst case frontside to backside gradient after eclipse exit (taken from a transient analysis).	0.00017	0.00012
Current Design Goals	0.001	0.001

TABLE 2-3. GAIN LOSS vs REFLECTOR RMS ERROR

(Frequency = 60 GHz, wavelength = 5.0 mm)

RMS ERROR	GAIN LOSS	
mm	dB	%
.025	0.02	0.5
.05	0.07	1.6
.10	0.27	6.0
.12	0.40	8.8
.15	0.62	13.3
.20	1.10	22.4
.25	1.71	32.5
.30	2.47	43.4
.35	3.36	53.9
.40	4.39	63.6
.50	6.86	79.4

Gimbals

Independently gimballed antennas consisting of a reflector and subreflector are used. Two orthogonal-axis gimbals are required for the range of motions required. Use of beam waveguide will require a 0.15-m hole through the center of the gimbals for passage of focussed 60 GHz radiation. Figure 2-4 shows a detail of the baseline gimbal plus beam waveguide concept.

2.1.8 Host Spacecraft Interfaces

The host spacecraft interfaces, as discussed on page 2.5-83 of the proposal, have been fully baselined. They are discussed in the following areas of this document or in Monthly Progress Reports which are appendices to this document.

- o Structure
  -   Sections 5.1.7 and 5.2.7 of this document.
- o Attitude Control Requirements
  -   Monthly Progress Report #8.
- o Thermal Control
  -   Sections 5.1.3 and 5.2.3. of this document.
- o Electrical Power
  -   Sections 5.1.7 and 5.2.7 of this document.
- o Tracking Control
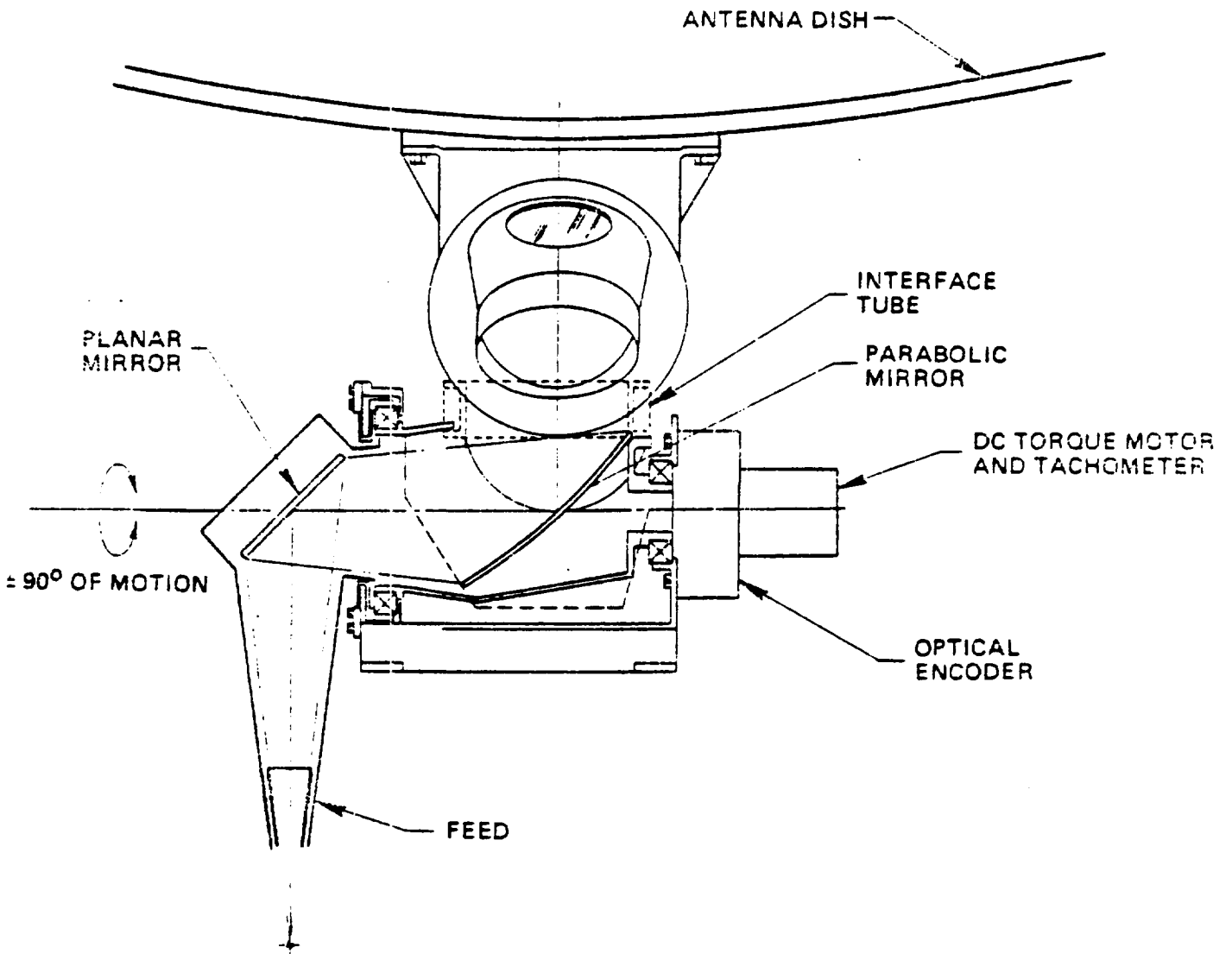 -   Section 1.1.2.2 of this document.

ANTENNA DISH

INTERFACE TUBE

PARABOLIC MIRROR

DC TORQUE MOTOR AND TACHOMETER

PLANAR MIRROR

OPTICAL ENCODER

± 90° OF MOTION

FEED

FIGURE 2-4. GIMBAL DETAIL, WITH BEAM WAVEGUIDE

2.2 TDAS ANTENNA DESIGN FOR GEO - LEO LINK

2.2.1 System Considerations

Five separate GEO-LEO links will be formed by five separate gimballed reflectors on the TDAS satellite. The factors determining antenna design are as follows.

- Full duplex operation: Maximum data rates are
  - 1 Mbps data rate for GEO-LEO command link, transmit 57.8 GHz RHCP
  - Up to 300 Mbps data rates for LEO-GEO link, receive 60.0 GHz LHCP
- LEO satellites tracked over an up to 32 degree field of view,
  LEO satellite altitudes from 160 to 5000 km.
  [30,000 to 51,000 km ranges, 218 to 222 dB path loss]
- Simultaneous communications links with three to five LEO satellites
- 0.6 W RF power amplifier on TDAS, 7.5 W on LEO satellite
- 360 K low noise receiver available (1990's)

Table 1.1.1-6 gives the GEO-LEO link budget with sun effects. Depending on LEO satellite orbit inclination and height, and solar declination, the solar effect could occur not at all or up to once every orbit as the LEO satellite passes the limb of the earth. Orbital period varies from 90 min for 160-km altitudes to 200 min for 5000-km orbits.

Table 2-4 gives the baseline antenna parameters. The system block diagram is shown in Figure 2-5.

TABLE 2-4. BASELINE GEO-LEO LINK ANTENNA

DESCRIPTION

o Five separate antennas required for different satellite links.
o Axially fed Cassegrain antenna with shaped reflectors for best efficiency.
o Mechanically steered around two axes via gimbals to cover required field of view with necessary acquisition and slew speeds.
o Each antenna has two channels for the transmit and receive links. Separation between channels will be on the basis of frequency and polarization.

PERFORMANCE ESTIMATE

Loss Budget

Factor	Efficiency (dB)
Aperture	-0.40
Blockage	-0.50
Spillover	-0.70
Phase	-0.10
Polarization	-0.10
Surface RMS (.10 mm)	-0.30
NET EFFICIENCY	-2.00

Antenna Gain

The ideal gain of a 0.9-m reflector at 60 GHz (wavelength = 5.0 mm) is 55.0 dB. The net gain, using the above efficiency, is 53.0 dB. When the 0.9-m reflector is used as a transmitting antenna at 57.8 GHz, the net gain is 52.7 dB.
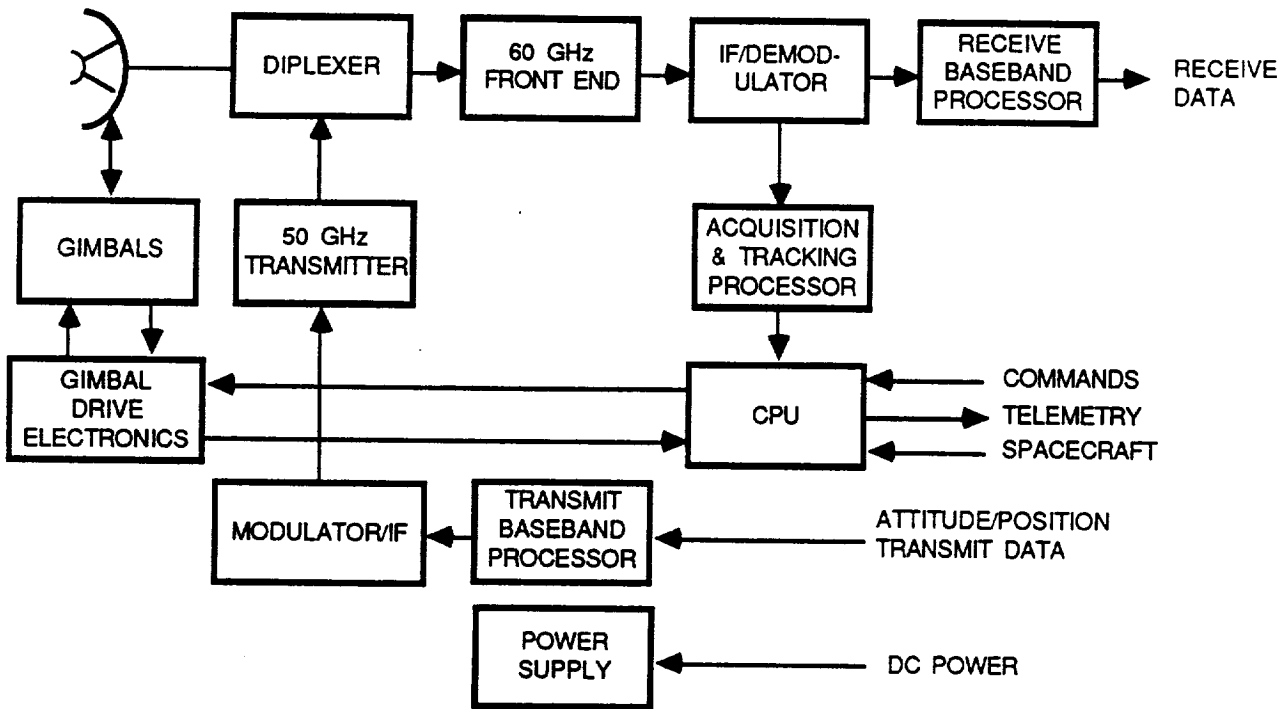
FEED DESIGN

o The feed is an aperture-matched horn with -20 dB subreflector edge taper.
o Circular polarization is implemented via a septum polarizer.
o System magnification is three. Focal length is chosen such that the feed to receiver/transmitter unit connection is short.
o Beam waveguide (a system of guiding mirrors) is used to transmit the RF signal through the center of gimbals. This allows the receiver/transmitter unit to be located on the body of the satellite and reduces inertial loads.
o Tracking is achieved by a monopulse system (single horn) using TE21 modes for the error pattern and TE11 for the main beam.
o Acquisition is accomplished by mechanically steering the antenna to each search position.

MECHANICAL DESIGN

o Composite materials will be used for maximum strength, minimum weight, and thermal stability in the space environment.
o Mass of the antenna system is estimated as follows.

0.9 m dia. reflector	2.0 kg
0.135 m subreflector	0.3 kg
Subreflector support	1.0 kg
Feed horn assembly	1.5 kg
TOTAL	4.8 kg

o The five one-piece, 0.9-m reflectors will fit in the shuttle for launch, and should not pose any packaging and deployment problems.

FIGURE 2-5. GEO-LEO COMMUNICATIONS SYSTEM BLOCK DIAGRAM

2.2.2 Antenna Geometry

Antenna geometry is shown in Figure 2-6. The major design consideration is high efficiency in order to keep antenna size to a minimum. An axially fed Cassegrain antenna design is used with reflectors shaped for enhanced efficiency. The combination of feed horn taper and shaped subreflector gives low aperture and spillover losses (0.3 dB). Magnification and focal length are chosen to minimize blockage and to place the feed position close to the vertex of the antenna.

2.2.3 Beam Waveguide

Beam waveguide is used for low loss transmission of RF energy through the gimbals to the body of the spacecraft. The baseline assumption was that the loss due to beam waveguide would be offset by the electrical and mechanical advantages of having the electronics package (receivers and transmitters) on the body of the spacecraft.
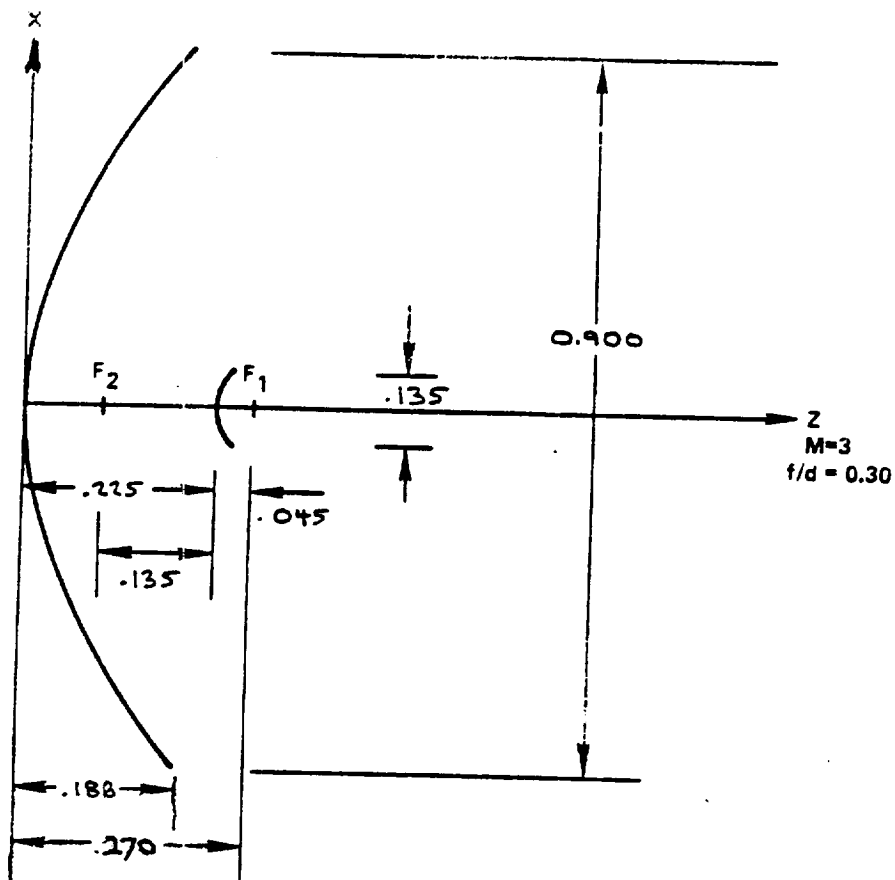
FIGURE 2-6. DIMENSIONS OF BASELINE GEO-LEO LINK ANTENNA

2.2.4 Feed Horn

An aperture-matched horn (Burnside design) with -20 dB subreflector edge taper is chosen. For the 20 degree subreflector coverage angle, the smoothly flared horn will be 3 to 5 wavelengths long.

2.2.5 Monopulse Tracking System

The monopulse tracking system couples TE21 mode energy from the feed horn to produce the error pattern signals. For each H and V polarization, signal coupling from four symmetric positions around the waveguide are required. Tracking will be carried out only on the receive signal. However, due to possible link reconfiguration, either polarization could be the receive signal, and eight coupled signals must be brought out. Some of the direct TE11 mode (H and V) is also coupled off to produce the sum and difference tracking signals.

2.2.6 Septum Polarizer

The septum polarizer separates the circularly polarized incoming signal into RHCP and LHCP components. The outputs of the septum polarizer go to filters for separation into the transmit and receive bands.

2.2.7 Mechanical Design

Composite Materials

The proposed design for the 0.9 meter diameter GEO-LEO link reflector is a thick honeycomb sandwich shell with high modulus graphite epoxy skins. The honeycomb shell consists of 2.0 lb/cu. ft. aluminum core faceskins. Each faceskin is a quasi-isotropic lay-up of pitch 75 unidirectional prepreg in a gore configuration. The fiber properties and the particular lay-up guarantee a very stiff and low distortion structure over temperature. Doublers will be added at each insert location to provide adequate margin of safety during launch. The exposed honeycomb edges are sealed with a pressure sensitive tape and then perforated to allow for atmospheric depressurization during ascent. The front surface will be coated with vapor-deposited aluminum passivated with a thin layer of silicon dioxide to enhance RF reflectivity. A provision should be made for optical alignment at sub-system and spacecraft integration. The subreflector will be a monoque aluminum design with tubular graphite epoxy support struts.

Misalignments and Surface Distortion

The reflector rms surface error is .10 mm, which will give a 0.3-dB loss in efficiency.

Gimbals

Independently gimballed antennas consisting of a reflector and subreflector are used. Two orthogonal-axis gimbals are required for the range of motions required. Use of beam waveguide will require a .15-m hole through the center of the gimbals for passage of focussed 60 GHz radiation.

2.3 LEO SPACECRAFT ANTENNA

The baseline approach to the antenna on the LEO satellite for the LEO-GEO telemetry link is a 1.4-m reflector antenna shown in Figure 2-7 and described in Table 2-5. Transmit is at 60.0 GHz LHCP, and receive at 57.8 GHz RHCP. Tables 1.1.1-3 and 1.1.1-4 show the link budget calculations. Two cases are considered.

- o 300 Mbps data rate without solar effects.
- o 50 Mbps data rate with solar effects present.

Solar effects can cause up to 6.7-dB deterioration in link performance. Depending on LEO satellite orbit height and inclination, and solar declination, the solar effects can occur once every orbit (90 to 200 min). The Space Station will be in a continuously varying orbit of 300 to 500 km altitude with period of 92 to 96 min.

TABLE 2-5. BASELINE LEO TELEMETRY LINK ANTENNA

DESCRIPTION

o One antenna required for TDAS satellite link.

o Axially fed Cassegrain antenna with shaped reflectors for best efficiency.

o Mechanically steered around two axes via gimbals to cover required field of view with necessary acquisition and slew speeds.

o The antenna has two channels for the transmit and receive links. Separation between channels will be on the basis of frequency and polarization, with channels capable of being switched between links.

PERFORMANCE ESTIMATE

Loss Budget

Factor	Efficiency (dB)
Aperture	-0.40
Blockage	-0.50
Spillover	-0.70
Phase	-0.10
Polarization	-0.10
Surface RMS (.10 mm)	-0.30
NET EFFICIENCY	-2.00

Antenna Gain

The ideal gain of a 1.4-m reflector at 60 GHz (wavelength = 5.0 mm) is 58.9 dB. The net gain, using the above efficiency, is 56.9 dB. When the 1.4-m reflector is used as a receiving antenna at 57.8 GHz, the net gain is 56.5 dB.

FEED DESIGN

o The feed is an aperture-matched horn with -20 dB subreflector edge taper.

o Circular polarization is implemented via a septum polarizer.

o System magnification is three. Focal length is chosen such that the feed to receiver/transmitter unit connection is short.

o Beam waveguide (a system of guiding mirrors) is used to transmit the RF signal through the center of gimbals. This allows the receiver/transmitter unit to be located on the body of the satellite and reduces inertial loads.

o Tracking is achieved by a monopulse system (single horn) using TE21 modes for the error pattern and TE11 for the main beam.

o Acquisition is accomplished by mechanically steering the antenna to each search position.

MECHANICAL DESIGN

o Mass of the antenna system is estimated as follows.

1.4 m dia. reflector		4.0 kg
0.21 m subreflector		0.4 kg
Subreflector support		1.4 kg
Feed horn assembly		1.5 kg
	TOTAL	7.3 kg

TABLE 2-5. BASELINE LEO TELEMETRY LINK ANTENNA. CONTINUED

1.4-Meter Reflector Design

The proposed design configuration for the 1.4 meter diameter reflector to be used on a low earth orbit (LEO) satellite is similar to the 3.2 meter TDAS reflector. A thin sandwich shell of Kevlar core and graphite epoxy skins is supported by a backup rib structure, which also provides support to the subreflector struts and interfaces to the gimbal mechanism. A sacrificial layer of low modulus graphite epoxy fibers on the reflector front surface will be machined after completion of the reflector assembly in order to meet the 0.10 mm RMS surface error requirement. Secondary requirements for this reflector are mainly related to the LEO environment. The long term stability within the space environment is always a major concern for a variety of spacecraft components used on large space antenna systems.

For LEO applications, the key environmental variables are atomic oxygen, ultraviolet radiation, high vacuum, and thermal cycling. The thirty years space mission durability requires an evaluation of the existing materials such as thin films, thermal control coatings, structural composites and adhesives in order to establish a level of confidence for the design of an economical system. All of these variables should be carefully investigated in the design phase.
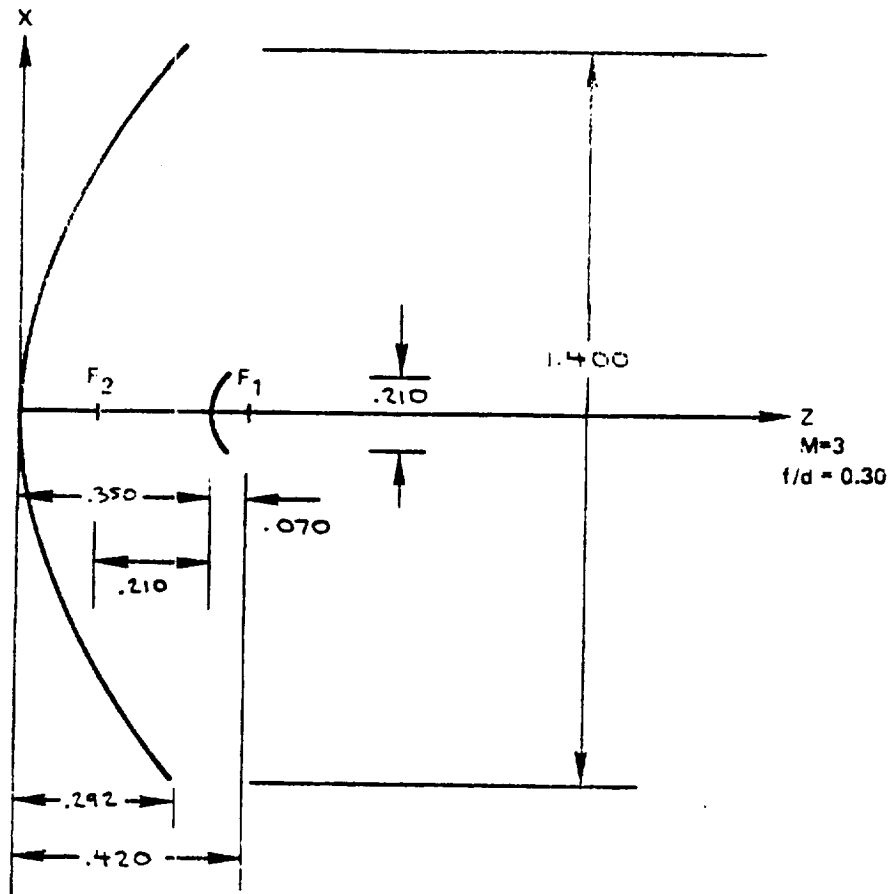
FIGURE 2-7. DIMENSIONS OF BASELINE LEO ANTENNA FOR DATA LINK

SECTION 3

TRANSMITTERS

TABLE OF CONTENTS, FIGURES & TABLES

3.0 TRANSMITTER DESCRIPTION

3.1 Overview

There are three different transmitter subsystems: one for the links between the GEO TDASs (the crosslink), one for link from the GEO TDAS to the low earth orbit (LEO) user spacecraft, and one for the link from the LEO spacecraft to the GEO TDAS. Because of the differing data rates for these links and the antenna characteristics of the baseline approach for each of these links, each of these three transmitters will have different requirements. However, because of the similarity of the requirements the implementation of these transmitters will draw on a common reservoir of EHF power amplifier technology. Similarly the transmitters will make use of the same modulator and frequency source technology. This section will summarize the EHF power amplifier and frequency source technology which will be available for all of the transmitter and receiver systems.

3.1.1 Power Amplifier Technology

Four types of power devices are candidates for use in the transmitter: IMPATT diodes, Field Effect Transistors (FETs), Gunn diodes and Traveling Wave Tube Amplifiers (TWTAs). The first three are solid state devices and the fourth is a thermionic vacuum tube. The status and characteristics of each of these devices are described in detail below.

3.1.1.1 IMPATT Diodes

IMPATT diodes can be made from either gallium arsenide or silicon (1,2). At frequencies below about 60 GHz, gallium arsenide diodes have proven to be the superior device with respect to both power output capability and efficiency of the DC to RF conversion. For example, 2.15 Watts at 14.4% efficiency has been achieved by Raytheon at 44 GHz (3). At higher frequencies silicon devices have given superior performance to date. Both silicon and gallium arsenide have produced approximately one Watt at 60 GHz. Silicon diodes with several hundred milliwatts output capability to well above 60 GHz are now commercially available (4). Gallium arsenide IMPATTs using a Read doping profile in a double drift configuration have produced 1 Watt with 13% efficiency at 56 GHz (5). Gallium arsenide's promise of higher efficiency is a strong argument in its favor although at the present its more demanding processing requirements make its use less well established than silicon at 60 GHz.

The present performance of IMPATT diodes is summarized in Figure 3.1.1-1 (5). It is seen that the performance of the two materials currently is similar at 60 GHz. The superior performance of GaAs at the lower frequencies, however, suggests that the best hope for improved 60 GHz performance lies in extending the superior GaAs performance to higher frequencies. This will require realizing for 60 GHz the double drift Read profiles which have given the superior GaAs performance at lower frequencies. This difficult task is the objective of at least two R&D programs. It is not unreasonable that 2 Watts will be achieved at 60 GHz by 1989. However, it is important, particularly in the case of IMPATT diodes, to make a distinction between state-of-the-art results and performance which can be achieved at a reliable, long life operating point usable in a space application. For such a High Rel application we feel that 1.5 Watts is a reasonable expectation for 1989. If this seems unduly pessimistic, it should be noted that IMPATTs represent a relatively mature technology. (Laboratory results of 1 Watt at 50 GHz were reported as long ago as 1971 (6)). Therefore we expect that space qualified

IMPATTs in 1989 will not offer much more capability than present state-of-the-art devices. Our projections are summarized in Figure 3.1.1-2. The projection given in this figure assumes operation at a reliable, space-applicable operating condition.

IMPATTs are two terminal devices which can be used as two port amplifiers in either of two modes: as an injection-locked oscillator or as a stable amplifier. Either can be implemented by the general circuit of Figure 3.1.1-3 where the matching circuit determines which mode is operative. The IMPATT is effectively a negative resistance in association with some reactance. With an appropriate matching circuit the load presented to the diode will not cause oscillation, but can still allow amplification of an applied signal. On the other hand in the injection-locked mode the matching circuit presents an impedance to the diode which causes it to oscillate. Under certain conditions the oscillator will lock to an applied input signal. Specifically the oscillator will lock to the input signal if it lies within a band, centered at the oscillator's free-running frequency, given by:

$$\frac{BW}{f_o} = \frac{2}{Q_e} \sqrt{P_{in}/P_{out}}$$

P_{in} and P_{out} are the input power and power out of the free-running oscillator respectively. Q_e is a function of the circuit but in practice will lie in the 20-100 range. A more accurate analysis would include the effect of the circulator VSWR, but in any event the locking bandwidth is related to the ratio of the input and output powers, much as a stable amplifier is subject to a gain-bandwidth limitation.

The choice of modes is important from a systems viewpoint. The injection-locked oscillator (ILO) cannot reproduce amplitude modulation, multiple-carrier signals or anything other than an angle modulated signal. In fact the free-running output will be present with no signal input unless a separate mechanism is included to turn off the diode when no input is present. On the other hand, the ILO mode gives more gain than a stable amplifier for the same bandwidth and power output. This translates to fewer stages and better size, weight, and efficiency. The smaller number of components and the somewhat lower temperature can lead to better reliability. It has been demonstrated that both ILOs and stable amplifiers can reproduce high data rate phase modulated signals if their bandwidth is sufficient, but the stable amplifier mode is more suitable for broad band applications (7,8,9).

A typical transfer characteristic of an IMPATT power amplifier operated as a stable amplifier (i.e. not as an injection-locked oscillator) is shown in Figure 3.1.1-4, taken from Kuno and English (26). To achieve the power output and efficiency used in the baseline transmitters (discussed in succeeding sections of this document), the power amplifiers must be operated near saturation at a point corresponding approximately to the 980 mW output point in Figure 3.1.1-4. At this point the slope of the transfer characteristic is about 0.25 dB/dB and the gain is down to about 10 dB from a small signal value of over 22 dB. The AM/PM conversion at such an operating point, on the basis of Kuno and English, would be on the order of 5 degrees per dB. Any signal degradation caused by this amount of AM/PM distortion has been included in the link budgets (Tables 1.1.1-1 through 1.1.1-6) as "Miscellaneous Hardware Losses".

Figure 3.1.1-1

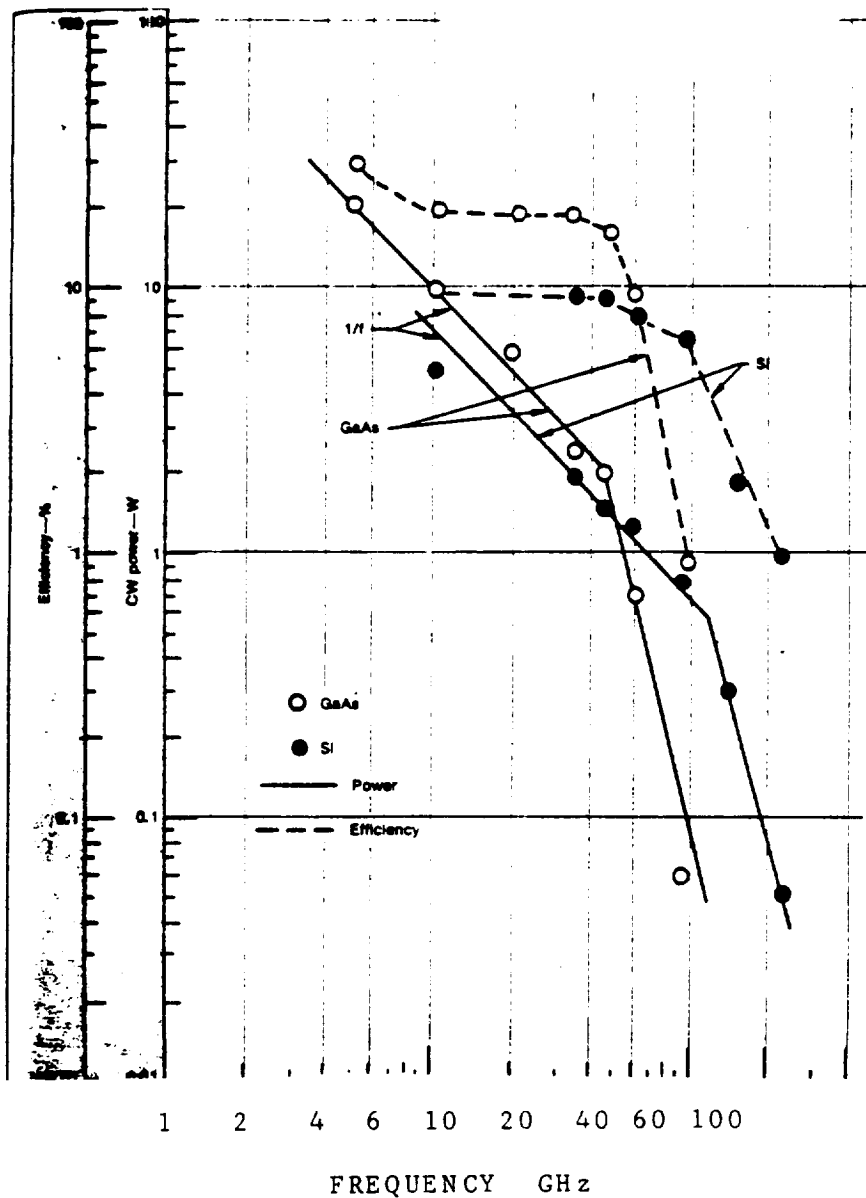Fig. 3.1.1-1 — A COMPARISON OF GaAs AND Si
              IMPATT DIODES (From Haugland Ref. 5)
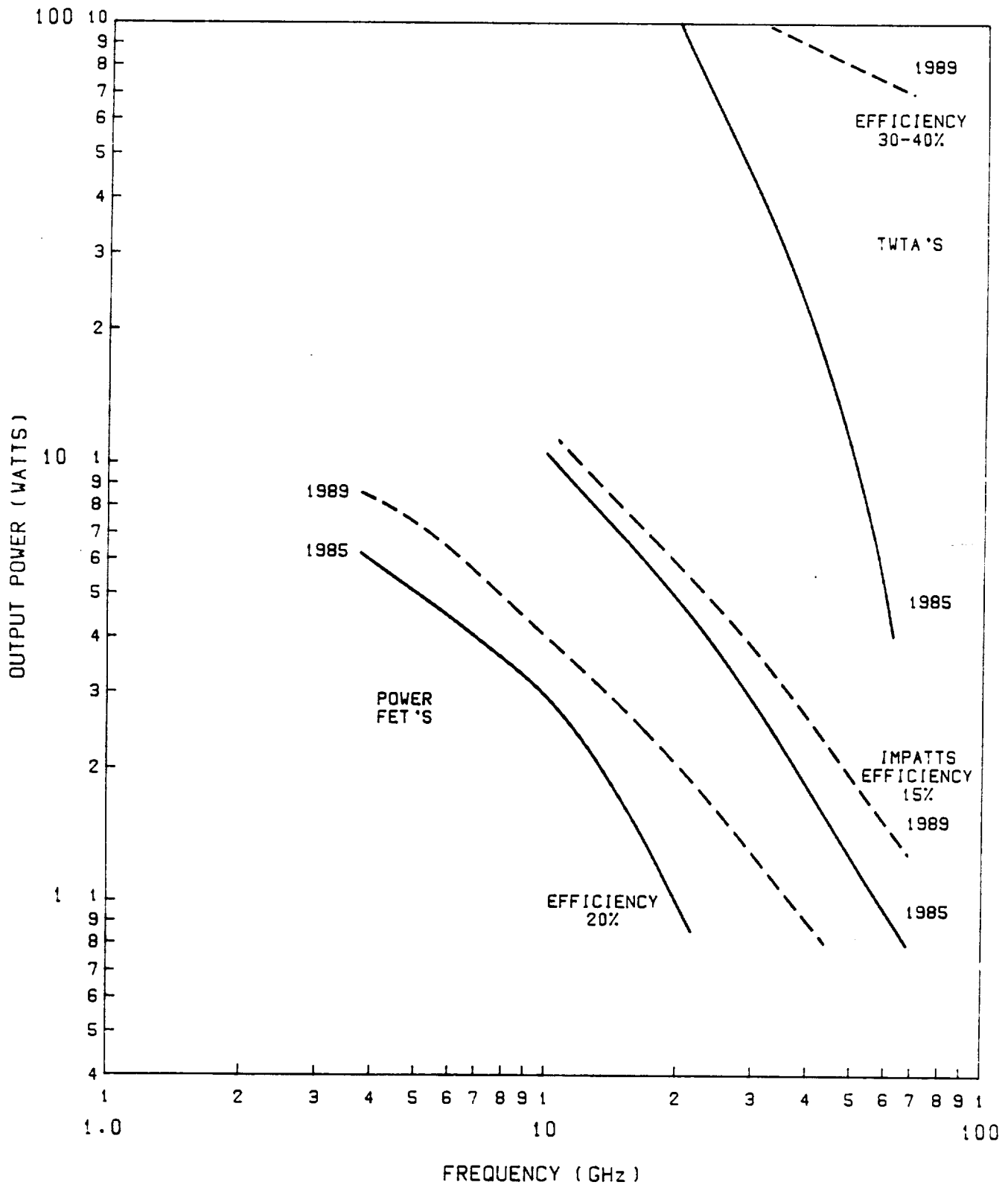
FIGURE 3.1.1-2
PRESENT AND ANTICIPATED PERFORMANCE OF MILLIMETER -
WAVE POWER SOURCES
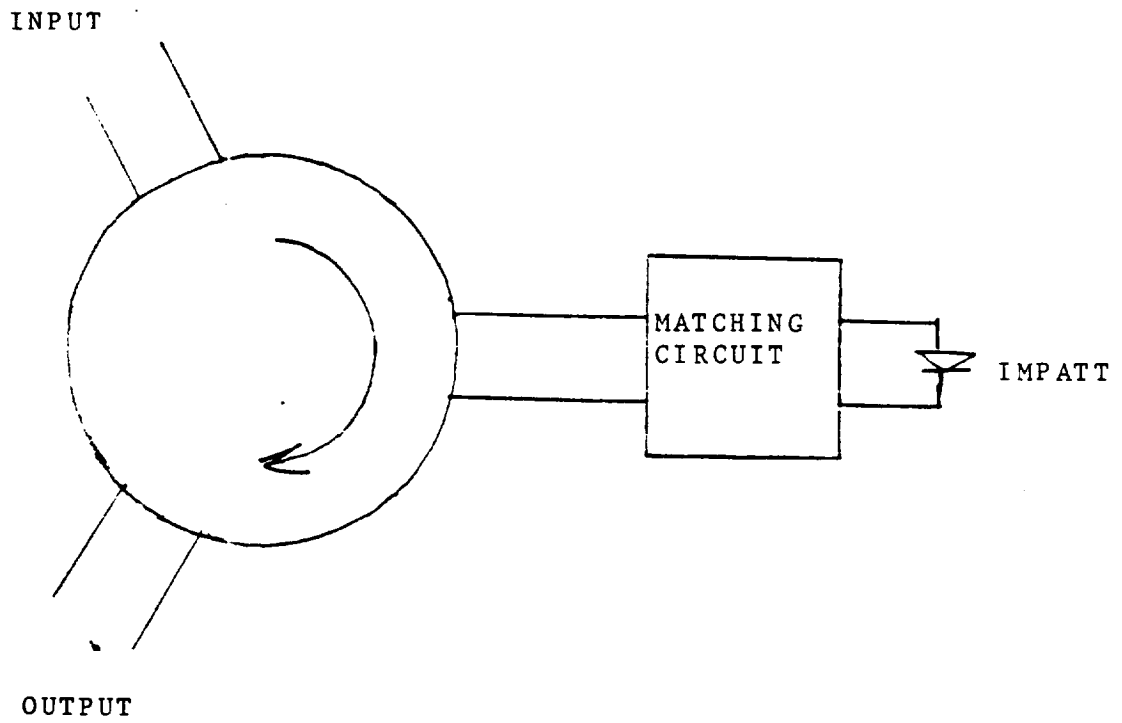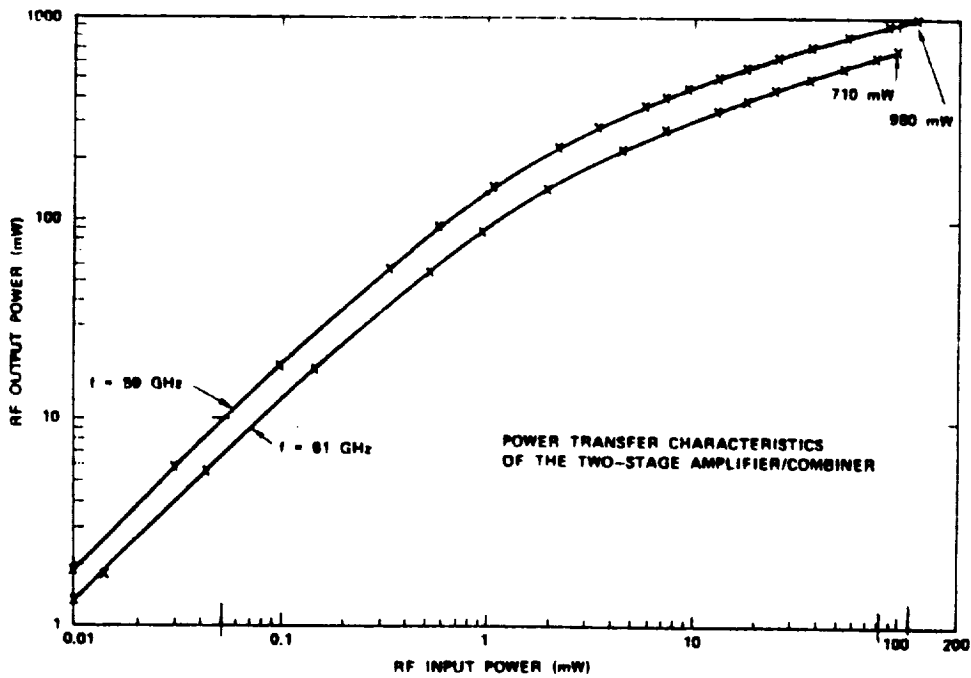
INPUT

MATCHING
CIRCUIT

IMPATT

OUTPUT

Figure 3.1.1-3

BASIC CIRCUIT FOR IMPATT AMPLIFIER
OR INJECTION LOCKED OSCILLATOR

Figure 3.1.1-4

TRANSFER CHARACTERISTIC OF A 60 GHz IMPATT AMPLIFIER

(FROM KUNO & ENGLISH)

3.1.1.2 FETs

In contrast to the relatively mature IMPATT technology, GaAs FET technology has made dramatic strides in recent years, replacing IMPATT and Gunn devices at lower frequencies and moving rapidly into the EHF range. Devices operating as high in frequency as 69 GHz have been demonstrated (10). Devices capable of one Watt of output power at 20 GHz are now commercially available (11,12). 93 milliwatts at 35 GHz has been reported. With further advances in photolithography, E-beam lithography, and material growth techniques, and the development of new devices such as the High Electron Mobility Transistor (HEMT), devices with usable output power at 60 GHz will be realized by 1989. The use of FETs offers several advantages. They are three-terminal devices which do not require bulky circulators to separate the input and output. The design of a stable broadband amplifier is considerably easier with a three-terminal device than with a two-terminal one. At lower frequencies such as 10 or 20 GHz where FETs are well developed, they offer efficiency superior to that of IMPATTs. On the other hand, even though FET technology is moving rapidly, it is very speculative to expect that FETs will be able to produce reliably as much as one Watt at 60 GHz by 1989. This is shown in Figure 3.1.1-2.

3.1.1.3 Gunn Effect Device

Gunn effect devices, like IMPATTs, are two-terminal devices. Unlike IMPATTs, however, they are "bulk effect" devices which do not utilize a p-n junction. Instead, their operation depends on a transferred electron effect which takes place in certain semiconductors, notably Gallium Arsenide and Indium Phosphide. This transferred electron effect in which for a certain range of voltages an increasing voltage excites electrons to move to a lower mobility state, under some circumstances can make the Gunn device act like a negative resistance. By proper circuit adjustment this negative resistance can be used to make an oscillator or a stable amplifier. The vast majority of Gunn diodes are based on GaAs technology. Recently it has been demonstrated that InP offers better performance at millimeter wavelengths such as 60 GHz (14). The efficiency of InP is about twice as high as that of GaAs. The transferred electron effect in InP is effective to about twice as high a frequency as in GaAs and a higher threshold voltage in InP is advantageous at millimeter wavelengths. As a result at 60 GHz 200 milliwatts has been obtained from an InP Gunn effect diode with an efficiency of about 6% (15), whereas GaAs Gunn diodes are capable of around 100 milliwatts at this frequency.

As in the case of IMPATTs, Gunn effect devices are a rather mature technology. Even InP development at 60 GHz extends back at least 9 years. (78 milliwatts in V-band was reported in 1976 (16)). Therefore we do not expect that much more than 200 milliwatts per device will be achievable on a space qualified basis in 1989. Thus Gunn effect devices will not be competitive with IMPATTs for a transmitter power source. On the other hand, Gunn devices have substantially superior noise characteristics to IMPATTs and are much more suitable than IMPATTs for use in LOs for mixers and upconverters and for small signal amplifiers.

3.1.1.4 Traveling Wave Tubes

Traveling wave tubes have filled a crucial role in the history of communication satellites. Their use as space based transmitters at frequencies up to 20 GHz is well established. In comparison with other types of tubes, they offer the best combination of high gain, broad bandwidth and high efficiency. Their performance in space has been impressive. More than 2800 space TWTs have been produced and have clocked more than 24 million hours of operation with a random catastrophic failure rate of about 200 per 10^9 hours (17).

At higher frequencies such as 60 GHz the TWT design problem becomes more challenging. Higher voltages are required and at the same time the physical size of the structure decreases so that higher voltage stresses are present not only in the tube but also in the DC/DC converter. Cathode current density must increase and this degrades the lifetime of the tube. 60 GHz tube technology has not been developed as extensively as at lower frequencies. For these reasons it is unreasonable to expect the same level of reliability at 60 GHz as at lower frequencies. Nevertheless the TWT is a leading candidate for a power amplifier for the ISL.

Two basic types of TWTs can be considered, corresponding to the type of slow wave structure used. The helical slow wave structure offers the greatest bandwidth, but a coupled cavity structure can dissipate more heat and can handle much higher power levels. The present state-of-the-art for helix tubes is 5 Watts output. Such a tube with 35 dB gain has 15% efficiency and weighs 3.3 pounds. NASA-Lewis has a program under way to develop a space type 75 Watt, 60 GHz coupled cavity tube with a 3 GHz bandwidth and 40% efficiency.

3.1.2 Power Combining Techniques

The candidate solid state devices for 60 GHz power amplifiers were described in Section 3.1.1 along with projections of anticipated 1989 performance. The highest power device is, and promises to be in 1989, the IMPATT. Even it, however, is only capable of around 1 Watt per device at the present, and at a conservative, reliable, low junction temperature operating point probably not much more than 1.5 Watt will be attainable in 1989. Therefore, to meet a 10 Watt output power requirement from solid state devices, the output of several devices will have to be combined. Several techniques are available for combining active devices. These will be described, and their advantages and disadvantages considered, in this section. The combining techniques can be divided into three categories: (1) chip level combining, (2) circuit level combining and (3) spatial combining.

3.1.2.1 Chip Level Combining

By "chip level combining" we mean making a series or parallel connection of semiconductor chips in a region which is small compared to a wavelength. This approach is severely limited at 60 GHz. The wavelength is so small that very few active devices can be combined in this manner. If the devices extend over an area which is not small compared to a wavelength, instabilities, unwanted modes, and interconnection parasitics complicate the response and must be taken into account explicitly by using circuit combining techniques. In addition the power output of solid state devices is typically limited by heating in such a way that trying to combine many devices in a small area does not necessarily avoid the limitation. One method of chip

level combining which offers some promise is the series connected IMPATT arrangement studied by Rucker at 40 GHz (18). However, even at 40 GHz the results had poor reproducibility and only 2 or 3 chips could be combined. As a result, we feel that chip level combining does not have the potential of the other two approaches for 60 GHz.

3.1.2.2 Circuit Level Combining

Many circuit level combining techniques have been studied and used at various frequencies. These have been reviewed in papers by Chang and Sun (19) and by Russell (20). Circuit combining techniques include resonant combining circuits, radial line combiners, hybrid combiners, chain coupled combiners, etc. All of these must be considered for this application at 60 GHz in terms of their bandwidth, efficiency, size, weight and number of devices which can be combined.

N-way combiners combine an almost arbitrary number of devices, N, in one circuit. Probably the most widely used N-way combiner is the resonant combiner, either the rectangular version of Kurokawa and Magalhaes (21) or the cylindrical version used by Harp and Stover (22), in which N active devices are placed in a resonant cavity at appropriate symmetrical locations to couple to the resonance. This technique has been used quite successfully at lower frequencies and somewhat less successfully at millimeter wavelengths. For instance in the cw mode at V-band a two-diode combiner with 1.4 Watt output and a four-diode combiner with 2.1 Watt output have been reported (23). At about 40 GHz, a twelve-diode rectangular resonant cavity combiner has produced 10 Watts of power (24).

The resonant combining technique, especially at lower frequencies, is capable of combining many devices efficiently and in a small size. It suffers from two important limitations for our 60 GHz application. As frequency increases either the cavity size must shrink, placing a limit on the number of diodes it is physically possible to place in the cavity, or else an over-moded cavity is used with the danger of instability and the excitation of unwanted modes. In addition the resonant combiner is narrowband with a bandwidth generally of less than 3%.

Another type of N-way combiner is the radial combiner, in either a waveguide or a microstrip version. This type of combiner has the advantage of broad bandwidth as a result of the fact that it is nonresonant. The typical trade off applies with respect to loss and physical size. A large waveguide version has low loss, whereas a microstrip approach reduces the size at the price of higher loss. TRW has reported a 16-way radial combiner at 60 GHz in waveguide (25). The loss is less than 1 dB over the 55-67 GHz range. It is about 3.5 inches in diameter. Our laboratory developed a 20 GHz, 8-way microstrip radial combiner which was only 1 inch in diameter. It also had only 1 dB of loss. However, at 60 GHz the loss would be higher and the size even smaller than 1 inch.

The combined output from the TRW radial combiner is probe coupled to coaxial line and then probe coupled to rectangular waveguide. Another approach which to the best of our knowledge has not been described previously, would be particularly desirable if one wants to take the output from the combiner in the TE_{01} mode of circular guide. This mode has the advantage that the loss is much less than in conventional rectangular guide and rotary joints can be readily incorporated in the TE_{01} mode guide. A radial combiner as shown in Figure 3.1.2-1 would couple directly and efficiently to the TE_{01} mode of

the circular guide. It should be possible to combine the outputs into the TE_{01} mode in this way more efficiently than the power can be combined into rectangular waveguide since a circularly symmetric mode is the natural output of a radial combiner.

Another nonresonant combiner uses hybrid couplers. This technique is widely used at microwave frequencies to combine transistors, in which case interdigitated microstrip hybrids are used. At 60 GHz waveguide hybrids are used to minimize loss. A 4-way combiner is shown in Figure 3.1.2-2. The hybrids also separate the input and the output of the reflection type amplifier. Such 4-diode combiners have been used extensively at millimeter wavelengths as efficient, broadband power combiners. The major limitation of the hybrid approach is that for combining more than four devices the approach becomes unwieldy and the efficiency depends strongly on the hybrid loss and the gain per device. Figure 3.1.2-3 is a plot of efficiency (the ratio of the power at the output to the power of N devices) as a function of the number of stages for a hybrid loss of 0.3 dB and a gain per device of 4, 6, or 10 dB. This plot is based on the following equation from Chang and Sun (19):

$$\eta = L^{-K}\left(1 - \frac{L}{G}^{2K}\right)$$

L is the hybrid loss expressed as a power ratio greater than unity, G is the gain per device and K is the number of stages. The efficiency is considerably better with more gain per device, but the 4-6 dB range is realistic for an amplifier meeting the bandwidth requirement of high data rate QPSK with anticipated IMPATT characteristics.

3.1.2.3 Spatial Combining

In spatial combining the outputs of many coherent radiating elements are made to add in a particular direction by proper control and adjustment of the phase of all the radiators. Whether spatial combining is an appropriate solution depends on many systems level considerations regarding the applicability of a phased array approach. The beam width and scanning angles determine the required number of radiating elements and their size. Generally overall systems requirements will determine whether an array approach is appropriate. If it is, the power amplifier problem is simplified in the sense that less power is required from an individual element. On the other hand, new requirements regarding size, heat sinking, phase accuracy and phase tracking become important.

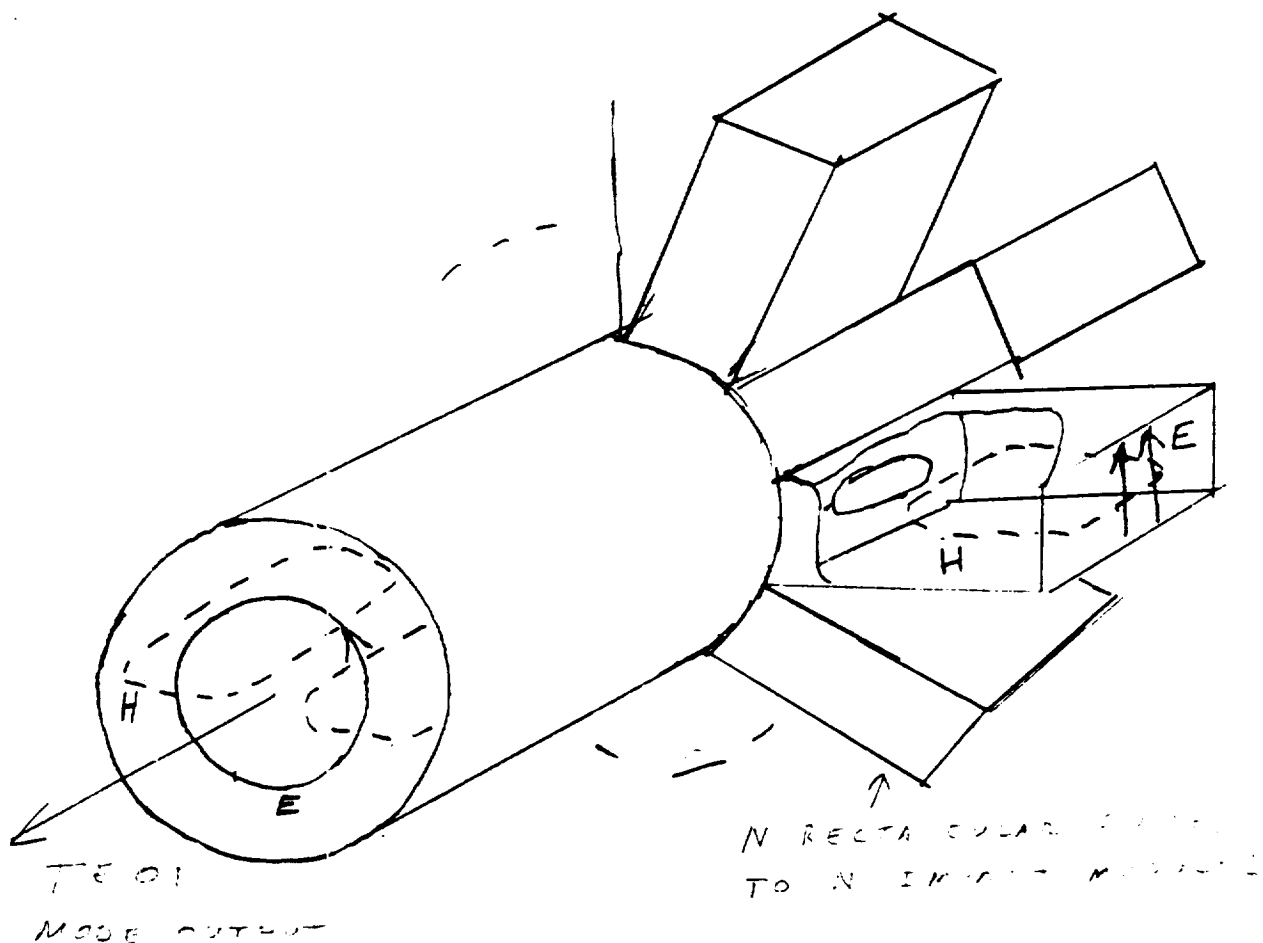The characteristics of important types of combiners are summarized in Figure 3.1.2-4.

FIGURE 3.1.2-1

Sketch showing coupling of N rectangular waveguides (excited in phase) to the TEOI mode of circular guide.

2-IMPATT MODULE

3-dB HYBRID
COUPLER

INPUT

OUTPUT
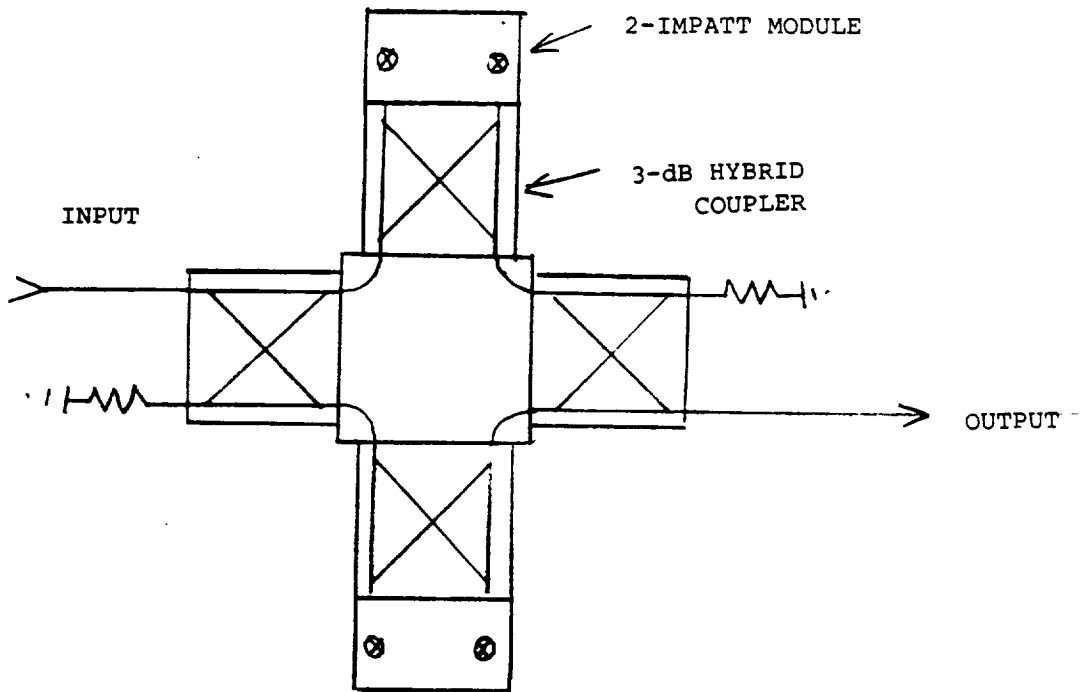
FIGURE 3.1.2-2

4-IMPATT Hybrid Combiner
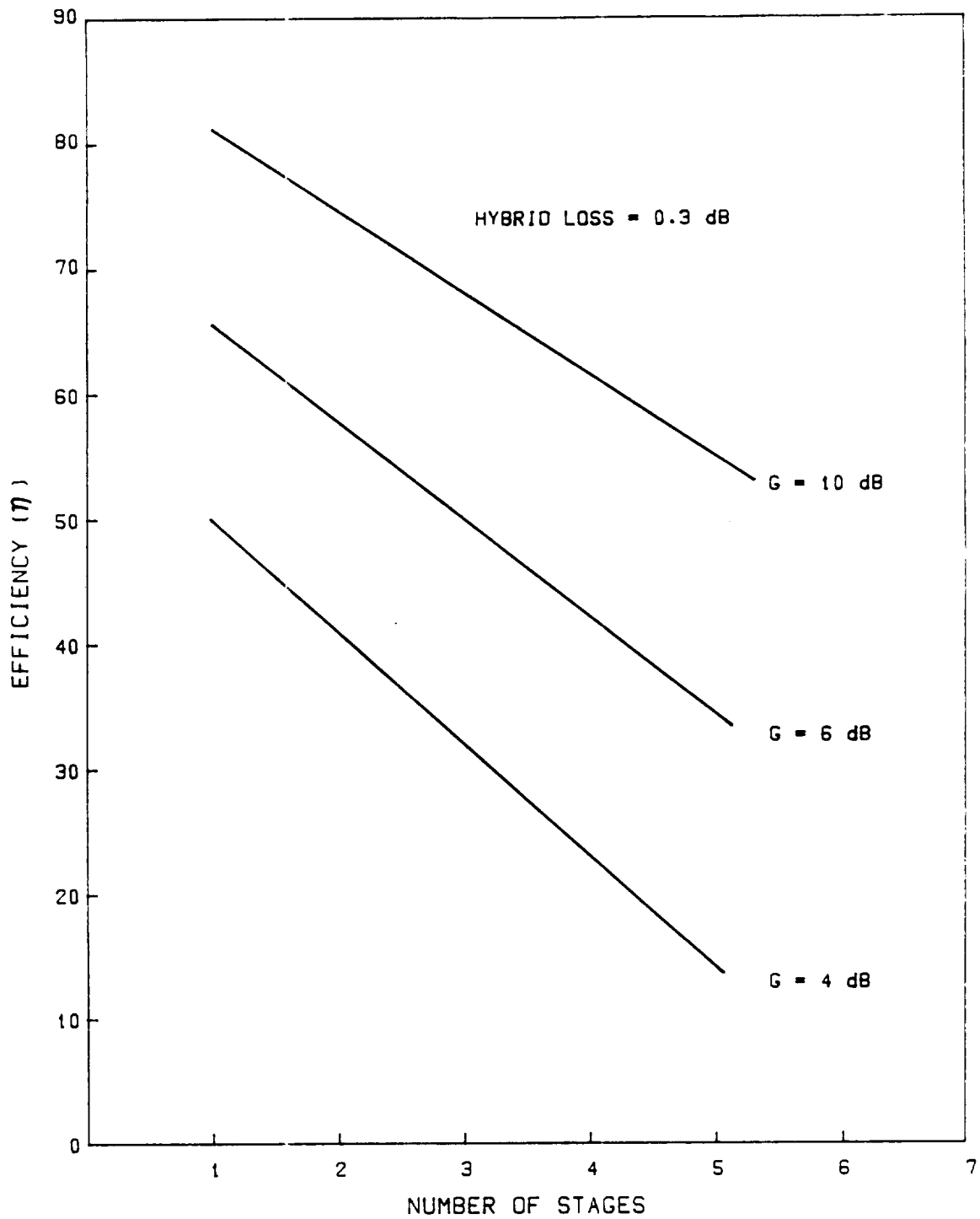
FIGURE 3.1.2-3
EFFICIENCY OF A HYBRID COMBINED FOR SEVERAL VALUES
OF GAIN. HYBRID LOSS 0.3 dB

POWER
COMBINING TECHNIQUES

N-WAY

ADVANTAGE: (a) SMALL
(b) LIGHT
(c) EFFICIENT

RESONANT
CAVITY

ACTIVE
DEVICES
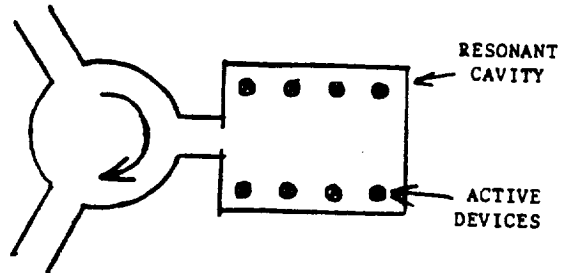
DISADVANTAGE: AT HIGH FREQUENCIES EITHER

(a) CIRCUIT BECOMES SMALL, LIMITS NUMBER OR DEVICES
OR

(b) IF CIRCUIT IS NOT SMALL, SUPPORTS MANY MODES, BECOMES UNSTABLE

(c) NARROW BAND (2%)

HYBRID COMBINER

ADVANTAGE: BROAD BAND (5%)

STRAIGHT FORWARD
"BRUTE FORCE" APPROACH

DISADVANTAGE: BECOMES LARGE, HEAVY
AND INEFFICIENT WHEN
NUMBER OF DEVICES IS
LARGE

ACTIVE
DEVICES

INPUT

OUTPUT
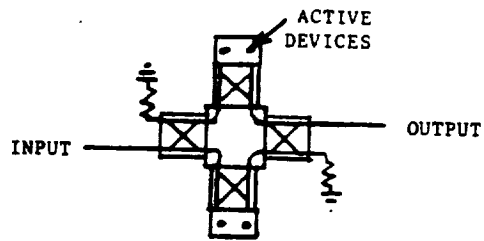
4 DEVICE HYBRID COMBINER

SPATIAL COMBINING

ADVANTAGE: o SUITABLE FOR PHASED ARRAY
o EFFICIENT

DISADVANTAGE: o MAY BE UNNECESSARILY COMPLEX
FOR SOME APPLICATIONS

POWER AMPLIFIERS

RADIATING
ELEMENTS
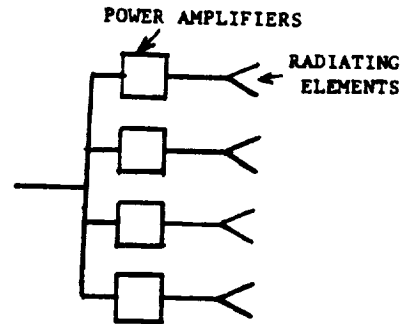
FIGURE 3.1.2-4

Summary of important combining techniques

3.1.3 10 Watt Power Amplifier

None of the candidate solid-state devices can produce close to the desired 10 Watts with a single device. Of the solid-state devices, IMPATTs promise still to have the highest power output at 60 GHz in the 1989 time frame. The power outputs shown in Figure 3.1.1-2 for IMPATTS are the power outputs from an optimally matched IMPATT oscillator. It has been shown by Kuno (8) that when an IMPATT is used in a reflection type of amplifier and operated at 3 dB saturated gain, the ADDED power will be equal to the output of the device used as an optimally matched oscillator. At 6 dB gain the amplifier output power is approximately 1.25 times that of an optimum oscillator. Thus, there is reason to expect an IMPATT amplifier to produce slightly more power output than shown in Figure 3.1.1-2. On the other hand when a number of devices are combined the combining efficiency will be less than one. In a narrow band amplifier (1% bandwidth) a low loss circulator can be used to separate the input and output of the amplifier, and a narrow band, efficient combiner can be used so that the output will approach the ideal. In a broadband approach, as is required here to handle the 2 Gbit/s data rate, a broadband combining approach such as the hybrid combiner will be necessary with a consequent reduction in efficiency. As a result of all these considerations, for our broadband case the amplifier output from a stage which combines N IMPATTs will be approximately N times the power shown in Figure 3.1.1-2 for an optimum oscillator. That this is true is demonstrated by the results of Kuno and English (26) who combined four IMPATTs, each producing 250-300 milliwatts as oscillators, in a four-way combiner with a 6 GHz bandwidth at 60 GHz, and obtained 1 Watt as the output power.

On this basis, then, it can be expected that 10 Watts should be attainable from an output stage which combines eight IMPATTs of the sort which should be available on a high-rel basis in 1989.

Kuno has demonstrated that either Injection Locked Oscillators (ILOs) or stable IMPATT amplifiers are capable of following high data rate phase modulation if the bandwidth of the amplifier is sufficient. Specifically, the bandwidth must be greater than the reciprocal of the phase-switching time. If 1 nanosecond is taken as the absolute maximum switching time for 2 Gbit/s QPSK, then the amplifier would be required to have 1 GHz bandwidth. In practice the bandwidth should be greater than this. Kuno found that a 3.5 GHz bandwidth IMPATT amplifier could be operated successfully with 4 Gbit/s QPSK. For our baseline design we will plan on a 2 GHz bandwidth for the 2 Gbit/s rate. Such a bandwidth is achievable, but it does impact the amplifier design substantially, restricting the design to broadband techniques such as hybrid combining or radial combining, and requiring low gain per stage in accordance with the gain-bandwidth limitation.

On the basis of these considerations and those described in Section 3.1.2, the baseline approach for a 10 Watt output stage will be an 8-way version of the radial combiner described by Hsu and Simonutti. The output will be in rectangular waveguide to feed the beam waveguide. The 10 Watt output stage with 2 GHz bandwidth would be expected to have approximately 3 dB gain, so that it must be driven by a four-diode, 5 Watt driver, probably using hybrid combiners. This, in turn, will be driven by a two-diode stage, driven by a one-diode stage, at which point the signal level should be down to a level attainable from a FET amplifier. Higher gains could be achieved in the IMPATT stages if the bandwidth were considerably less, but for the 2 GHz bandwidth, the gains assumed here are realistic.

The 10 Watt IMPATT amplifier is shown in Figure 3.1.3-1. The isolators and circulators are assumed to be of the junction type. Such devices can give less than 0.4 dB loss and a bandwidth of 3 GHz at 60 GHz. Broader band Faraday rotation isolators have higher loss, about 1.5 dB.

The amplifier of Figure 3.1.3-1 is based on the availability of IMPATTs which can produce about 1.5 Watts at a reliable, long life operating point. Such IMPATTs are the goal of present R&D programs and there is a good probability they will be available in 1989. In the event that they are not, more, lower power diodes would have to be combined in a radial combiner, increasing the size and weight. For instance the "lowest risk" scenario would use a 24-diode radial combiner as the output stage, adding considerably to the size and weight. In addition, the efficiency of these less advanced diodes would not be as good, so that more DC power would be required.

Table 3.1.3-1 shows the estimated performance and weight of 10 Watt IMPATT power amplifiers assuming either 1.5 Watt or 0.5 Watt devices. Also shown is the estimated weight of the DC to DC converters.

The only viable alternative to the IMPATT combiner is the TWTA. As indicated in Section 3.1.1.4, the present state-of-the-art is a 5 Watt tube with 15% efficiency. In principal a 10 Watt tube could be developed; however, unless development of such a tube is begun immediately, it will not be available in the 1989 time frame. Therefore, it is assumed that a 10 Watt TWTA in 1989 would combine two 5 Watt TWTs. On this basis, Table 3.1.3-1 compares the characteristics of the candidate power amplifiers. The TWTA promises the best efficiency. The IMPATT amplifiers, particularly, of course, the version based on 1.5 Watt devices, offer considerably less weight. For a particular power level, the DC to DC converter for the IMPATT amplifier is smaller and lighter than for the TWTA since the TWT requires a high voltage (approximately 6 KV) whereas the IMPATTs will be biased at about 15 volts. The efficiency of the DC to DC converters will be about 85% in either case.

TABLE 3.1.3-1

10 WATT POWER AMPLIFIERS

CHARACTERISTIC	TWTA	IMPATT (assuming 1.5 W devices)	IMPATT (assuming 0.5 W devices)
GAIN	38 dB	38 dB	38 dB
BANDWIDTH	2 GHz	2 GHz	2 GHz
POWER OUTPUT	10 W	10 W	10 W
DC POWER INPUT	67 W	111 W	200 W
EFFICIENCY	15 %	9 %	5 %
WEIGHT OF RF AMPLIFIER	6.6 lbs.	1.6 lbs.	3.7 lbs.
WEIGHT OF DC/DC CONVERTER	6.6 lbs.	3.3 lbs.	6.6 lbs.
TOTAL WEIGHT	13.2 lbs.	4.9 lbs.	10.3 lbs.
POWER INTO DC/DC CONVERTER	80 W	130 W	235 W
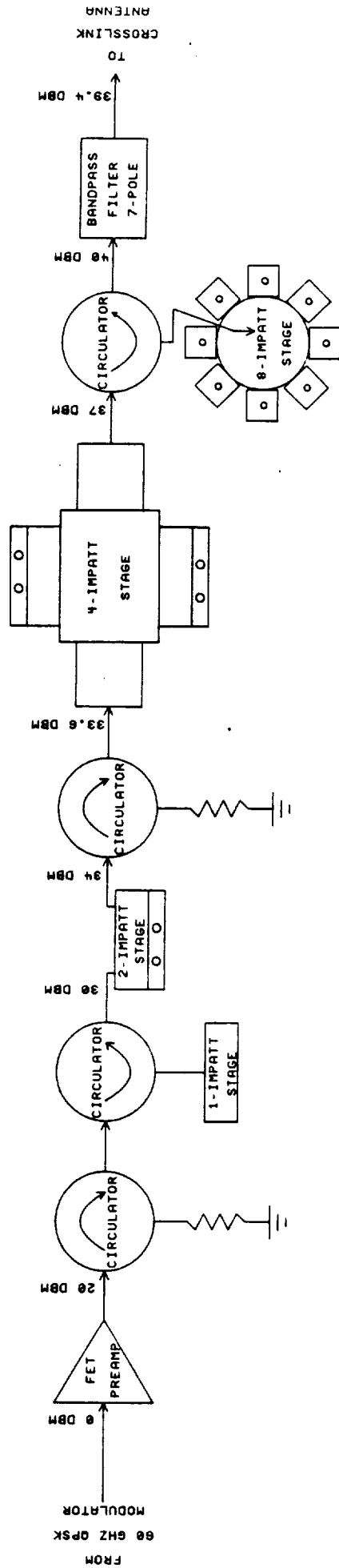
10 WATT POWER AMPLIFIER

FIGURE 3.1.3-1

3-18

3.1.4   0.6 Watt Power Amplifier

The GEO-LEO link requires a 0.6 Watt transmitter aboard the GEO spacecraft. It should be possible to realize this in 1989 with an output stage which uses a single IMPATT diode. This output stage will have sufficient gain to be driven by a FET amplifier. Thus, the amplifier will consist essentially of the FET amplifier and the first IMPATT stage of the 10 Watt transmitter, but with a slightly lower power IMPATT diode. The much smaller bandwidth of this amplifier in comparison to the GEO-GEO amplifier will make this amplifier significantly easier to achieve. The characteristics of the GEO-LEO power amplifier are shown in Figure 3.1.4-1.
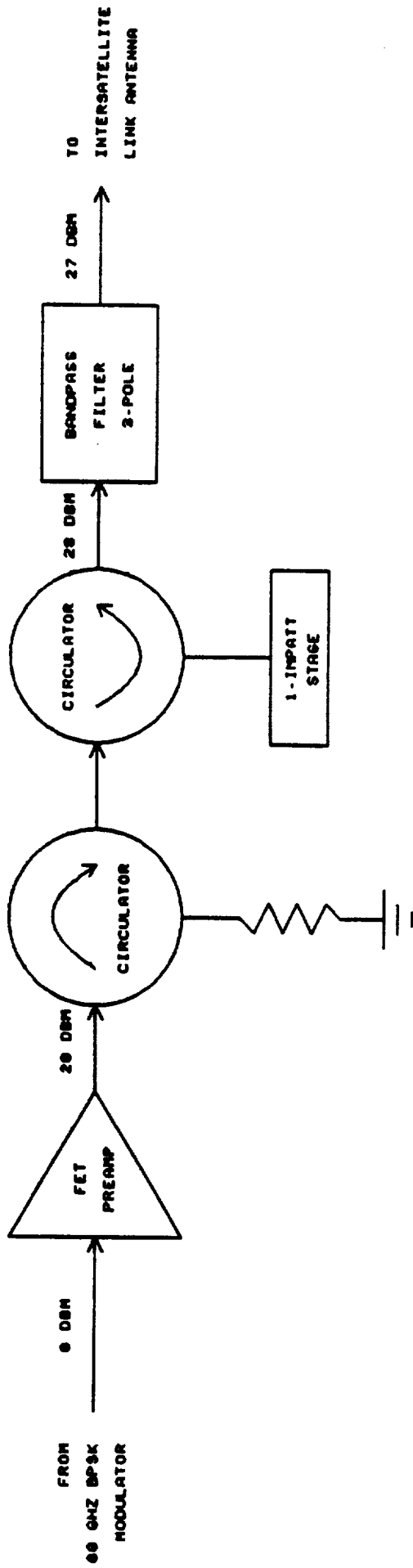
3.1.5   Frequency Source Technology

A stable RF source is required in the transmitter either to drive an upconverter or to provide a signal to be directly modulated. The technology available for such a source is the same as that for the local oscillator described in detail in section 4.1.3. The frequency source for the transmitter will be the same as the crystal stabilized oscillator proposed for the LO.

3.1.6   Modulator Technology

Although BPSK modulation is acceptable for the low data rate (1 Mbps) on the Command link, the high data rates involved in both the Crosslink and Return link, coupled with severe bandwidth limitations, force a higher M-PSK modulation for those data paths. Frequency planning per Figure 1.1.1-2 allows data communication at the specified rates to be within the bounds of the WARC-79 frequency allocations if QPSK modulation is used. Due to the broad bandwidth of the Crosslink (2 GHz) a stable amplifier will be required (see Section 3.1.1.1); thus offset QPSK, which might be desireable using an ILO as the amplifier, will not be necessary, since stable amplifiers are capable of following high data rate phase modulation.

Direct QPSK modulation at 60 GHz has been shown to be feasible by Grote and Chang(27). Their concept of the modulator circuitry, which includes an in-phase power divider and an in-phase power combiner, two biphase switches and a 90 degree phase shifter (implemented by increased microstrip path length before one of the switches), has been adopted as the baseline modulator. The QPSK modulator is shown in Figure 3.1.6-1.

A simplified version of the circuitry implementing only one biphase switch will be used for direct BPSK modulation at 60 GHz. Such a circuit is shown in Figure 3.1.6-2.

FROM 60 GHZ BPSK MODULATOR

0 DBM

FET PREAMP

20 DBM

CIRCULATOR

CIRCULATOR

1-IMPATT STAGE

28 DBM

BANDPASS FILTER 2-POLE

27 DBM

TO INTERSATELLITE LINK ANTENNA

GEO-LEO

0.6 WATT TRANSMITTER SUBSYSTEM

Figure 3.1.4-1

3-20
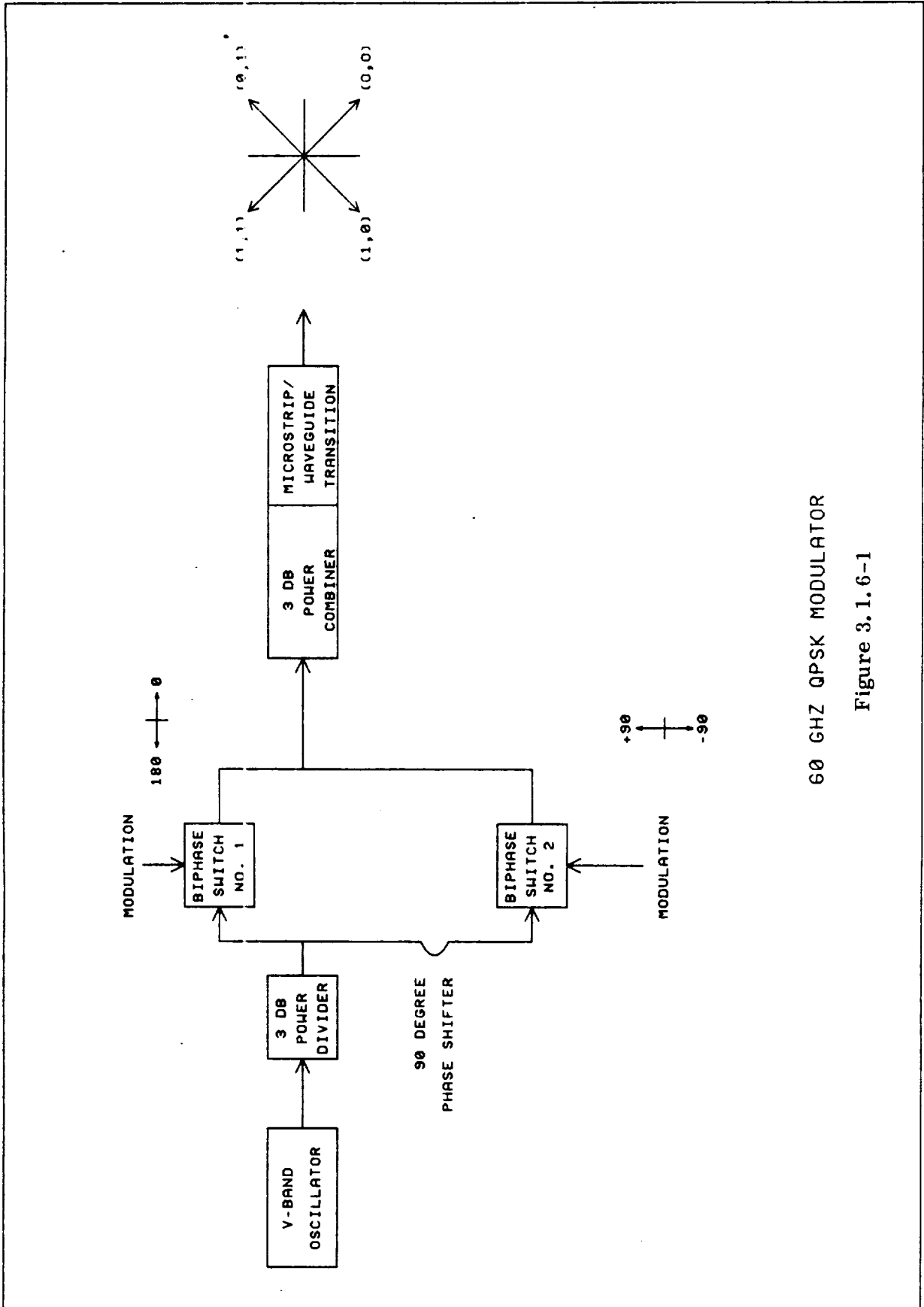
60 GHZ QPSK MODULATOR

Figure 3.1.6-1

60 GHZ BPSK MODULATOR

Figure 3.1.6-2

3.2   GEO-LEO Transmitter

The GEO-LEO transmitter is the simplest of the transmitter designs. Because of the low data rate (1 Mb/s) only 600 milliwatts is required from the transmitter in the baseline system and, therefore, its output stage will require only one active device. The baseline design uses an IMPATT for the output stage. If FETs develop at a rapid pace, the FET could be a more efficient approach in 1989. However, IMPATTs will be assumed because of their established capability for meeting this requirement.

The baseline transmitter will consist of the 0.6 watt power amplifier shown in Figure 3.1.4-1 integrated with the BPSK modulator of Figure 3.1.6-2. The frequency source is the crystal stabilized Gunn oscillator of Figure 4.1.3-2. The IMPATT stage will be in waveguide to minimize losses. The overall size, weight and power consumption will be dominated by the crystal controlled oscillator.

3.2.1   Cooling System

The baseline transmitter cooling system will utilize a variable conductance heat pipe (VCHP) and radiator system plus heaters for thermal control. The VCHP's will be mounted in an aluminum faceskins, aluminum honeycomb panel such as to be part of the panel structure. FACC anticipates utilizing high purity (99.999%) ammonia as the hea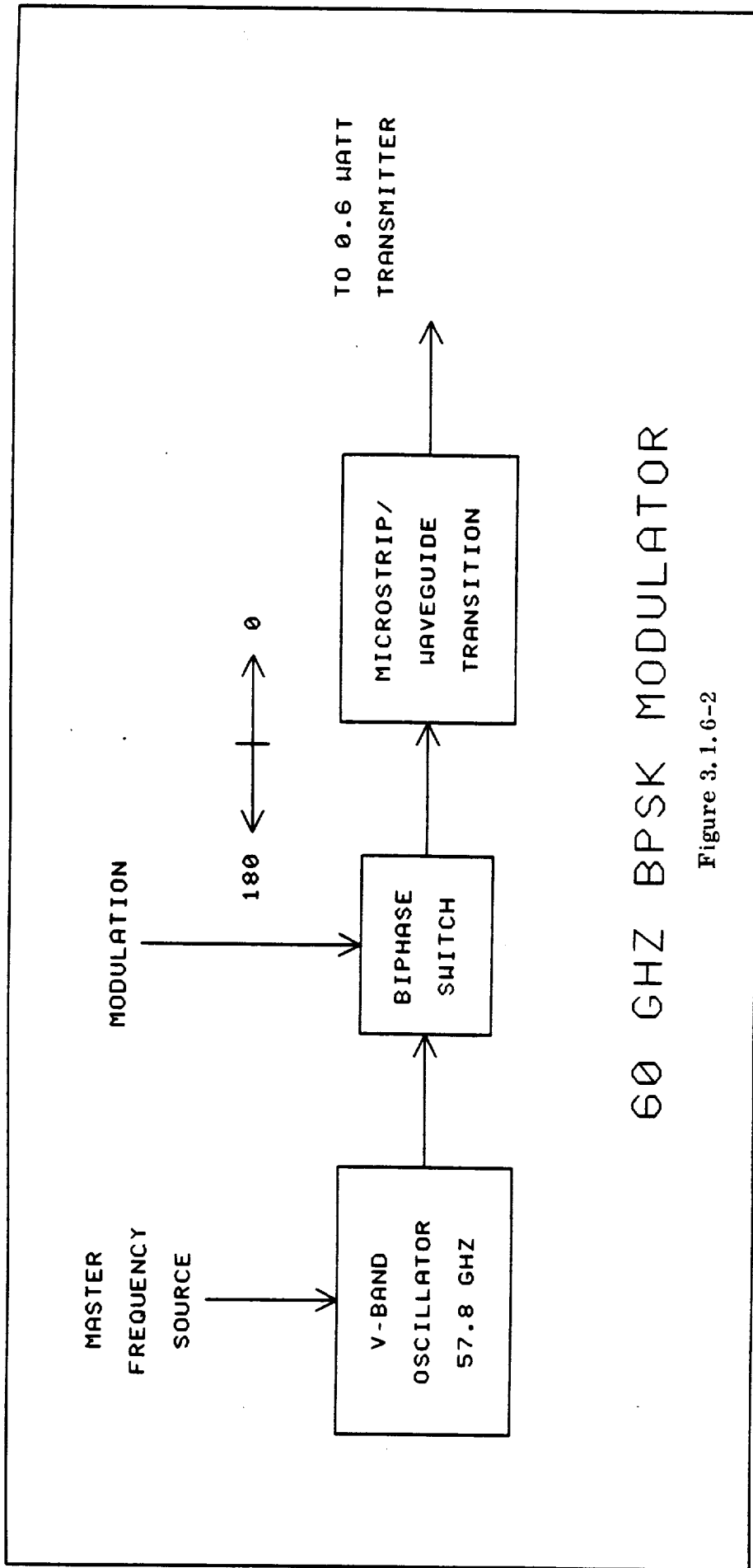t transport fluid contained by an aluminum tube. The transmitter will be attached to the honeycomb panel at the inner faceskin interface. OSR's will be applied to the outer faceskin interface and multilayer insulation will cover all other exposed surfaces of the ICL.

3.3   LEO-GEO Transmitter

The LEO-GEO transmitter, in the baseline plan, must be capable of transmitting 7.5 Watt if using the maximum data rate of 300 Mb/s. The power amplifier will be essentially the same as the 10 Watt amplifier, but with diodes biased at a lower power operating point. This will result in a conservative estimate of weight and power consumption since the larger gain per stage that can be achieved over the narrower bandwidth of this link could be exploited to improve these characteristics.

The baseline LEO-GEO transmitter is thus an integration of the power amplifier of Figure 3.1.3-1 and the QPSK modulator of Figure 3.1.6-1. The frequency source again is the crystal-controlled oscillator of Figure 4.1.3-2.

Those users who do not need the full 300 Mbps data rate may prefer to utilize a smaller transmitter and/or antenna. For a minimum data rate of 100 Kbps, the RF transmitters could be 0.5 Watt or less, so that the output stage could use only one active device, as in the GEO-LEO transmitter.

3.3.1 Cooling System

The baseline transmitter cooling system will utilize a variable conductance heat pipe (VCHP) and radiator system plus heaters for thermal control. The VCHP's will be mounted in an aluminum faceskins, aluminum honeycomb panel such as to be part of the panel structure. FACC anticipates utilizing high purity (99.999%) ammonia as the heat transport fluid contained by an aluminum tube. The transmitter will be attached to the honeycomb panel at the inner faceskin interface. OSR's will be applied to the outer faceskin interface and multilayer insulation will cover all other exposed surfaces of the ICL.

3.4 GEO-GEO Transmitter

The GEO-GEO link imposes the most difficult transmitter requirements of the three types of links. Not only is the required power output (10 Watts) higher than in the previous cases, but the bandwidth (2 GHz) makes this power harder to achieve. The baseline approach combines the 10 Watt power amplifier described in Section 3.1.3 with the QPSK modulator described in Section 3.1.6 and the stable source of Figure 4.1.3-2.

3.4.1 Cooling System

The baseline transmitter cooling system will utilize a variable conductance heat pipe (VCHP) and radiator system plus heaters for thermal control. The VCHP's will be mounted in an aluminum faceskins, aluminum honeycomb panel such as to be part of the panel structure. FACC anticipates utilizing high purity (99.999%) ammonia as the heat transport fluid contained by an aluminum tube. The transmitter will be attached to the honeycomb panel at the inner faceskin interface. OSR's will be applied to the outer faceskin interface and multilayer insulation will cover all other exposed surfaces of the ICL.

REFERENCES

1. R.S.Ying, "Solid-State Sources Power Millimeter Transmitters", MSN, Vol. 13, No. 12, November, 1983, p280.

2. F.A. Myers, "Performance Parameters Examined for Millimeter-Wave Solid State Devices", MSN, Vol. 14, No.7, July, 1984, p266.

3. L.H.Holway & S.L.Chu,"Broadband Characteristics of EHF IMPATT Diodes", IEEE Transactions on Microwave Theory and Techniques,Vol.30, No.11, p1893.

4. Hughes Millimeter-Wave Products 1985 Catalog.

5. Edward J. Haugland,"NASA Seaking High-power 60 GHz IMPATT Diodes", MICROWAVES & RF, August 1984, p100.

6. Thomas E. Seidel, Ronald E. Davis, David E. Iglesias,"Double-Drift-Region Ion-Implanted Millimeter-Wave IMPATT Diodes", Proc. of the IEEE, Vol.59, No.8, Aug 1971, p1222.

7. Yu-Wen Chang, H.J.Kuno, D.L.English, "High Data Rate Solid-State Millimeter Wave Transmitter Module", IEEE Trans. on Microwave Theory and Techniques, Vol.MTT-23, No.6, June, 1975, p470.

8. H. J. Kuno, "Analysis of Nonlinear Characteristics and Transient Response of IMPATT Amplifiers", IEEE Trans. on Microwave Theory and Techniques, Vol. MTT21, No11, Nov. 1973, p694.

9. H. J. Kuno & D. L. English, "Nonlinear and Large-Signal Characteristics of Millimeter-Wave IMPATT Amplifier", IEEE Trans. on Microwave Theory and Techniques, Vol.MTT-21, No.11, Nov. 1973, p703.

10. D. W. Maki, J. M. Schellenberg, H. Yamasaki, L.C.T. Liu, "A 69 GHz Monolithic FET Oscillator", 1984 IEEE MTTS International Microwave Symposium Digest, p62.

11. Raytheon product information.

12. Y. Hirachi, Y. Takeuchi, M. Igarashi, K. Kosemura, S. Yamamoto, "A Packaged 20GHz 1 Watt GaAs MESFET with a Novel Via-Hole Plated Heat Sink Structure" IEEE Transaction on Microwave Theory and Techniques, Vol. MTT-32, No.3 March, 1984.

13. Yong-Hoon Yun, G. C. Taylor, D. S. Bechtle, S. T. Jolly, S. G. Liu, R. L. Camisa, "Ka-Band GaAs Power FET's", 1983 IEEE MTTS International Microwave Symposium Digest, p.136.

14. F. Berin Fank, "InP Emerges as Near Ideal Material for Prototype Millimeter Wave Devices",MSN, February, 1982, p.59.

15. F. B. Fank & J. D. Crowley, "Gunn Effect Devices Move Up in Frequency and Become More Versatile", Microwave Journal, Sept. 1982, p. 143.

16. R. J. Hamilton, Jr., R. D. Fairman, S. I. Long, M. Omori, F. B. Fank, "InP Gunn Ef Devices for Millimeter-Wave Amplifiers and Oscillators", IEEE Transactions on Microwave Theory and Techniques, Vol. MTT-24, No.11, Nov. 1976.

17. T. A. Appleby, "Space Tubes: Past, Present, and Future", Hughes Aircraft Co., Electron Dynamics Division, Torrance, CA.

18. C.T.Rucker, J.W.Amoss, G.N.Hill, "Chip Level IMPATT Combining at 40 GHz", 1981 IEEE MTTS International Microwave Symposium Digest, p.347.

19. K. Chang and C. Sun, "Millimeter-Wave Power Combining Techniques", IEEE Transactions on Microwave Theory and Techniques, Vol. MTT-31, No.2, Feb. 1983, p.91.

20. K. J. Russell, "Microwave Power Combining Techniques", IEEE Transactions on Microwave Theory and Techniques, Vol. MTT-27, No.5, May, 1979, p.472.

21. K. Kurokawa, F. M. Magalhaes,"An X-Band 10 Watt Multiple-IMPATT Oscillator", Proceedings of the IEEE, Jan. 1971, p.102.

22. R. S. Harp & H. L. Stover, "Power Combining of X-Band IMPATT Circuit Modules", 1973 IEEE-ISSCC Digest of Technical Papers, Feb., 1973, p.118.

23. Y. Ma & C. Sun, "Millimeter Wavelength Combiner at V-Band",Proceedings of the Seventh Cornell Electrical Engineering Conference, Aug. 1979, p.299.

24. D. W. Mooney & F. J. Bayuk, "41 GHz 10 Watt Solid State Amplifier", Proceedings of the 11th European Microwave Conference (Amsterdam) Sept.1981, p.876.

25. T. Hsu, M. Simonutti, "A Wideband 60 GHz 16-Way Power Divider/Combiner Network", 1984 IEEE MTTS International Microwave Symposium Digest p. 175.

26. H. J. Kuno & David L. English, "Millimeter-Wave IMPATT Power Amplifier/ Combiner", IEEE Transactions on Microwave Theory and Techniques, Vol. MTT-24, No.11, p. 758, Nov.1976.

27. Albert Grote & Kai Chang, "60-GHz Integrated-Circuit High Data Rate Quadriphase Shift Keying Exciter and Modulator", IEEE Transactions on Microwave Theory and Techniques, Vol. MTT-32, No.12, p. 1663, Dec. 1984.

SECTION 4

RECEIVERS

TABLE OF CONTENTS, FIGURES & TABLES

4.0 RECEIVER

4.1 RF Technology Overview

Three receivers must be considered in this study. Since their requirements are similar in many respects, they will utilize much the same RF technology. This section summarizes the current and projected 1989 technology applicable to the realization of the RF portions of the receiver.

A general block diagram for the RF portion of a receiver is shown in Figure 4.1.1-1. The receiver noise temperature, T_e, is given by:

$$T_e = T_A + ((L_D t_D - 1)T_0 + L_D T_{IF})/G_A$$

The antenna loss and line losses before the receiver will be accounted for separately in the link calculations. Single sideband operation is assumed by the equation. If a high performance RF preamplifier is available with a low noise temperature, T_A, and a gain, G_A, sufficient to make the second term in the brackets negligible compared to T_A, the receiver noise temperature will be that of the preamplifier. On the other hand the state of preamp technology relative to mixer and IF amplifier technology may be such that the lowest noise temperature is achieved by omitting the preamp and accepting the noise temperature set by the mixer conversion loss and noise temperature of the IF amplifier. The following sections discuss the 60 GHz technology for low noise preamplifiers, mixers and local oscillators.

4.1.1 60 GHz Low Noise Amplifiers

Up to the present time at 60 GHz only parametric amplifiers have offered noise temperatures low enough to be capable of making a receiver with a lower noise figure than that obtained by going straight in to a low noise mixer followed by a low noise amplifier. This is seen in Figure 4.1.1-2. A noise figure of around 3 dB can be obtained at 60 GHz from a cooled, non-cryogenic paramp and 4.5 dB from an ambient temperature paramp(1). Although paramps have been used in space to a limited extent at lower frequencies, their complexity, size, weight, poor reliability, and requirement for a pump at greater than 100GHz for low noise at 60 GHz, make them unsuitable for an ISL preamp.

Gallium Arsenide and Indium Phosphide Gunn amplifiers have been built at EHF but their noise figures of around 15 dB are not competitive with direct conversion.

The situation is changing rapidly and dramatically, however, with the rapid advances in Gallium Arsenide FET technology and in High Electron Mobility Transistors (HEMTs).

In a very short time GaAs FETs have come to dominate low noise amplifier technology at microwave frequencies. Recent results indicate that they are moving rapidly into the 30-60 GHz range. Watkins, et al, from Hughes have reported amplifier noise figures as low as 2.0 dB at 30 GHz using one-quarter micron gate FETs(2,3,4). At 60 GHz they report noise figures of 7.1 to 8.9 dB with an associated gain of 3.1 to 5.8 dB. A three stage-amplifier achieved 17.4 +/-1.0 dB gain from 56 to 60 GHz. Biased for minimum noise, this amplifier demonstrated a 9.2 dB noise figure with 12 dB gain. Avantek has reported 7 dB gain and 3.5 dB noise figure at 44 GHz with their quarter-micron FET(5). Clearly the results at 30 and 44 GHz are substantially better than the early 60 GHz results, but it would be expected that further development at 60 GHz will yield significant improvement.
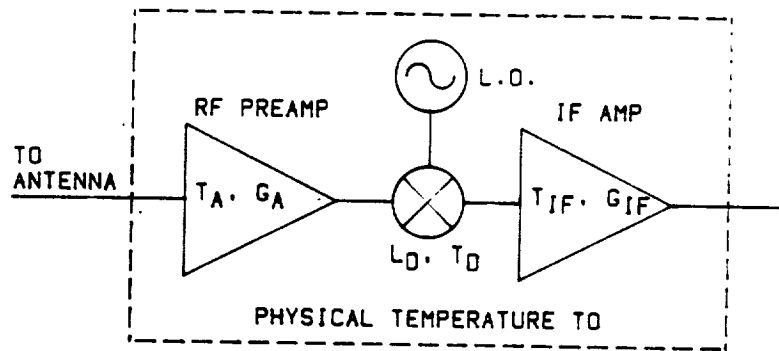
FIGURE 4.1.1-1 GENERAL BLOCK DIAGRAM
FOR RF PORTION OF RECEIVER

FIGURE 4.1.1-2

4-3
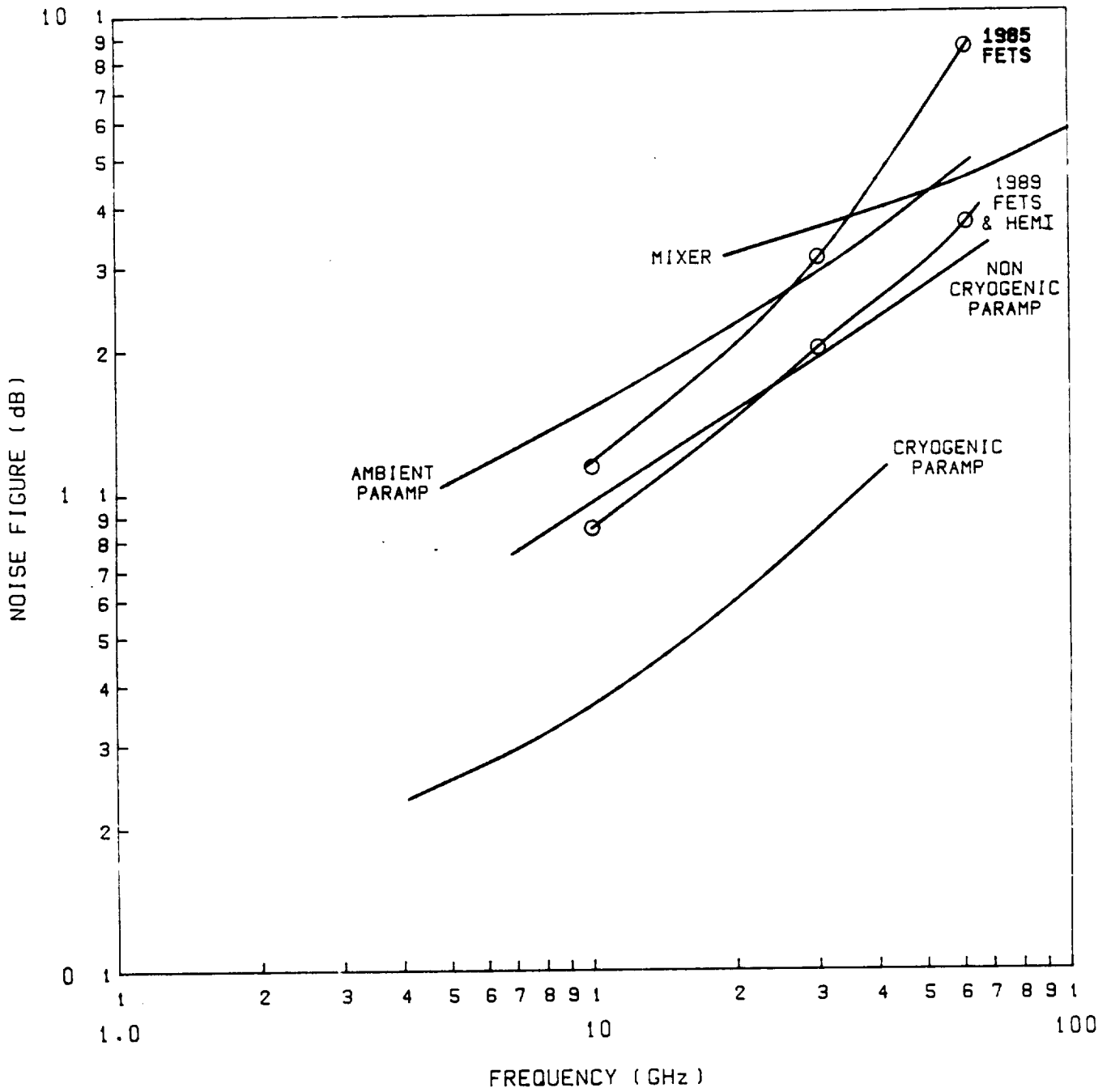
4.1.2 Mixers

As discussed previously, if a preamplifier with a sufficiently high gain and low noise figure is available, it will establish the receiver noise figure, and the loss of the mixer and the noise figure of the IF amplifier will not be critical. If an amplifier with the required characteristics is not available, however, the lowest noise figure will be achieved by going directly into a high performance mixer. In that case the noise temperature of the receiver becomes:

$$T_e = (L_D t_D - 1)T_0 + L_D T_{IF}$$

t_D will be approximately unity for the high IF frequencies of the ISL application, and the noise figure, F, becomes:

$$F = (L_D - 1)(-1 + T_0/290) + L_D F_{IF}$$

If the temperature of the mixer is approximately room temperature, this becomes the familiar result that the noise figure is the sum of the mixer conversion loss and the IF noise figure with all quantities expressed in dB.

Since adequate low noise amplifiers have not been available, up to now, at millimeter wavelengths, considerable effort has been devoted to development of low loss mixers. The development in recent years of high quality beam lead Schottky diodes has resulted in good EHF mixer performance. The reliability should be better than with the older point-contact diodes if the beam lead diodes are mounted properly on a hard substrate such as fused silica and if hermetic sealing is provided. Some representative results are summarized below.

Paul, et al(ref 8)   63 GHz LO, 57 GHz signal, 6 dB conversion loss

Chang, et al(ref 9)   57 GHz LO, 63 GHz signal, 6 dB conversion loss

Whelehan (ref 10)   60 GHz LO, 1.5 GHz IF, 9-10 dB noise figure
                                                (including 5 dB IF noise
                                                figure contribution)

Alpha Industries(ref 11)60 GHz signal, 4 GHz IF, 6 dB conv. loss (typ)
                                                7 dB conv. loss (max)

Hughes (ref 12)   60 GHz signal, 4 GHz IF, 6 dB conversion loss

Some of these results use Duroid substrates which are convenient for experimental work, but unsuitable for high-reliability use in this application. The Alpha Industries performance is for a "high reliability" mixer with hermetic sealing. All of these results are for singly-balanced (two-diode) mixers. A photograph of a 60 GHz balanced mixer developed at Ford Aerospace and Communications Corporation is shown in Figure 4.1.2-1. This mixer uses two beam lead diodes bonded to thin film metalization on a fused silica substrate, and mates directly to waveguide for the signal and LO connections. This mixer has given conversion loss as low as 5.5 dB (13).

The noise figure of the IF amplifier must be added to the conversion loss of the mixer to obtain the noise figure of the receiver. This IF noise figure will depend on the bandwidth and frequency of the IF. For a relatively narrowband situation (up to approximately 500 MHz bandwidth) the IF noise figure can be as little as about 1 dB. For a broad bandwidth such as 2 GHz, the IF noise figure contribution will be significantly higher, approximately 4 dB.

The mixer performance potentially can be improved significantly by means of image enhancement. In principal, performance can be improved by close to 3 dB by providing a reactive termination to the image and sum frequencies. This is accomplished by placing a bandpass filter an appropriate distance from the diodes. This filter in the signal path introduces some loss which will offset to some extent the benefit of image enhancement. By using an IF frequency in the low microwave range, it is possible to keep the loss of the image reject filter low, while still using a low enough IF frequency to keep the IF noise figure low. Thus, if a 6 dB conversion loss of the basic mixer is improved by 2.5 dB by image enhancement and degraded by a 1.5 dB IF, the resulting noise figure would be 5 dB. Whelehan(10) has used the mixer theory of Barber(14) and Dickens and Maki(15) to calculate the achievable performance of image enhanced mixers, including the effect of filter loss. The result, assuming a 1.5 dB IF contribution, is the "mixer" curve of Figure 4.1.1-2.

The noise performance of the mixer can also be improved by cooling. As indicated by the above expression for noise figure, this can be very effective as long as the IF noise contribution is small and the conversion loss of the mixer remains low. This is illustrated by Figure 4.1.2-2. By using a cooled paramp as the IF amplifier and cooling the mixer diodes to 15 Kelvin, extremely low noise temperatures of 350 Kelvin (3.4 dB noise figure) at 85 GHz and 260 Kelvin (2.8 dB noise figure) at 33 GHz have been reported by Weinreb and Kerr(16). The Super-Schottky diode, a super conductor-semiconductor tunneling junction, is claimed to be the most sensitive detector of microwaves. Diode temperatures of 5 Kelvin at 92 GHz have been reported(17), but an 18 dB conversion loss makes the use of an ultra low noise IF amplifier, such as a cryogenic paramp, necessary to realize the benefit of the low diode noise temperature. Although the cryogenic cooling approach is useful for such applications as radio astronomy where a great deal of equipment complexity can be tolerated to obtain the lowest possible noise, this is not the case in the ISL application. Nevertheless, these cryogenic results indicate the ultimate that can be achieved with the direct down conversion approach.
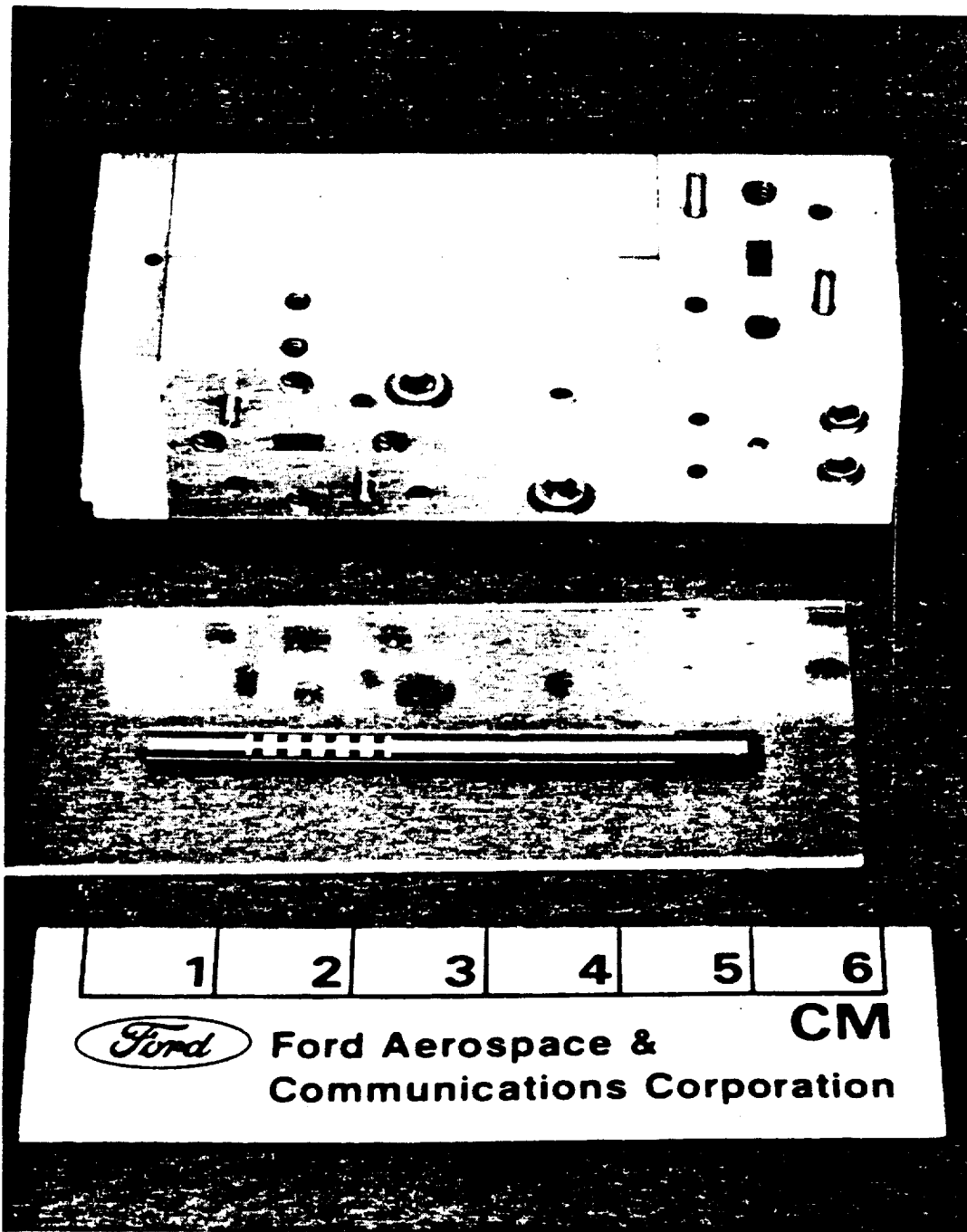
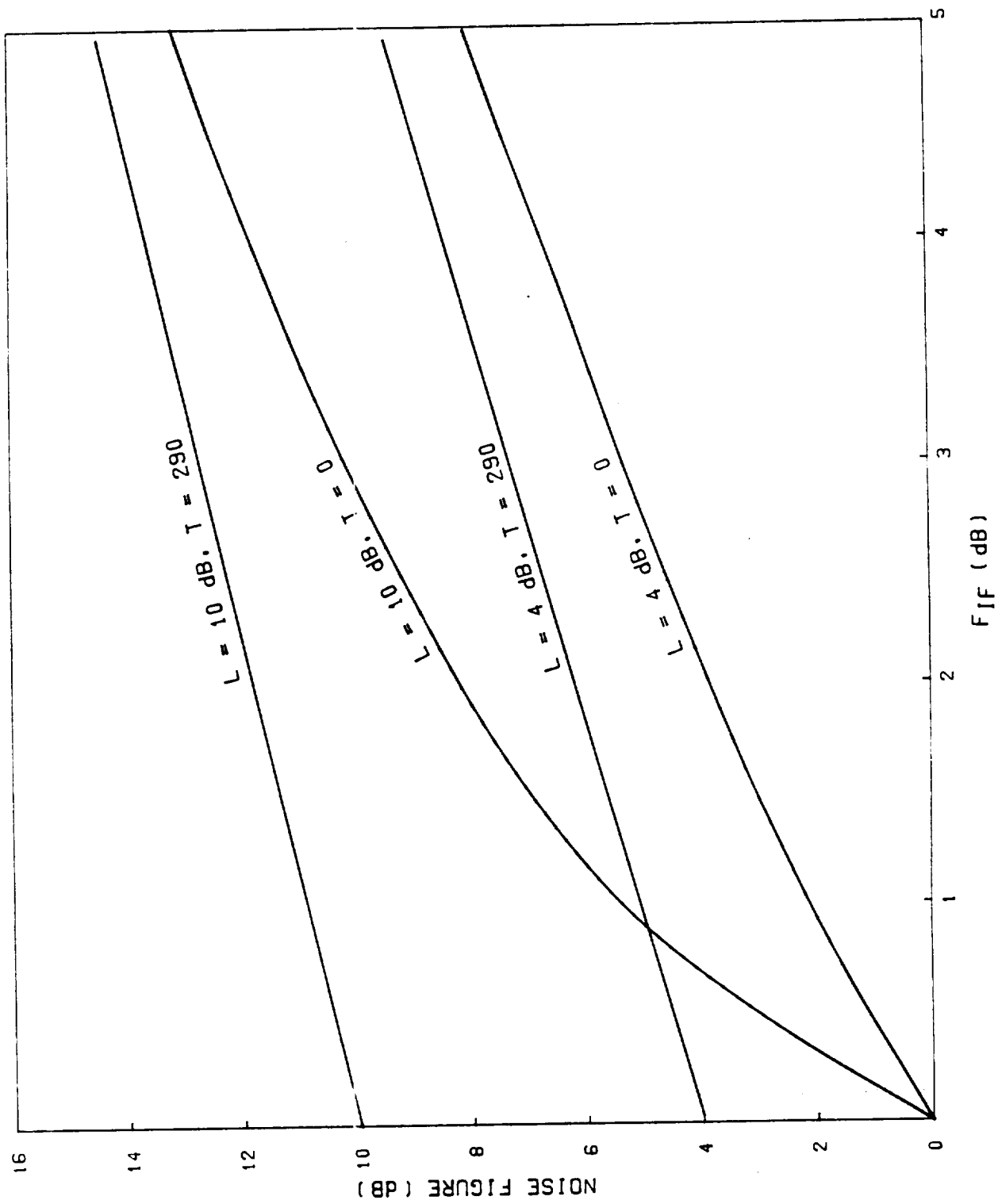Figure 4.1.2-1   Photograph of 60 GHz Balanced Mixer

4-6

FIGURE 4.1.2-2
OVERALL NOISE FIGURE VS IF NOISE FIGURE FOR SEVERAL VALUES
OF MIXER LOSS AND MIXER TEMPERATURE

4.1.3 Local Oscillator

The RF power sources available for use as the local oscillator are the same as the solid-state devices considered for use as the transmitter: Gunn diodes, IMPATTs and FETs. About 7-10 dBm will be required to drive the mixer, so that even with an isolator and connecting losses, 10-15 dBm from the LO will be sufficient. Tight stability and noise requirements will have to be met by the LO so that methods of stabilizing the oscillator must be considered. Present and projected 1989 power capability for the candidate devices are shown in Figure 4.1.3-1. Characteristics of each of these devices are reviewed in the following paragraphs and compared in Table 4.1.3-1.

(a) Gunn Diodes

Gunn diodes are currently the lowest noise solid-state oscillators for use at millimeter wavelengths. They are bulk effect devices making use of a transferred-electron effect which occurs in certain semiconductor materials, notably Gallium Arsenide and Indium Phosphide. By far most Gunn oscillator technology is based on GaAs, but in recent years it has been demonstrated that InP has important advantages for use at millimeter wavelengths. Some of these advantages are summarized in Table 4.1.3-2(18). As seen from Figure 4.1.3-1, Gunn diodes of both types have adequate power output for LO application around 60 GHz. Gunn diodes of either type have spectral characteristics superior to those of IMPATTs or FETs. They are about 10-20 dB better than IMPATTs in AM and FM noise, and are better than FETs in terms of noise close to the carrier.

(b) IMPATT Diodes

IMPATTs are useful devices for transmitter power sources because they offer more power output than any other solid-state device at 60 GHz. However, their noise characteristics are inferior to those of Gunn devices. Some evidence (19) indicates that these inferior noise characteristics can be avoided by careful material control and by biasing at about 75 % of maximum power. Filtering (20) can also be used to reduce noise at the expense of added complexity and weight. But even with these additional efforts, the noise, at best, only approaches that of the Gunn's, so that for the power levels of interest here, the Gunn is the superior candidate.

(c) Field Effect Transistor

FET technology is moving rapidly into the EHF region. FET oscillators at lower frequencies offer higher efficiency, broader bandwidth and advantages associated with being a three-terminal device. To date their noise characteristics close to the carrier are inferior to Gunn's. At the present FETs are not capable of the power output we require at 60 GHz. 2.5 milliwatts has been reported at 57.3 GHz from a laboratory device(21). With the rapid advances that are being made in this technology it is probable that FETs will soon produce usable power at 60 GHz, and it is possible that they will be competitive with Gunn oscillators at 60 GHz by 1989.

Several stabilization techniques exist which can be used with any of these solid-state frequency sources:

(a) The millimeter-wave oscillator can be locked to a low frequency (~10 Mhz) temperature-controlled crystal oscillator. The crystal can be used to establish extremely good long and short term stability and low phase noise close to the carrier. This can be implemented either by multiplying the reference frequency to 60 GHz by a varactor multiplier, or by means of a phase-locked loop. The phase-locked loop can be realized more simply and with less hardware, but in some applications, where the frequency must be changed rapidly, the use of a phase-locked loop is not compatible with the time required to establish lock.

(b) A high-Q, temperature stable (Invar) reference cavity can be coupled to the free-running oscillator in either a reflection or transmission mode.

(c) A high-Q, temperature-stable frequency discriminator can be used, sampling the oscillator output and feeding correction signals back to the voltage-tuned oscillator.

(d) Dielectric resonators can be used for obtaining very high stability. The dielectric resonators are small, high-Q, temperature stable resonators. Since the development of temperature stable resonators within the past few years, they have found important applications in microwave filters and oscillators. By coupling the resonator to the active device extremely good stability, such as 0.001% over a 100 degree C temperature range, has been achieved. A dielectric resonator-stabilized Gunn oscillator for 60 GHz is currently under development at Ford Aerospace.

Systems analyses on this project reported earlier show that very good stability will be required of the LOs. Both range accuracy requirements and the requirement for handling a 2 Gbit/s data rate translate into tight requirements on LO stability. Both criteria can be met by requiring a short term oscillator stability of 10^{-8}/sec. Range rate accuracy, however, requires a short term oscillator stability of 10^{-10}/sec. Either an atomic standard or a crystal oscillator can achieve the accuracy needed. To meet the specification, we propose the circuit of Figure 4.1.3-2 as the baseline approach for the LOs. A voltage-tuned Gunn Dielectric Resonator Oscillator (DRO) is used as the 60 GHz source. It is readily capable of producing the required 10-15 dBm power output on a reliable basis. The DRO is phase-locked to a low frequency reference to meet the stability requirement. A crystal oscillator establishes the long and short term stability while the SAW oscillator establishes low noise close to the carrier. The bandwidth of the loop locking the Gunn oscillator is chosen so that far away from the carrier, where the noise of the DRO is lower than that of the locking source, the noise will be that of the DRO. Close to the carrier, where the noise of the locking source is better than that of the DRO, the output noise level will be that of the locking source. Such an LO is capable of meeting the 10^{-10}/sec stability specification. The SAW oscillator establishes a low noise level at moderate distances from the carrier as illustrated by Figure 4.1.3-3. At offset frequencies of greater than 10 kHz, the single-sideband FM noise of the SAW oscillator is of the order of -170 dBc/Hz (22).

Although such a circuit is capable of meeting the requirements of the GEO LO, further consideration will be given to the possibility of simplifying the hardware · by using, for instance, a sampling phase detector such as described by Takano, et al (23).

The size, weight, and power consumption of the LO are summarized in Table 4.1.3-3.
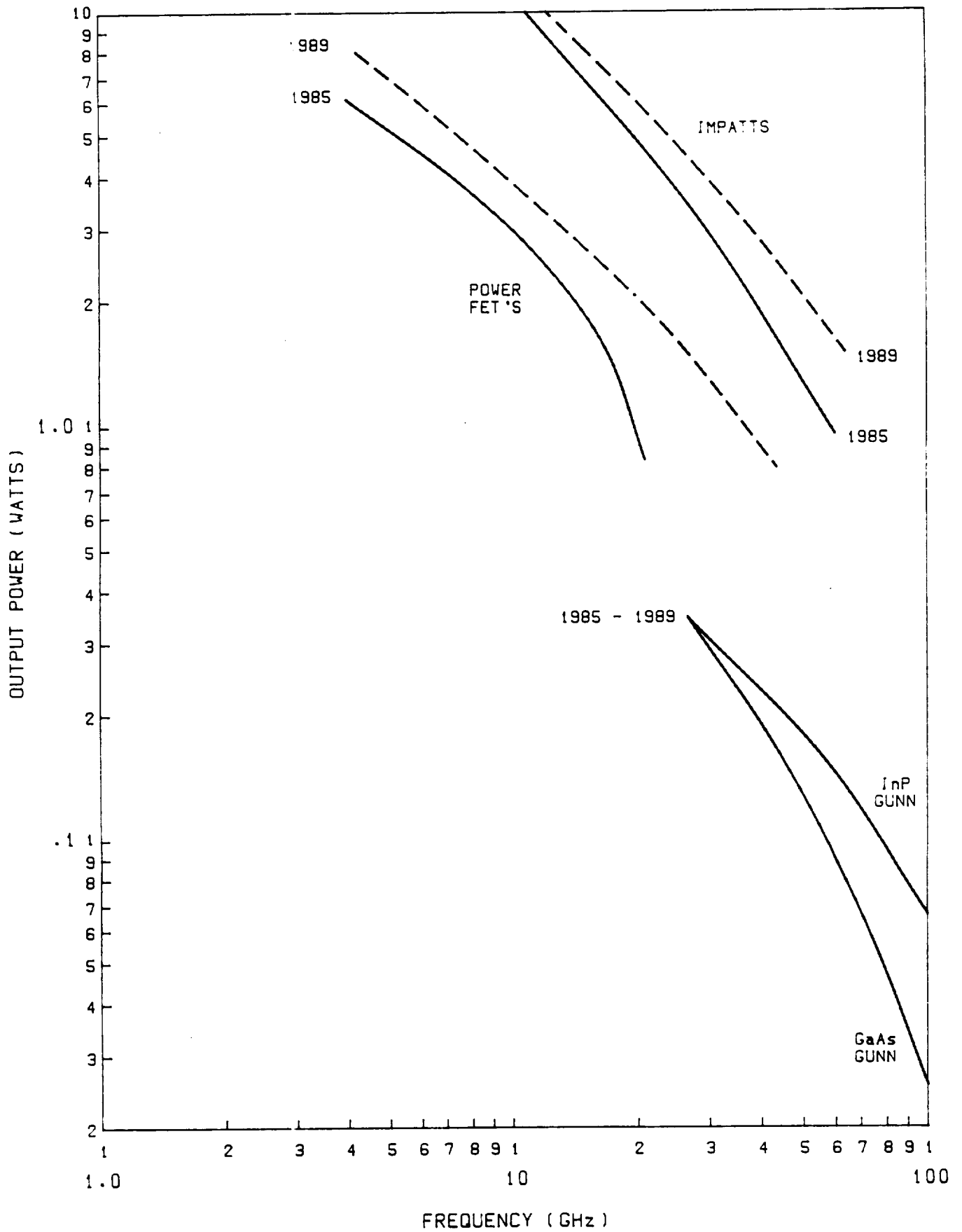
FIGURE 4.1.3-1
COMPARISON OF SOLID STATE LO DEVICES
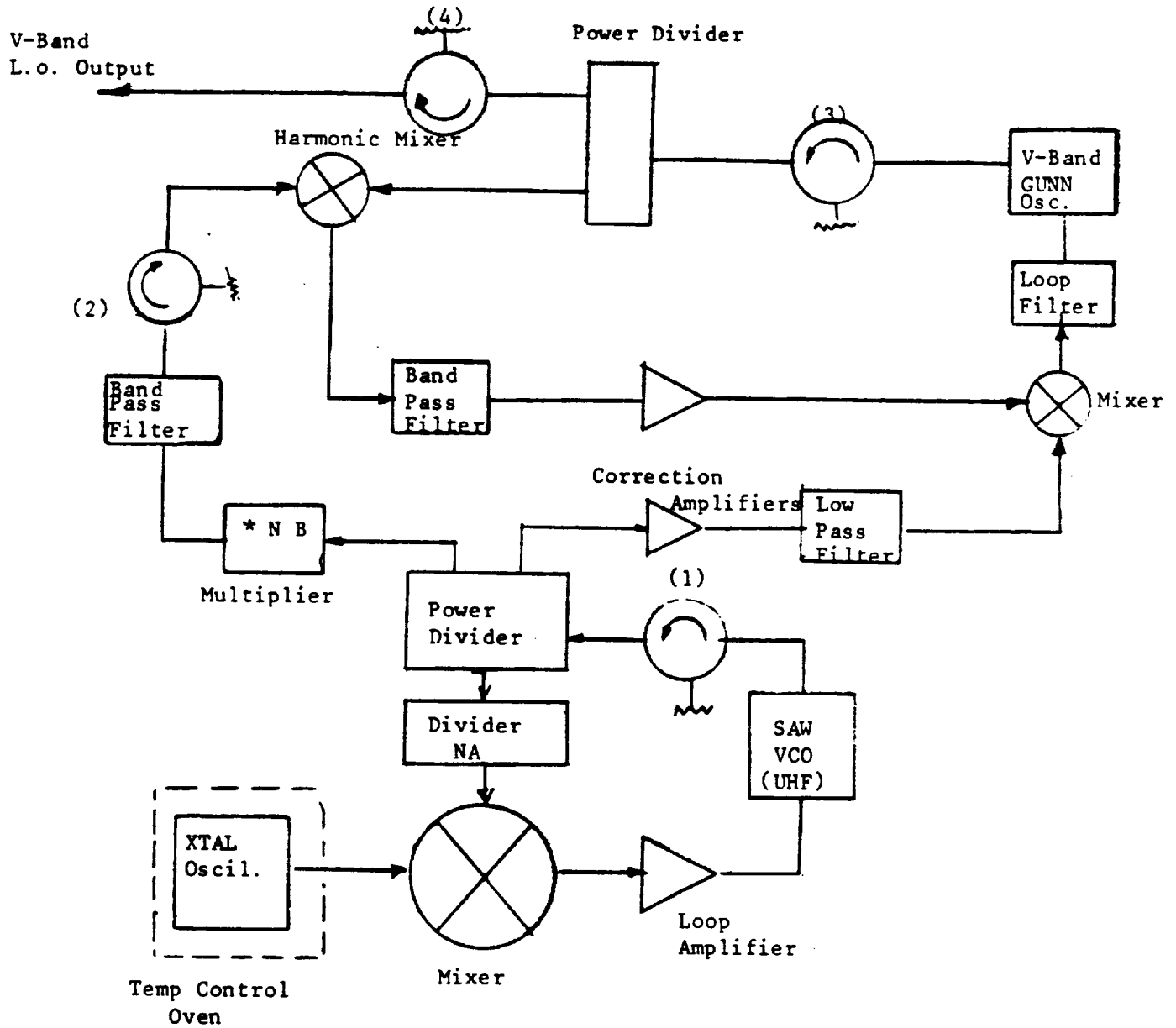
Figure 4.1.3-2 Schematic Diagram of V-Band L.O.

FREQUENCY OFFSET
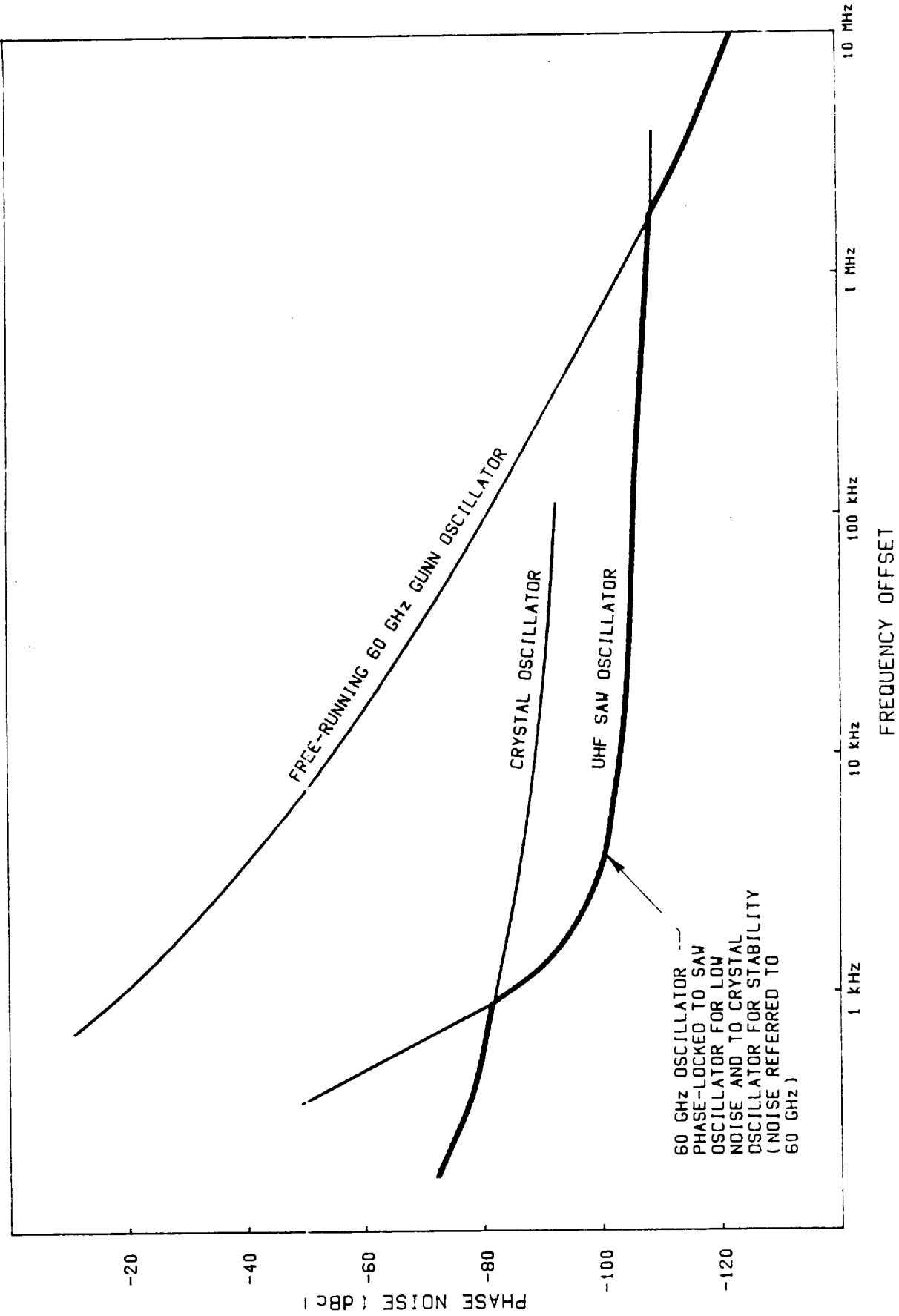
FIGURE 4.1.3-3
ESTIMATED NOISE FOR LOCAL OSCILLATOR

FREE-RUNNING 60 GHz GUNN OSCILLATOR

CRYSTAL OSCILLATOR

UHF SAW OSCILLATOR

60 GHz OSCILLATOR
PHASE-LOCKED TO SAW
OSCILLATOR FOR LOW
NOISE AND TO CRYSTAL
OSCILLATOR FOR STABILITY
(NOISE REFERRED TO
60 GHz)

PHASE NOISE (dBc)

-20
-40
-60
-80
-100
-120

1 kHz
10 kHz
100 kHz
1 MHz
10 MHz

Table 4.1.3-1

Comparison of FET/DRO, GUNN & IMPATT Oscillators

PARAMETER	GaAs FET DRO	GUNN OSCILLATOR Phase-Locked	IMPATT OSCILLATOR Phase-Locked
Power Out	20-30 mw	100 mw	300 mw
Efficiency	20%	2%	- -
Short Term Stability	1×10^{-7}	1×10^{-10}	1×10^{-10}
FM Noise	< Depends on the Circuit - Q >		
AM Noise (DSB)	- -	-160	-140 dBc/Hz
SSB -Noise Improvement (dBc/Hz)	- -	40 dB	50 dB @ 100 kHz

Table 4.1.3-2

Comparison of GaAs and InP Materials for GUNN Diodes

Parameter	GaAS (GUNN)	InP (GUNN)
1) Peak-to-Valley Ratio	1 (unit):	2
2) Efficiency	2%	4%
3) High Frequency Limit	100 GHz	200 GHz
4) Noise prop to D/	142 cm2/S	72 cm2/S
(D=Diffusion coefft of electron) (=Negative diff. mobility)		
5) Thermal conductivity W/cm^{o}C	.54	.68
6) Threshold Field	3.5 kv/cm	10.5 kv/cm
7) Active Region Length	- -	x2 of GaAs

Table 4.1.3-3

LOCAL OSCILLATOR
Size, weight, power consumption estimate.

ITEM	SIZE (inches)	WEIGHT (ounces)	POWER CONSUMPTION (Watts)
Crystal Oscillator	2X4X2	24	7
SAW Oscillator	1X2X1/2	2	3
Loop Amplifiers (2 req)	3/4X3/4X1/2	4 (total)	2
L.P.Filter	1X2X1/2	2	0
Multipliers (5 req)	1X1X1/2	10 (total)	0
Mixers (3 req)	1X2X1/2	3 (total)	0
B.P. Filters (3 req)	1X2X1/2	4 (total)	0
Isolator (UHF)	1.25X1.125X0.5	4	0
Isolator (microwave)	1X1.25X0.5	3	0
Isolator (EHF) (2 req)	0.75X0.75X1.25	4	0
Gunn Oscillator	1.1X1.5X1.25	4	5
TOTAL	~5X4X2	64	17

4.2   Baseline RF Receivers

4.2.1   GEO-LEO RF Receiver

The baseline LEO receiver has a 3.5 dB noise figure (360 K), but is only required to handle a data rate of 1 Mbps. On the basis of the receiver technology discussion, we conclude that the requirement for a 3.5 dB noise figure can be met by a direct downconversion receiver, without a preamp, only by means of a cryogenic mixer and an ultra-low noise IF amplifier such as a cooled paramp. This is not a viable approach for the ISL. However, it is projected that by 1989 low noise 60 GHz preamplifers using FET and/or HEMT devices will be capable of the required noise figure. Because of the low data rate, the IF noise figure for the LEO receiver can be very low, ~1 dB, and the mixer noise figure will be less than for the larger IF bandwidths of the other receivers. A preamp with a gain of 25 dB will be sufficient to overcome the noise contribution of both the IF amplifier and an MIC mixer, making it pos-sible to use a small MIC mixer integrated with the preamp and IF amplifier instead of a large waveguide mixer.

Therefore, the baseline LEO RF receiver is as shown in Figure 4.2.1-1 and the receive RF filter has been included in the receiver subsystem. It should be noted that this realization depends on adequate R&D funds being devoted to the 60 GHz low noise amplifier area to develop the technology in this time frame. The estimated size, weight, and power consumption of the receiver components, including the LO, are shown in Table 4.2.1-1.

TABLE 4.2.1-1

SIZE, WEIGHT, POWER CONSUMPTION
GEO-LEO RF RECEIVER

ITEM	SIZE (INCHES)	WEIGHT (OUNCES)	POWER CONSUMPTION (WATTS)
RF FILTER	1.0X0.8X0.8	2	--
LOCAL OSCILLATOR (per Table 4.1.3-3)	5X4X2	64	17
PREAMP, MIXER, LO MODULE	1X3X0.75	4	10
IF FILTER	2.5X1.0X1.0	3	--
TOTAL		73	27

-116.7 DBM
57.8 GHZ

FROM
ANTENNA

BPF
3-POLE
L = 0.5 DB

-117.2 DBM

RF PREAMP
(HEMT)
G = 30 DB

-87.2 DBM

LO
56.8 GHZ

-93.2 DBM

BPF
3-POLE
L = 0.2 DB

-93.4 DBM

IF AMPL
(GaAs FET)
G = 45 DB

-48.4 DBM
1.0 GHZ

TO
DEMODULATOR

RF EQUIPMENT

ISL USER RECEIVER SUBSYSTEM

Figure 4.2.1-1
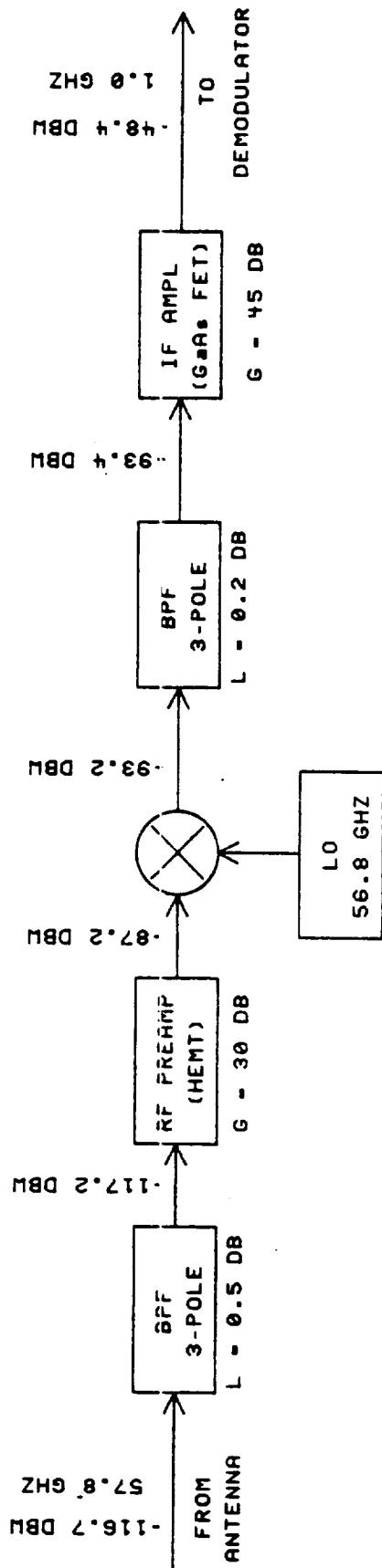
4.2.2 LEO-GEO RF Receiver

The baseline receiver for the LEO-GEO link has a 3.5 dB noise figure (360 K), and is required to handle a maximum data rate of 300 Mbps. On the basis of the receiver technology discussion, we conclude that the requirement for a 3.5 dB noise figure can be met by a direct downconversion receiver, without a preamp, only by means of a cryogenic mixer and an ultra-low noise IF amplifier such as a cooled paramp. This is not a viable approach for the ISL. However, it is projected that by 1989 low noise 60 GHz preamplifiers using FET and/or HEMT devices will be capable of the required noise figure. Even with a 300 Mbps data rate, the IF noise figure for the LEO receiver can be very low, ~1 dB. Therefore, a preamplifier with a gain of 30 dB will be sufficient to overcome the noise contribution of both the IF amplifier and the MIC mixer, making it possible to use a small MIC mixer integrated with the preamp and IF amplifier instead of a large waveguide mixer.

The baseline LEO-GEO RF receiver is as shown in Figure 4.2.2-1. The estimated size, weight, and power consumption, including the LO, the RF filter and the (1st) IF filter are shown in Table 4.2.2-1.

TABLE 4.2.2-1

SIZE, WEIGHT, POWER CONSUMPTION
LEO-GEO RF RECEIVER

ITEM	SIZE (INCHES)	WEIGHT (OUNCES)	POWER CONSUMPTION (WATTS)
RF FILTER	1.0X0.8X0.8	2	--
LOCAL OSCILLATOR (per Table 4.1.3-3)	5X4X2	64	17
PREAMP, MIXER, LO MODULE	1X3X0.75	4	10
IF FILTER	2.5X1.0X1.0	3	--
TOTAL		73	27

FROM ANTENNA
60.0 GHZ
-105.36 DBM

BPF 3-POLE
L = 0.5 DB

-105.86 DBM

RF PREAMP (HEMT)
G = 30 DB

-75.86 DBM

LO 34 GHZ

-83.86 DBM

SWITCHABLE BP FILTER 3-POLE
L = 0.2 DB

-84.06 DBM

IF AMPL (GaAs FET)
G = 35 DB

-49.06 DBM
26.0 GHZ

TO DEMODULATOR

RF EQUIPMENT

ISL LEO-GEO RECEIVER SUBSYSTEM

Figure 4.2.2-1

4.2.3 GEO-GEO RF Receiver

The GEO-GEO receiver is the most difficult of the three receiver types because of the bandwidth required to handle the 2 Gb/s rate. The requirement to handle approximately a 2 GHz bandwidth impacts the receiver sensitivity by degrading the noise figure of both the RF and IF amplifiers from what is achieved with the more optimum match that can be obtained over a narrow band, and, to a lesser extent, through the poorer performance of a broadband mixer. The requirement for a 2 GHz bandwidth will seriously affect the noise figure of the IF amplifier, making it about 4 dB instead of the 1 dB which can be obtained over a narrow band. On the other hand, the noise figure of a 60 GHz preamp will not be affected so much since 2 GHz is a relatively narrow percentage band at 60 GHz.

On the basis of the receiver technology discussion, we conclude that the requirement of the baseline system for a 3.5 dB noise figure (360 K) can be met by direct downconversion only with a cryogenic mixer and ultra-low noise IF amplifier such as a cooled paramp. This is not a viable approach for the ISL. However, it is projected that by 1989 low noise 60 GHz preamplifiers using FET and/or HEMT devices will be capable of the required noise figure. A preamp gain of 30 dB will be sufficient to overide the noise contribution of a mixer with 6 dB conversion loss and an IF noise figure of 4 dB, so that the overall noise figure will be negligibly greater than that of the preamp. If, as projected, amplifiers with 3.5 dB noise figure are available, the 360 K noise temperature can be achieved in this way. In fact, with this preamp it will be possible to use an MIC mixer, instead of the waveguide mixer, reducing the size and weight with a small (~0.1 dB) increase in noise figure.
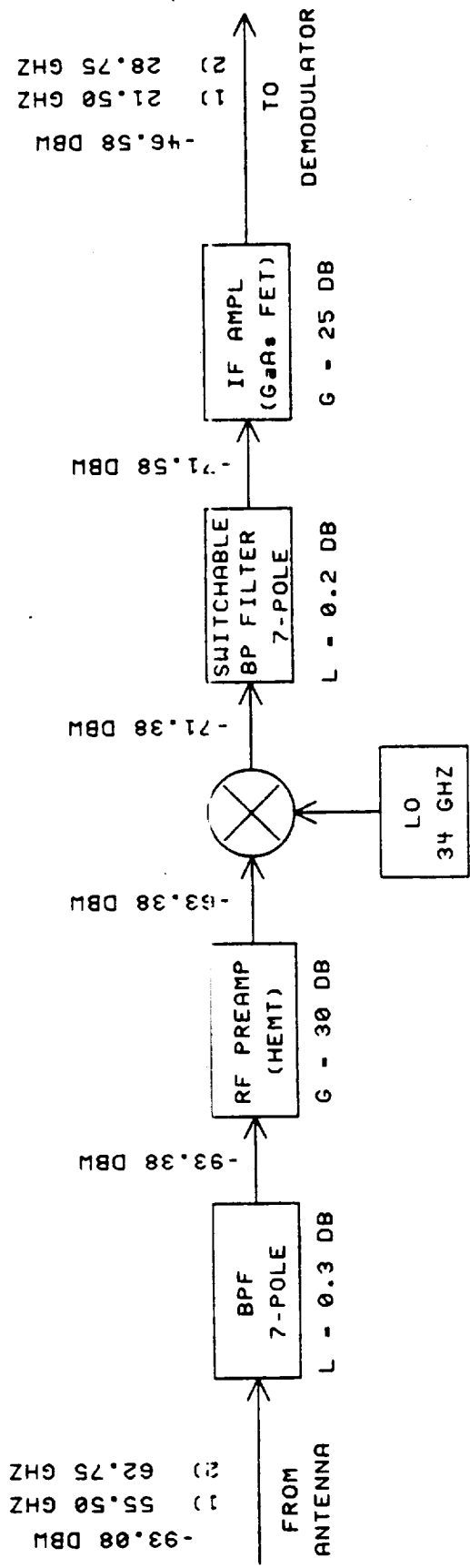
The GEO-GEO RF receiver is as shown in Figure 4.2.3-1. The estimated size, weight, and power consumption is shown in Table 4.2.3-1.

TABLE 4.2.3-1

SIZE, WEIGHT, POWER CONSUMPTION
GEO-GEO RF RECEIVER

ITEM	SIZE (INCHES)	WEIGHT (OUNCES)	POWER CONSUMPTION (WATTS)
RF FILTER	2.0X0.8X0.8	3	--
LOCAL OSCILLATOR (per Table 4.1.3-3)	5X4X2	64	17
PREAMP, MIXER, LO MODULE	1X3X0.75	4	10
IF FILTER	3.5X1.0X1.0	4	--
TOTAL		75	27

RF EQUIPMENT

ISL GEO-GEO RECEIVER SUBSYSTEM

FROM ANTENNA
-93.08 DBM
1) 55.50 GHZ
2) 62.75 GHZ

BPF 7-POLE   L = 0.3 DB

-93.38 DBM

RF PREAMP (HEMT)   G = 30 DB

-63.38 DBM

LO 34 GHZ

-71.38 DBM

SWITCHABLE BP FILTER 7-POLE   L = 0.2 DB

-71.58 DBM

IF AMPL (GaAs FET)   G = 25 DB

-46.58 DBM
1) 21.50 GHZ
2) 28.75 GHZ
TO DEMODULATOR

Figure 4.2.3-1

4.3 Effect of Ranging Requirements on Oscillator Short Term Stability

4.3.1 Effects of Velocity Error

At 60 GHz a velocity change of 2×10^{-3} m/s results in a 0.4 Hz change in doppler frequency. If the doppler shift is measured by counting cycles (rather than measuring a fraction of a period), the averaging time of the counter must be greater than 1 second, which exceeds the ranging delay. Using Develet's (26) formulas the velocity error from oscillator instability is given by:

$$r_e = (C/2\pi f_o T)(T/T_c)^{1/2}$$

where r_e = velocity error

   C = speed of light

   f_o = carrier frequency

   T = counter averaging time

   T_c = 1 radian coherence time of the oscillator

Using the specification of 2 mm/second the above equation becomes

$$2\times10^{-3} = (3\times10^8/2(2\pi)(60\times10^9))(1/TT_c)^{1/2}$$

$$2\times10^{-3} = 5.623\times10^{-4}(1/TT_c)^{1/2}$$

$$(1/TT_c)^{1/2} = 3.557$$

$$(1/TT_c) = 12.65$$

$$T_c = 1/12.65\ T$$

For an averaging time T of $1/0.04 = 2.5$ sec

$$T_c = 1/(12.65\ (2.5)) = 0.0316\ \text{sec}$$

The required oscillator stability S (caused by the maximum range rate error of 2 mm/sec) given by $S = 1/(2\pi T_c f_o)$ is thus

$$1/(2\pi \times 0.0316 \times 60\times10^9) = 8.39\times10^{-11}\ \text{or approximately}\ 1\times10^{-10}.$$

4.3.2 Frequency Errors Due to 2.5 Sec Averaging

For an orbital period of 5400 seconds,

$$f = 1.8 \times 10^{-6} \sin(2\pi t/5400)$$

and $2\pi t/5400$ is the angle from nadir.

$$\int f \, dt = 1.8 \times 10^{6} \sin(2\pi t/5400) \, dt$$

$$= - (5400 \times 1.8 \times 10^{6}/2\pi)(\cos(2\pi(2.5)/5400) - \cos 0)$$

$$= - 1.547 \times 10^{9} (-4.231 \times 10^{-6})$$

$$= 6544.8184 \text{ Hz sec}$$

$$(1/T) \int f \, dt = 2617.9274 \text{ Hz}$$

The average frequency is given by $(f_1 + f_2)/2$ and if $f_1 = 0$ and

$$f_2 = 1.8 \times 10^{6} \sin(2\pi(2.5)/5400) = 5235.9803 \text{ Hz}$$

then the average frequency is 2617.9902 Hz and the frequency error is thus
0.0628 Hz. This error can be reduced by calculating the known acceleration
error and subtracting.

4.3.3 Velocity Errors Due to Thermal Noise

Again according to Develet [26] the effect of additive noise on range rate error can be given in terms of a normalized range rate error β' and a normalized smoothing factor α.

$$\beta' = \dot{r}_e (\omega'_o/\omega_n C)(2(S/N))^{1/2}$$

A carrier to noise ratio of 95 dB and an undamped second-order phase-locked loop natural frequency of 5 KHz results in S/N = 43 dB. Thus,

$$\beta' = \dot{r}_e (60 \times 10^9 / 5 \times 10^3 \times 3 \times 10^8)(2 \times 20000)^{1/2}$$

or, $\dot{r}_e = \beta/8$.

$\alpha = \omega'_n T$ and for T = 2.5 sec, $\alpha = 78540$. For large α,

$\beta = 1/\alpha\sqrt{2} = 9 \times 10^{-6}$ and

$\dot{r}_e = 1.125 \times 10^{-4}$ cm/sec, which is negligible.

4.4   Demodulation and Detection Technique Selection Trades

The signal at the input of the receiver consists of a modulated carrier plus noise. This signal must be processed to extract the useful digital data. Because of the presence of noise and the consequent possibility of incorrect detection of the data, the demodulation and detection processes must be implemented as effectively as possible. The most energy efficient data transmission scheme requires coherent carrier demodulation and matched filter synchronous detection to extract the data from the noisy input signal.

4.4.1   Carrier Acquisition and Tracking

Four alternative methods may be used to acquire the phase and frequency of the carrier of a suppressed carrier quadriphase signal. They are:

a. Times-four circuit followed by a narrow bandpass filter
b. Times-four circuit followed by a narrowband phaselocked loop
c. Double Costas loop
d. Decision-directed feedback technique

In all cases, the acquired carrier is used to coherently demodulate the inphase and quadrature components of the four-phase signal.

The most commonly used method is the times-four circuit with a phaselocked loop. This method is relatively simple to implement, and it provides a stable signal for coherent carrier demodulation. Phase ambiguity of the acquired carrier is resolved either through differential encoding of the data, or through unique data word recognition.

When carrier acquisition is performed at a high IF frequency, circuits at four times the IF frequency may be difficult to implement. In such cases, a double Costas loop or a decision-directed feedback technique may be easier to build.

Carrier acquisition with QPSK and MSK signals utilizing times-four circuitry is more sensitive to data patterns than carrier acquisition utilizing other techniques. With QPSK and MSK, certain nonrandom data patterns may result in a low reconstructed carrier-to-noise ratio. For this reason, decision-directed feedback techniques are often used with QPSK and MSK modulation schemes.

A trade-off among the alternative acquisition methods must take all of the above factors into account. From the standpoint of bit-error-rate performance, the alternative carrier acquisition schemes provide similar results. The decision on which scheme to use is often based on circuit implementation complexity and individual past experience.

4.4.2   Symbol Timing Recovery

Optimum bit-error-rate performance is achieved with synchronous detection of the demodulated baseband signal. To provide the correct sampling time, it is necessary to extract the timing information from the baseband data.

When the carrier is acquired with a double Costas loop, or with the decision-directed feedback method, the data clock acquisition process becomes

an integral part of the carrier acquisition circuit.   Alternative data clock acquisition methods are as follows:

    a. Inphase and midphase detection
    b. Early and late phase detection
    c. Half symbol delay and multiply technique
    d. Rectify and filter technique
    e. Differentiate, rectify, and filter technique

The first two methods have integrate-and-dump circuits operating on the baseband signal. They provide good performance even at low signal-to-noise ratios. In the last three methods, diodes are used to perform multiplication and rectification, and the circuit performance is degraded at low signal-to-noise ratios.

From the standpoint of circuit complexity, the rectify and filter technique is the simplest one to implement. The schemes that have phaselocked loops require additional components but provide a data clock with less jitter. Bit-error-rate performance is degraded with excessive jitter.

The trade-offs involved in selecting the timing recovery method should also consider the problem of clock cycle slippage, which results in the loss of data bit integrity. Introduction of an extraneous data bit, or deletion of a valid data bit in block-synchronized data systems, may result in a significant loss of information.

4.4.3   Matched Filter Detection

Matched filter detection of digital data provides the lowest bit error rate because the matched filter maximizes the signal-to-noise ratio at the decision circuit. Integrate-and-dump circuits serve as matched filters for wideband BPSK and QPSK data. Weighted integrate-and-dump circuits must be used for wideband MSK matched filter detection.

In practice, lowpass filters are often used instead of integrate-and-dump circuits. When cosine rolloff spectral shaping is used, the lowpass filter transfer function at the receiver is designed in conjunction with the shaping filter at the transmitter to produce the desired effect.

Adaptive equalizers must be used in cases where the receiver has to work with significantly different signals and channel characteristics, or when the bit-error-rate performance is marginal and must be improved.

4.4.4   Error Correction

When convolutional encoding is used at the transmitter, a convolutional decoder is used at the receiver to decode the data and correct the errors. The power efficiency improvement that can be realized with one-half-rate error correction encoding is about 4 dB. Other error correction coding schemes provide alternative trade-offs of power efficiency, bandwidth efficiency, and equipment complexity.

4.5 Baseline Demodulator Systems

4.5.1 GEO-GEO

The baseline GEO-GEO demodulator is as shown in the block diagram of Figure 4.5-1. The double Costas loop approach was chosen because of the difficulties of building phase-stable frequency multipliers at EHF. The Costas loop also avoids hang-up problems associated with decision directed feedback techniques and alleviates some of the noise that is present in frequency multiplier systems. A similar demodulator has been built (along with a corresponding modulator) as an IR&D project and the modem operates at a 2 Gbps data rate at 20 GHz. The current performance is a degradation of 2.5 dB at a BER of 10^{-6}, but performance should be improved to a degradation of only 2.0 dB at that BER by 1989. Such improvement may require adaptive equalizers.

The timing recovery method, as shown in the demodulator block diagram, is half symbol delay and multiply. It was chosen for its simplicity and reliability. The propagation delays are too high for the sophisticated bit synchronizers required by either inphase/midphase or early/late phase detection. The circuit performance degradation caused by a rectify and filter method was deemed to be excessive.

4.5.2 LEO-GEO

The large number of data rates prevents a single conventional data demodulator to be implemented for the entire range. Handling the entire demodulation process digitally creates difficulties because extreme frequency accuracy is required to keep sampling rates manageable. A hybrid approach to the problem provides a solution that is both technically manageable and weight efficient. In a demodulator with a FEC decoder, the signals from the I and Q channel are usually processed in an analog manner to obtain the PLL feedback and clock signals. The I&Q signals are also A to D converted to provide the inputs for the FEC decoder which derives the data. Once converted to digital data, however, the PLL error signal and the clock and bit sync extraction can be done digitally. The digital VCO error signal is then processed by a D to A converter which drives the VCO input. The actual data rate adaption is done in the Costas Loop Algorithm and verified in the Bit Sync Output.

Such a hybrid demodulator has been selected as the baseline for the LEO-GEO communications link. The block diagram is shown in Figure 4.5-2.

This approach is not without problems. Normally data is converted from its analog to a 2 bit digital form (sign and quality), which is sufficient to achieve most of the benefit from FEC algorithms. Quantization noise in the PLL could drive the precision level to 8 bits (approximately 40 dB dynamic range). This places a great deal of dependence on A to D converter technology. It requires the development of a reliable 8 bit A to D converter capable of 150 M conversions per second. One such device is under development by Sony.

Analysis of the carrier acquisition is the second major problem. The complexities of the interaction of carrier and clock prior to lock will require extensive simulation. When these difficulties are overcome the result is a data detector which can be optimized for any bit rate below its maximum by changing software (or firmware).
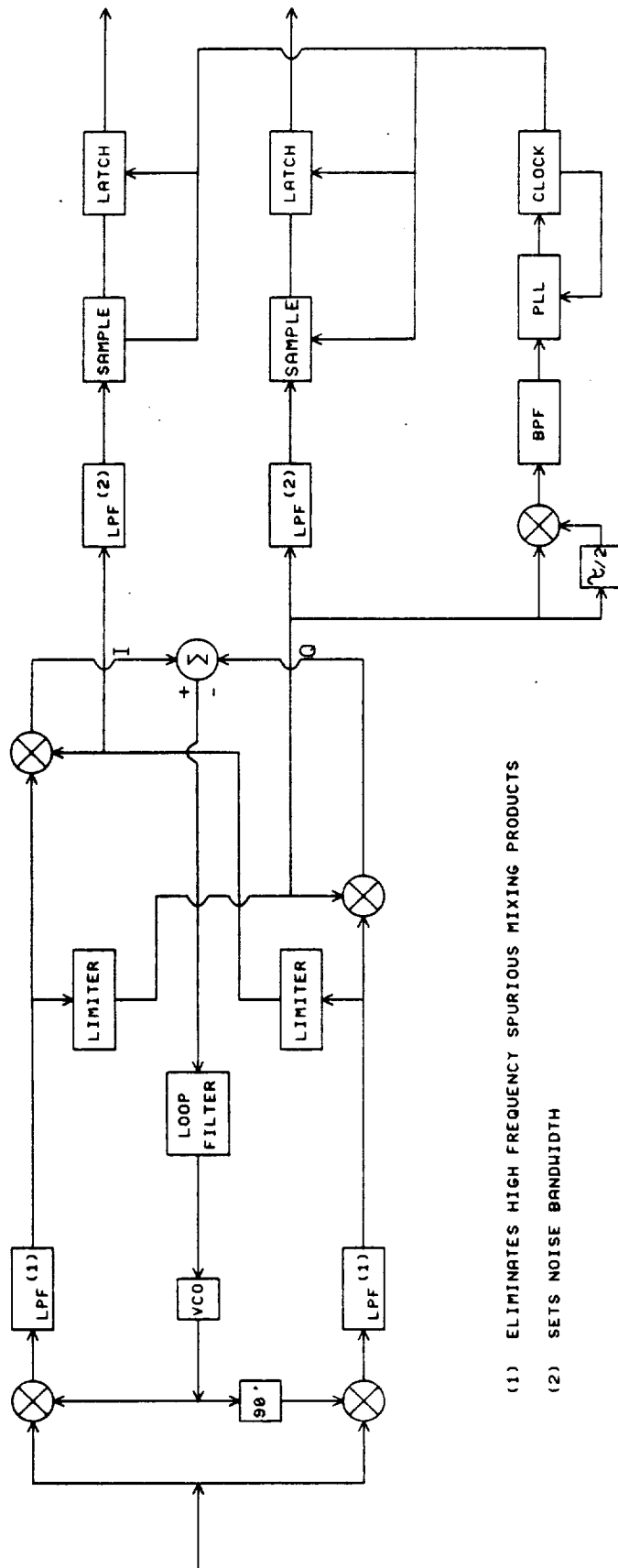
QPSK DEMODULATOR SUBSYSTEM

(1) ELIMINATES HIGH FREQUENCY SPURIOUS MIXING PRODUCTS

(2) SETS NOISE BANDWIDTH
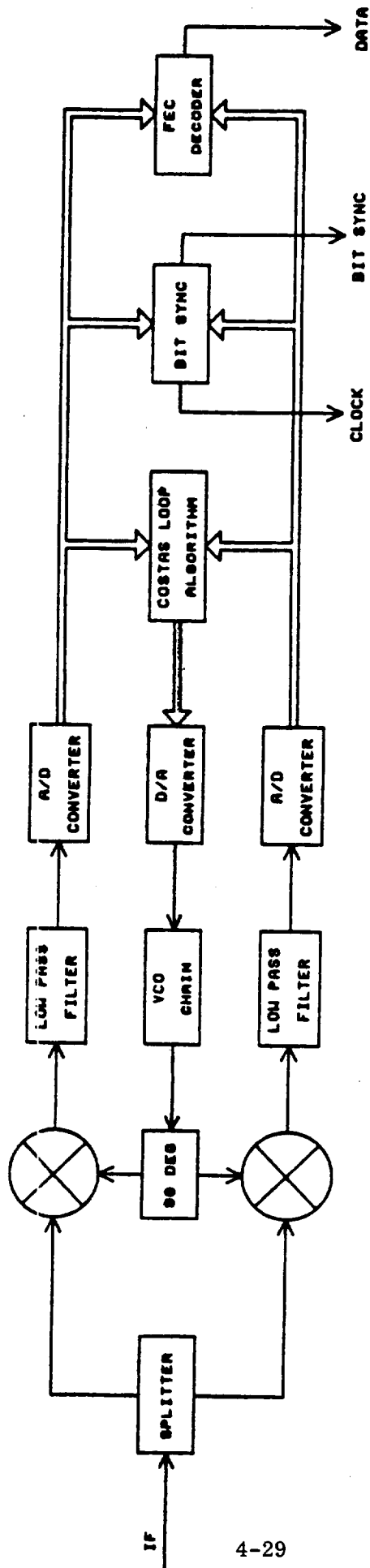
Figure 4.5-1

VARIABLE DATA RATE DEMODULATOR

Figure 4.5-2
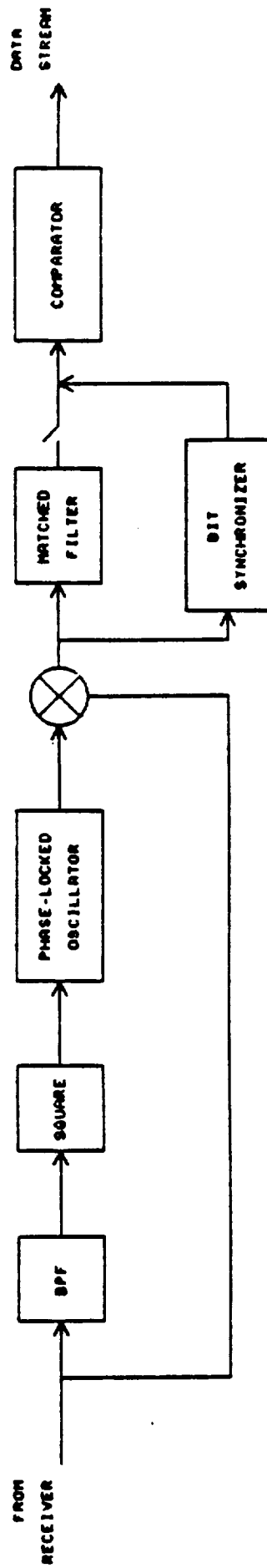
BPSK DEMODULATOR

Figure 4.5-3

4.5.3 GEO-LEO

The BPSK demodulator for the GEO-LEO link (equipment aboard the USAT) is shown in Figure 4.5-3.

4.5.4 Forward Error Correction Codes

The LEO-GEO communications link will utilize FEC coding when operating at the maximum data rate of 300 Mbps (or 50 Mbps with solar interference) but at lower data rates this is optional. We recommend a rate 5/6 Low Complexity code and an Algorithm B-type decoder. The 5.4 dB coding gain assumed in the link budgets (Tables 1.1.1-3 and 1.1.1-4) is conservative. A code of this type for a quadri-phase signal has recently been developed and the theoretical expected gain is 6 dB.

The GEO-GEO link budgets, Tables 1.1.1-1 and 1.1.1-2, show link margin of more than 1.0 dB. If more power is required in this link, two different LC codes (a rate 8/9 and a rate 11/12) have been designed to operate at 2 Gbps. Although the encoders and decoders are still in development, they should be available in the TDAS-required time frame.

The GEO-LEO link requires no forward error correction coding.

4.6 Doppler Compensation

Effects of Ranging Dynamics on PLL Bandwidths

A second order phase lock loop as used in phase lock receivers can be expected to track both phase and frequency (doppler) errors. If the feedback path between the phase detector and VCO has a perfect integrator (a good approximation), the dc gain in this path approaches infinity and the velocity error or static phase error approaches zero. Acceleration error (frequency rate) will have a finite value given by (27)

$$\Theta_a = \frac{\Delta\dot{\omega}}{\omega_n^2}$$

where Θ_a = phase error (radians)

$\Delta\dot{\omega}$ = frequency rate (radians/sec^2)

ω_n = loop natural frequency (radians/sec)

Jerk error (frequency acceleration) does not produce a constant error so that its effects must be estimated over the time of occurence. Assuming a second order loop transfer function in standard notation, the transfer function can be written as

$$\Theta_o/\Theta_i = s^2/(s^2 + 2\zeta\omega_n + \omega_n^2)$$

or

$$\Theta_o = \Theta_i s^2/(s^2 + 2\zeta\omega_n + \omega_n^2)$$

Assuming a frequency acceleraton (jerk) input of

$$\Theta_i = \Delta\ddot{\omega}/s^4$$

then

$$G_o = (1/s^2)(\Delta\ddot{\omega})/(s^2 + 2\zeta\omega_n + \omega_n^2)$$

Simplifying to a critically damped loop (an approximation)

$$\Theta_o = \Delta\ddot{\omega}((1/s^2)(1/(s+\omega_n)^2))$$

The time domain solution can be found to be

$$\Theta_o(t) = \Delta\ddot{\omega}/\omega_n^3)(\omega_n t - 2(1-e^{-\omega_n t}) + \omega_n t e^{-\omega_n t})$$

If $\omega_n t$ is expected to be greater than 100 then the error can be approximated by:

$$\Theta_o(t) = (\Delta\ddot{\omega}/\omega_n^2)\, t \quad \bigg|\ \omega_n t > 100$$

Given a maximum acceleration of 10.47 m/sec^2 (3002 Hz/sec) and a maximum jerk of .012m/sec^3 (40.02 Hz/sec^2) and assuming constant jerk, the time period for the jerk can be calculated as:

$$A(t) = \int_0^T J(t)\,dt \quad \text{or} \quad \Delta\ddot{\omega} = \int_0^T \Delta\dddot{\omega}\,dt$$

where T is the time to reach maximum acceleration.

T is then equal to $\Delta\ddot{\omega}/\Delta\dddot{\omega}$ or 75 seconds.

If acceleration goes from maximum negative to maximum positive then the total time that the acceleration can change is 150 seconds. Assuming a maximum allowable phase error of 15° (.262 radian) then the minimum loop natural frequency can be calculated as follows:

The total phase error Θ_e which is composed of the acceleration and jerk errors is given by

$$\Theta_e = -3002/\omega_n^2 + 40.02(150)/\omega_n^2 = 0.262$$

where the acceleration is the first term and the jerk is the second term.

The natural frequency, ω_n is thus

$$((-3002 + 40.02(150))/0.262)^{1/2} = 107 \text{ radians/sec} = 17 \text{ Hz.}$$

The minimum PLL bandwidth for the user therefore is 17 Hz and the TDAS which sees twice the dynamics would require a 107 Hz loop bandwidth to allow for doppler tracking with large loop safety factors. Since it is desireable to have larger loop bandwidths for other reasons such as phase noise, doppler compensation for loop dynamics will be unnecessary.

4.7 Receiver Reliability and Redundancy

Considerable attention has been paid to the expected reliability of the components whose use is anticipated. It is a useless exercise to build a system design around components that will not be available in the required timeframe. It is almost as useless to specify components that may be available but will be so unreliable as to preclude their use in any operational system. It is essential that the system concept developed and thus the hardware configuration assumed in the ICLS study be reliable over the specified 8-year mission life of the host satellite.

This is especially important in a spaceborne system where repair or replacement of failed components is virtually impossible. That situation is changing, as evidenced by the recent repair of the Solar Maximum Mission satellite (in LEO) by STS Mission 41-C. GEO satellites, however, are still out of the range of reasonable repair missions. In any case, it is much more cost effective to ensure mission lifetime by using high reliability components and appropriate levels of redundancy rather than relying on in-situ repair operations.

The receiver subsystem is critical to consider from a reliability standpoint. The failure rates of low-noise front ends can approach those of the power amplifiers, depending on frequency, power level, and noise figure desired and the specific technologies used. Their sensitivity to burnout from a number of mechanisms (overdrive, static discharge effects, EMP, etc.), though not necessarily a function of their actual reliability, is nevertheless an externally induced failure mode that must be considered along with the usual internally generated failure.

High-speed digital circuitry, as would be used in the demodulator, could also be a reliability driver. Digital technology has improved dramatically in recent years, but space-qualified (or qualifiable) hardware operating in the gigabit range is not yet available. This implies that anything that might be available in 1989 would have to be analyzed carefully to assess its impact on system reliability.

If individual component reliabilities are not sufficient to meet overall system reliability requirements, redundancy must be added to provide backup capability in the event of a component failure. Depending on the actual failure rates, different levels of redundancy may be necessary for different components. Suitable switching must be provided to allow changeover of input and output lines, power, commands, and telemetry. This switching adds losses in RF lines and interface complexity in power, command, and telemetry lines. It is also costly to fly equipment that is not normally (non-failure-mode) needed. It is therefore necessary to trade off the cost and complexity of the redundant equipment against its expected failure rate to optimize the overall system.

As part of our effort on the ICLS Study, we have evaluated the various receiver technologies in terms of predicted reliability in the 1989 timeframe. These evaluations are factored into the baseline architecture. We have also defined recommendations for appropriate levels of redundancy for the various components of the receiver subsystem. These recommendation are given in Section 1.1.14.

REFERENCES

1. Herman C. Okean and Alexander J. Kelly, "Low-Noise Receiver Design Trends Using State-of-the-Art Building Blocks", IEEE Transactions on Microwave Theory and Techniques, Vol. MTT-25, No. 4, April 1977, p. 254.

2. E. Watkins, J. M. Schellenberg and H. Yamasaki, "A 30 GHz FET Receiver", 1982 IEEE Microwave Theory and Techniques Symposium Digest, p. 16.

3. Edward T. Watkins, "GaAs FET Amp Uses One-Quarter Micron Gate, Heralding MIC Opportunities at UP to 60 GHz", MSN, December 1983, p. 52.

4. E. T. Watkins, J. M. Schellenberg, L. H. Hackett, H. Yamasaki and M. Feng, "A 60 GHz GaAs FET Amplifier", 1983 IEEE Microwave Theory and Techniques Symposium, p. 145.

5. Private Communication, May 1984.

6. N. Niori and T. Saito, "A 20 GHz High Electron Mobility Transistor Amplifier for Satellite Communications", 1983 IEEE International Solid State Circuits Conference Digest, February 1983, p. 198.

7. J. J. Berenz, K. Nakano, and K. P. Weller, "Low Noise High Electron Mobility Transistors", IEEE 1984 Microwave and Millimeter-Wave Monolithic Circuits Symposium Digest of Papers, p. 83.

8. J. Paul, L. Yuan, & P. Yen, "Beam Lead Dielectric Crossbar Mixers from 60 to 140 GHz," 1982 IEEE Microwave Theory and Techniques Symposium Digest, p. 372.

9. Kai Chang et al, "V-Band Low Noise Integrated Circuit Receiver," IEEE Transactions on Microwave Theory and Techniques, Vol MTT-31, No. 2, February 1983, p. 146.

10. James J. Whelehan, "Low Noise Millimeter-Wave Receivers," IEEE Transactions on Microwave Theory and Techniques, Vol MTT-25, no. 4, April 1977, p. 268.

11. Alpha Industries Brochure, "Active Millimeter-Wave Components and Subsystems," Alpha Industries, Inc., Woburn, MA. 01801.

12. Hughes, "Millimeter-Wave Products 1985 Catalog," Hughes Aircraft Co., Microwave Products Division, Torrance, CA.

13. Y. Vaddiparty, unpublished results.

14. M. R. Barber, "Noise Figure and Conversion Loss of the Schottky Barrier Mixer Diode," IEEE Transactions on Microwave Theory and Techniques, Vol. 15, No. 11, November 1967.

15. L. E. Dickens and D. W. Maki, "An Integrated-Circuit Balanced Mixer, Image and Sum Enhanced," IEEE Transactions on Microwave Theory and Techniques, Vol. MTT-23, March 1975.

16. Sander Weinreb and Anthony R Kerr, "Cryogenic Cooling of Mixers for Millimeter and Centimeter Wavelengths," IEEE Journal of Solid-State Circuits, Vol. SC-8, No. 1, February 1973.

17. Robert L. Dickman, William J. Wilson, and Gerald G. Berry, "Super-Schottky Mixer Performance at 92 GHz," IEEE Transactions on Microwave Theory and Techniques, Vol. MTT-29, No. 8, August 1981.

(18) L. Wandinger, "mm-Wave InP Gunn Devices: Status and Trends", Microwave Journal, March 1981, p. 71.

(19) F. A. Myers, "Performance Parameters Examined for Millimeter-Wave Solid-State Devices", MSN, July 1984, Vol. 14, No. 7, p. 266.

(20) G. A. Ediss et al, "AM Noise from IMPATT Oscillator", IEEE Transactions on Microwave Theory and Techniques, Vol. 30, NO. 11, Nov 1982, p. 2012.

(21) J. M. Schellenberg, H. Yamasaki and D. W. Maki, "A 69 GHz FET Oscillator", Symposium Digest, 1981 IEEE MTT-S Symposium, p. 328.

(22) T. E. Parker, "SAW Controlled Oscillators", Microwave Journal, October 1978, p. 66.

(23) T. Takano, et al, "Novel GaAs FET Phase Detector Operable to Ka-Band", Symposium Digest, 1984 IEEE MTT-S Symposium, p. 381.

(24) K. W. Lee et al , "A varactor tuned X-band Dielectric Resonator GaAs FET oscillator", 1982 IEEE MTT-S Symposium, p. 274.

(25) Robert H. Merriam, "Gunn Technology's Low Noise Advantages." MSN, August, 1983, pp. 80-96.

(26) Jean A. Develet, Jr., "Fundamental Accuracy Limitations is a Two-Way Coherent Doppler Measurement System", 1961 IRE Transactions on Space Electronics and Telemetry, p. 80.

(27) Floyd M. Gardner - "Phaselock Techniques", 2nd ed.

SECTION 5

MECHANICAL DESIGN

TABLE OF CONTENTS, FIGURES & TABLES

5.0   MECHANICAL DESCRIPTION

5.1   GEO-LEO Mechanical Design

5.1.1   Thermal and Mechanical Error Budget

The summation pointing error budget in link subsystem azimuth and elevation is shown in Table 5.1-1 by time behavior. The method of segregating spacecraft/payload pointing error by time behavior for prior spacecraft programs has been extensively utilized. In this method, pointing errors are grouped into constant, long period, short period and daily errors. Constant errors are due to mechanical alignment. Long period errors include seasonal and aging effects. Short period errors have epochs or periods of not longer than approximately 30 minutes. Daily period errors include strictly diurnal, circadian and other effects lasting approximately 1 hour or more (e.g., eclipse effects). Tables 5.1-2 through 5.1-5 indicate the RSS contribution by each type of time behavior errors and link subsystem tracking mode.

Table 5.1-1

60 GHz LINK SUBSYSTEM POINTING ERRORS (SUM)

ERROR SOURCE	OPEN LOOP MODE ERROR CONTRIBUTIONS (DEGREES)		CLOSED LOOP MODE ERROR CONTRIBUTIONS (DEGREES)	
	AZIMUTH	ELEVATION	AZIMUTH	ELEVATION
CONSTANT TERMS	0.0613	0.0613	0.0000	0.0000
LONG TERMS	0.0254	0.0254	0.0112	0.0112
SHORT TERMS	0.0316	0.0316	0.0316	0.0316
DAILY TERMS	0.0537	0.0537	0.0197	0.0197
TOTAL ERROR (DEGREES)	0.1788	0.1788	0.0625	0.0625

Table 5.1-2

60 GHz LINK SUBSYSTEM POINTING ERRORS (CONSTANT TERMS)

ERROR SOURCE	OPEN LOOP MODE ERROR CONTRIBUTIONS (DEGREES)		CLOSED LOOP MODE ERROR CONTRIBUTIONS (DEGREES)	
	AZIMUTH	ELEVATION	AZIMUTH	ELEVATION
GIMBAL/S/C ALIGNMENT (to nominal bearing axes)	0.050	0.050	0.00	0.00
ORTHOGONALITY OF GIMBAL AXES	0.010	0.010	0.00	0.00
ENCODER RESOLUTION (2 TO 14 BIT, ERROR IS 1/2 OF RESOLUTION)	0.022	0.022	0.00	0.00
ENCODER ALIGNMENT	0.010	0.010	0.00	0.00
BEAM WAVEGUIDE ALIGN.	0.020	0.020	0.00	0.00
GRAVITY COMPENSATION FIXTURE	0.020	0.020	0.00	0.00
S/C POINTING KNOWLEDGE	0.003	0.003	0.00	0.00
SUM OF SQUARES	0.003985	0.003985	0.00	0.00
RSS ERROR (DEGREES)	0.0613	0.0613	0.00	0.00

Table 5.1-3

60 GHz LINK SUBSYSTEM POINTING ERRORS (LONG TERMS)

ERROR SOURCE	OPEN LOOP MODE ERROR CONTRIBUTIONS (DEGREES)		CLOSED LOOP MODE ERROR CONTRIBUTIONS (DEGREES)	
	AZIMUTH	ELEVATION	AZIMUTH	ELEVATION
RUNOUT IN BEARING AXIS	0.020	0.020	0.00	0.00
CLEARANCES IN BEARINGS	0.000	0.000	0.00	0.00
GIMBAL STEP SIZE (MOTOR RES)	0.010	0.010	0.010	0.010
ENCODER ACCURACY (1/2 LSB)	0.011	0.011	0.00	0.00
RF SENSOR	0.005	0.005	0.005	0.005
SUM OF SQUARES	0.000646	0.000646	0.000125	0.000125
RSS ERROR (DEGREES)	0.0254	0.0254	0.0112	0.0112

Table 5.1-4

60 GHz LINK SUBSYSTEM POINTING ERRORS (SHORT TERMS)

ERROR SOURCE	OPEN LOOP MODE ERROR CONTRIBUTIONS (DEGREES)		CLOSED LOOP MODE ERROR CONTRIBUTIONS (DEGREES)	
	AZIMUTH	ELEVATION	AZIMUTH	ELEVATION
CONTROL LOOP RESPONSE	0.030	0.030	0.030	0.030
AUTOTRACKING ACCURACY	0.010	0.010	0.010	0.010
SUM OF SQUARES	0.0010	0.0010	0.0010	0.0010
RSS ERROR (DEGREES)	0.0316	0.0316	0.0316	0.0316

Table 5.1-5

60 GHz LINK SUBSYSTEM POINTING ERRORS (DAILY TERMS)

ERROR SOURCE	OPEN LOOP MODE ERROR CONTRIBUTIONS (DEGREES)		CLOSED LOOP MODE ERROR CONTRIBUTIONS (DEGREES)	
	AZIMUTH	ELEVATION	AZIMUTH	ELEVATION
GIMBAL THERMAL DISTORTION	0.050	0.050	0.00	0.00
CLEARANCES IN BEARINGS	0.00	0.00	0.00	0.00
ANTENNA DISTORTION	0.017	0.017	0.017	0.017
WAVEGUIDE THERMAL DISTORTION	0.010	0.010	0.010	0.010
SUM OF SQUARES	0.002889	0.002889	0.000389	0.000389
RSS ERROR (DEGREES)	0.0537	0.0537	0.0197	0.0197

5.1.2   System Structure/Mechanical Design

The baseline ICL structure for the electronics module will be a truss framework and brackets of graphite-epoxy composites attached to an aluminum faceskins/aluminum honeycomb panel to which are mounted the electronic components and contain the variable conductance heat pipes (VCHP's) for temperature control.

The antenna will be an axial fed Cassegrain. The reflectors will be graphite epoxy faceskins with a Kevlar honeycomb core. The tripod holding the subreflector to the main reflector is fabricated of graphite epoxy tubes.

The baseline design is such (Figure 5.1.2-1) that no masts or booms are necessary in order to deploy the five 0.9 meter antennas. The dual axis Gimbals will provide that function.

5.1.3   Thermal Control Concepts

The baseline thermal control concepts are;

a. The electronic module containing all the GEO-LEO ICL electronic components including the transmitter, receiver and microprocessor will be a box of truss structure which contains a panel constructed of aluminum faceskins covering an aluminum honeycomb core. Variable conductance heat pipes (VCHP) are embedded in the panel. All electrical and electronic components are mounted to the interior of the panel. The exterior of the panel will contain optical solar reflectors (OSR's). All surfaces not covered in OSR's and the truss structure will be covered by multilayer aluminized Kapton multilayer blankets. A heater system will be employed. A tradeoff of required electronic module radiator area (a function of module dissipation for various spacecraft locations, sun angles) is indicated by Figures 5.1.3-1 through 5.1.3-3.

b. The Beam Waveguide assembly is internal to the dual axis gimbal/electronic module which will be covered by aluminized Kapton multilayer blankets. No heater system will be employed for thermal control of these assemblies.

c. The electro mechanical systems (gimbals) will employ a thermistor controlled heater system and will employ a multilayer blanket system where the two axis movement will allow.

FIGURE 5.1.2-1
TOAS LAYOUT

FIGURE 5.1.3-1

X-axis: RADIATOR SURFACE AREA ~ FT^2

Y-axis: ELECTRONICS MODULE DISSIPATION ~ WATTS

Legend box:
- 23.5° SUN AGLE
- WINTER SOLSTICE
- HEAT PIPES/OSRs
- $\alpha = 0.21$
- $\epsilon = 0.80$
- 50° C COMPONENT
- 50° C BLOCKAGE
- HEAT PIPES 100% EFF.
- PANEL ΔT 0°C

Curves labeled: 10% BLOCKAGE, 30% BLOCKAGE, 50% BLOCKAGE, 70% BLOCKAGE

FIGURE 5.1.3-2

60° SUN AGLE
WINTER SOLSTICE
HEAT PIPES/OSRs
$\alpha = 0.21$
$\epsilon = 0.80$
50° C COMPONENT
50° C BLOCKAGE
HEAT PIPES 100% EFF.
PANEL ΔT 0°C

RADIATOR SURFACE AREA ～ FT²

ELECTRONICS MODULE DISSIPATION ～ WATTS

10% BLOCKAGE
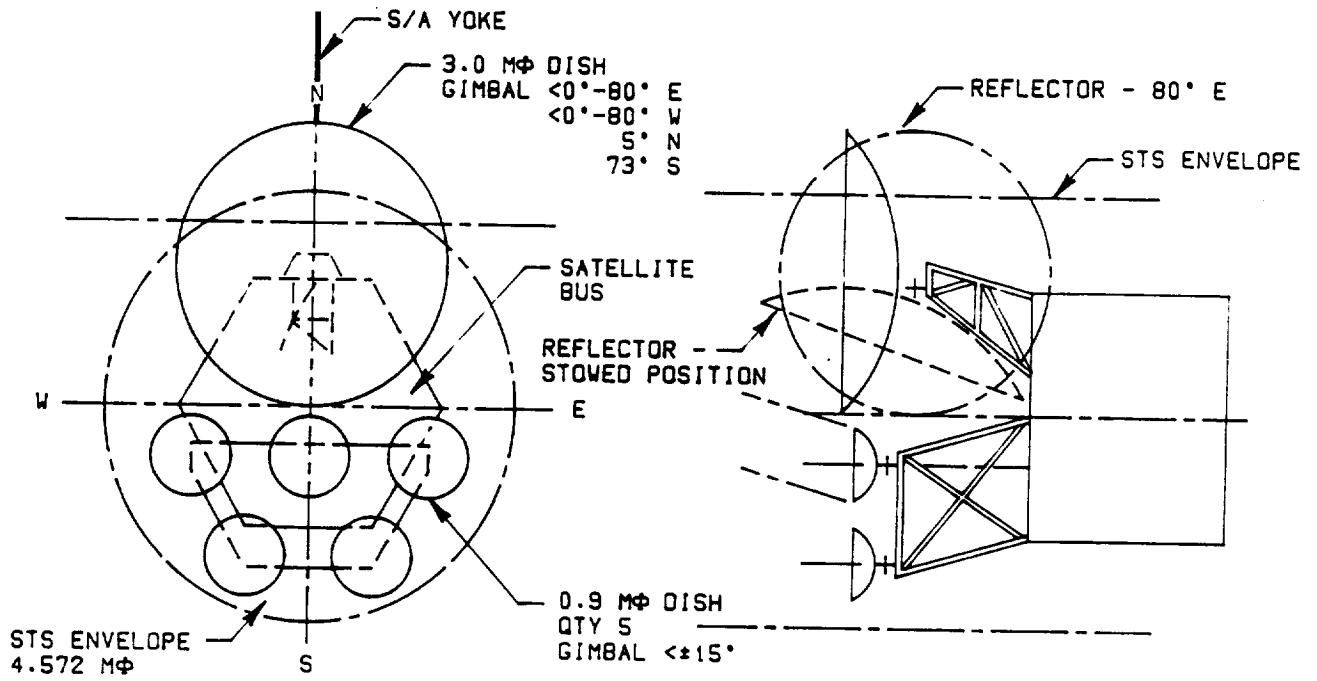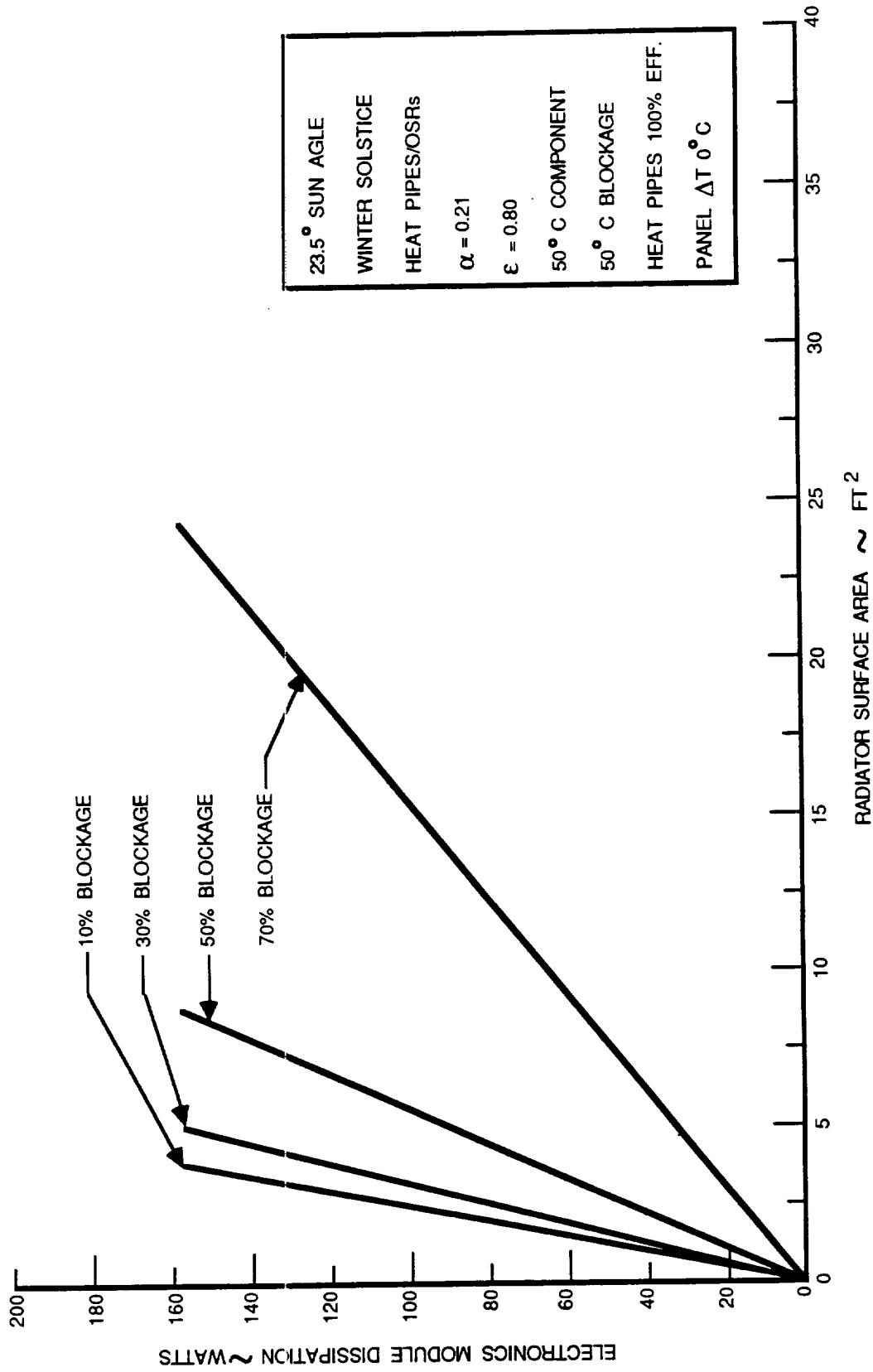
30% BLOCKAGE

50% BLOCKAGE

FIGURE 5.1.3-3

Legend box:

83.5° SUN AGLE

WINTER SOLSTICE

HEAT PIPES/OSRs

$\alpha = 0.21$

$\epsilon = 0.80$

50° C COMPONENT

50° C BLOCKAGE

HEAT PIPES 100% EFF.

PANEL ΔT 0° C

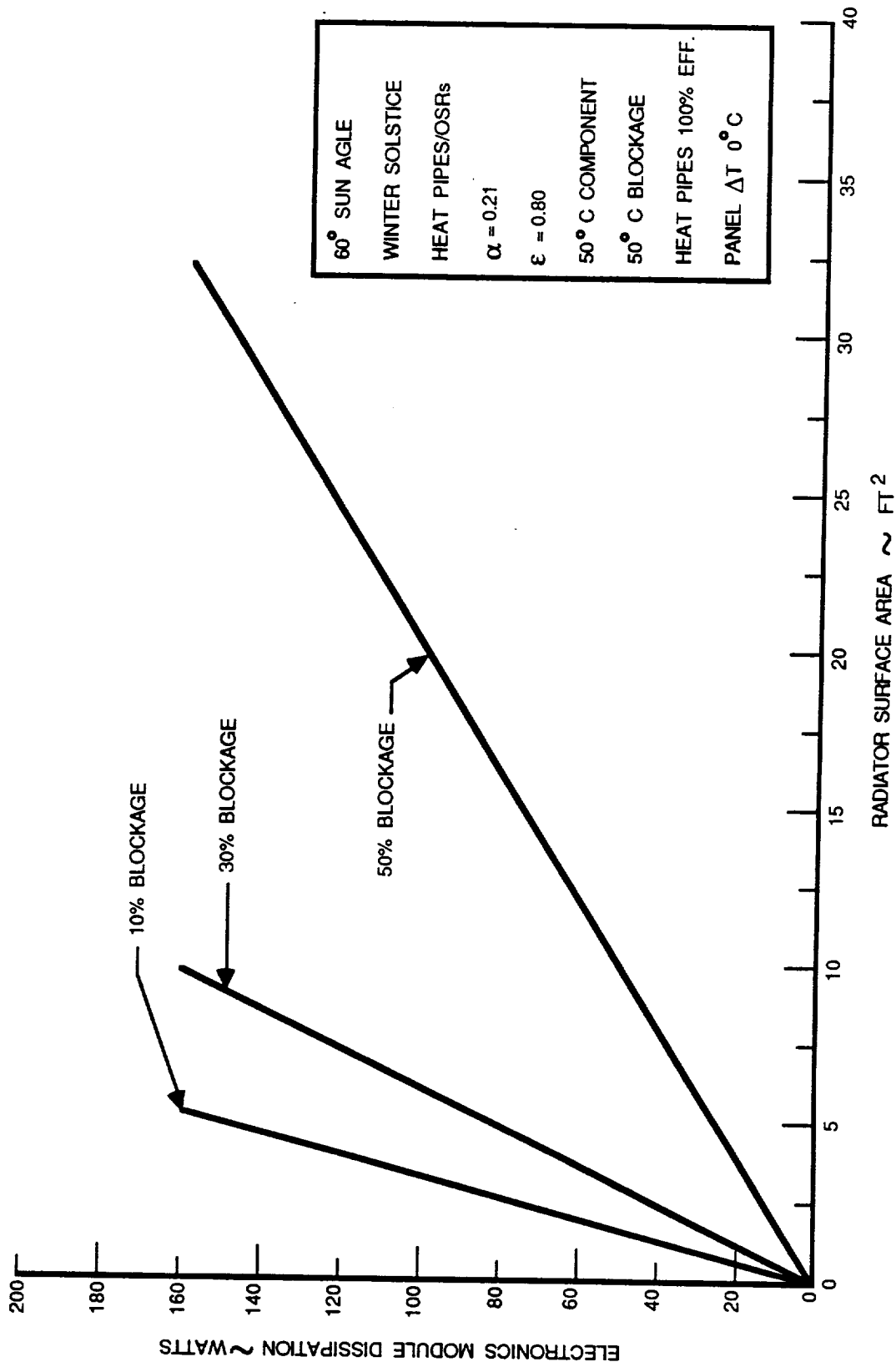X-axis: RADIATOR SURFACE AREA ~ FT^2

Y-axis: ELECTRONICS MODULE DISSIPATION ~ WATTS

Curve labels: 10% BLOCKAGE, 30% BLOCKAGE, 50% BLOCKAGE
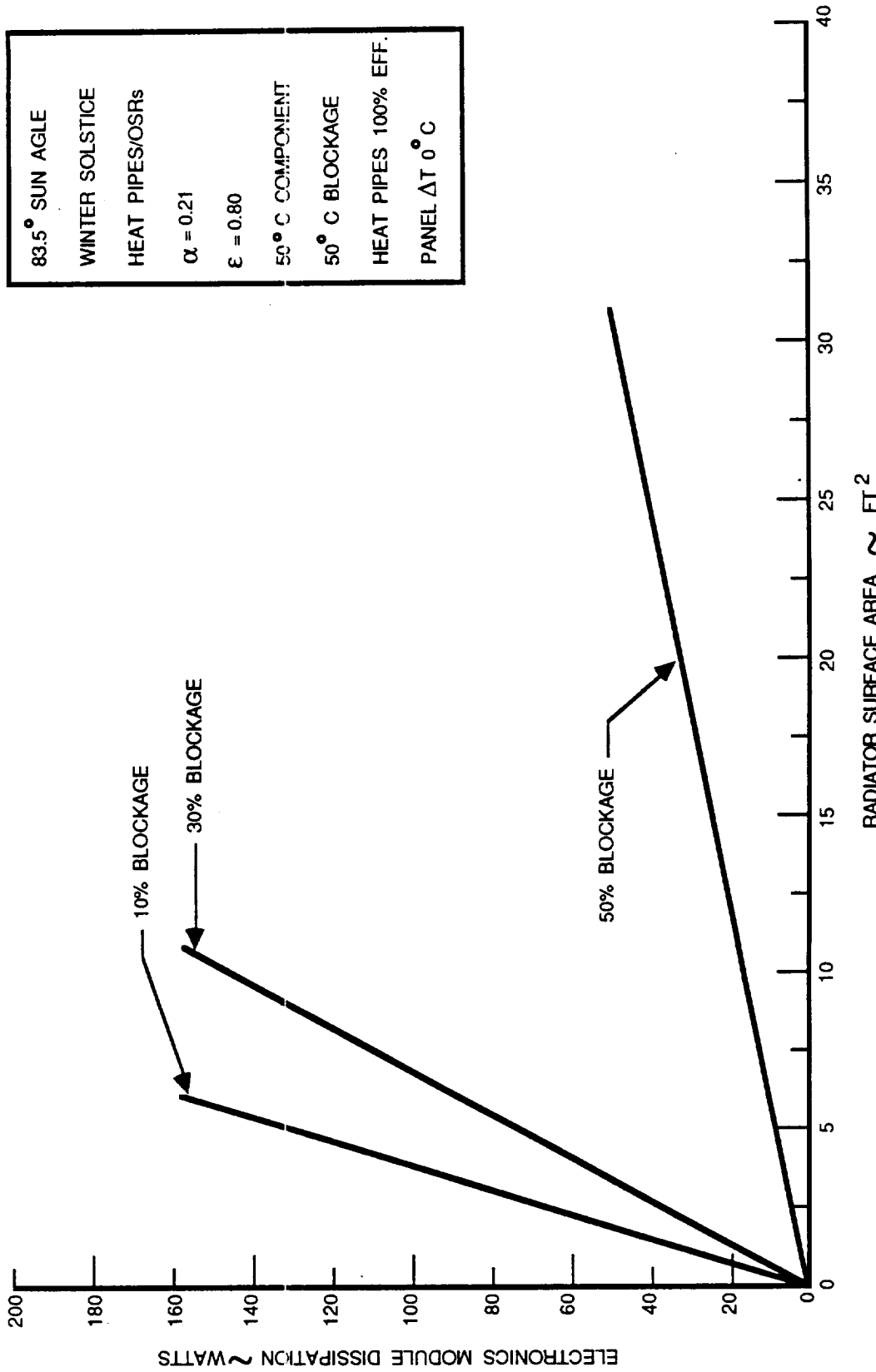
5.1.3   Thermal Control Concepts. Cont.

   d. The Cassegrain reflector system will have aluminized kapton multi-
       layer blankets attached to the gimbal side of the main reflector
       and on the concave side of the subreflector.   All other surfaces
       will be coated with white paint to act as a second surface mirror
       system and to provide diffuse reflections in the solar spectrum.
       All areas that are to employ multilayer blankets will be examined
       to determine if the blankets could cause multiple equivalent
       insolation to other critical spacecraft and ICL surfaces.   Any
       blanket that could contribute such an effect will be painted with
       a diffuse black coating which is standard FACC practice.   All
       blankets will be grounded to the spacecraft structure.

   e. A detailed thermal analysis for six sun conditions can be found in
       Monthly Progress Report No. 13.

5.1.4   System Contamination

        Figure 5.1.2-1 indicates the baseline layout of the GEO spacecraft
(TDAS) with the 3.2 meter GEO-GEO antenna and the five 0.9 meter GEO-LEO
antennas depicted mounted to the TDAS earth face (+Z axis).   It is seen that
none of the reflector RF radiating surfaces are within the line of sight of
any thruster plumes for any mission phase e.g., perigee, apogee, north/south
stationkeeping or east/west stationkeeping firings.   Referring to Figure
5.1.2-1 again, it is intended that the baseline radiators utilized for elec-
tronic module thermal control will be mounted on a north facing surface for
the 3.2 meter GEO-GEO antenna and on a south facing surface for the five 0.9
meter antennas.   Again, similar to the antennas RF radiating surfaces, no
mission phase thruster firings have direct line of sight access to the thermal
radiator surfaces. Based on flight experience and the discussions presented
by sections 2.3.4.3 through 2.3.4.3.4 of WDL-TP6033 "60 GHz Intersatellite
Links Definition Study" Volume II-Technical Proposal 30 April 1984, thruster
plume contamination should not be a problem for the system.

        With regard to contamination from other sources, materials are
selected to minimize outgassing and consequent contamination of optical and
thermal surfaces, as well as other deleterious effects.   Maximum allowable
out-gassing values for acceptable materials are 1.0% TWL (Total Weight Loss)
and 0.1% VCM (Volatile Condensable Material) when the sample is exposed to
125° for 24 hours at 10^{-6} torr, and the condensate is collected on a polished
aluminum condenser plate at 25^oC. Testing is per ASTM E595, Method of Test
for Total Mass Loss and Collected Volatile Condensable Materials from
Outgassing in a Vacuum Environment.

        In summary then, contamination of the system is considered unlikely,
i.e., low technical risk since in general:

   o   Materials same as past spacecraft.
   o   Propellants same as past spacecraft.
   o   Relative location of optical surfaces same as past spacecraft.
   o   History indicates degradation not contamination of optical
        surfaces.
   o   Shielding will protect from direct thruster plume impingement
        if necessary.

5.1.5   Antenna System Control Electronics (ASCE)

A study was made to determine a possible configuration of the ASCE which could meet the requirements of the Intersatellite Link Study. The requirements used to define the configuration of the ASCE are as follows:

- o   Acquire and track 5 LEO's
- o   Acquire and track 1 GEO
- o   Fixed scan search pattern
- o   Trajectory data uploaded from ground and stored in RAM
- o   Ability to track 3 LEO's while acquiring 2 LEO's
- o   Contain 24 hours of stored trajectory data (10 minute intervals) ·for each satellite to be tracked
- o   Capable of tracking each satellite for 24 hours open loop
- o   Capable of dithering antenna position based on RF feedback
- o   Estimate size, weight, power, and technology required to implement design
- o   Acquisition capability limited by slew rate of Gimbal Mechanism

Based on the above requirements, a system has been studied which can meet the requirements based on 1989 technology.

5.1.5.1 ASCE Design

A block diagram of the design that was investigated is shown in Figure 5.1.5-1. The design consists of two basic components, an Antenna Control Microprocessor, and a LEO/GEO Antenna Controller. Each component will be described separately.
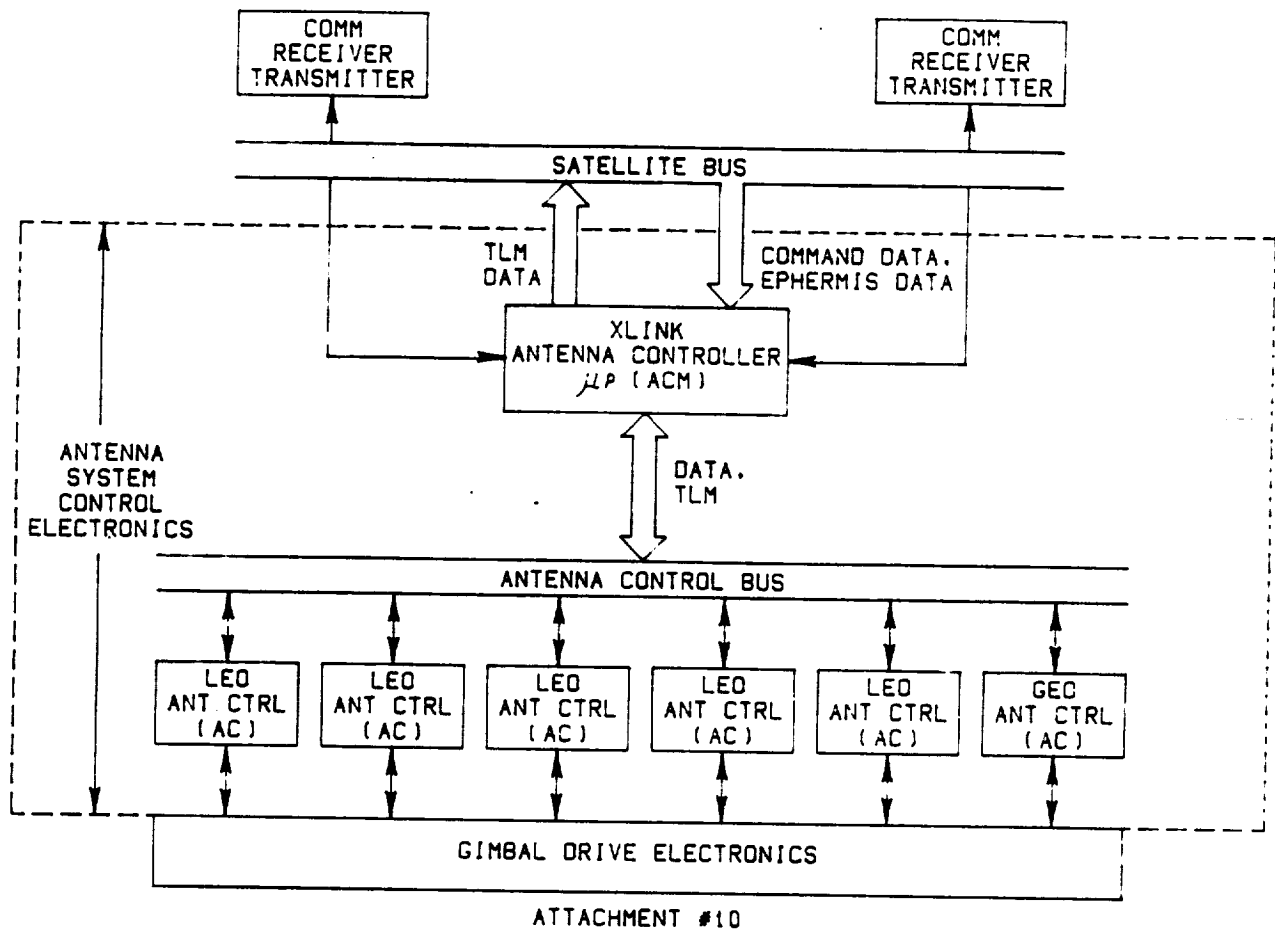
FIGURE 5.1.5-1
INTERSATELLITE LINK ANTENNA SYSTEM CONTROL ELECTRONICS

5.1.5.2 Antenna Control Microprocessor (ACM)

The ACM functions as the Controller for the ASCE. All communications with the Spacecraft and the communication system receiver/transmitter are controlled by the ACM. All data or commands from ground to ASCE must pass into the ACM. All decisions on how to employ the data or commands are determined by the ACM. When a ground command to search, acquire, or track a LEO or GEO satellite has been received by the ACM and processed, it will be passed to one of the Antenna Controller (AC) units which will then proceed with the commanded function. Position and status data from each of the six AC's is received by the ACM and reformatted for TLM transmission over the Satellite Bus, the Satellite, and thence, to ground.

A summary of the functions proposed for the ACM are as follows:

o Provide Command Decoder for Antenna Control Functions
o Provide communication path from RF communication Link to AC's
   from closed loop tracking
o Provide temporary storage for LEO and GEO tracking data uploaded
   from ground to AC's
o Provide TLM formatting for AC position and status data
o Provide ACM error checking
o Provide all control functions to cause AC's to search, acquire,
   and track target satellites
o Provide ASCE status to TLM

5.1.5.3 Antenna Controller (AC)

The AC consists of six identical controllers which are capable of controlling one antenna gimbal drive electronics. Each of the six controllers have identical designs and contain a microprocessor, 4Kx8 ROM, and 8Kx8 RAM. These components consist of Radiation Hard CMOS devices. The programs stored in ROM are identical and provide for a fixed pattern search sequence, an acquisition sequence, and a tracking sequence.

In addition, the necessary functions are provided to receive 24 hours worth of tracking data from the ACM and save it in RAM and to provide the ACM with position and status data from the controlled antenna gimbal drive. A self test function for the AC is also included in ROM.

A summary of the AC functions is as follows:

o Provide Antenna Slew command before Search Sequence.
o Provide a fixed pattern search pattern based on Ephemeris
   data and target satellite position uploaded from ground.
o Provide acquisition sequence after receiving RF acquisition
   status from communication system.
o Provide 24 hour tracking of target satellite based on tracking
   data uploaded from ground.
o Provide dithering of tracking function based on RF error signals
   from communication system.
o Provide position and status TLM data to ACM.
o Provide self test mode for error checking.

5.1.5.4 Weight, Power and Size

An estimate of the size, weight and power required is shown below.

	AC (Qty 6)	ACM (Qty 1)	TOTAL
Size (inches)	4x8x1/2	4x8x1/2x	112 in^3
Weight (pounds)	0.5	0.5	3.5 lbs
Power (watts)	0.1w	0.4w	1.0w

5.1.6   Electromechanical Mechanisms

5.1.6.1 General Requirements

The electro-mechanical mechanism used for antenna pointing, position-ing and tracking will be a two-axis gimbal mechanism. Transmission of the RF signals will be via a four reflector, beam waveguide routed through the gimbal axis. This gimbal mechanism will be virtually identical for the three proposed missions (GEO-LEO, LEO-GEO, and GEO-GEO). There will be minor varia-tions in mechanism configuration to allow for the mission specific antenna and angular pointing range requirements. The three missions are detailed below with their despin critical assumptions.

a. Geosynchronous - Low Earth Orbit Link - The primary requirement for this system is to have the TDAS spacecraft communicating with up to five (5) low altitude spacecraft which may have orbital altitudes from 160 km to 5000 km. Figure 5.1.6-1 shows this system configuration. The gimbal mechanism will have the follow-ing capabilities:

1. Five (5) gimbals will be required on the geosynchronous spacecraft. Each gimbal will support a zero point nine (0.9) meter diameter antenna.

2. The gimbal will have an angular range of +/-20 deg in each of two orthogonal axes allowing complete coverage of the 5000 Km altitude zone. If these antennas are also required to track Molniya orbits then the angular range will be extended accordingly. Such a change may require a modification of the gimbal installation to permit the necessary field of view.
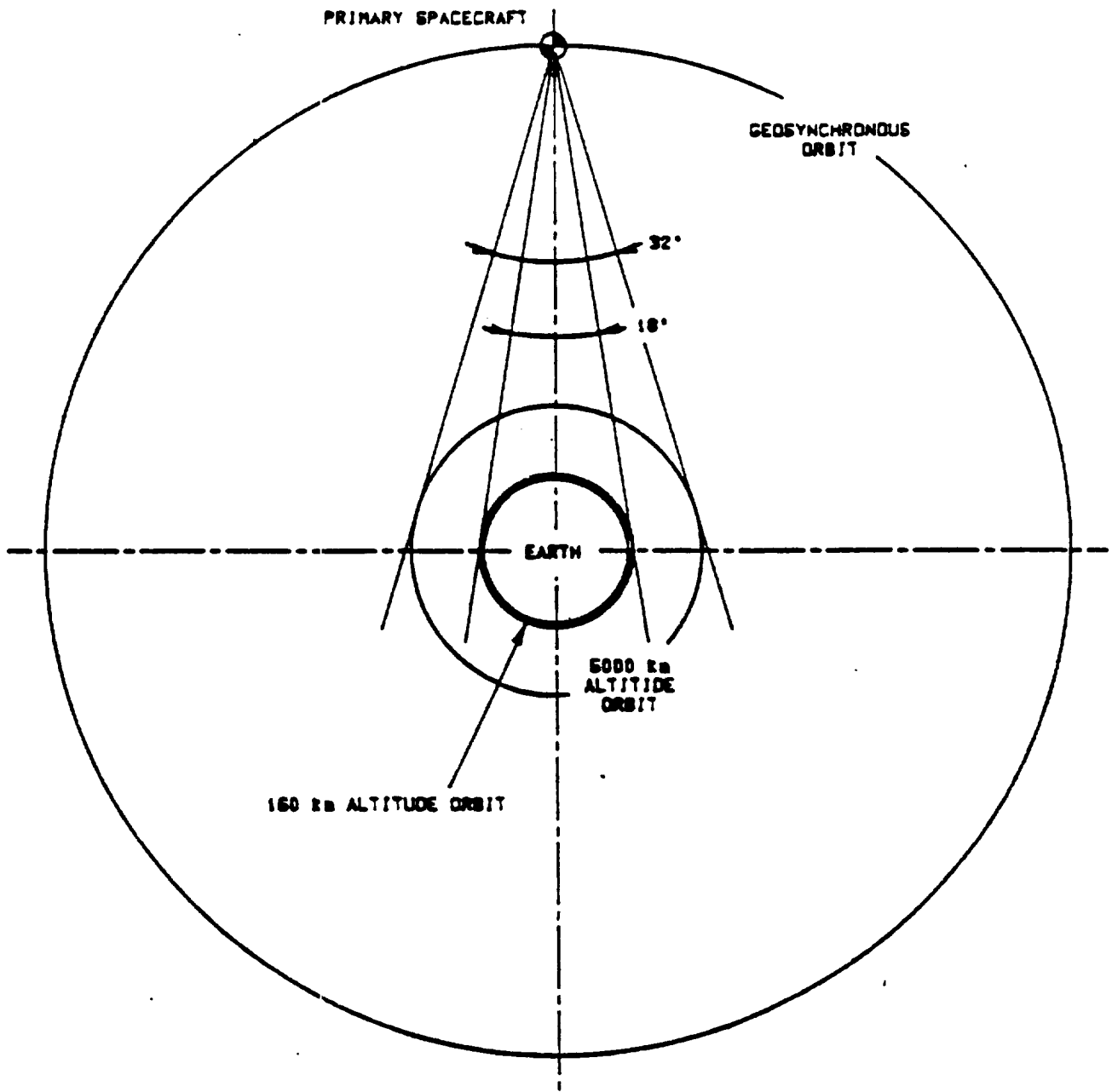
Figure 5.1.6-1   Geosynchronous - Low Earth Orbit
System Configuration

5.1.6.1 General Requirements, Cont.

3. The angular resolution will be 0.011 deg which should maintain adequate pointing and RF reception margins.

4. The acquisition time will vary according to the slew angle and the degree of scanning required to eliminate initial acquisition pointing errors. Assuming that the GEO spacecraft adequately illuminates the LEO target, the acquisition times will be less than 2 minutes.

5. Maximum tracking rate, allowing for LEO orbital and GEO attitude motions, will be approximately 6.0 deg/min for spacecraft in the 160 km to 5000 km orbits.

b. **Low Earth Orbit - Geosynchronous Link** - This terminal is effectively the reverse of the GEO-LEO system with the exception of only one low orbit spacecraft linked to one geosynchronous spacecraft. Figure 5.1.6-2 shows the system configuration. The gimbal mechanism will be identical to that for the GEO-LEO link with the following differences.

1. The maximum angular range will be +/-90 deg in both axes. Location of the antenna and gimbal on the host spacecraft will determine whether the full 180 deg can be used. Due to the mechanics of the gimbal a change in coordinate pointing systems cartesian to polar, occurs. This may cause target tracking problems in two extreme regions of the pointing range. Unfortunately, these points lie close to many of the expected acquisition coordinates.

5.1.6.2 Gimbal Mechanism Design

The three different missions will all be performed by the same basic gimbal design. Minor mechanism configuration changes will result in several gimbal options, each optimized for a particular mission. The characteristics are summarized in Table 5.1-6.

a. **Acquisition Assumptions** - The gimbal design is driven by the system requirements in terms of angular range, speeds, inertias, etc. Of prime importance is the target acquisition method and its mechanical scanning requirements. The following assumptions are made concerning acquisition:

1. Geosynchronous spacecraft guarantees to illuminate the low Earth orbit spacecraft throughout the acquisition attempt.

2. Low Earth orbit spacecraft will perform a pre-programmed scan motion to detect the geosynchronous spacecraft.

3. High speed scanning (approx. 1 deg/sec, cycling with a frequency of approx. 1 Hz) of an entire antenna will cause unacceptable disturbances to the host spacecraft.

4. Acquisition scanning speeds must be of the same order as those used during closed loop tracking.

5.1.6.2 Gimbal Mechanism Design. Cont.

b. Gimbal Configuration - To minimize disturbances to the host spacecraft the beam scanning motions will be performed at relatively slow speeds. The gimbal will perform slewing motions and acquisition tracking motions and the superimposed acquisition scanning.

Only LEO-GEO missions require scanning to acquire a target and this should be limited due to accurate position knowledge. Therefore, the scanning speeds should not have an adverse effect on the total acquisition time.

The gimbal is centered on a four (4) reflector beam waveguide RF transmission system. The feed radiates the beam on to a fixed planar reflector which turns the beam through 90 degrees. The beam then strikes a shaped reflector which can be rotated about the beam axis. The beam is turned through another 90 degrees and is directed toward the third reflector. The third and fourth reflectors are essentially identical to the second and first respectively. Their arrangement is a mirror image of the others and set at an orthogonal axis. Thus, the fourth reflector is fixed relative to the antenna.

Each shaped reflector is housed within a tube structure which is supported by the gimbal bearings. The support bearings are all within the drive sections of the gimbal which are located behind the shaped reflectors.

Mounted on the protruding shaft are the motor, tachometer and optical enccder. The bearings and drive components are mounted onto a highly sculpted housing. The housing consists of bearing support rings which are heavily braced by webs from a box structure strongback. This configuration permits three functions to be accomplished. These are:

1. To provide a stiff load path to transmit launch loads.

2. To maintain accurate alignment and orientation of the reflectors.

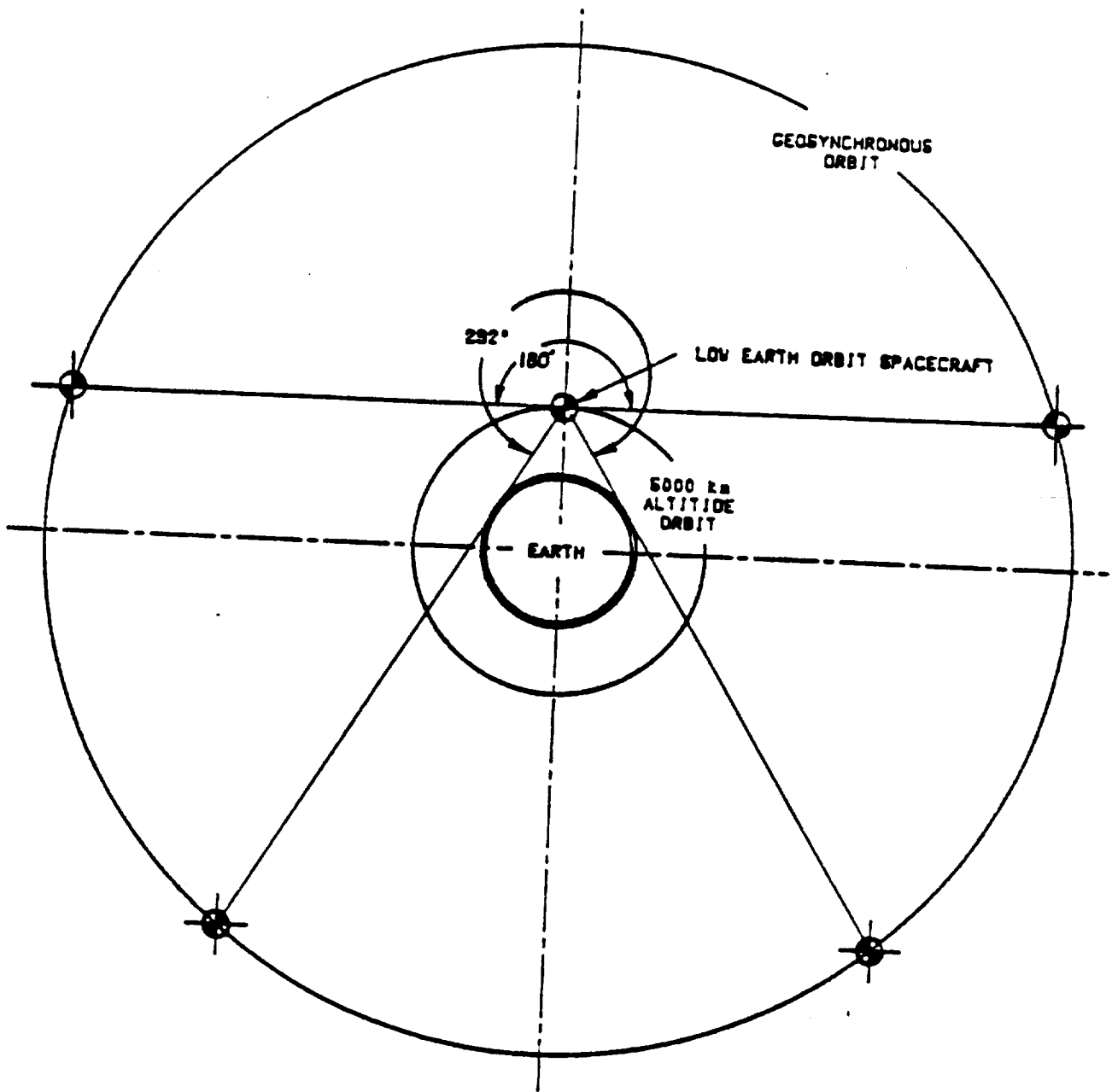3. To permit simple mounting of the motor, tachometer and encoder.

Figure 5.1.6-2   Low Earth Orbit to Geosynchronous
System Configuration

TABLE 5.1-6 GIMBAL CHARACTERISTICS

PARAMETER	Gimbal Crosslink Mission		
	GEO-LEO	LEO-GEO	GEO-GEO
Mechanisms/Spacecraft	5	1	1
Antenna Diameter	0.9 meters	1.4 meters	3.2 meters
Angular Range, Elevation	+/-20 deg.	+/-90 deg.	+/-10 deg.
Azimuth	+/-20 deg.	+/-90 deg.	+/-35 deg.
Maximum Slew Rate	5.0 deg/sec	5.0 deg/sec	2.0 deg/sec
Maximum Acquisition Time	1 min.	1 min.	1 min.
COMMON CHARACTERISTICS			
Angular Resolution	0.011 deg.		
Maximum Tracking Rate	6.0 deg/min.		
Gimbal Mass.	12.7 Kg		
Power Consumption	9W avg./32W peak		

c. Motor/Drive System - A geared stepper motor drive will be used to drive each axis of the gimbal. Ramping of the motor step rates will be used to minimize disturbances to the host spacecraft. These mechanisms are discussed in detail in Monthly Report No. 10.

d. Position Sensor - Position knowledge is required for telemetry and acquisition purposes. Pointing errors must be minimized if expedient acquisitions are to be achieved. Therefore, the encoder must provide position information to an accuracy of approximately 0.01 degrees (ie., approx. 5% of the beam width). Only an optical encoder can provide this 2^{15} performance under the environmental conditions and for the required lifetime. Therefore a 2^{15} optical encoder with redundant readout stations will be incorporated.

The encoder will be mounted directly to the shaft, just as for the motor. As a maximum of 180 deg of motion is required from the gimbal the encoder could be geared to increase its resolution. However, only a 2:1 improvement could be achieved by a standard installation (to be used for all missions) and this would be more than offset by the reduction in accuracy due to backlash.

e. Structural Design - The construction of the gimbal does not permit it to support the antennas through launch without some form of caging. The smaller antennas will be caged for launch and released once on station. The larger antennas will be stowed against the spacecraft body during launch and deployed once on orbit. A caging system may still be necessary depending upon the stowed configuration.

The caging device prevents antenna rotation, while the gimbal transmits the major loads. The main structural members of the gimbal mechanism will be sized to withstand launch and acceleration loads imposed by the various antenna launch configurations.

f. Thermal Design - The material selections for the gimbal design will be based on the thermal conditions in orbit. From previous FACC experience, with similar equipment, the thermal environment will exhibit large temperature variations.

It is assumed that the main gimbal structures will be of titanium to maintain compatibility with the bearings and to reduce beam waveguide thermal distortion. Active thermal control will be used to maintain a relatively benign thermal environment within the mechanism. Where possible, multi-layer blanketing will be installed, though the large angular gimbal motions will not allow extensive use of such insulating techniques.

5.1.7   Power, Size and Weight

Paragraph 1.1.13 indicates the power, weight and size for the electromechanical and RF components for the GEO-LEO crosslink module. The module has three radiator/ heatpipe panels facing south, southeast and southwest. The south panel, which handles three 0.9 meter antenna crosslink elements, has an area of 3.2 square meters. The southwest and southeast radiator panels have an area of 1.4 square meters each for a total module radiator area of 6 square meters weighing a total of 21.3 Kg. The module truss, blankets, brackets etc., have an estimated mass of 25 Kg including margin. The module truss overall dimensions are scaled from Figure 5.1.2-1.

The total mass of the GEO-LEO crosslink module is then:

Electromechanical and Rf components	188.0 Kg
Radiators and heat pipes	21.3 Kg
Truss, blankets, brackets etc.	25.0 Kg
Total Mass	234.3 Kg

5.1.8   Reliability

Reliability is discussed in Section 1.1.14.

5.1.9 System Integration and Sketches

Figure 5.1.2-1 indicates the baseline layout of the GEO spacecraft (TDAS) with the 3.2 meter GEO-GEO antenna and the five 0.9 meter GEO-LEO antennas depicted mounted to the TDAS earth face (+ Z axis). The electronics modules thermal control radiators for the GEO-GEO system and the five GEO-LEO systems antennas are located on the north and south spacecraft surfaces respectively. Some features of the layout are:

1. Concepts follow the "Bolt-on" concept of attaching the crosslink packages.

2. No deployment booms or mast are necessary thereby raising system reliability and lowering mass while increasing stiffness.

3. Reduced number and length of components to spacecraft interface thereby reducing pointing errors.

4. The single 3.2 meter GEO-GEO antenna can face either east or west depending on spacecraft location in orbit.

5. Electronics packages are placed directly behind the two axis gimbals thereby cutting down on RF losses by shortening beam waveguide runs.

6. The electronics for the five 0.9 meter antennas can be incorporated in a single module.

7. The thermal control system will be more efficient by requiring less radiator area since those radiators can be part of the north or south facing panels. Less radiator area also requires less heater power when the system is not operating.

If the projected TDAS uses a larger bus (body) as is expected, then the truss structures supporting the various antennas can have their south/north components acting as extensions of the TDAS north/south panels which would provide easy stowage interfaces for a larger solar array if that becomes necessary.

5.2   GEO-GEO Mechanical Design

5.2.1   Thermal and Mechanical Error Budget

The writeup of paragraph 5.1.2 of this report provides the subject budget for both the GEO-GEO ICL and the GEO-LEO ICL.

5.2.2   System Structure/Mechanical Design

The baseline ICL structure for the GEO-GEO electronics module will be a truss framework and brackets of graphite-epoxy composites attached to an aluminum faceskins/aluminum honeycomb panel to which are mounted the electronic components and contain the variable conductance heat pipes (VCHP's) for temperature control.

The antenna will be an axial fed Cassegrain. The reflectors will be graphite epoxy faceskins with a Kevlar honeycomb core. The tripod holding the subreflector to the main reflector is fabricated of graphite epoxy tubes.

The baseline design is such (Figure 5.1.2-1) that no masts or booms are necessary in order to deploy the three meter antenna. The dual axis Gimbals will provide that function.

5.2.3   Thermal Control Concepts

The baseline thermal control concepts are;

a.   The electronic module containing all the GEO-GEO ICL electronic components including the transmitter, receiver and microprocessor will be a box of truss structure which contains a panel constructed of aluminum faceskins covering an aluminum honeycomb core. Variable conductance heat pipes (VCHP) are embedded in the panel. All electrical and electronic components are mounted to the interior of the panel. The exterior of the panel will contain optical solar reflectors (OSR's). All surfaces not covered in OSR's and the truss structure will be covered by multilayer aluminized Kapton multilayer blankets. A heater system will be employed. A tradeoff of required electronic module radiator area (a function of module dissipation for various spacecraft locations, sun angles) is indicated by Figures 5.1.2-2 through 5.1.2-4.

b.   The Beam Waveguide assembly is internal to the dual axis gimbal/electronic module which will be covered by aluminized Kapton multilayer blankets. No heater system will be employed for thermal control of this assembly.

c.   The electro mechanical systems (gimbals) will employ a thermistor controlled heater system and will employ a multilayer blanket system where the two axis movement will allow.

5.2.3   Thermal Control Concepts. Cont.

d.   The Cassegrain reflector system will have aluminized kapton multi-
     layer blankets attached to the gimbal side of the main reflector
     and on the concave side of the subreflector. All other surfaces
     will be coated with white paint to act as a second surface mirror
     system and to provide diffuse reflections in the solar spectrum.
     All areas that are to employ multilayer blankets will be examined
     to determine if the blankets could cause multiple equivalent
     insolation to other critical spacecraft and ICL surfaces. Any
     blanket that could contribute such an effect will be painted with
     a diffuse black coating which is standard FACC practice. All
     blankets will be grounded to the spacecraft structure.

5.2.4   System Contamination

     The contamination problem for the GEO-GEO 60 GHz crosslink system is
covered by the discussion of paragraph 5.1.4 of this report.

5.2.5   Microprocessor Pointing Control

     The pointing control electronics for the GEO-GEO crosslink are dis-
cussed in Section 5.1.5.

5.2.6   Electromechanical Mechanisms

     The design of the gimbal mechanism for GEO-GEO applications is con-
sidered in Section 5.1.6.

     In this system, one primary spacecraft is required to crosslink to
another similar spacecraft at an orbit angular separation of up to +/-160 deg.
The minimum orbital separation is assumed to be 25 deg. Figure 5.2.6-1
illustrates this configuration. This gimbal is required to support and steer
a 3.2 meter antenna.

     The larger inertia of the GEO-GEO antennas result in slower allowable
motions than for the other missions. However, this is not a concern for the
following reasons:

     Acquisition

     1.   Slew angles are relatively small permitting short slew times.

     2.   The GEO-LEO and LEO-GEO antennas are not tracking during GEO-GEO
          slewing.

     3.   The target spacecraft is always visible and GEO-GEO links will be
          long term. Therefore, a longer initial acquisition period is
          acceptable.

5.2.6   Electromechanical Mechanisms. Cont

Tracking

1. The target spacecraft does not move relative to the host
    spacecraft and so angular tracking rates will be lower (rates
    depend on host spacecraft attitude rates).

    The GEO-GEO gimbals would be one of the options on the basic gimbal.
Configuration of the beam waveguide, motors, encoders would be as for any
other mission. Differences would be restricted to the gimbal range, control
loop gains, caging arrangement and acquisition system.

5.2.7   Power. Size and Weight

    Paragraph 1.2.8 indicates the power, weight and size for the elec-
tromechanical and RF components of the GEO-GEO crosslink module.

    The module has a radiator/heat pipe panel facing north of 1.1 square
meters area which weighs 8.7 Kg. The module truss, blankets, brackets etc.,
have an estimated mass of 5 Kg including margin. The truss overall dimensions
are indicated by Figure 5.1.2-1. The total mass of the GEO-GEO crosslink
module is then:

Electromechanical and RF components	71.3 Kg
Radiators and heat pipes	8.7 Kg
Truss, blankets, brackets etc.	5.0 Kg
Total Mass	85.0 Kg

5.2.8   Reliability

    Reliability is discussed in Section 1.1.14.

5.2.9   System Integration and Sketches

    Paragraph 5.1.9 of this report covers system integration for both the
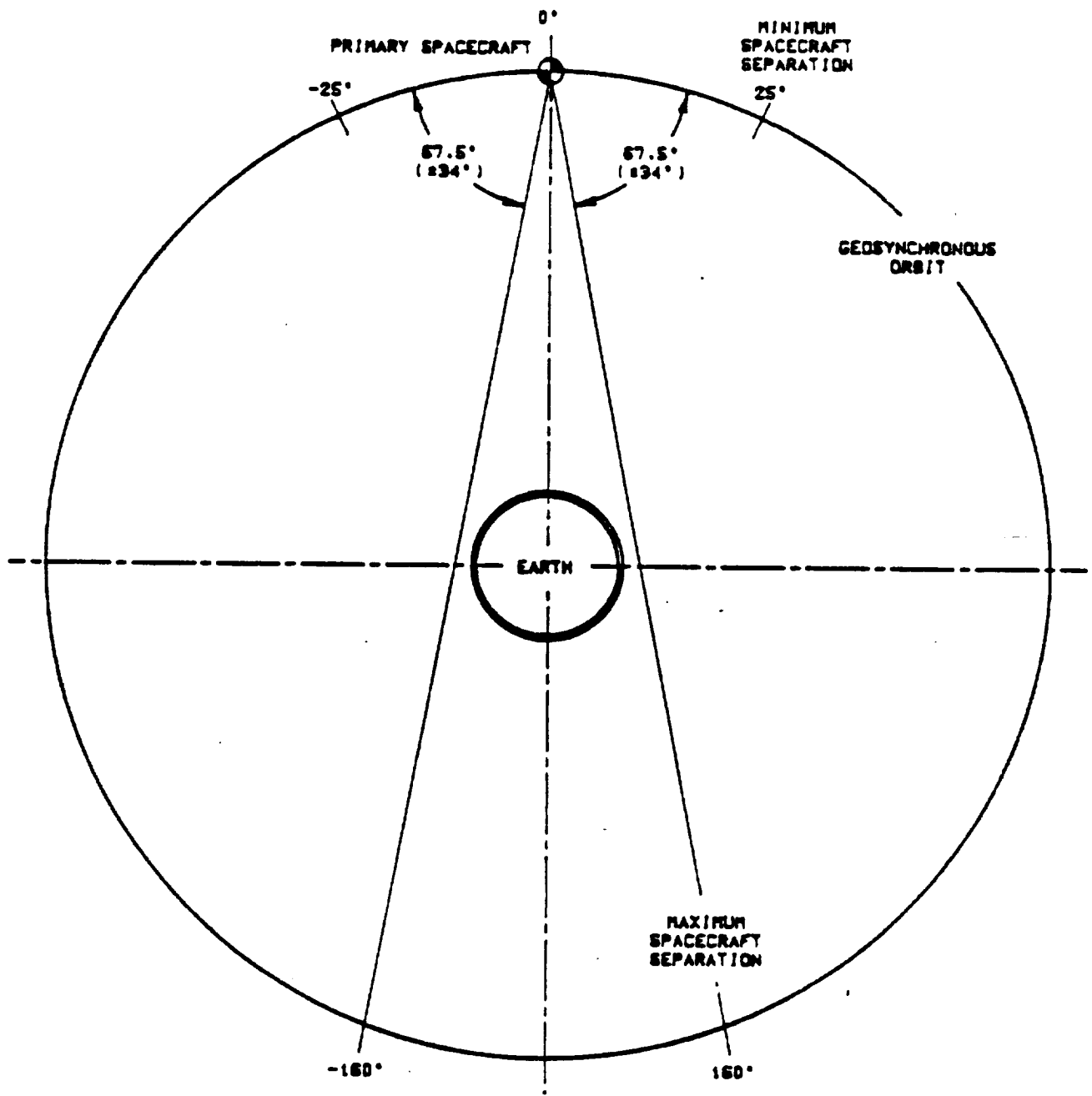GEO-GEO and GEO-LEO ICL packages.

Figure 5.2.6-1 Geosyncnronous Crosslink Configurarion